Analytical and Numerical Approaches to Initiation of Excitation Waves

Submitted by **Burhan Bezekci,**
to the University of Exeter as a thesis for the degree of
Doctor of Philosophy in Mathematics, in **November 2016.**

Signature: . . . . . .

ABSTRACT

This thesis studies the problem of initiation of propagation of excitation waves in one-dimensional spatially extended excitable media. In a study which set out to determine an analytical criteria for the threshold conditions, Idris and Biktashev [68] showed that the linear approximation of the (center-)stable manifold of a certain critical solution yields analytical approximation of the threshold curves, separating initial (or boundary) conditions leading to propagation wave solutions from those leading to decay solutions.

The aim of this project is to extend this method to address a wider class of excitable systems including multicomponent reaction-diffusion systems, systems with non-self-adjoint linearized operators and in particular, systems with moving critical solutions (critical fronts and critical pulses). In the case of one-component excitable systems where the critical solution is the critical nucleus, we also extend the theory to a quadratic approximation for the purpose of improving the accuracy of the linear approximation. The applicability of the approach is tested through five test problems with either traveling front such as Biktashev model, a simplified cardiac excitation model or traveling pulse solutions including Beeler-Reuter model, near realistic cardiac excitation model.

Apart from some exceptional cases, it is not always possible to obtain explicit solution for the essential ingredients of the theory due to the nonlinear nature of the problem. Thus, this thesis also covers a hybrid method, where these ingredients are found numerically. Another important finding of the research is the use of the perturbation theory to find the approximate solution of the essential ingredients of FitzHugh-Nagumo system by using the exact analytical solutions of its primitive version, Zeldovich-Frank-Kamenetsky equation.

ACKNOWLEDGEMENTS

I would like to thank all help and support I have received from the following people during the course of my PhD research.

My deep and sincere gratitude and appreciation go first to my supervisor Prof Vadim N. Biktashev for his continuous support, motivation and patience throughout my PhD research. As my supervisor, Vadim deserves thanks for making a huge effort to guide me, to answer my questions, to lead me into some programming languages and to be available every time I need help. Without his guidance and constant feedback, this PhD would not have been achievable and it has been an honor to have a chance studying under his supervision.

I am happy to acknowledge my debt to my second supervisor Peter Ashwin especially for his understanding and invaluable advices during my tough times in the first year.

My sincere appreciation also goes to all of my colleagues and other staff members in the College of Engineering, Mathematics and Physical Sciences for such a warm academic atmosphere, especially to Ibrahim Kucukkoc, Ummu Atiqah Mohd Roslan, Abdullah Aldurayhim, Saad Almuaddi, Harun Baldemir. My gratitude extends to Courtney Quinn, Tomas Stary, Ovinda Wijeyaratne for proofreading and all members of Exeter Turkish Society for preventing and managing homesickness.

I am extremely grateful for the financial support of the Ministry of National Education of the Republic of Turkey. I cannot thank them enough for providing me the necessary fund to carry out this research in the UK.

Finally, I would like to express my deepest gratitude to every single member of my family for helping me survive all the stress. I owe them much more than I would ever be able to express.

I dedicate this thesis to my beloved mum ZAIDE BEZEKCI.

TABLE OF CONTENTS

LIST OF TABLES

TABLE **Page**

LIST OF FIGURES

FIGURE **Page**

CHAPTER 1

INTRODUCTION

1.1 Threshold Phenomenon

The threshold phenomenon *"deals with the minimal, an event, or stimulus just strong enough to be perceived or to produce a response"* [118] and the presence of it *"imposes the restriction on the types of mathematical model suitable to describe"* biological/chemical systems [45]. Despite its extreme importance, it is not completely understood. Below, we list some examples of how understanding the threshold phenomenon can be rather important:

- Propagation of excitation in the heart involves action potential and threshold value controls if an applied stimulus is sufficient enough to generate an action potential. Understanding the mechanisms of initiation of propagating is extremely crucial as successful propagation enables continuous electrical and chemical communication between cells and failure may lead to serious medical conditions [140].

- Another typical example of how the threshold phenomenon plays a key role is prey-predator system, popular area of extensive study of the relation between species and their environment. The threshold phenomenon in a prey-predator system must be carefully examined as the effect would just be so dramatic [96]. Starting from low population densities of the prey and predator, a typical interaction between two species can be as follows [129]: initially, there occurs an

increase of the prey population until self-limitation mechanisms take part so no further growth is possible. On the other hand, the predator population starts increasing as long as the prey density is above a certain threshold. As the excess predators cause the prey population to decrease, the predator population then declines rapidly due to starvation or emigration.

- Threshold phenomenon also plays a key role in understanding many age-related diseases such as Alzheimer and Parkinson. Studies on neuronal changes in brain suggest that the threshold hypothesis helps to explain *"some of the associations between clinical and pathological findings"* [1, 113]. The importance of the threshold concept in the clinical analysis of such diseases lies in its implications for diagnosis and further research into treatment.

1.2 An Introduction to Excitable Media

Originally, the term *excitability* has come to be used to refer to the *"property of living organisms to respond strongly to the action of a relatively weak external stimulus"* [141]. A well-known example of excitability is the ability of nerve cells to generate and propagate electrical activity. To better understand the mechanisms of the electrical activity in cells, it is helpful to categorise all cell types into two distinct types, *excitable* and *non-excitable*.

Many cells maintain a stable equilibrium electric potential. For some, if electric currents are applied to the cell for a short period of time, the potential returns directly to its equilibrium value once the applied current is removed. These type of cells are called *non-excitable*. The epithelial cells that line the walls of the gut are typical examples of *non-excitable* cells. *Excitable* cells, however, are characterized by an ability to respond to sufficiently strong applied current in a specific way such that the membrane potential goes through a large excursion, called an action potential, before eventually returning to rest. Some classic examples are cardiac cells, smooth and skeletal muscle cells, secretory cells, and most neurons [74].

By definition, an excitable medium is a spatially distributed system, each element of which possesses the property of excitability and it is usually defined as nonlinear reaction-diffusion system, where the reaction term defines how the constituents of the system are transformed into each other, and the diffusion part provides propagation of information [7, 55, 141].

The phenomenon of the excitability can be widely seen in nature and one example of which is forest fire [6, 35]. By way of illustration, consider a forest consisting of fully grown trees. Each individual tree may be in one of the following three states: quiescent (the tree is healthy, unburnt), excited (the tree is on fire) and refractory (the tree is temporarily unable to become excited). If a tree is excited, it will transfer its excitation to its nearest neighbors, and hence the fire on a site will spread through diffusion, followed by refractory period, during which a tree is no longer responsive to a fire. After a certain amount of time, the site eventually returns more or less back to its original state as the forest regrows. Thus, the entire forest can be considered a notable example of excitable media. Figure 1.1 illustrates a typical process of a tree on a site with excitability features in order.

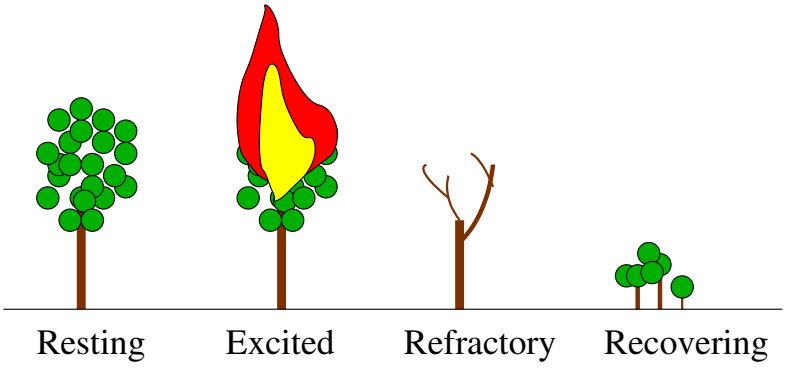

Figure 1.1: A tree with the features of excitability. Copyright 2016 by J. P. Keener [73]. Reprinted with permission.

There are a wide variety of areas where the term “excitable medium” has been used repeatably for decades in many fields including physical, chemical and biological systems and so on [32, 71, 87]. Some prominent examples of excitable media can be listed as follow [40, 123, 141]:

- propagation of electrical excitation in various biological tissues, including nerve fiber and myocardium,
- concentration waves in the bromate-malonic acid reagent (the Belousov-Zhabotinsky reaction),
- waves of spreading depression in the retina of eye,
- pattern formation on tongue,

- the Mexican wave (or La Ola).

1.3 Problem Statement and Aims

This thesis considers the problems of initiation of propagating waves in terms of one-dimensional reaction-diffusion system,

$$\frac{\partial \mathbf{u}}{\partial t} = \mathbf{D}\frac{\partial^2 \mathbf{u}}{\partial x^2} + \mathbf{f}(\mathbf{u}), \tag{1.1}$$

where $\mathbf{u} : \mathbb{R} \times \mathbb{R} \to \mathbb{R}^k$ is a k-component reagents field, $k \geq 1$, defined for $x \in \mathbb{R}$ and $t \in \mathbb{R}_+$, vector-function $\mathbf{f} : \mathbb{R}^k \to \mathbb{R}^k$ describes the reaction rates and $\mathbf{D} \in \mathbb{R}^{k\times k}$ is the matrix of diffusivity. Equation (1.1) is assumed to be an excitable medium that is a system composed of elementary segments or cells, each of which possesses the following properties [41]:

- an equilibrium resting state $\mathbf{u}_r$ such that the solution to (1.1) will decay to it whenever the initial datum is below a certain threshold,
- a threshold for excitation such that any applied stimulus below this threshold produces no persistent change in the system while a stimulus above this threshold induces the cell to change from resting state to an excited state,
- a diffusive-type coupling to its nearest neighbors.

Our aim is to analyse wave motion in (1.1) that has been a topic of extensive studies, both in biological media as well as in chemical processes according to following initial and boundary conditions

$$\mathbf{u}(x,0) = \mathbf{u}_r + U_\mathrm{s}\mathbf{X}(x), \quad \mathbf{D}\mathbf{u}_x(0,t) = -I_\mathrm{s}\mathbf{T}(t), \tag{1.2}$$

where $\mathbf{X}$ and $\mathbf{T}$ describe the shape of the initial and boundary profiles, U_s and I_s are amplitude and strength of those profiles, respectively. The cases of initial value problem and boundary value problem are handled separately as follow:

- Case 1: $U_\mathrm{s} = 0, I_\mathrm{s} \neq 0$. This is the case when the current is injected at the boundary point $x = 0$ during some time interval. For a fixed boundary profile $\mathbf{T}(t)$, there exist a corresponding threshold strength value ${I_\mathrm{s}}^*$ such that the solution tends to propagating wave ("ignition") as $t \to \infty$ whenever $I_\mathrm{s} > {I_\mathrm{s}}^*$, and the solution tends to resting state ("failure") otherwise. This fixed value is called a threshold,

and the corresponding curve that illustrates a graphical representation of the relationship between a set of boundary profiles and the corresponding threshold values is called a strength-duration curve.

- Case 2: $U_{\mathrm{s}} \neq 0, I_{\mathrm{s}} = 0$. Here the perturbation is instantaneous at $t = 0$, but is spread in space. For a fixed initial profile $\mathbf{X}(x)$, there exist a corresponding threshold strength value ${U_{\mathrm{s}}}^*$ such that the solution tends to propagating wave as $t \to \infty$ whenever $U_{\mathrm{s}} > {U_{\mathrm{s}}}^*$, and to resting state otherwise. This fixed value is called a threshold, and we shall call the corresponding critical curve a strength-extent curve.

From a mathematical point of view, the problem of initiation of propagation of excitation waves in one-dimensional spatially extended excitable media is spatially-distributed, non-stationary, nonlinear. Due to the complex nature of the problem, it is not always possible to solve the initiation problem analytically, and hence the solution is mostly approximated by numerical simulations. However, it is highly desirable to have a closed-form analytical solutions to this kind of problems and there have been numerous phenomenological and heuristic approaches aiming to obtain such answers *e.g.* [58, 79, 103, 115].

The motivation for this research is based on the results of McKean and Moll [88] and Flores [48], who established that the boundary in the space of initial data of the equation between the basins of attraction of the resting state and the propagating wave solution is a stable manifold of a certain "standing wave" solution, later alternatively called as *critical nucleus*.

The critical nucleus is a unique unstable nontrivial time independent solution of the one-component case of (1.1) with exactly one positive eigenvalue. It plays a key role in understanding the threshold phenomenon in one-component excitable media. The reason is that the critical nucleus does not depend on the sort of initial data and it appears as a long transient if the initial data are very near the threshold between ignition and decay. One of the analytical approaches attempting to describe the critical conditions benefits from this understanding. In [101], Neu and co-workers derived an analytical expression for the relationship between the parameters of the initial condition using Galerkin style approximations. Another analytical approach to determine the critical conditions is based on the idea of the stable manifold of the critical solution. Idris and Biktashev [68] have demonstrated that linearisation of the stable manifold in the functional space leads to an analytical expression for initiation criteria for a simple

bistable model.

The purpose of this thesis is to quantify the threshold curve performing the boundary between initial (or boundary) conditions leading to propagation wave solution and initial (or boundary) conditions leading to the resting state as an extension further study of [68]. Moreover, as the analytical ignition criteria for the one-component case do not agree very well with their numerically obtained critical curves, we investigate the feasibility of improving the accuracy by using a quadratic rather than a linear approximation of the critical manifold, and related problems. Finally, we extend the method to the case where there are no critical nucleus solutions. This is observed in multicomponent reaction-diffusion systems, where it has been previously demonstrated that instead of critical nucleus, one has unstable propagating waves, such as critical pulses [49] or critical fronts [67].

1.4 Thesis Outline

The contents of the thesis are divided into seven chapters. This chapter was intended to give a brief introduction about the main area of the study, initiation problem. Definitions of some concepts needed for the understanding of the problem have been shortly provided. We will end the chapter by describing the contents of the thesis.

Introduction chapter is followed by the literature review beginning with the description of some concepts and terminologies including reaction-diffusion system and action potential in Chapter 2. We then describe some well-known mathematical models of excitable cells and excitability properties of each starting with the classic Hodgkin-Huxley model, its logical reduction FitzHugh-Nagumo (FHN) model and its generalisation version Beeler-Reuter model. We also explain the generic form of spatially extended excitable systems and their traveling wave solution. Details of the test problems for two different traveling wave solutions are given. The first, models with traveling front, consists of Zeldovich-Frank-Kamenetsky (ZFK) equation, McKean equation and the simplified front model due to Biktashev. The second, models with traveling pulse, includes spatially extended FitzHugh-Nagumo system and spatially extended Beeler-Reuter model. The chapter is then closed with a brief history of the mathematical approaches to the initiation problem and a review of some essential numerical methods.

Chapter 3 describes the proposed analytical methods, including both the linear and quadratic approximations of the one-component case, and the linear approxi-

mation for the multicomponent case. Subsequent sections are dedicated to specific examples of application of the described method.

Though the method is analytical in nature, it is generally unlikely to obtain the essential ingredients analytically due to the nature of the equations having nonlinear term(s). Therefore, we need to take the aid of numerical methods for calculating these ingredients numerically. Further, these numerical methods can be handled as a verification of the analytical derivation. We also describe direct numerical simulations of the threshold curves in order to compare them with their analytical approximation. A detailed outline of the technique introducing the numerical approaches to the initiation problem is given in Chapter 4.

The applicability of the approach is demonstrated on five test problems and Chapter 5 is devoted to one-component test problems with critical nucleus solutions. The models considered are Zeldovich-Frank-Kamenetsky and McKean equations and both the linear and quadratic approximations are employed for comparison with direct numerical simulations.

In Chapter 6, we test the ignition criteria for the multicomponent systems. The theory will be carried out on Biktashev model with moving critical front, and FitzHugh-Nagumo system and Beeler-Reuter model with moving critical pulses where their ingredients are found numerically. As ZFK equation is a one-component version of FHN system (with $\gamma = 0, v \equiv 0$), the perturbation method is performed to analytically obtain the ingredients of FHN with small excitability parameter β. Both strength-extent and strength-duration curves are examined for all models except Biktashev model where only the strength-duration case is considered as its strength-extent analysis has been performed by Idris [66].

In Chapter 7, we summarise the work in this thesis. We present a short review of the results and some possible further directions.

Finally, due to discontinuity of the right-hand sides of McKean and Biktashev models some non-standard numerical techniques are discussed in the appendices.

Some of the material contained in this thesis is used in the following publications:

- B. Bezekci, I. Idris, R. D. Simitev and V. N. Biktashev, Semi-analytical approach to criteria for ignition of excitation waves, *Phys. Rev. E*, **92**:042917, 2015.
- B. Bezekci and V. N. Biktashev, Strength-duration relationship in an excitable

medium, submitted to *Phys. Rev. E*.

- B. Bezekci and V. N. Biktashev, Fast-slow asymptotic for semi-analytical ignition criteria in FitzHugh-Nagumo system, in preparation, to be submitted to *Chaos*.

CHAPTER 2

LITERATURE REVIEW

2.1 Chapter Introduction

In this chapter, review of the relevant literature is given. Section 2.2 explains definitions and description of several key concepts including reaction-diffusion systems and action potential. Section 2.3 describes some of the research on excitable cells and their mathematical models of how action potentials in the cells are initiated and propagated. Section 2.4 begins with the generic form of one-dimensional spatially extended excitable systems followed by some forms of traveling wave solutions of it and finally we then progress onto the models that we consider in the following chapters. We shall then outline various mathematical approaches to the initiation problem listed according to their publication year in Section 2.5. The chapter is concluded with some essential numerical methods in Section 2.6 which can be used to find numerical threshold curve or to obtain the ingredients of explicit analytical expression of the threshold curve.

2.2 Fundamentals and Definitions

In this section, we introduce some concepts that will be needed for the understanding of the topic.

2.2.1 Reaction-Diffusion Systems

One of the much studied nonlinear and chaotic dynamics is reaction-diffusion systems since they, rather typically, arise in many areas such as physical, chemical, biological media and so on. The study of these phenomena requires a variety of different methods from many areas of mathematics for instance bifurcation and stability theory, singular perturbations, numerical analysis, just to mention a few. Typically, a reaction-diffusion system is obtained by combining Fick's law of diffusion with the chemical reaction rate law [120, p. 783-789]. One-component reaction-diffusion system is considered as the simplest which is known as the KPP (Kolmogorov-Petrovsky-Piskounov) equation [77]

$$\frac{\partial u}{\partial t} = D\frac{\partial^2 u}{\partial x^2} + f(u), \tag{2.1}$$

where t and x respectively represent time and space position in one dimension, $u = u(x,t)$ is a state variable and describes density/concentration of a substance and D is the diffusion coefficient. $f(u)$ describes a local reaction kinetics and when it is equal to zero, the equation represents a pure diffusion process called as heat equation in the literature. There are various well-known choices of $f(u)$ and here we introduce some of them [53] :

- $f(u) = u(1-u)$ yields Fisher's equation named after R. A. Fisher who [44] described the spatial spreading of biological population u over a one-dimensional habitat,
- $f(u) = u\left(1-u^2\right)$ is known as Newell-Whitehead-Segel equation [102, 122] arising after carrying out a suitable normalization in the study of thermal convection of a fluid heated from below. Considering the perturbation from a stationary state, the equation describes the evolution of the amplitude of the vertical velocity if this is a slowly varying function of time t and position x,
- $f(u) = u(1-u)(u-\theta), \quad 0 < \theta < 1$ (or its particular degenerate case $f(u) = u^2 - u^3$) gives the general Zeldovich-Frank-Kamenetsky equation [139] that mainly emerges in the combustion theory. This equation also known as Nagumo equation modeling the transmission of electrical pulses in a nerve axon,
- $f(u) = -u + \mathrm{H}(u-a)$ is a variant of Nagumo equation named as one-component McKean model [89] with $\mathrm{H}(\cdot)$ being Heaviside step function and in terms of having piecewise smooth kinetics it is similar to "realistic" cardiac models.

The last two equations will be further reviewed in the following sections in details as they are the only ones with threshold parameters. On the other hand, two component reaction-diffusion systems also have a great deal of importance especially in chemical reaction systems, epidemiology and pattern formation research. A classical two-component activator-inhibitor system is described by the following partial differential equations

$$\begin{aligned} \frac{\partial u}{\partial t} &= D_1 \frac{\partial^2 u}{\partial x^2} + f_1(u,v), \\ \frac{\partial v}{\partial t} &= D_2 \frac{\partial^2 u}{\partial x^2} + f_2(u,v), \end{aligned} \tag{2.2}$$

where D_1 and D_2 are nonnegative diffusion coefficients, u and v are the state of the system, f_1 and f_2 are the local dynamics. In a 1952 article in Biomathematics, Alan Turing proposed that pattern formation could be understood using a simple two-component system of reaction-diffusion equations [130]. Since then, there have been further experimental and theoretical studies based on Turing's theoretical work.

Additionally, reaction-diffusion systems with more than two components have been widely investigated and one of the major areas of interest within the field of electrophysiology is the mathematical description of the excitation and propagation of nerve impulses firstly proposed by Hodgkin and Huxley [61]. In their Nobel Prize work, they described how action potentials in neurons are initiated and propagated. Another example of the system of equations (2.2) is promoted by the FitzHugh-Nagumo model [47] that is a simplified version of the Hodgkin-Huxley model and is accepted as the prototype of an excitable system. These two models will be explained in detail in the following sections.

2.2.2 Action Potential

Neurons are specialized cells in the body of living organisms and they are basically responsible for transmitting information to other nerve cells or other types of cells, such as muscles. Transient electrical signals are considered to be particularly important as they carry time-sensitive information over long distances and these electrical signals are produced by changes in the current flow into and out of the cell, driving the electrical potential across the cell membrane away from its resting value [70].

Membrane potential (also transmembrane potential or membrane voltage) refers to the electrical potential difference in the concentration of ions on each side of the

membrane. When the membrane potential is consistent so that there is no distinguishable change in it, the membrane potential is held at a stable value called resting potential, *i.e.* unstimulated, polarized state of a neuron and it varies among different cell types.

A typical action potential is initiated by a sudden change in the transmembrane potential. During this event, the membrane potential changes rather dramatically and noticeably usually from negative to positive. An action potential can be divided into three phrases: depolarization, repolarization and hyperpolarization and we briefly describe each of which below.

An action potential is not produced unless a stimulus current of a sufficient magnitude is injected. **Depolarization phase, or rising phase** occurs once when a large enough positive stimulus exceeding a certain value, at which point the neuron generates an action potential, is inputted. A simplified picture is that there is a certain value of the minimum membrane potential giving rise to the action potential is called as **threshold potential**. In this phase, the negative membrane potential becomes positive for a very short time and it reaches its most positive value such that the depolarization phase is then completed.

The next phase of the action potential is called **repolarization, or falling phase** referring to the change in the membrane potential that returns it to a negative value just after the action potential has reached its maximum. The membrane repolarizes beyond the resting state due to the flow of potassium out of the cell where the third phase called as **hyperpolarization** starts. This phase causes the potassium channels to close so the membrane potential level it with the steady state resting potential.

The duration of an action potential can be divided into two phases. **Absolute refractory period** comes immediately after the start of an action potential. During this period, it is impossible to produce a second action potential no matter how strong a stimulating current is applied. **Relative refractory period** follows the first phase immediately and lasts until the membrane returns to the resting state. During this phase, another action potential can be produced only if the stimulus is stronger than those normally required to reach the threshold.

It is very important to bear in mind that the intensity of a stimulus does not affect the strength of the action potential. If that stimulus exceeds the necessary threshold, the neuron or, in general, any excitable cell will give a complete response and an action potential will be transmitted from one end of the axon to the other. Otherwise, there is no response. This characteristic property of action potentials is called as “all

or none" principle.

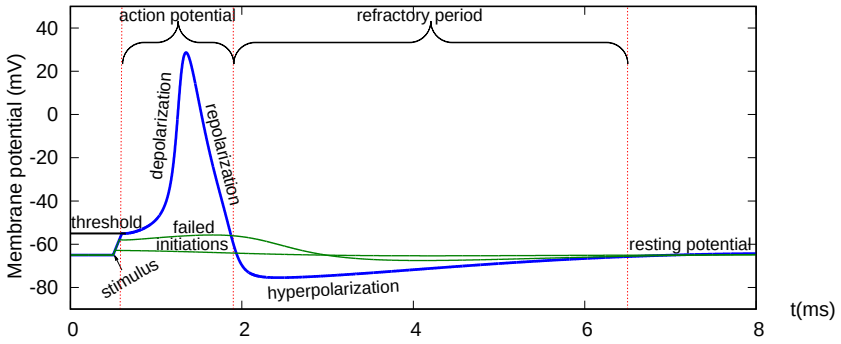

Figure 2.1: General shape of the phases of a typical action potential with respect to time and voltage, adopted from [22].

Figure 2.1 shows the typical shape of an action potential on an expanded time scale. The various parts of the action potential are labeled and the responses of the stimulus current below the threshold that do not cause enough depolarization to trigger an action potential are labeled as "failed initiation".

2.3 Mathematical Models for Excitable Cells

The purpose of this chapter is to review several mathematical models describing the generation of action potential.

2.3.1 Hodgkin-Huxley Model

Action potential has been the subject of extensive research in the field of electrophysiology due to its dominant feature of the nervous system. In 1952, Alan Hodgkin and Andrew Huxley conducted one of the most valuable studies in this research area. In their work, Hodgkin and Huxley developed a mathematical model to analyse and explain the ionic mechanisms underlying the initiation and propagation of action potentials in a giant squid [61]. They received the 1963 Nobel Prize in physiology and medicine together with John Eccles. Considering that they developed the model well before the advent of electron microscopes or computer simulations, one could say this Nobel Prize was well earned.

To describe the cell membrane, Hodgkin and Huxley constructed a simple electrical equivalent circuit, as shown in Figure 2.2. The cell membrane is a lipid bilayer and it acts as a capacitor with constant capacitance, C. During their experiments,

Hodgkin and Huxley determined the sodium (Na^+) and potassium (K^+) ions to be two most important species implied in the generation of the action potential. The Na^+ and K^+ channels are considered to be resistors described by voltage-dependent conductances g_{Na} and g_K, respectively. The ionic currents of these two are denoted by i_{Na} and i_K. The model also considers a third ionic current lumping together all other ions designated by i_L and a third leak conductance, g_L, being independent of the membrane potential. The electrochemical gradients driving the flow of ions are represented by an electric source with voltages V_{Na}, V_K and V_L.

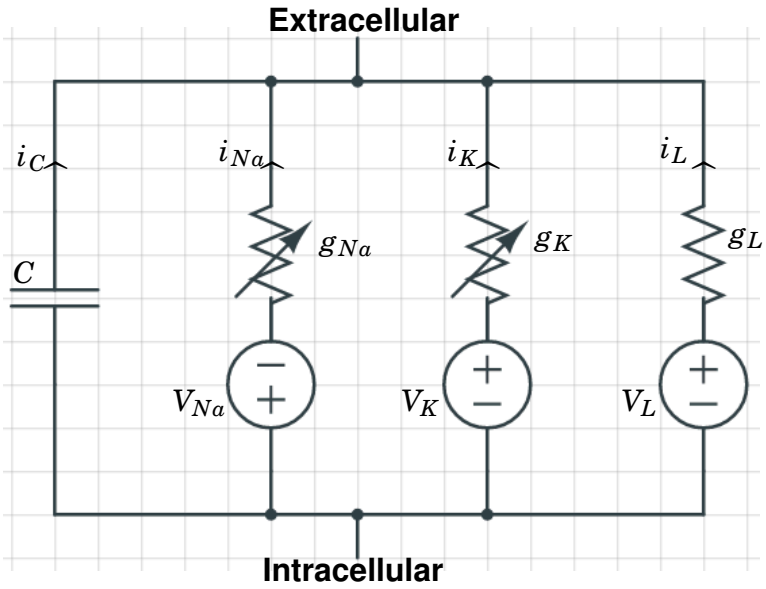

Figure 2.2: The typical representation of the membrane as an electric circuit containing active Na^+ and K^+ channels, a leakage channel and a membrane, adapted from [61].

By employing Kirchhoff's law, we have the following relationship between the sum of ionic currents, the capacitive current i_C and an externally applied current I_{ext}

$$i_{Na} + i_K + i_L + i_C = I_{ext}, \tag{2.3}$$

where the capacitive current can be mathematically written as

$$i_C = C\frac{\mathrm{d}V}{\mathrm{d}t}. \tag{2.4}$$

The membrane voltage, V, is the potential difference between intracellular and extracellular environments and is the same for each parallel branch of the circuit. As a result, Hodgkin and Huxley described the individual ionic current as

$$i_s(V) = g_s(V - V_s), \tag{2.5}$$

for sodium, potassium and leak branches, *i.e.* $s = Na^+$, K^+ and L. Substituting this quantity for each current into (2.3) and employing (2.4) give a mathematical formulation of electrical activity as a first-order differential equation

$$C\frac{\mathrm{d}V}{\mathrm{d}t} = I_{ext} - g_{Na}(V - V_{Na}) - g_K(V - V_K) - g_L(V - V_L). \tag{2.6}$$

Hodgkin and Huxley proposed the specific forms for the sodium and potassium conductances as a product of gating variables and maximum conductances. Particularly, they found

$$g_K(n) = n^4\bar{g}_K, \quad g_{Na}(m,h) = m^3h\bar{g}_{Na},$$

where $\bar{g}_K$ and $\bar{g}_{Na}$ are constants. The unknown functions n, m and h are gating variables representing activation of the potassium current, activation of the sodium current and inactivation of the sodium current, respectively and they all have dimensionless values in the range of $(0,1)$. Each of these gating variables obeys a simple linear differential equation

$$\frac{\mathrm{d}s}{\mathrm{d}t} = \alpha_s(1-s) - \beta_s s, \tag{2.7}$$

where α_s, β_s, $s = n,m,h$ are the rate constants that describe the transition rates of permissive and non-permissive gates. Further, applying the voltage clamp experimental technique let Hodgkin-Huxley fix the membrane voltage, V, at almost any desired value. Thus, steady-state of the gating variables can be found using the fact that the rates of opening and closing are equal at steady-state

$$s_\infty = \frac{\alpha_s}{\alpha_s + \beta_s}, \quad t \to \infty.$$

An analytical solution of (2.7) can then be found as

$$s = s_\infty - (s_\infty - s_0)\exp(-t/\tau_s), \tag{2.8}$$

where s_0 is the initial condition and the quantity τ_s is called the time constant defined in terms of the rate constants at a constant membrane potential

$$\tau_s = \frac{1}{\alpha_s + \beta_s}.$$

We summarise the equations proposed by Hodgkin and Huxley to describe the nerve action potential as follows:

$$C\frac{\mathrm{d}V}{\mathrm{d}t} = I_{ext} - \bar{g}_{Na}(V - V_{Na})m^3h - \bar{g}_K(V - V_K)n^4 - g_L(V - V_L), \tag{2.9a}$$

$$\frac{\mathrm{d}m}{\mathrm{d}t} = \frac{m_\infty - m}{\tau_m}, \tag{2.9b}$$

$$\frac{\mathrm{d}h}{\mathrm{d}t} = \frac{h_\infty - h}{\tau_h}, \tag{2.9c}$$

$$\frac{\mathrm{d}n}{\mathrm{d}t} = \frac{n_\infty - n}{\tau_n}. \tag{2.9d}$$

Hodgkin and Huxley were able to fit their experimental data to derive the following expressions for voltage-dependent rate constants

$$\alpha_n(V) = \frac{0.01(V+55)}{1-\exp[-(V+55)/10]}, \quad \beta_n(V) = 1.125\exp[-(V+65)/80], \tag{2.10a}$$

$$\alpha_m(V) = \frac{0.1(V+40)}{1-\exp[-(V+40)/10]}, \quad \beta_m(V) = 4\exp[-(V+65)/18], \tag{2.10b}$$

$$\alpha_h(V) = 0.07\exp[-(V+65)/20], \quad \beta_h(V) = \frac{1}{1+\exp[-(V+35)/10]}. \tag{2.10c}$$

The values of the constants are given in Table 2.1. As (2.9) is a set of four coupled

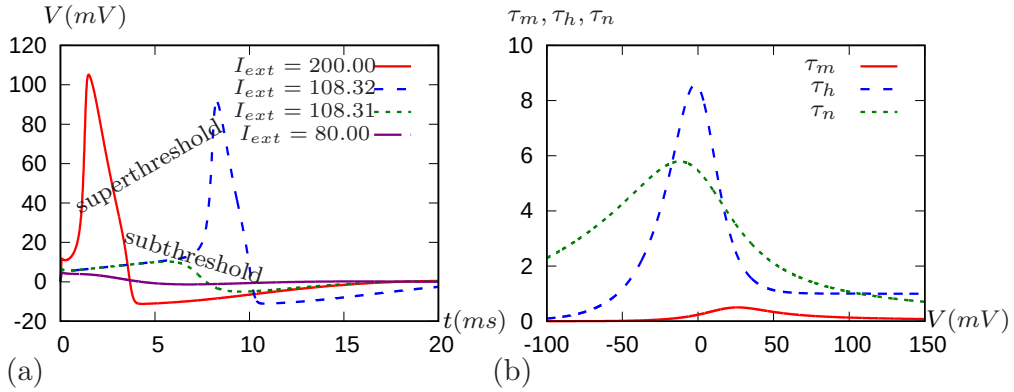

Figure 2.3: (a) Hodgkin-Huxley waveform of the membrane potential with different external currents applied at $t = 0$ ms and lasting for 0.05 ms, (b) the time constants of the model.

nonlinear ordinary differential equations, it is impossible to find an explicit solution. Hence, computer simulations are required to numerically approximate the action potential of Hodgkin-Huxley squid axon model. In Figure 2.3, the voltage profile for four different applied external stimuli (a) and time constants for $I_{ext} = 200$ (b) are plotted.

The initial conditions are fixed as $(V_0, m_0, h_0, n_0) = (0, 0.0529, 0.5961, 0.3177)$, to four places of decimals.

Action potential generation in Hodgkin-Huxley model is a threshold phenomenon and a great deal of effort has been made to determine such threshold experimentally. The effect of a stimulus on the membrane potential varies according to its amplitude. A smaller amplitude stimulus results in small magnitude response in the membrane potential but it is insufficient to produce an action potential. This insufficient stimulus is known as **subthreshold stimulus**. In the figure, two subthreshold external stimuli $I_{ext} = 80$ and $I_{ext} = 108.31$ are shown such that the change in the voltage is small and when the applied current is turned off, the magnitude of the potassium current increases that acts to repolarize the membrane voltage so it returns to the resting potential.

On the other hand, a large enough stimulus that produce an action potential is called as **superthreshold (or suprathreshold) stimulus** (see $I_{ext} = 108.32$ and $I_{ext} = 200$ cases in the figure). In this case, the applied external stimulus can cause a large change in the membrane potential and sodium influx via voltage-dependent sodium channels further depolarizes the membrane potential until the membrane potential reaches to the sodium equilibrium potential. Then, the potassium channels open that cause potassium efflux from the cell and the cell becomes hyperpolarized due to a small undershoot in the membrane potential. Finally, the recovery stage back to the steady-state resting potential is associated with the action of sodium and potassium pumping.

In the Hodgkin-Huxley model, some certain strength of the injected current can produce partial-amplitude spike that is neither “none” nor “all” response. This intermediate response will be further detailed in the FitzHugh-Nagumo model analysis.

Parameters	Value	Units
Membrane capacitance (C)	1	$\mu F/cm^2$
Maximum sodium conductance ($\bar{g}_{Na}$)	120	mS/cm^2
Maximum potassium conductance ($\bar{g}_K$)	36	mS/cm^2
Leak conductance ($\bar{g}_L$)	0.3	mS/cm^2
Sodium equilibrium potential (V_{Na})	115	mV
Potassium equilibrium potential (V_K)	-12	mV
Leak equilibrium potential (V_L)	10.613	mV

Table 2.1: Hodgkin-Huxley model constant parameters.

2.3.2 FitzHugh-Nagumo Model

2.3.2.1 Bonhoeffer-van der Pol Model

The Hodgkin-Huxley model has to be judged one of the most successful mathematical models in the field of electrophysiology. Ever since their publication in 1952, many researchers have tended to focus on the generation of the nerve action potential. Due to the complexity of a 4-variable system, a particular attention has been devoted to obtain simpler and more mathematically tractable reduced-order systems.

In 1961, Richard FitzHugh sought to obtain two-dimensional simplification of the Hodgkin-Huxley model by means of his observation indicating that the gating variable m is much faster than that of the variables n and h, and that for the parameters values specified by Hodgkin and Huxley the value of $n+h$ remains approximately constant during the action potential of the system [46, 47]. Therefore, he obtained following two-variable model

$$C\frac{\mathrm{d}V}{\mathrm{d}t} = I_{ext} - \bar{g}_{Na} m_{\infty}^{3}(0.8-n)(V-V_{Na}) - \bar{g}_{K} n^{4}(V-V_{K}) - g_{L}(V-V_{L}), \tag{2.11a}$$

$$\frac{\mathrm{d}n}{\mathrm{d}t} = \frac{n_{\infty}-n}{\tau_{n}}. \tag{2.11b}$$

Furthermore, FitzHugh discovered that the nullcline of V and n had approximately cubic and linear shapes, respectively. This led to the following two-variable model

$$\frac{\mathrm{d}V}{\mathrm{d}t} = I_{ext} + V - \frac{V^{3}}{3} - W, \tag{2.12a}$$

$$\frac{\mathrm{d}W}{\mathrm{d}t} = \epsilon(V - a - bW), \tag{2.12b}$$

where V and W are dimensionless, normalized dynamic state variables being excitation (fast) and recovery (slow) variables respectively, a, b and ϵ are constant parameters.

FitzHugh in his original papers called this model the **Bonhoeffer-van der Pol model** as he devised the model in the same way as the Van der Pol equation was devised. Van der Pol equation known as the first model representing the heart's dynamics [132] is the special case of (2.12) with $a = b = I_{ext} = 0$. In another well-known study, Nagumo *et al.* [98] described a prototype of a single cell excitable system and came up with essentially the same form as (2.12). Thus, these equations (2.12) have tended to be known as the FitzHugh-Nagumo model.

It is very useful to sketch the phase-plane for understanding the qualitative behaviour of the system (2.12). Figure 2.4 aims to illustrate the typical phase plane for

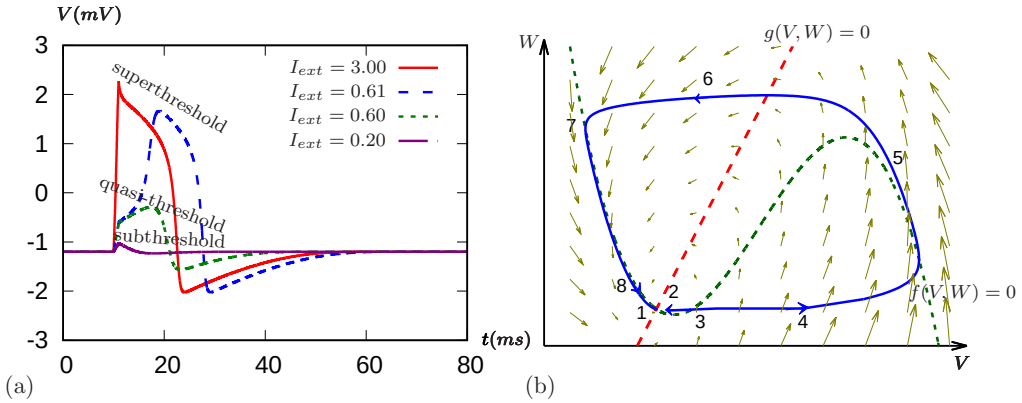

Figure 2.4: (a) Excitation variable solution of equations (2.11) with different external currents applied at $t = 10$ ms and lasting for 1 ms, (b) typical phase plane for Bonhoeffer-van der Pol model. Dotted green and red lines are nullclines of V and W where $\mathrm{d}V/\mathrm{d}t = 0$ and $\mathrm{d}W/\mathrm{d}t = 0$, respectively. Other remaining lines are the time parametrized trajectories. The resting state of the system (1) is stable. Subthreshold perturbations (2) result in a simple return to resting state, but superthreshold perturbations (3) generate a large excursion (action potential) before returning to rest. First, there is a phase (4) of rapid excitation, followed by a period (5) when the system remains in the excited state. After the end of excitation phase (6), the system is at absolute refractory period (7) and then recovers excitability (8) as it returns to the resting state [131].

Bonhoeffer-van der Pol model exhibiting the threshold behaviour along with excitation variable behaviour over time at varying values of applied current, I_{ext}. The initial condition are set to be resting steady state $(V_0, W_0) = (1.2, -0.625)$ for parameter values $\epsilon = 0.08$, $a = 0.7$, $b = 0.8$. The chosen value of weak stimulus (subthreshold) that does not lead to excitation is 0.2, and that of stronger stimuli (superthreshold) that cause excitation to occur are 0.61 and 3.

A remarkable property of excitability in neuronal cells conducted by FitzHugh [45, 46], who explained the absence of all-or-none responses in the Hodgkin-Huxley model is such that any intermediate response between “all” and “none” can be obtained if the stimulus intensity is well-adjusted. In other words, the Hodgkin-Huxley model does not have a well-defined firing threshold. This property is called “quasi-threshold” and is also valid for the FitzHugh-Nagumo model. As can be seen in Figure 2.4, the injected stimulus $I_{ext} = 0.6$ produce this intermediate response between sub- and superthreshold.

2.3.2.2 The Generalized FitzHugh-Nagumo Model

There are also many other equivalent forms of the system, some of which can be found in [112]. Here, we only introduce the generalized FitzHugh-Nagumo equation that is in the following form

$$\epsilon \frac{\mathrm{d}v}{\mathrm{d}t} = f(v,w), \tag{2.13a}$$

$$\frac{\mathrm{d}w}{\mathrm{d}t} = g(v,w), \tag{2.13b}$$

where $0 \leq \epsilon \ll 1$ represents the ratio of time scales. The nullcline $f(v,w) = 0$ resembles a cubic shape and the nullcline $g(v,w)$ only has one intersection with $f(v,w)$.

2.3.3 Beeler-Reuter Model

Following the Hodgkin and Huxley, many researchers have extended their pioneering formulation to describe the electrophysiology of various specific cell types. In 1977, G.W. Beeler and H. Reuter [12] developed one of the simplest physiologically-based model and successfully proposed a mathematical model of the action potential of mammalian cardiac ventricular muscle cell based on experimental data from the guinea pig.

Beeler-Reuter model is the first study taking into account the calcium currents. Hence, compared to Hodgkin-Huxley model (with three ionic currents), the model consists of four ionic conductance components. These are: the usual fast inward current carried primarily by sodium, I_{Na}; a slow inward current carried mostly by calcium, I_s; a time-activated outward current based mainly on potassium ions, I_{x1}; and an outward time-independent potassium current, I_{K_1}. Kirchhoff's law gives the following total ionic current expression as a combination of sum of these four currents, capacitive current I_C, and an externally applied current I_{ext}

$$I_{Na} + I_{K_1} + I_{x1} + I_s + I_C = I_{ext}. \tag{2.14}$$

The equation for the membrane potential is then

$$\frac{\mathrm{d}V}{\mathrm{d}t} = \frac{1}{C_m}\left(I_{ext} - I_{Na} - I_s - I_{K_1} - I_{x1}\right), \tag{2.15}$$

where C_m is the membrane capacitance. The fast inward sodium current I_{Na} has an extra inactivation variable j as opposed to the standard Hodgkin-Huxley formulation

$$I_{Na}(V,m,h,j) = \left(\widetilde{g_{Na}} m^3 h j + \widetilde{g_{Na_c}}\right)(V - E_{Na}), \tag{2.16}$$

where $\widetilde{g_{Na}}$ is the maximum sodium conductance, $\widetilde{g_{Na_c}}$ is the steady-state sodium conductance, and E_{Na} is the sodium reversal potential. Similarly, the slow inward current I_s is determined by

$$I_s(V,d,f,\mathrm{Ca}) = \widetilde{g_s}\, d\, f(V - E_s(\mathrm{Ca})), \tag{2.17}$$

where $\widetilde{g_s}$ is the fully activated channel conductance of slow currents, d and f are the activation and inactivation gate variables, respectively. The reversal potential E_s depends on the intracellular calcium ion concentration (using Nernst's equation)

$$E_s(\mathrm{Ca}) = -82.3 - 13.0287 \ln(\mathrm{Ca}). \tag{2.18}$$

The time-independent outward potassium current I_{K_1} is simply a function of the membrane potential given by

$$I_{K_1}(V) = 0.0035 \left[\frac{4\left(\mathrm{e}^{0.04(V+85)} - 1\right)}{\mathrm{e}^{0.08(V+53)} + \mathrm{e}^{0.04(V+53)}} + \frac{0.2(V+23)}{1 - \mathrm{e}^{-0.04(V+23)}} \right] \tag{2.19}$$

and time-activated outward potassium current has a single gating variable x_1

$$I_{x1}(V,x_1) = 0.8 x_1 \frac{\mathrm{e}^{0.04(V+77)} - 1}{\mathrm{e}^{0.04(V+35)}}. \tag{2.20}$$

The time evolution of the intracellular calcium concentration is described by

$$\frac{\mathrm{dCa}}{\mathrm{d}t} = -10^{-7} I_s + 0.07(10^{-7} - \mathrm{Ca}) \tag{2.21}$$

and each dimensionless gating variable $y = m, h, j, d, f, x_1$ obeys

$$\frac{\mathrm{d}y}{\mathrm{d}t} = \frac{y_\infty - y}{\tau_y}, \tag{2.22a}$$

$$\tau_y = \frac{1}{\alpha_y + \beta_y}, \tag{2.22b}$$

$$y_\infty = \frac{\alpha_y}{\alpha_y + \beta_y}, \tag{2.22c}$$

where y_∞ is the steady-state curve, τ_y is the time constant curve, α_y and β_y represent

the opening and closing rates. The values for the rate constants are found as

$$\alpha_m(V) = \frac{-(V+47)}{e^{-0.1(V+47)}-1}, \quad \beta_m(V) = 40\,e^{-0.056(V+72)}, \tag{2.23a}$$

$$\alpha_h(V) = 0.126\,e^{-0.25(V+77)}, \quad \beta_h(V) = \frac{1.7}{e^{-0.082(V+22.5)}+1}, \tag{2.23b}$$

$$\alpha_j(V) = \frac{0.055\,e^{-0.25(V+78)}}{e^{-0.2(V+78)}+1}, \quad \beta_j(V) = \frac{0.3}{e^{-0.1(V+32)}+1}, \tag{2.23c}$$

$$\alpha_d(V) = \frac{0.095\,e^{-0.01(V-5)}}{e^{-0.072(V-5)}+1}, \quad \beta_d(V) = \frac{0.07\,e^{-0.017(V+44)}}{e^{0.05(V+44)}+1}, \tag{2.23d}$$

$$\alpha_f(V) = \frac{0.012\,e^{-0.008(V+28)}}{e^{0.15(V+28)}+1}, \quad \beta_f(V) = \frac{0.0065\,e^{-0.02(V+30)}}{e^{-0.2(V+30)}+1}, \tag{2.23e}$$

$$\alpha_{x1}(V) = \frac{0.0005\,e^{0.083(V+50)}}{e^{0.057(V+50)}+1}, \quad \beta_{x1}(V) = \frac{0.0013\,e^{-0.06(V+20)}}{e^{-0.04(V+20)}+1}. \tag{2.23f}$$

Parameters	Value	Units
Membrane capacitance (C_m)	1	$\mu F/cm^2$
Maximum sodium conductance ($\widetilde{g_{Na}}$)	4	mS/cm^2
Steady-state sodium conductance ($\widetilde{g_{Na_c}}$)	0.003	mS/cm^2
Sodium reversal potential (E_{Na})	50	mV
Fully activated conductance of slow inward ions ($\widetilde{g_s}$)	0.09	mS/cm^2

Table 2.2: Beeler-Reuter model constant parameters.

$$(V_0, \mathrm{Ca}_0, m_0, h_0, j_0, d_0, f_0, x_{10}) = \left(-84.624, 1.782\times10^{-7}, 0.011, 0.988, 0.975, 0.003, 0.999\right). \tag{2.24}$$

The values of the Beeler-Reuter model parameters are displayed in Table 2.2 and the solution of the model with the resting steady-state initial conditions given by (2.24) is shown in Figure 2.5. Two out of four consecutive (above-threshold) stimuli generate action potentials in the same way as Hodgkin-Huxley model. In both models, the rapid upstroke of the action potential is mainly due to the sodium current, I_{Na}. However, there are some significant differences between the two, for example their plateau shapes. The plateau shape and duration of an action potential generated by the Beeler-Reuter model highly depend on the presence of the activation of I_{x1} or the inactivation of I_s and these can be changed via alterations in the parameters. For example, the increased I_s produces a higher plateau and longer action potential. Similarly, a significant decrease in the parameter $\widetilde{g_s}$ yields an action potential similar to the Hodgkin-Huxley model.

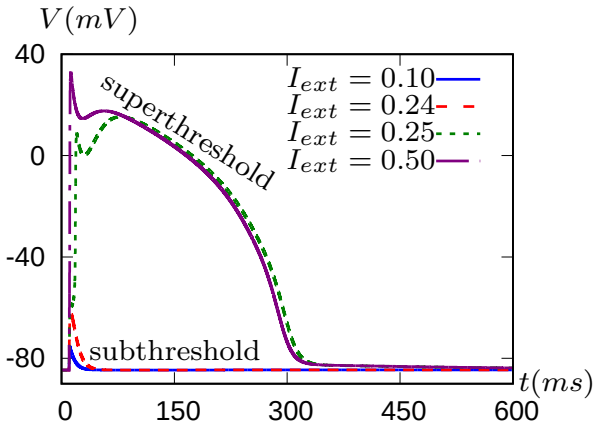

Figure 2.5: Standard Beeler-Reuter model waveform of the membrane potential with different external currents applied at $t = 10$ ms and lasting for 1 ms.

2.4 Spatially Extended Excitable Systems

In the previous section, the excitability has been formulated for a number of single-cell systems, *i.e.* in terms of ordinary differential equations (ODEs). Here, we are presenting traveling waves in excitable media by means of a diffusion term leading to the spreading excitation from one cell to another. In this thesis, our interests are restricted to models in one spatial dimension. Thus, the theory of wave propagation in excitable media is based on the following reaction-diffusion system of partial differential equations (PDEs)

$$\frac{\partial \mathbf{u}}{\partial t} = \frac{\partial}{\partial x}\left(\mathbf{D}\frac{\partial \mathbf{u}}{\partial x}\right) + \mathbf{f}(\mathbf{u}), \tag{2.25}$$

where $\mathbf{u} : \mathbb{R} \times \mathbb{R} \to \mathbb{R}^k$ is a k-component dynamic variable, $k \geq 1$, defined for $x \in \mathbb{R}$ and $t \in \mathbb{R}_+$, vector-function $\mathbf{f} : \mathbb{R}^k \to \mathbb{R}^k$ describes the nonlinear kinetics of the system and $\mathbf{D} \in \mathbb{R}^{k\times k}$ is the matrix of diffusivity. Although $\mathbf{D}$ can be a function of space, time and/or the density of the modeled species, we restrict our attention to the systems where the properties of $\mathbf{D}$ do not depend on the space and time variables.

In the late 1930's, the one-component case of equation (2.25) with particular kinetic term was first proposed by Fisher who intended to describe the propagation of advantageous genes [44] and was studied mathematically by Kolmogorov, Petrovskii and Piskunov [76] followed by Zeldovich and Frank-Kamenetsky [138] who developed a model for flame propagation in the following year.

2.4.1 Traveling Wave Solutions

Now, we present an approach called traveling wave that allows to reduce the reaction-diffusion system from PDEs to ODEs. This helps us to describe the profile of the wave under the assumption that wave propagates at a constant velocity without changing the profile. In the transformed equation, the dynamic variable gives the profile as a function of traveling wave coordinate.

From a mathematical point of view, if the solution of (2.25) can be written in the following form

$$\mathbf{u}(x,t) = \mathbf{U}(\xi,t) \qquad \xi = x - ct, \tag{2.26}$$

then $\mathbf{u}(x,t)$ is a traveling wave and it moves at a positive constant speed c in the positive x direction. Hence, (2.25) reads

$$\mathbf{U}_t = \mathbf{D}\partial_{\xi\xi}\mathbf{U} + c\partial_{\xi}\mathbf{U} + \mathbf{f}(\mathbf{U}). \tag{2.27}$$

Note that the traveling wave solution is the stationary solution of the equation (2.27), *i.e.* $\mathbf{U}_t = 0$ [97].

2.4.2 Classification of the Traveling Waves

Any stationary solution of (2.27) gives a traveling wave with a constant speed c. In particular, if the velocity $c = 0$, then the traveling wave is called the standing wave. When $c \neq 0$, consider two points P and Q such that $P > Q$. Some examples of traveling waves can be categorised in one dimension as [42, 75]:

- Periodic wave trains of wavelength L are represented by limit cycles of period L in the profile equation.
- Traveling front where $U(-\infty)$ and $U(\infty)$ exist and are different from each other:

$$\lim_{\xi\to-\infty} U(\xi) = P, \quad \lim_{\xi\to\infty} U(\xi) = Q.$$

- Traveling back satisfying the opposite condition:

$$\lim_{\xi\to-\infty} U(\xi) = Q, \quad \lim_{\xi\to\infty} U(\xi) = P.$$

- Traveling pulse where U is not a constant and $U(-\infty)$ and $U(\infty)$ exist and are the same:

$$\lim_{\xi\to\pm\infty} U(\xi) = R, \quad \text{where } R = P \text{ or } Q.$$

There also are forms in two dimensions such as $(x = (a,b), a = r\cos(\theta), b = r\sin(\theta))$

- Target patterns where $\mathbf{u}(x,t) = U(r,t)$ and U is periodic in t.

- Rotating patterns (including *e.g.* spiral waves) where $u(x,t) = U(r,\theta - ct)$ and U is periodic in the second argument.

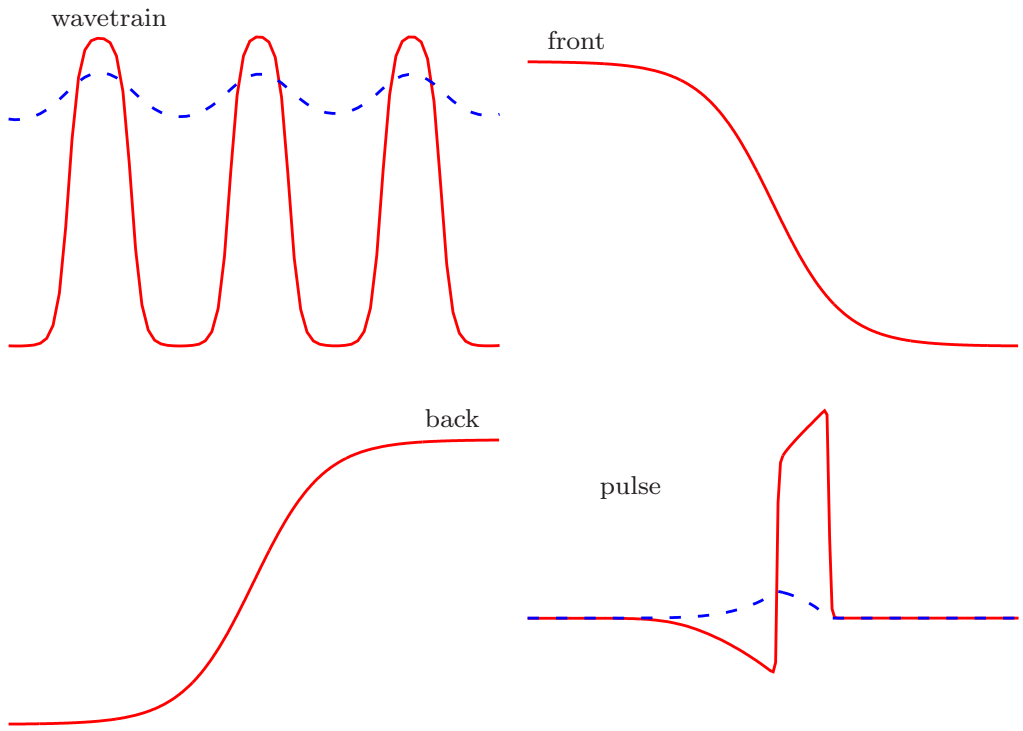

Figure 2.6: Representation of some traveling wave patterns. Solid red lines represent the membrane potential variable, while dashed blue lines are for the inactivation variable.

A front solution is always a connection between two different points as $\xi \to \pm\infty$. This connection is called a heteroclinic orbit. A pulse solution connects a single point by a loop to itself as $\xi \to \pm\infty$. These connections are called homoclinic orbits. Traveling fronts and traveling pulses are of particular importance in applications. Hence, the models with these two traveling waves are reviewed in the following section.

2.4.3 Models with Traveling Front

2.4.3.1 Zeldovich-Frank-Kamenetsky (ZFK) equation

In 1962, Nagumo *et al.* [98] who characterized the FitzHugh model as an equivalent electrical circuit proposed a mathematical model of the nerve axon as

$$\frac{\partial^3 z}{\partial t \partial x^2} = \frac{\partial^2 x}{\partial t^2} + \mu\left(1 - z + \epsilon z^2\right)\frac{\partial z}{\partial t} + z, \tag{2.28}$$

where $\mu > 0$, $0 < \epsilon < \frac{3}{16}$ and z is the normalized potential. In the following year, same authors [99] introduced a more general active transmission equation in neuron

$$\frac{\partial u}{\partial t} = \frac{\partial^2 u}{\partial x^2} - (u+1)(u-m)(u-1), \tag{2.29}$$

where $-1 < m \leq 0$. ZFK equation (also known as Nagumo's equation or Bistable equation) is a generic form of (2.29) [74, 89, 139]

$$\frac{\partial u}{\partial t} = \frac{\partial^2 u}{\partial x^2} + f(u), \tag{2.30}$$

where $f(u) = -(u-u_1)(u-u_2)(u-u_3), \quad u_1 < u_2 < u_3, \quad u_2 < (u_1+u_3)/2$ and $f(u)$ has three roots at u_1, u_2, u_3. The values $u = u_1$ and $u = u_3$ are stable steady solutions of the ordinary differential equation $\mathrm{d}u/\mathrm{d}t = f(u)$. Meanwhile, u_2 is the threshold state. The ZFK equation has the traveling front solution connecting two different steady states (heteroclinic trajectory) at each end of the domain.

Time independent solution of (2.30) is found in [101] and such solution is called critical nucleus. Specifically, (2.30) with the quadratic kinetic term, $f(u) = u(\theta - u)$ has a unique critical nucleus as

$$\hat{u}(x) \approx \frac{3\theta}{2}\mathrm{sech}^2\left(\frac{\sqrt{\theta}}{2}x\right), \tag{2.31}$$

while the critical nucleus solution for the cubic kinetic term, $f(u) = u(\theta - u)(1-u)$ can be found analytically [48, 68] [1]

$$\hat{u}(x) = \frac{3\theta\sqrt{2}}{(1+\theta)\sqrt{2} + \cosh(x\sqrt{\theta})\sqrt{2 - 5\theta + 2\theta^2}}. \tag{2.32}$$

[1] Actually, expressions given in both of these works contain typos.

2.4.3.2 McKean equation

Another one-component simplification of the FitzHugh-Nagumo system was carried out by McKean [89]. He started with the following equivalent form

$$\frac{\partial u}{\partial t} = \frac{\partial^2 u}{\partial x^2} + u(1-u)(u-a) + v, \tag{2.33a}$$

$$\frac{\partial v}{\partial t} = \beta u - \gamma v, \tag{2.33b}$$

with $0 < a < 1$, $\beta \geq 0$, $\gamma \geq 0$. McKean suggested the piecewise-linear representation of (2.33) as a simplification version as follow

$$\frac{\partial u}{\partial t} = \frac{\partial^2 u}{\partial x^2} - u + \mathrm{H}(u-a) + v, \tag{2.34a}$$

$$\frac{\partial v}{\partial t} = \beta u - \gamma v, \tag{2.34b}$$

where $\mathrm{H}(\cdot)$ is the Heaviside step function defined as

$$\mathrm{H}(w) = \begin{cases} 1, & \text{if } \ w \geq 0 \\ 0, & \text{if } \ w < 0. \end{cases}$$

It has commonly been assumed that ZFK equation with cubic kinetic term and u-component of McKean model have a similar phase plane for large values of the threshold parameters θ and a as piecewise-linear function has a similar shape to the cubic function (see Figure 2.7). Fast subsystem of (2.34) can be obtained neglecting the recovery component of the system by setting $v \equiv 0$, $\beta = 0$, and $\gamma = 0$

$$\frac{\partial u}{\partial t} = \frac{\partial^2 u}{\partial x^2} - u + \mathrm{H}(u-a). \tag{2.35}$$

Equation (2.35) is known as McKean equation and provided $0 < a < 1/2$, it has a unique critical nucleus solution found in [90] as

$$\hat{u}(x) = \begin{cases} a\mathrm{e}^{x+m}, & \text{if } \ x \leq -m, \\ 1 - \mathrm{e}^{-m}\cosh(x), & \text{if } \ x < m, \\ a\mathrm{e}^{-x+m}, & \text{if } \ x \geq m, \end{cases}$$

where $m = -\ln(1-2a)/2$. The key role of the critical nucleus will be outlined in more detail later in this chapter. The propagating front solutions of ZFK and McKean models are sketched in the left panel of Figure 2.8.

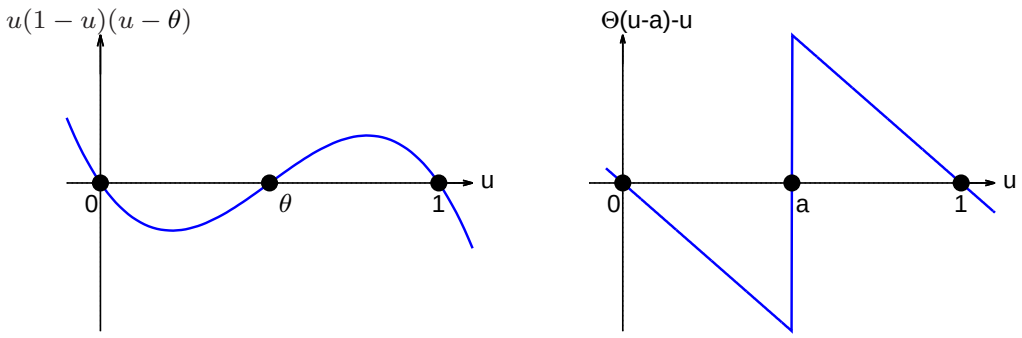

Figure 2.7: Comparison between cubic and piecewise-linear functions for same chosen parameters $\theta = a = 0.5$.

2.4.3.3 Biktashev Model

The FitzHugh-Nagumo model has been one of the most studied excitable media since the 1960s as it allows a fair amount of analytical and qualitative study. However, it has been realized that this model does not adequately produce some phenomena. Biktashev [16, 17] made the observation that the widely used FitzHugh-Nagumo model is not able to capture the propagation failure due to the dissipation of the wavefront, a phenomenon seen in more realistic models.

The construction of the Biktashev model is based on spatially extended version of the original Hodgkin-Huxley model

$$\frac{\partial E}{\partial t} = \frac{\partial^2 E}{\partial x^2} - \bar{g}_{Na}(E - E_{Na})m^3 h - \bar{g}_K(E - E_K)n^4 - g_L(E - E_L), \tag{2.36a}$$

$$\frac{\partial m}{\partial t} = \frac{m_\infty(E) - m}{\tau_m(E)}, \tag{2.36b}$$

$$\frac{\partial h}{\partial t} = \frac{h_\infty(E) - h}{\tau_h(E)}, \tag{2.36c}$$

$$\frac{\partial n}{\partial t} = \frac{n_\infty(E) - n}{\tau_n(E)}, \tag{2.36d}$$

where a diffusion term is only added into the membrane potential equation (represented in different letter E) and the membrane capacitance parameter C is fixed at the value 1. Biktashev aimed to formulate the front separately from other phases of the waves as a simplified model based on the Hodgkin-Huxley model. As the sodium current i_{Na} is more responsible for the rapid increase of the membrane potential in the front than all other ionic currents, a limit $\bar{g}_{Na} \to \infty$ was considered. Thus, the variable n is neglected while m and h which are responsible for the sodium current i_{Na} remain.

Another simplification to notice is that the values of $\tau_m(E)$ (as seen in Figure 2.3-(b)) at the front are considerably small compared to other time constants of the problem. Therefore, the differential equation for m is eliminated on account of it always being close to its quasi-stationary value $m_\infty(E)$. Thus, the remaining two equations are

$$\frac{\partial E}{\partial t} = \frac{\partial^2 E}{\partial x^2} + I_{Na}(E) m_\infty^3(E) h, \tag{2.37a}$$

$$\frac{\partial h}{\partial t} = \frac{1}{\tau_h(E)} (h_\infty(E) - h), \tag{2.37b}$$

where $I_{Na}(E) = g_{Na}(E_{Na} - E)$. This system differs from the FitzHugh-Nagumo model in that there is an assumption that the variable h is a slow variable. Here, both dynamic variables E, h are considered as fast variables. Another simplification is based on qualitative considerations where $m_\infty(E)$ and $h_\infty(E)$ are assumed to be step-like functions. Hence, they are replaced with

$$m_\infty(E) = \mathrm{H}(E - E_m) = m_\infty^3(E), \quad h_\infty(E) = \mathrm{H}(E_h - E),$$

where $\mathrm{H}(\cdot)$ is the Heaviside step function. Further simplifications can be made by replacing $\tau_h(E)$ and $I_{Na}(E)$ with constants and by suitable rescaling so that $E_h = 0$, $E_m = 1$. Hence, (2.37) finally becomes

$$\frac{\partial E}{\partial t} = \frac{\partial^2 E}{\partial x^2} + \mathrm{H}(E - 1) h, \tag{2.38a}$$

$$\frac{\partial h}{\partial t} = \frac{1}{\tau_*} (\mathrm{H}(-E) - h), \tag{2.38b}$$

where τ_* is a dimensionless parameter. In the original paper [16], this parameter was taken to be τ. However, we find it convenient to replace it by τ_* in order not to clash with the notation in the rest of this thesis, where τ is used to designate time in the moving frame of reference.

As (2.38) is a simplified model of the excitation front, one of the attractions of the Biktashev model is to have analytical solutions such as traveling wavefront. The traveling front solution of (2.38), going rightwards, is in the form

$$E(x,t) = \widetilde{E}(z), \quad h(x,t) = \widetilde{h}(z), \quad z = x - ct,$$

where $c > 0$ is the wave speed. Hence, (2.38) becomes

$$-c\widetilde{E}' = \widetilde{E}'' + \mathrm{H}\big(\widetilde{E} - 1\big)\widetilde{h}, \tag{2.39a}$$

$$-c\widetilde{h}' = \frac{1}{\tau_*} \big(\mathrm{H}(-\widetilde{E}) - \widetilde{h}\big), \tag{2.39b}$$

with the following auxiliary conditions

$$\widetilde{E}(-\infty) = \omega > 1, \quad \widetilde{E}(+\infty) = -\alpha < 0, \tag{2.40a}$$

$$\widetilde{h}(-\infty) = 0, \quad \widetilde{h}(+\infty) = 1 \tag{2.40b}$$

and the phase of the front solution is chosen such that $\widetilde{E}(0) = 0$ at $z = 0$, $\widetilde{E}(-\Delta) = 1$ at $z = -\Delta$ requiring that $\widetilde{E}(z) \in C^1$ and $\widetilde{h}(z) \in C^0$. This problem has a family of propagating front solutions depending on one parameter, the pre-front voltage α,

$$\widetilde{E}(z) = \begin{cases} \omega - \frac{\tau_*{}^2 c^2}{1+\tau_* c^2} \exp\left(-\frac{z}{\tau_* c}\right) & (z \le -\Delta), \\ -\alpha + \alpha \exp(cz) & (z \ge -\Delta), \end{cases} \tag{2.41a}$$

$$\widetilde{h}(z) = \begin{cases} \exp\left(-\frac{z}{\tau_* c}\right) & (z \le 0), \\ 1 & (z \ge 0), \end{cases} \tag{2.41b}$$

where $\omega = 1 + \tau_* c^2(\alpha + 1)$, $\Delta = \frac{1}{c}\ln\left(\frac{1+\alpha}{\alpha}\right)$ and c is an implicit function of τ_* and α,

$$\tau_* c^2 \ln\left(\frac{(1+\alpha)\left(1+\tau_* c^2\right)}{\tau_*}\right) + \ln\left(\frac{\alpha+1}{\alpha}\right) = 0. \tag{2.42}$$

Note that here the pre-front voltage α is fixed and the only parameter is τ_*. The transcendental equation (2.42) has two solutions for c if $\tau_* > \hat{\tau}_* \approx 7.674$ and it has been shown that the propagating front solution (2.41) with smaller speed value is unstable with exactly one positive eigenvalue while the solution (2.41) with bigger speed value is stable [16, 60]. The propagating front solution (2.41) is sketched in the right panel of Figure 2.8.

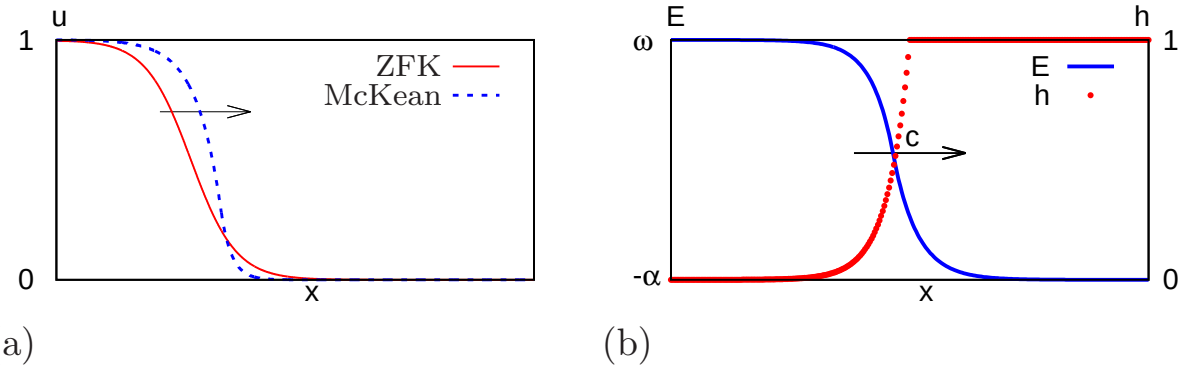

Figure 2.8: Propagating front profiles for three front models, (a) ZFK (red solid line) and McKean (blue dashed line), (b) Biktashev models.

2.4.4 Models with Traveling Pulse

2.4.4.1 Spatially extended FitzHugh-Nagumo system

There are many different forms derived from the original FitzHugh-Nagumo model that have been used as to model the cardiac/neuron dynamics. One of which (in spatially extended form) has been introduced in [101] as

$$u_t = u_{xx} + f(u) - v, \tag{2.43a}$$

$$v_t = \gamma(\alpha u - v), \tag{2.43b}$$

where $f(u)$ is cubic polynomial function in the form $f(u) = u\big(u-\beta\big)(1-u)$, the variables u and v represent respectively membrane potential and the recovery variables, γ is a small parameter describing the ratio of time scales of the variables u and v, and α is a constant. The parameter β plays a key role in the fast dynamics of the model as it is the threshold state of the system that must be in the range $(0, 1/2)$ in order for the system to have a qualitative electro-physiological meaning [84, 85].

A propagating pulse solution to equation (2.43) is a function of the single variable $\xi = x - ct$, *i.e.* $(u(\xi), v(\xi))$ that satisfies

$$-cu' = u'' + f(u) - v, \quad -cv' = \gamma(\alpha u - v), \tag{2.44}$$

where $(u, v) \to (0, 0)$ as $\xi \to \pm\infty$. There is a large volume of published studies on the FitzHugh-Nagumo model and some of them particularly need to be mentioned. For example, one study by Hastings [56] proven that the FitzHugh-Nagumo model has two propagating pulse solutions with different values of speed c such that when $c = c_s$, the solution is called slow pulse solution and when $c = c_f$, the solution is called the fast pulse solution with $0 < c_s < c_f$. Yet another major study based on the significance of small γ reviewed singular perturbation theory analysis of the FitzHugh-Nagumo model where the propagating pulse solution can be derived by piecing together solutions of certain reduced systems [27]. In addition, there are many other studies about the stability of the propagating pulse solution stating that the slow pulse solution is unstable and fast pulse is stable (see, for example [26, 27, 38, 56, 69]).

2.4.4.2 Spatially extended Beeler-Reuter model

Generally speaking, the analysis of models with several variables is much more complicated than the fever variables models. The original Beeler-Reuter model has 8 vari-

ables, with widely different time scales. The membrane potential equation of the spatially extended Beeler-Reuter model is in the form

$$V_t = D\nabla^2 V + I_T,$$

where D is the diffusion constant and I_T is the instantaneous total ionic current

$$I_T = -I_{K_1}(V) - I_{x1}(V, x_1) - I_{Na}(V, h, j) - I_s(V, d, f, \mathrm{Ca}).$$

Other 7 other variables' equations and the values for the rate constants are held same as described in Subsection 2.3.3. Several attempts have been made to obtain the propagating pulse solution of the spatially extended Beeler-Reuter model, see for example [31, 125]. One popular approach is to calculate conduction velocity restitution curve that splits into two branches, one for the stable pulse velocity and one for the unstable pulse velocity.

2.5 Mathematical Approaches to Initiation Problem

2.5.1 An Introduction the Initiation Problem

In this section, we will look at the literature investigating the behaviour of the solutions of the nonlinear reaction-diffusion equation

$$\frac{\partial \mathbf{u}}{\partial t} = \mathbf{D}\frac{\partial^2 \mathbf{u}}{\partial x^2} + \mathbf{f}(\mathbf{u}), \quad t > 0. \tag{2.45}$$

We start by specifying the perturbation of the initial and boundary conditions in the following form

$$\mathbf{u}(x,0) = \mathbf{u}_0(x) = \mathbf{u}_r + U_{\mathrm{s}}\mathrm{H}(x_{\mathrm{s}} - x)\mathbf{e}, \quad \mathbf{D}\mathbf{u}_x(0,t) = -\mathbf{I}_{\mathrm{s}}(t) = -I_{\mathrm{s}}\mathrm{H}(t_{\mathrm{s}} - t)\mathbf{e}, \tag{2.46}$$

where $\mathbf{u}_r$ is the resting state, x_{s} is the spatial extent, U_{s} is the stimulus amplitude, I_{s} is the strength of the current lasting for time duration t_{s}, $\mathrm{H}(\cdot)$ is the Heaviside step function and $\mathbf{e}$ determines which reagents are being injected.

For convenience and brevity, the above notation will be adopted for all articles referred even though the problem itself is different in some mentioned papers.

2.5.2 A Brief History of the Mathematical Approaches

In the following, we state some of the crucial literature according to the publication date:

Weiss(1901): There have been several experimentally tested theoretical models addressing the relationship between the minimum stimulus amplitude required to excite an axon and the duration for which the stimulus is applied even well before the development of intracellular and voltage-clamp techniques. The study of the charge-duration relation was first carried out by Weiss [135] who experimentally derived the following linear equation

$$Q = a + bt_{\mathrm{s}}, \tag{2.47}$$

where Q is the threshold charge, a and b are unknown constants. In his original formula, Weiss did not interpret the constants a and b physically and hence they were later on replaced by the rheobasic current multiplied by the chronaxie, $I_{rh} \times \tau$ and the the rheobasic current, I_{rh} [24] so (2.47) becomes

$$Q = I_{rh}(\tau + t_{\mathrm{s}}), \tag{2.48}$$

which is known as the Weiss excitation law for the charge. In neuroscience, the rheobasic current refers to the minimal current amplitude of indefinite duration required to evoke an action potential and the chronaxie is a duration measurement for electrical stimulation related to the time constant of the cell membrane [109, 136].

Lapicque(1907): Another empirical equation was developed by Lapicque [79] (see also its translated version [25]) who reiterated Weiss's equation in a different form for which the relation between the pulse strength and duration was instead formulated. This relation is named as strength-duration curve. Lapicque observed that the strength of the current I_{s} required to stimulate an action potential increased as the duration t_{s} was decreased. Hence, he proposed the following current law for excitation

$$I_{\mathrm{s}} = I_{rh}\left(1 + \frac{\tau}{t_{\mathrm{s}}}\right). \tag{2.49}$$

As previously pointed out that the rheobase current, I_{rh} may be defined as the minimal current amplitude of infinite duration for which threshold can be reached and also note that the chronaxie time of the cell, τ refers to the value of the pulse duration t_{s} at twice the rheobase current. Another important relation is the one between the charge, Q and the stimulus strength, I_{s} represented by $Q = I_{\mathrm{s}}t_{\mathrm{s}}$ and hence Weiss

excitation law for the charge (2.48) actually reduces to the Lapicque current law for excitation (2.49). These two empirical laws are two different ways aiming to express the requirement for excitation.

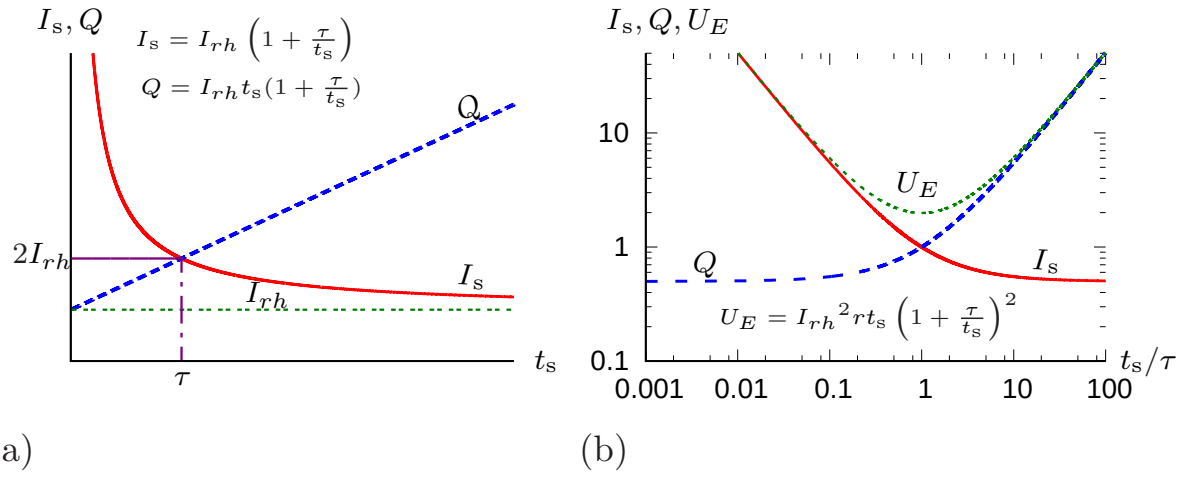

Figure 2.9: (a) Lapicque hyperbolic strength-duration curve for current I_s and the Weiss linear strength-duration relationship for charge Q. (b) Universal strength-duration curves in the logarithmic form, for current, energy and charge, with the duration axis divided by the chronaxie [52].

The sketch of the Lapicque hyperbolic strength-duration curve and the Weiss linear charge-duration relationship is shown in Figure 2.9. Another electrical parameter that is used to describe a stimulus is energy, the minimum of which is located at pulse duration equal to the chronaxie. It is also plotted in the right panel of Figure 2.9 for illustration purposes only.

Blair(1932): An alternative expression for threshold stimulating current was based on the realization that the nerve cell membrane could be represented by a parallel resistance R and capacitance C. In 1932, Blair [20, 21] published a purely phenomenological method relying on an RC network to formulate the strength-duration curve. He proposed the following exponential function for the current required to stimulate the nerve

$$I_s = \frac{I_{rh}}{1 - \exp(-t_s/\tau)}. \tag{2.50}$$

In view of all models that have been mentioned so far, Blair's formula is closely related to that of Lapicque (2.49) and to Weiss's law (2.48), and they all nearly fit the same data [20].

Rashevsky(1933), Monnier(1934) and Hill(1936): Blair's model has a number of at-

tractive features and to give two of them: fairly accurately fit experimental outcomes and mathematically simple descriptive approach for the strength-duration curve. Thus, a number of researchers began to focus on it, among which three important ones are Rashevsky, Monnier and Hill [58, 94, 108]. They developed a "two-factor" mathematical model of excitation and inhibition (the two extended Blair's model). The equations they considered are equivalent and so are their results. Based on the literature observed, higher priority has been given to Hill's article, and therefore we use his notation.

Hill examined the relationship among the stimulus, the excitability of the tissue, and its accommodation, where the term "accommodation" [100] is used to describe the membrane potential response to a sufficiently slow increase in the stimulating current without exciting. This phenomenon of accommodation resulted in Hill's two time-constant model

$$I_{\mathrm{s}} = \frac{I_{rh}\,(1-\kappa/\lambda)}{\exp(-t_{\mathrm{s}}/\lambda)-\exp(-t_{\mathrm{s}}/\kappa)}, \tag{2.51}$$

where κ, λ are the time constant of excitation and the time constant of accommodation, respectively. The constants κ and λ satisfy $\lambda \gg \kappa$ and in particular when $\lambda/\kappa \to \infty$, Hill's equation (2.51) reduces to Blair's equation (2.50).

All above approaches are basically experimental and the parameters of the equations can be measured and calculated through some data fitting algorithms such as Levenberg-Marquardt method, one of the most used iterative procedure that will be explained in the following section.

Rushton(1937): Study of spatially extended excitable media goes as far back as 1937, when Rushton [115] first introduced a concept of the "liminal length". This concept is based on very impressive result that the ability of a stimulus to initiate a wave depends also on its spatial extent. We can exemplify this in one of the model we consider, *i.e.* Zeldovich-Frank-Kamenetsky equation. As pointed out earlier, the kinetic term in (2.30) is a cubic polynomial with two of its three zeros are stable and the other (its middle zero) is unstable. For any initial condition with the stimulus amplitude above the unstable zero, the solution initiates the propagation wavefront and it tends to its smaller stable zero otherwise [126].

Noble and Stein(1966): One of most noticeable features of the strength-duration curve is that the threshold reduces when the time duration increases. Based on simplification of the Hodgkin-Huxley membrane equations, Noble and Stein [104] explored the influence of the membrane activation time and accommodation on the strength-

duration curve. They also deduced that the strength-duration curve time constant is highly dependent on the geometry of the stimulus.

Aronson and Weinberger(1975): There have been a lot of works on the semi-linear diffusion equation after the publication of the classical papers by Fisher [44] , Kolmogorov, Petrovski and Piskunov [76] (both in the year 1937), and Zeldovich and Frank-Kamenetsky [139] (in 1938)

$$\frac{\partial u}{\partial t} = \frac{\partial^2 u}{\partial x^2} + f(u), \tag{2.52}$$

where $f(u)$ is the continuous nonlinear function allowed to have various qualitative behaviour. Aronson and Weinberger [3] systematically investigated the behaviour of the solution of (2.52) as $t \to \infty$. They pointed out that the solution of (2.52) converges to a traveling wave under some assumptions on the function f and the initial condition $u(x,0)$. For example, they introduced "heterozygote inferior" case with the following feature of f

$$f \in C^1[0,1], \quad f(0) = f(1) = 0, \quad f'(0) < 0, \quad f(u) < 0 \text{ in } (0,a), \tag{2.53a}$$

$$f(u) > 0 \text{ in } (a,1) \text{ for some } a \in (0,1), \quad \int_0^1 f(u)\,\mathrm{d}u > 0, \tag{2.53b}$$

where the equilibrium states $u = 0$ and $u = 1$ are stable while $u = a$ is unstable. It is pointed out for this case that if $u(x,0) \in [0,a)$, then $\lim_{t\to\infty} u(x,t) = 0$ and that if the initial distribution $u(x,0) \in [a,1]$ for every x, then $\lim_{t\to\infty} u(x,t) = 1$ uniformly on $\mathbb{R}$. Consequently, this case exhibits a threshold phenomenon. Subsequent well-known work by ***Fife and McLeod*** [43] proved the existence, uniqueness, and stability for traveling front solutions to the equation (2.52) in the case

$$f(0) = f(1) = 0, \quad f'(0) < 0, \quad f'(1) < 0. \tag{2.54}$$

McKean and Moll(1986): Another systematic study of (2.52) was reported by McKean and Moll [90] who studied equation (2.52) with the kinetic term specified as a piecewise-linear function introduced first by McKean [89], $f(u) = -u + \mathrm{H}(u-a)$ provided that $a < 1/2$. This study set out with the aim of investigating the asymptotic behaviour of the solution as $t \to \infty$ and made a noteworthy contribution to the previous understanding of the asymptotic behaviour of the solution. They demonstrated that there exists a threshold surface in the space of initial data that separates collapsing solutions (subthreshold case) from expanding ones (superthreshold case).

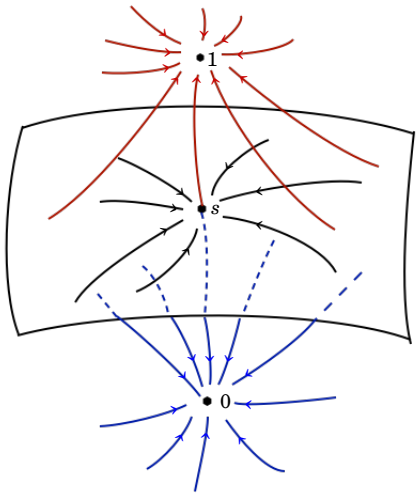

Figure 2.10: Illustration of the threshold surface separating initial conditions tending to the equilibrium value 0 (blue lines) from those leading to the excited value 1 (red lines). The initial conditions on the critical surface (black lines) tend towards a saddle point designated by s. This figure is adapted from [90].

There is another important insight from this study: apart from these two resting and excited state solutions, there is a unique, nontrivial, time-independent solution on the threshold surface that satisfies,

$$\frac{\partial^2 \hat{u}}{\partial x^2} + f(\hat{u}) = 0. \tag{2.55}$$

This unstable solution is known as the critical nucleus (or standing wave) and it separates the set of initial conditions leading to the excited state, from the set of initial conditions evolving towards its resting state. Hence, it acts as a threshold separating two outcomes and is a saddle of codimension one. Figure 2.10 illustrates this threshold surface.

In the following years, ***Flores*** [48, 49] who studied (2.52) for $f(u) = u(1-u)(u-a)$ used Sturm's theorem to prove that the linearization spectrum of the equation around the critical nucleus has exactly one positive eigenvalue, while all other eigenvalues are negative.

Moll and Rosencrans(1990): After the observation of the existence of a threshold surface introduced by McKean and Moll [90], a number of researchers showed an increased interest in determining such threshold surface. In another major study, Moll and Rosencrans [93] tried to trace this threshold surface numerically. They chose rectangular pulse initial condition lying on the surface and analysed if the resulting

solution would either decay to the resting state 0 or expand into a propagation wave. If the eventual solution is a decay solution, they increased the amplitude of the initial condition and decreased it otherwise. By repeating the procedure, they eventually obtained the threshold surface as a relation between the amplitude and the width of the initial pulse.

Neu et al.(1996): One of the analytical approaches to the initiation problem is based on the method of projected dynamics, introduced by Neu, Preissig and Krassowska [101] in 1996. They proposed that the equation (2.52) can be written as the gradient flow of an energy functional

$$\frac{\partial u}{\partial t} = -\frac{\delta E(u)}{\delta u}, \tag{2.56}$$

where E is energy and $\delta E/\delta u$ is the variational derivative. For potential $u(x,t)$ with $u(x,t) \to 0$ as $x \to \infty$, energy can be defined as

$$E(u) = \int_{-\infty}^{\infty} \left(\frac{u_x^2}{2} + F(u) \right) \mathrm{d}x, \tag{2.57}$$

where $F(u) = -\int f\left(u'\right) \mathrm{d}u'$. The potential $u(x,t)$ can be parametrized in the form $u(x,t) = U(x, a(t))$ where $a(t) = a_1(t), \cdots, a_N(t)$ is a time-dependent vector of parameter. If the exact solution is in this from, then (2.56) gives a system of ordinary differential equations of the form

$$\mathbf{M} \frac{\mathrm{d}a}{\mathrm{d}t} = -\nabla E, \tag{2.58}$$

where $\nabla_i = \partial/\partial a_i$ and $\mathbf{M}$ is an $N \times N$ symmetric matrix whose components are given by

$$m_{ij} = \int_{-\infty}^{\infty} \frac{\partial U}{\partial a_i} \frac{\partial U}{\partial a_j} \mathrm{d}x. \tag{2.59}$$

They then specifically chose the Gaussian pulse with time-dependent parameters for the amplitude $a(t)$ and the pulse width $1/k(t)$ [2]

$$U(x,t) = a(t) \mathrm{e}^{-(k(t)x)^2}. \tag{2.60}$$

Inserting the Gaussian representation of u (2.60) into the projected dynamics (2.58) yields a pair of ordinary differential equations

$$\dot{a} = -a\left(2k^2 + 1 - pa\right), \tag{2.61a}$$

$$\dot{k} = -k\left(2k^2 - qa\right), \tag{2.61b}$$

[2] though not every equation can be written in this form.

where p and q are constants

$$p = \frac{7\sqrt{6}}{18} \approx 0.9526, \quad q = \frac{\sqrt{6}}{9} \approx 0.2722. \tag{2.62}$$

The phase plane for the projected dynamics (2.61) has resting state at $(0,0)$ and critical nucleus at $(1.47, 0.447)$. The stable manifolds of the critical nucleus divide the phase plane into two regions: non-excitable and excitable. The non-excitable region corresponds to the initial conditions that fail to start the propagation of excitation while the excitable region refers to the initial conditions that succeed in starting the propagation.

Idris and Biktashev(2008): As emphasized previously, the stable manifold of the critical nucleus is the threshold surface separating initial conditions leading to initiation of propagation and to decay. Idris and Biktashev [68] showed that approximation of this manifold by its tangent linear space yields an analytical criterion of initiation. They considered the linearization of (2.52) near the critical nucleus and obtained analytical expressions for both strength-duration and strength-extent curves.

2.6 Review of Some Essential Numerical Methods

Numerical methods are necessary to study the initiation problem since analytical results are not always possible to obtain explicitly. Even when analytical solutions are feasible it can be convenient to validate and estimate their accuracy by means of some numerical procedure. In this section, we will present a brief introduction to finite difference and finite element methods for simulation of the initiation problem and some numerical methods for the computation of the ingredients of the analytical solution to the problem. Eigenvalues and eigenfunctions play an important part in formulating the analytical solution to the initiation problem. Any discretized version of the linear differential operator can be written in a matrix form so that the eigenpairs of the system become the eigenpairs of such discrete matrix. There exist several iterative methods for finding eigenpairs, two of which will be outlined in this section: power iteration and Arnoldi methods. Least-squares fitting is a common technique to find the best fitting curve. One of the most widely used iterative estimation technique is Levenberg-Marquardt method, and thus it will also require to be mentioned. Finally, we will introduce Piecewise Cubic Hermite Interpolating Polynomial (PCHIP) method, a method for interpolation scattered data to obtain a smooth continuous set of data.

2.6.1 Finite Difference Method

One of the simplest and of the oldest methods to solve (partial) differential equations is the finite difference methods. The main idea is to replace the derivatives in the equations by their finite difference approximations. This converts the main equations into a system of algebraic equations, which can be conveniently implemented in various computational programming languages and packages (C, Maple, Matlab, Mathematica, *etc.*).

In all cases, for simulation of time-dependent problems, we discretize the problems on a regular space grid on a finite interval $x \in [0, L]$ as an approximation of $x \in [0, \infty)$, with fixed space step Δ_x and a regular time grid with time step Δ_t. We first introduce a rectangular mesh or grid consisting of points (t_n, x_i) with

$$0 = t_0 < t_1 < t_2, \cdots, \quad 0 = x_1 < x_2 < \cdots < x_N = L \tag{2.63}$$

so that

$$x_i = (i-1)\Delta_x, \quad t_n = n\Delta_t, \quad i = 1, \ldots, N \quad n = 0, \ldots. \tag{2.64}$$

The grid function $\hat{\mathbf{u}}_i^n$ denotes the numerical approximation, of $\mathbf{u}(x_i, t_n)$

$$\hat{\mathbf{u}}_i^n \approx \mathbf{u}(x_i, t_n).$$

Approximate time derivative with the explicit Euler forward difference is

$$\frac{\partial \hat{\mathbf{u}}_i^n}{\partial t} = \frac{\hat{\mathbf{u}}_i^{n+1} - \hat{\mathbf{u}}_i^n}{\Delta_t} + \mathcal{O}(\Delta_t). \tag{2.65}$$

Except where stated otherwise, we use explicit second-order central difference approximations in space for the diffusion term

$$\frac{\partial^2 \hat{\mathbf{u}}_i^n}{\partial x^2} = \frac{\hat{\mathbf{u}}_{i+1}^n - 2\hat{\mathbf{u}}_i^n + \hat{\mathbf{u}}_{i-1}^n}{{\Delta_x}^2} + \mathcal{O}\left({\Delta_x}^2\right). \tag{2.66}$$

Hence, the discretization formula for (2.45) is

$$\hat{\mathbf{u}}_i^{n+1} = \hat{\mathbf{u}}_i^n + \mathbf{D}\Delta_t \left(\frac{\hat{\mathbf{u}}_{i+1}^n - 2\hat{\mathbf{u}}_i^n + \hat{\mathbf{u}}_{i-1}^n}{{\Delta_x}^2} \right) + \Delta_t \mathbf{f}\left(\hat{\mathbf{u}}_i^n\right). \tag{2.67}$$

Notice that the approximate time and space discretizations have errors of size $\mathcal{O}(\Delta_t)$ and $\mathcal{O}\left({\Delta_x}^2\right)$, respectively. Hence, approximate solution (2.67) has an associated error of

$$\Delta\hat{\mathbf{u}} = \mathcal{O}(\Delta_t) + \mathcal{O}\left({\Delta_x}^2\right).$$

The proposed finite difference approximation scheme is said to be consistent if this error goes to zero as $\Delta_x \to 0$ and $\Delta_t \to 0$. According to the von Neumann stability analysis (which is detailed in *e.g.* [127]), this numerical scheme is stable if

$$\frac{\max(\mathbf{D})\Delta_t}{{\Delta_x}^2} < \frac{1}{2},$$

where $\max(\mathbf{D})$ is the maximum value of the elements of $\mathbf{D}$.

2.6.2 Finite Element Method

Another widely used numerical technique for finding the approximate solution to the (partial) differential equations is the finite element method (FEM), also known as finite element analysis (FEA). The main concept of the FEM is to subdivide the mathematical model into smaller components of simple geometry called finite elements. To summarise in general terms how the FEM works, we shall study the method for the approximate solution of the initiation problem (2.45). For simplicity, here we consider one-component case so that the diffusion term of which component becomes scalar, *i.e.* $\hat{D} = \mathbf{D}(m,m)$ for $m-th$ component, and repeat the same procedure for any other remaining component equation in the system.

First of all, as in the finite difference method, the finite interval domain $x \in [0,L]$ is to be used as an approximation of $x \in [0,\infty)$. We then divide this domain into smaller regions such that $0 = x_1 < x_2 < \cdots < x_N = L$ where the constant mesh spacing is assumed, *i.e.* $\Delta_x = L/(N-1)$. Next, we construct suitable basis (also known as trial or shape) functions $\Phi_j(x)$ with $j = 1,\cdots,N$. There are a number of choices available for the type of basis function. For example, nodal kind of basis function satisfies

$$\Phi_j(x_i) = \begin{cases} 1, & \text{if} \quad i = j, \\ 0, & \text{if} \quad i \neq j, \end{cases}$$

where $i,j = 1,2,\cdots,N$. We then multiply one-component case of equation (2.45) with an arbitrary test function $V(x)$ so that integrating the resulting expression over the domain leads to

$$\int_0^L \left\{ \frac{\partial \hat{u}}{\partial t} - \hat{D}\frac{\partial^2 \hat{u}}{\partial x^2} - f(\hat{u}) \right\} V(x)\, \mathrm{d}x = 0, \tag{2.68}$$

which is known as the weak formulation (or variational form) [124, 128]. Using homogeneous Neumann (no-flux) boundary condition, this further simplifies to

$$(\hat{u}_t, V) + \hat{D}(\nabla \hat{u}, \nabla V) = (f, V), \tag{2.69}$$

where $(a,b) = \int_0^L \overline{a}^\top b \, \mathrm{d}x$. An approximate solution is expressed as a linear combination of the basis functions

$$\hat{u}(x,t) = \sum_{j=1}^{N} \alpha_j(t)\Phi_j(x), \tag{2.70}$$

where $\alpha_j(t)$ are unknown coefficients yet to be determined by minimising the error between the exact and the approximate solutions. Substituting the ansatz (2.70) into the equation (2.69) yields

$$\sum_{j=1}^{N} \alpha_j'(t)\left(\Phi_j, V_i\right) + \hat{D}\sum_{j=1}^{N} \alpha_j(t)\left(\nabla\Phi_j, \nabla V_i\right) = (f, V_i).$$

In the Galerkin finite element method, the test function is the same as the basis function [30], *i.e.* $V_i = \Phi_i$, $i = 1,2,\ldots,N$

$$\sum_{j=1}^{N} \alpha_j'(t)\left(\Phi_j, \Phi_i\right) + \hat{D}\sum_{j=1}^{N} \alpha_j(t)\left(\nabla\Phi_j, \nabla\Phi_i\right) = (f, \Phi_i). \tag{2.71}$$

Since $\Phi_j\left(x_j\right) = 1$ and $\Phi_j(x_i) = 0$ for all $j \neq i$, the expansion coefficients α can be replaced with approximate solution $\hat{u}$. Thus, (2.71) can be written in a matrix form as

$$\mathbf{A}\frac{\mathrm{d}\hat{u}}{\mathrm{d}t} + \hat{D}\mathbf{B}\hat{u} = \mathbf{F}(\hat{u}), \tag{2.72}$$

where $\mathbf{A} = \left(A_{i,j}\right)$ is known as the mass matrix with entries $A_{i,j} = \left(\Phi_i, \Phi_j\right)$, $\mathbf{B} = \left(B_{i,j}\right)$ is known as the stiffness matrix with entries $B_{i,j} = \left(\nabla\Phi_i, \nabla\Phi_j\right)$ and $\mathbf{F}(\hat{u}) = (f(\hat{u}), \Phi_i)$. An explicit piecewise linear representation of the basis functions is given by

$$\Phi_j(x) = \frac{1}{\Delta_x}\begin{cases} x - x_{i-1}, & x \in [x_{i-1}, x_i], \\ x_{i+1} - x, & x \in [x_i, x_{i+1}], \\ 0, & \text{otherwise}, \end{cases}$$

and its derivative is

$$\Phi_j'(x) = \frac{1}{\Delta_x}\begin{cases} 1, & x \in [x_{i-1}, x_i], \\ -1, & x \in [x_i, x_{i+1}], \\ 0, & \text{otherwise}. \end{cases}$$

This basis function is shown in Figure 2.11. For the given basis function, the elements

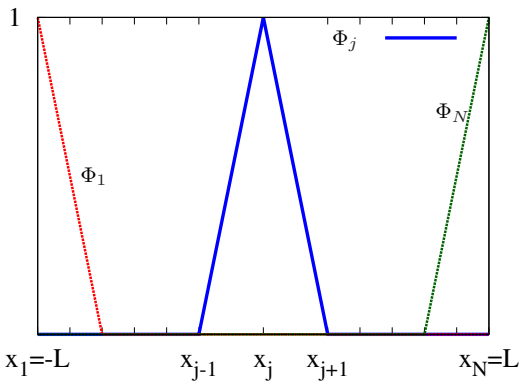

Figure 2.11: An illustration of the basis function.

of the mass matrix $\mathbf{A} = [a_{i,j}]$ can be calculated as

$$\mathbf{A} = \frac{\Delta_x}{6}\begin{pmatrix} 2 & 1 & 0 & \cdots & 0 \\ 1 & 4 & 1 & & \vdots \\ 0 & \ddots & \ddots & \ddots & 0 \\ \vdots & & 1 & 4 & 1 \\ 0 & \cdots & 0 & 1 & 2 \end{pmatrix}, \tag{2.73}$$

while the elements of the stiffness matrix $\mathbf{B} = [b_{i,j}]$ are

$$\mathbf{B} = \frac{1}{\Delta_x}\begin{pmatrix} 1 & -1 & 0 & \cdots & 0 \\ -1 & 2 & -1 & & \vdots \\ 0 & \ddots & \ddots & \ddots & 0 \\ \vdots & & -1 & 2 & -1 \\ 0 & \cdots & 0 & -1 & 1 \end{pmatrix}. \tag{2.74}$$

In the finite difference formulation, the time derivative is expressed in forward Euler form. However, here we employ the generalized trapezoidal rule (also known as θ-scheme) [110], in which the residual is evaluated at $n+\theta$, with this notation implying

$$\hat{\mathbf{u}}^{n+\theta} = \theta\hat{\mathbf{u}}^{n+1} + (1-\theta)\hat{\mathbf{u}}^{n}, \tag{2.75}$$

where $0 \leq \theta \leq 1$ is a real parameter. Based on the above, the fully discrete problem (2.72) becomes

$$\left[\mathbf{A} + \Delta_t\theta\hat{D}\mathbf{B}\right]\hat{\mathbf{u}}^{n+1} = \mathbf{F}\left(\hat{u}^{n+\theta}\right) + \left[\mathbf{A} - \Delta_t(1-\theta)\hat{D}\mathbf{B}\right]\hat{\mathbf{u}}^{n}. \tag{2.76}$$

For this scheme, the stability condition and error analysis are dependent upon the choice of the parameter θ. In scheme (2.76), $\theta = 0$ gives the explicit Euler method with truncation error proportional to $\mathcal{O}(\Delta_t) + \mathcal{O}\left({\Delta_x}^2\right)$, $\theta = 1/2$ gives the second-order neutrally stable Crank-Nicolson method with truncation error proportional to $\mathcal{O}\left({\Delta_t}^2\right) + \mathcal{O}\left({\Delta_x}^2\right)$, and $\theta = 1$ gives the first-order accurate implicit Euler rule that is unconditionally stable with truncation error proportional to $\mathcal{O}(\Delta_t) + \mathcal{O}\left({\Delta_x}^2\right)$ [23].

2.6.3 Power Iteration

The power iteration method (also known as the Von Mises iteration [91]) is very good at approximating the largest eigenvalue in the magnitude of a given diagonalisable matrix $\mathbf{A} \in \mathbb{C}^{n \times n}$ as well as its associated eigenvector. Recall that if λ and q are respectively eigenvalue and eigenvector for the matrix $\mathbf{A}$, then $\mathbf{A}q = \lambda q$. The power iteration method is motivated by this definition. Given any arbitrary vector of unit Euclidean norm as an initial approximation of the dominant eigenvector corresponding to the eigenvalue of largest magnitude, the power iteration method can then be computed via the following iterative procedure:

Input: Any given diagonalisable matrix $\mathbf{A} \in \mathbb{C}^{n \times n}$, a user-defined small parameter $\mathrm{tolerance}$ and an arbitrary initial vector $\mathbf{b} \in \mathbb{C}^n$
Output: The dominant eigenvalue and corresponding eigenvector of $\mathbf{A}$
Set: $\boldsymbol{q_1} = \boldsymbol{b}/\|\boldsymbol{b}\|_2$;
for $n = 1, 2, 3 \ldots$ **do**
  $\boldsymbol{v} = \mathbf{A}\boldsymbol{q_n}$;
  $\boldsymbol{q_{n+1}} = \boldsymbol{v}/\|\boldsymbol{v}\|_2$;
  $\boldsymbol{\lambda_{n+1}} = \boldsymbol{q_{n+1}}^{\top}\mathbf{A}\boldsymbol{q_{n+1}}$;
  if $\|\boldsymbol{q_{n+1}} - \boldsymbol{q_n}\|_2 < \mathrm{tolerance}$ **then**
    break
  end
end

Algorithm 1: The power method computation of the first eigenpair.

In the algorithm above, the eigenvector is normalized at each iteration so that it gets closer to the desired eigenvector. The power iteration method can be terminated

whenever the convergence criterion is met, *i.e.* the change in the eigenvector (or eigenvalue) is negligibly small. Note that the algorithm can be of interest when the matrix $\mathbf{A}$ is large and sparse and when there is a sufficient gap between the first two largest eigenvalues in magnitude [54]. The main advantage of this method is a faster convergence, especially when these two eigenvalues are distinct. However, the method also has some major drawbacks, like returning only an estimate of one eigenvector with the eigenvalue of largest magnitude.

2.6.4 Arnoldi Iteration

The power iteration method will only converge to a single eigenvalue of a given matrix $\mathbf{A}$. However, in many cases, it is likely that a small subset of the spectrum of a large-scale matrix is to be sought. There are several approaches to computing a small number of eigenvalues of such large matrix and one of the best-known approaches is the Arnoldi method.

In 1951, Arnoldi [2] described an algorithm to provide a relatively good approximation to some eigenvalues after a relatively small number of iterations. It was later discovered that his algorithm can indeed lead to an efficient technique for approximating eigenvalues of large sparse matrices. In the following, a general description of the Arnoldi method and one of its variations will be presented.

Basic Arnoldi Iteration

The basic idea of the Arnoldi algorithm is grounded on projecting a given matrix $\mathbf{A} \in \mathbb{C}^{n\times n}$ onto a properly chosen low-dimensional subspace, and then solving a rather small eigenvalue problem performing QR algorithm, an approach to compute the eigenvalues and eigenvectors of a given matrix developed by Francis [51]. The Arnoldi method [2, 116, 137] is an orthogonal projection method onto the k^{th} order Krylov subspace,

$$\mathcal{K}_k = \operatorname{span}\left\{q, \mathbf{A}q, \cdots, \mathbf{A}^{k-1}q\right\}, \tag{2.77}$$

where q can be any starting normalized vector in $\mathbb{C}^n$. For such given matrix $\mathbf{A} \in \mathbb{C}^{n\times n}$, QR factorization is defined as a decomposition of the form $\mathbf{A} = \mathbf{QR}$ where $\mathbf{Q} \in \mathbb{C}^{n\times n}$ is an orthogonal matrix and $\mathbf{R} \in \mathbb{C}^{n\times n}$ is an upper triangular matrix. However, the QR factorization of matrix $\mathbf{A}\mathcal{K}_k$ is unstable and thus, instead of using this subspace, the Arnoldi iteration derives the (stabilized) Gram-Schmidt procedure to produce an

orthonormal basis of the Krylov subspace,

$$\mathcal{K}_k = \text{span}\{q_1, q_2, \cdots, q_k\}. \tag{2.78}$$

Let $\mathbf{Q}_k$ be the $n \times k$ matrix formed by the Arnoldi vectors $q_1, q_2, \cdots, q_k$, each of which is constructed from the previous Arnoldi vectors except q_1, arbitrarily chosen normalized vector (see Algorithm 2 for the exact procedure). Then, $k-$step Arnoldi factorization is of the form,

$$\mathbf{A}\mathbf{Q}_k = \mathbf{Q}_k \mathbf{H}_k + h_{k+1,k} q_{k+1} \mathbf{e}_k^\top, \tag{2.79}$$

or equivalently

$$\mathbf{A}\mathbf{Q}_k = \mathbf{Q}_{k+1} \bar{\mathbf{H}}_k, \tag{2.80}$$

where $\mathbf{H}_k \in \mathbb{C}^{(k)\times k}$ and $\bar{\mathbf{H}}_k \in \mathbb{C}^{(k+1)\times k}$ are upper Hessenberg matrices, $\mathbf{Q}_{k+1} \in \mathbb{C}^{n\times(k+1)}$, and $\mathbf{e}_k = (0, 0, \cdots, 1)^\top$. Note that the matrices $\mathbf{Q}_k$, $\mathbf{H}_k$, $\mathbf{Q}_{k+1}$ and $\bar{\mathbf{H}}_k$ are uniquely determined by the first column of $\mathbf{Q}_k$, an arbitrary normalized initial vector q_1. The Arnoldi iteration can be essentially viewed in the following algorithm:

Input: Any given diagonalisable matrix $\mathbf{A} \in \mathbb{C}^{n\times n}$, a user-defined small parameter tolerance and an arbitrary initial vector $\mathbf{b} \in \mathbb{C}^n$
Output: Upper Hessenberg matrix and a set of $n+1$ orthonormal vectors
Set: $\boldsymbol{q_1} = \boldsymbol{b}/\|(\boldsymbol{b})\|_2$;
for $n = 1, 2, 3 \ldots$ *k* **do**
  $\boldsymbol{v} = \boldsymbol{A q_n}$;
  for *j=1:n* **do**
    $h_{jn} = \boldsymbol{v}^\top \boldsymbol{q_j}$;
    $\boldsymbol{v} = \boldsymbol{v} - h_{jn} \boldsymbol{q_j}$;
  end
  $h_{(n+1)n} = \|(\boldsymbol{v})\|_2$;
  if $h_{(n+1)n} < \text{tolerance}$ **then**
    break
  end
  $\boldsymbol{q_{n+1}} = \boldsymbol{v}/h_{(n+1)n}$;
end

Algorithm 2: Basic Arnoldi iteration method.

Note that the above procedure will stop if $h_{(n+1)n} < \text{tolerance}$ for some n and tolerance, a small parameter typically chosen to be equal to the machine precision. The advantage of this algorithm is that the matrix $\mathbf{H}_k$ has a modest number of nonzero

entries and it represents the orthogonal projection of $\mathbf{A}$ onto the Krylov subspace. The eigenvalues and eigenvectors of $\mathbf{H}_m$ can be computed efficiently using, for instance, the QR algorithm. The eigenvalues of $\mathbf{H}_k$ are called Ritz values and provide a good approximation for the eigenvalues of $\mathbf{A}$. Also, the Ritz eigenvector, $\mathbf{Q}_k y$, can be taken as an approximation of the eigenvector of $\mathbf{A}$ where y is an eigenvector of $\mathbf{H}_k$ associated with any considered eigenvalue of $\mathbf{H}_k$.

Implicitly Restarted Arnoldi Iteration

One of the main disadvantages of the basic Arnoldi iteration method is that the required number of steps is typically large. This is the main issue especially when the starting matrix, $\mathbf{A}$, is very large. Another problem with this approach is that one cannot set certain criteria for detection of the eigenvalues. For example, in some cases, only first k eigenvalues of the largest real part may be required. To date, various methods have been developed and introduced to compute a specific number of eigenpairs of a given matrix in a more efficient manner. A numerically stable approach, named as implicitly restarted Arnoldi method, that combines Arnoldi process with the implicitly shifted QR algorithm is to be introduced here.

The method was proposed by Lehoucq and Sorensen [80] and the technique has been also implemented in a freely available software package called ARPACK [81] by them. This process is more convenient than some traditional approaches since it lets the user specify in advance the number of eigenvalues with certain specified features such as largest real part or largest magnitude. Hence, the required storage is fixed.

The Implicitly Restarted Arnoldi Method can be accomplished in the following three steps [5]:

1. Extend a $k-$step Arnoldi factorization to a length $m = k + p$ Arnoldi factorization:

$$\mathbf{A}\mathbf{Q}_k = \mathbf{Q}_k\mathbf{H}_k + h_{k+1,k}q_{k+1}\mathbf{e}_k^\top \Rightarrow \mathbf{A}\mathbf{Q}_m = \mathbf{Q}_m\mathbf{H}_m + h_{m+1,m}q_{m+1}\mathbf{e}_m^\top. \tag{2.81}$$

2. Reorder the $m-$step Arnoldi factorization in such a way that the desired eigenvalues appear in the leading submatrix of $\mathbf{H}_m$:

$$\mathbf{A}\mathbf{Q}_m = \mathbf{Q}_m\mathbf{H}_m + h_{m+1,m}q_{m+1}\mathbf{e}_m^\top \Rightarrow \mathbf{A}\tilde{\mathbf{Q}}_m = \tilde{\mathbf{Q}}_m\tilde{\mathbf{H}}_m + \tilde{h}_{m+1,m}\tilde{q}_{m+1}\mathbf{e}_m^\top. \tag{2.82}$$

3. Truncate the reordered $m-$step Arnoldi factorization to get a new $k-$step Arnoldi factorization :

$$\mathbf{A}\tilde{\mathbf{Q}}_m = \tilde{\mathbf{Q}}_m\tilde{\mathbf{H}}_m + \tilde{h}_{m+1,m}\tilde{q}_{m+1}\mathbf{e}_m^\top. \Rightarrow \mathbf{A}\tilde{\mathbf{Q}}_k = \tilde{\mathbf{Q}}_k\tilde{\mathbf{H}}_k + \tilde{h}_{k+1,k}\tilde{q}_{k+1}\mathbf{e}_k^\top. \tag{2.83}$$

In step 2, $p = m - k$ steps of the shifted QR algorithm on the Hessenberg matrix $\mathbf{H}_m$ have been performed so that the eigenvalues of the leading principal submatrix $\tilde{\mathbf{H}}_m$ are ordered. In step 3, the unwanted eigenvalues are eliminated. Please refer to [80, 81], for more detailed explanations and derivations of some expressions.

2.6.5 Levenberg-Marquardt Algorithm

The Levenberg-Marquardt algorithm is one of the most widely used standard iterative technique to solve nonlinear least squares problems. This optimization algorithm, which was introduced firstly by Kenneth Levenberg in 1944 [82] and revised by Donald Marquardt in 1963 [86], provides a numerical solution to the following nonlinear least squares curve fitting problem:

$$S(\theta) = \sum_{i=1}^{m} [y_i - f(x_i, \theta)]^2, \tag{2.84}$$

where $(y_1, y_2, \cdots, y_m)$ is the desired output vector, $f(x, \theta)$ is the function of an independent variable x and n parameters θ, and $S(\theta)$ is the function to be minimised.

The Levenberg-Marquardt algorithm is an iterative technique that starts with an initial guess for the n parameters θ that are updated at every iteration until stopping criterion is satisfied, *i.e.* the absolute change in the parameter estimates between two consecutive iteration steps is less than a user-defined $\mathrm{tolerance}$ value. Furthermore, the Levenberg-Marquardt algorithm acts as a combination of two other well-known minimisation methods: the steepest descent method and the Gauss-Newton method. When the parameters are far from their optimal value, the Levenberg-Marquardt algorithm behaves like a steepest descent method. Similarly, it behaves like a Gauss-Newton method when the parameters are close to their optimal value.

2.6.6 Piecewise Cubic Hermite Interpolating Polynomial

Interpolation is a method of estimating and constructing new data points within the range of a finite set of known data points. One major purpose of using an interpolation technique is to construct a regular grid from an irregular set of data points. For this procedure, we focus on a shape-preserving interpolant method called piecewise cubic Hermite interpolating polynomial (PCHIP). It is beyond the scope of this study to rigorously and formally analyse this method, but reader should refer to [92] for its detailed explanation and MATLAB implementation.

There are two main advantages of the PCHIP interpolant [105]. First, this approach produces a monotone interpolant on each interval between two consecutive measurements, *i.e.* it never overshoots the data. Secondly, the resulting interpolant has one continuous derivative, which is reasonable provided that the signal being measured is expected to be continuous.

CHAPTER 3

ANALYTICAL THEORY

3.1 Chapter Introduction

The focus of this chapter is to describe the analytical framework of the research. The problem considered in this thesis is the ignition of propagating waves in one-dimensional bistable or excitable systems. In Section 3.2, this problem will be mathematically formulated. Analytical initiation criterion for such problem will be divided into two cases: stimulation by voltage and stimulation by current. Section 3.3 and Section 3.4 address how the linear approximation of the critical curves for each case can be derived. An extension of the method from a linear to a quadratic approximation of the (center-)stable manifold for both cases are also provided in each section. Finally, the summary of the chapter is presented in Section 3.5.

3.2 Problem Formulation

We consider the problems of initiation of propagating waves in one spatial dimension, which is formulated as a reaction-diffusion system,

$$\frac{\partial \mathbf{u}}{\partial t} = \mathbf{D}\frac{\partial^2 \mathbf{u}}{\partial x^2} + \mathbf{f}(\mathbf{u}), \tag{3.1}$$

where $\mathbf{u} : \mathbb{R} \times \mathbb{R} \to \mathbb{R}^k$ is a k-component reagents field, $k \geq 1$, defined for $x \in \mathbb{R}$ and $t \in \mathbb{R}_+$, vector-function $\mathbf{f} : \mathbb{R}^k \to \mathbb{R}^k$ describes the reaction rates and $\mathbf{D} \in \mathbb{R}^{k \times k}$ is the matrix of

diffusivity. We assume that this system has a stable spatially uniform equilibrium state, called resting state,

$$\mathbf{u}(x,t) = \mathbf{u}_r, \qquad \mathbf{f}(\mathbf{u}_r) = \mathbf{0}, \tag{3.2}$$

and a family of stable propagating wave solutions of the form

$$\begin{aligned} \mathbf{u}(x,t) &= \mathbf{u}_{\mathrm{w}}(x - c_{\mathrm{w}} t - s_{\mathrm{w}}), \\ \mathbf{u}_{\mathrm{w}}(\infty) &= \mathbf{u}_r,\ \mathbf{u}_{\mathrm{w}}(-\infty) = \mathbf{u}_-, \end{aligned} \tag{3.3}$$

where $\mathbf{u}_-$ is also a stable spatially uniform equilibrium, $\mathbf{f}(\mathbf{u}_-) = \mathbf{0}$, which may or may not coincide with $\mathbf{u}_r$. In this thesis, we restrict our attention to the two types of propagating wave solutions, and these are propagating *pulse*, which is the case when $\mathbf{u}_- = \mathbf{u}_r$ and propagating *front* otherwise. In (3.3), $c_{\mathrm{w}} > 0$ is a fixed constant, the wave propagation speed, and s_{w} is an arbitrary constant, the parameter of the family.

The main purpose of this study is to investigate the behaviour of the solutions of the system (3.1) set on $x \in [0,\infty)$, $t \in [0,\infty)$ subject to the following initial and boundary conditions,

$$\begin{aligned} &\mathbf{u}(x,0) = \mathbf{u}_0(x) = \mathbf{u}_r + \mathbf{u}_{\mathrm{s}}(x), \qquad x > 0, \\ &\mathbf{D}\mathbf{u}_x(0,t) = -\mathbf{I}_{\mathrm{s}}(t), \qquad t > 0. \end{aligned} \tag{3.4}$$

Typically, these solutions either approach the propagating wave solution ("ignition") or the resting state ("failure") as $t \to \infty$, as illustrated in Figure 3.1. [1] Without loss of generality, we assume that the functions $\mathbf{u}_{\mathrm{s}}(x)$ and $\mathbf{I}_{\mathrm{s}}(t)$ have a finite support, $\mathbf{u}_{\mathrm{s}}(x) \equiv \mathbf{0}$ for $x > x_{\mathrm{s}}$, and $\mathbf{I}_{\mathrm{s}}(t) \equiv \mathbf{0}$ for $t > t_{\mathrm{s}}$.

Our analysis is carried out focusing attention on the cases when only one of $\mathbf{u}_{\mathrm{s}}(\cdot)$ and $\mathbf{I}_{\mathrm{s}}(\cdot)$ is nonzero. If the dependence is on just one parameter, then one talks about threshold value(s) of the parameter, separating the two outcomes. When there are two parameters, one can talk about a *threshold curve*, or a *critical curve*. The simplest and standard formulations are:

- "Stimulation by voltage":

$$\mathbf{I}_{\mathrm{s}}(t) = \mathbf{0}, \qquad \mathbf{u}_{\mathrm{s}}(x) = U_{\mathrm{s}}\mathbf{X}(x). \tag{3.5}$$

[1] More precisely, since (3.4) is defined on half-line $x \in \mathbb{R}_+$ and the propagating wave solution (3.3) on the whole line $x \in \mathbb{R}$, the convergence should be understood in an appropriate sense, *e.g.* convergence in any finite interval fixed in a co-moving frame of reference.

That is, the initial condition is the resting state $\mathbf{u}_r$, displaced by the magnitude defined by parameter U_s with a normalized spatial profile defined by $\mathbf{X}(x)$. In all specific examples, we shall use simply a rectangular profile of a width x_s,

$$\mathbf{X}(x) = \mathrm{H}(x_\mathrm{s} - x)\mathbf{e}, \tag{3.6}$$

where $\mathrm{H}(\cdot)$ is the Heaviside step function and $\mathbf{e} \in \mathbb{R}^k$ is a constant vector defining the modality of the perturbation. Then the critical curve can be considered in the plane $(x_\mathrm{s}, U_\mathrm{s})$, and we call it "strength-extent curve".

- "Stimulation by current":

$$\mathbf{u}_\mathrm{s}(x) = \mathbf{0}, \qquad \mathbf{I}_\mathrm{s}(x) = I_\mathrm{s}\,\mathbf{T}(t). \tag{3.7}$$

That is, the initial condition is the unperturbed resting state, but there is a constant current injected through the left boundary of the interval, where I_s defines the strength of the current and $\mathbf{T}(t)$ its normalized temporal profile. Similar to stimulation by voltage case, we consider a rectangular profile of duration t_s,

$$\mathbf{T}(t) = \mathrm{H}(t_\mathrm{s} - t)\mathbf{e}, \tag{3.8}$$

where the fixed vector $\mathbf{e}$ determines which reagents are being injected. The critical curve will then be in the plane $(t_\mathrm{s}, I_\mathrm{s})$, and widely used standard term for it is "strength-duration curve".

We find it convenient to formalize the initiation problem as one posed on the whole real line $x \in \mathbb{R}$,

$$\begin{aligned} &\frac{\partial \mathbf{u}}{\partial t} = \mathbf{D}\frac{\partial^2 \mathbf{u}}{\partial x^2} + \mathbf{f}(\mathbf{u}) + \mathbf{h}(x,t), \quad (x,t) \in \mathbb{R} \times \mathbb{R}_+, \\ &\mathbf{u}(x,0) = \mathbf{u}_r + \mathbf{u}_\mathrm{s}(x), \qquad \mathbf{h}(x,t) \equiv \mathbf{0} \ \text{ for } \ t > t_\mathrm{s}, \end{aligned} \tag{3.9}$$

where the initial condition is an even continuation of the one in (3.4),

$$\mathbf{u}_\mathrm{s}(-x) \equiv \mathbf{u}_\mathrm{s}(x) = \begin{cases} U_\mathrm{s}\mathbf{X}(x), & x \geq 0, \\ U_\mathrm{s}\mathbf{X}(-x), & x < 0 \end{cases} \tag{3.10}$$

and the forcing term is formally represented by

$$\mathbf{h}(x,t) = 2I_\mathrm{s}\,\mathbf{e}\mathrm{H}(t_\mathrm{s} - t)\,\delta(x), \tag{3.11}$$

where $\delta(\cdot)$ is the Dirac delta function. This term is derived firstly by integrating (3.9) with respect to x from $-\epsilon$ to ϵ. Then, we take into account the boundary condition given by (3.4) and the fact that the solution to either (3.9) or (3.1) is an even and continuous function of x, while its derivative is discontinuous. Finally, we obtain the expression (3.11) by taking the limit $\epsilon \to 0$.

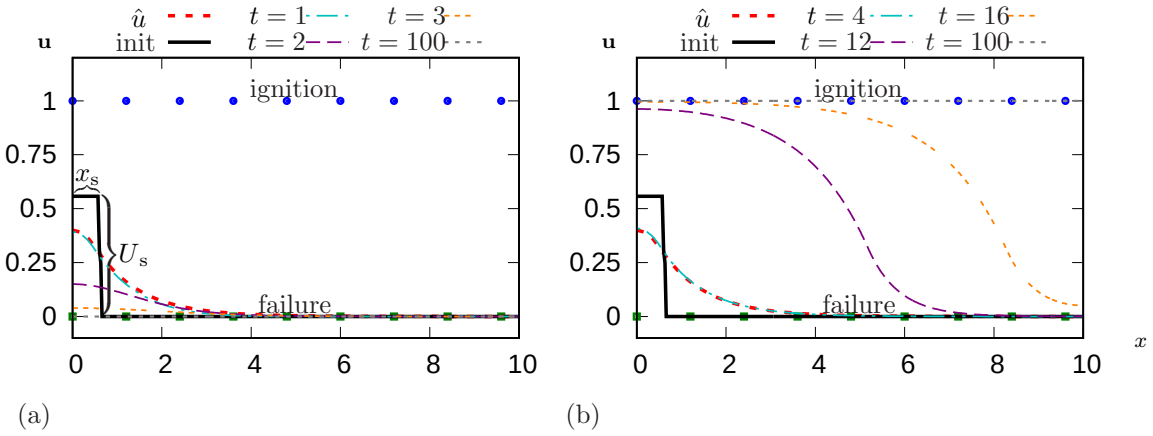

Figure 3.1: Response to slightly below- and slightly above-threshold initial conditions in the McKean model. Parameter values: $\theta = 0.05$, $I_s = 0$, $x_s = 0.6$, $U_s = 0.557123722019382$ (sub-threshold) (a) and $U_s = 0.557123722019383$ (super-threshold)(b).

3.3 Initiation by Voltage: Strength-Extent Curve

In this section, a mathematical formulation of the threshold curve in the (x_s, U_s)-plane that serves as a boundary between initial conditions leading to the propagating wave solution and initial conditions leading to the resting state is provided. To obtain the expression for the strength-extent curve, we consider the problem (3.9) with $\mathbf{h}(x,t) \equiv 0$ for all t and the initial conditions (3.10). We begin with the principal assumption that there exists a *critical solution*, which is defined as a self-similar solution,

$$\begin{aligned} \mathbf{u}(x,t) &= \hat{\mathbf{u}}(x-ct), \\ \mathbf{0} &= \mathbf{D}\frac{\mathrm{d}^2\hat{\mathbf{u}}}{\mathrm{d}\xi^2} + c\,\frac{\mathrm{d}\hat{\mathbf{u}}}{\mathrm{d}\xi} + \mathbf{f}(\hat{\mathbf{u}}), \\ \hat{\mathbf{u}}(\infty) &= \mathbf{u}_r, \quad \hat{\mathbf{u}}(-\infty) = \hat{\mathbf{u}}_- \end{aligned} \tag{3.12}$$

(where $\hat{\mathbf{u}}_-$ may be different from $\mathbf{u}_-$ but in our examples $\hat{\mathbf{u}}_- = \mathbf{u}_r$ when $\mathbf{u}_- = \mathbf{u}_r$) which is unstable with one unstable eigenvalue. Naturally, the speed c of the critical solution is also entirely different from the speed c_w of the stable wave solution.

Similar to the stable wave solution, there is then a whole one-parametric family of critical solutions,

$$\hat{\mathbf{u}}(x-ct-s), \qquad s \in \mathbb{R}. \tag{3.13}$$

Due to this translation invariance, this solution always has one zero eigenvalue. Hence its stable manifold has codimension two, whereas its center-stable manifold has codimension one and as such, it can partition the phase space, i.e. it can serve as a boundary between basins of different attractors (see Figure 3.3). Our strategy is to approximate this center-stable manifold. In the first instance, we consider a linear approximation.

3.3.1 Linear Approximation

Let us rewrite the reaction-diffusion system (RDS) (3.1) in a frame of reference moving with a constant speed c, so that $\mathbf{u}(x,t) = \tilde{\mathbf{u}}(\xi,\tau)$, $\xi = x - ct - s$, $\tau = t$,

$$\begin{aligned}
&\frac{\partial \tilde{\mathbf{u}}}{\partial \tau} = \mathbf{D}\frac{\partial^2 \tilde{\mathbf{u}}}{\partial \xi^2} + c\frac{\partial \tilde{\mathbf{u}}}{\partial \xi} + \mathbf{f}(\tilde{\mathbf{u}}),\\
&\tilde{\mathbf{u}}(\xi,0) = \mathbf{u}_r + \mathbf{u}_s(\xi+s).
\end{aligned}$$

We linearize this equation on the critical solution, which is stationary in the moving frame

$$\tilde{\mathbf{u}}(\xi,\tau) = \hat{\mathbf{u}}(\xi) + \mathbf{v}(\xi,\tau). \tag{3.14}$$

The linearization gives

$$\begin{aligned}
&\frac{\partial \mathbf{v}}{\partial \tau} = \mathbf{D}\frac{\partial^2 \mathbf{v}}{\partial \xi^2} + c\frac{\partial \mathbf{v}}{\partial \xi} + \mathbf{F}(\xi)\mathbf{v},\\
&\mathbf{v}(\xi,0) = \mathbf{u}_r + \mathbf{u}_s(\xi+s) - \hat{\mathbf{u}}(\xi),
\end{aligned} \tag{3.15}$$

where

$$\mathbf{F}(\xi) = \left.\frac{\partial \mathbf{f}}{\partial \mathbf{u}}\right|_{\mathbf{u}=\hat{\mathbf{u}}(\xi)} \tag{3.16}$$

is the Jacobian matrix of the kinetic term, evaluated at the critical solution.

Equation (3.15) is a linear non-homogeneous equation, with time-independent linear operator,

$$\partial_\tau \mathbf{v} = \mathscr{L}\mathbf{v}, \quad \mathscr{L} \triangleq \mathbf{D}\frac{\partial^2}{\partial \xi^2} + c\frac{\partial}{\partial \xi} + \mathbf{F}(\xi). \tag{3.17}$$

For the sake of simplicity, let us assume that the eigenfunctions of $\mathscr{L}$,

$$\mathscr{L}\mathbf{V}_j(\xi) = \lambda_j \mathbf{V}_j(\xi), \tag{3.18}$$

are simple and form a basis in an appropriate functional space, and the same is true for the adjoint $\mathscr{L}^+$ [2]. Then the general solution of problem (3.15) in that space can be written as a generalized Fourier series

$$\mathbf{v}(\xi,\tau) = \sum_j a_j(\tau)\mathbf{V}_j(\xi). \tag{3.19}$$

The coefficients a_j will then satisfy decoupled ODEs,

$$\begin{aligned} \frac{\mathrm{d}a_j}{\mathrm{d}\tau} &= \lambda_j a_j, \\ a_j(0) &= \left\langle \mathbf{W}_j(\xi) \middle| \mathbf{v}(\xi,0) \right\rangle, \end{aligned} \tag{3.20}$$

the scalar product $\left\langle \cdot \middle| \cdot \right\rangle$ is defined as

$$\left\langle \mathbf{a} \middle| \mathbf{b} \right\rangle = \int_{-\infty}^{\infty} \overline{\mathbf{a}}^{\top} \mathbf{b}\, \mathrm{d}\xi,$$

and $\mathbf{W}_j$ are eigenfunctions of the adjoint operator,

$$\mathscr{L}^+\mathbf{W}_j = \overline{\lambda_j}\mathbf{W}_j, \quad \mathscr{L}^+ = \mathbf{D}^{\top}\frac{\partial^2}{\partial\xi^2} - c\frac{\partial}{\partial\xi} + \mathbf{F}^{\top}(\xi), \tag{3.21}$$

normalized so that

$$\left\langle \mathbf{W}_j \middle| \mathbf{V}_k \right\rangle = \begin{cases} 1, & \text{if} \quad j = k, \\ 0, & \text{otherwise.} \end{cases} \tag{3.22}$$

Another assumption, which simplifies formulas and is true for all examples considered, is that all eigenvalues important for the theory are real. We shall enumerate the eigenpairs in the decreasing order of λ_j, so by assumption we always have $\lambda_1 > \lambda_2 = 0 > \lambda_3 > \ldots$.

The solution of (3.20) is

$$a_j(\tau) = \mathrm{e}^{\lambda_j \tau} a_j(0).$$

[2] This assumption will, of course, have to be verified in each particular case.

By assumption, $\lambda_1 > 0$, and due to translational symmetry, $\lambda_2 = 0$, and the rest of the spectrum is assumed within the left half-plane. Hence the condition of criticality is

$$a_1(0) = 0.$$

Using the definition of $a_1(0)$, we have, in terms of the original model (3.15),

$$\left\langle \mathbf{W}_1(\xi) \middle| \mathbf{u}_s(\xi + s) \right\rangle = \left\langle \mathbf{W}_1(\xi) \middle| \hat{\mathbf{u}}(\xi) - \mathbf{u}_r \right\rangle. \tag{3.23}$$

This is an equation of the center-stable space, i.e. a tangent space to the center-stable manifold of the critical solution. Note that this tangent space is different for every choice of the critical solution as identified by choice of s.

General Setting

Let us now consider the typical formulation, when the spatial profile of the initial perturbation is fixed and only its magnitude is varied,

$$\mathbf{u}_s(x) = U_s \mathbf{X}(x). \tag{3.24}$$

Then (3.23) gives

$$U_s \left\langle \mathbf{W}_1(\xi) \middle| \mathbf{X}(\xi + s) \right\rangle = \left\langle \mathbf{W}_1(\xi) \middle| \hat{\mathbf{u}}(\xi) - \mathbf{u}_r \right\rangle$$

or

$$U_s = \frac{\mathscr{N}_1}{\mathscr{D}_1(s)}, \tag{3.25}$$

where the numerator $\mathscr{N}_1$ is a constant, defined entirely by the properties of the model,

$$\mathscr{N}_1 = \left\langle \mathbf{W}_1(\xi) \middle| \hat{\mathbf{u}}(\xi) - \mathbf{u}_r \right\rangle, \tag{3.26}$$

and the denominator $\mathscr{D}_1$ depends on the shift s,

$$\mathscr{D}_1(s) = \left\langle \mathbf{W}_1(\xi) \middle| \mathbf{X}(\xi + s) \right\rangle. \tag{3.27}$$

Hence to get the ultimate answer, we need an extra condition to fix the value of the shift s.

The Case of Critical Nucleus

This is the case when $c = 0$, i.e. the critical solution is stationary, and moreover it is even in x. Then there is a natural choice of $s = 0$ prescribed by symmetry. It can also be motivated directly by considering the problem for $x \in \mathbb{R}$ as an even extension of the problem for $x \in \mathbb{R}_+$. In this case the position of the critical nucleus is fixed, there is no translational invariance, no associated zero eigenvalue, and we can consider the stable space, tangent to the stable manifold, as symbolised in Figure 3.2, rather than center-stable manifold.

That is, we have $x = \xi$, $t = \tau$, $\mathbf{u} = \tilde{\mathbf{u}}$, $\hat{\mathbf{u}}(-\xi) \equiv \hat{\mathbf{u}}(\xi)$, and (3.25) gives the explicit expression for the threshold

$$U_{\mathrm{s}} = \frac{\int\limits_0^\infty \mathbf{W}_1(\xi)^\top (\hat{\mathbf{u}}(\xi) - \mathbf{u}_r)\,\mathrm{d}\xi}{\int\limits_0^\infty \mathbf{W}_1(\xi)^\top \mathbf{X}(\xi)\,\mathrm{d}\xi}. \tag{3.28}$$

If, further, the stimulation is done by a rectangular perturbation of the resting state,

$$\mathbf{X}(\xi) = \mathrm{H}(x_{\mathrm{s}} - \xi)\mathrm{H}(x_{\mathrm{s}} + \xi)\mathbf{e}, \tag{3.29}$$

then we have

$$U_{\mathrm{s}} = \frac{\int\limits_0^\infty \mathbf{W}_1(\xi)^\top (\hat{\mathbf{u}}(\xi) - \mathbf{u}_r)\,\mathrm{d}\xi}{\int\limits_0^{x_{\mathrm{s}}} \mathbf{W}_1(\xi)^\top \mathbf{e}\,\mathrm{d}\xi}. \tag{3.30}$$

This case was first considered in [68].

The Case of Moving Critical Solution

This is the case when $c > 0$, and then we call the critical solution either a *critical pulse* (for $\mathbf{u}_- = \mathbf{u}_r$) or a *critical front* ($\mathbf{u}_- \neq \mathbf{u}_r$) [67]. The problem now does not have the symmetry $\xi \mapsto -\xi$ and the previous "intuitively obvious" choice of s is not generally applicable. Recall that our approach is based on linearization, whereas the original problem does not, in fact, contain small parameters. In this formulation, the criticality condition depends on an "arbitrary" parameter s.

We select an optimal value of the parameter, so as to minimise the error in the prediction. This is done based on a "skew-product" approach [14, 15, 50], which consider solutions $\mathbf{u}(x,t)$ of (3.1) in the form

$$\mathbf{u}(x,t) = \tilde{\mathbf{u}}(\xi,\tau),$$

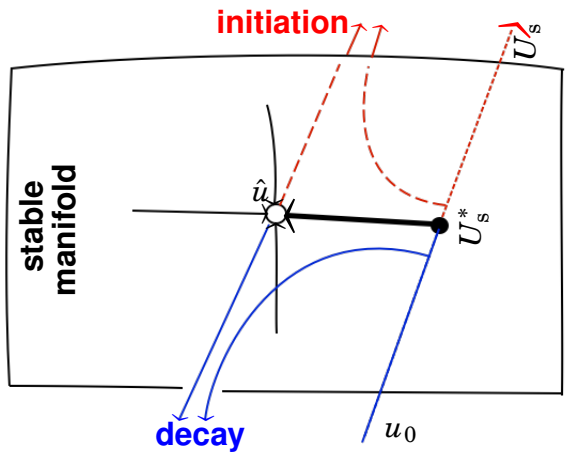

Figure 3.2: Diagram of a stable manifold of the stationary critical solution. The empty circle denotes the critical nucleus and thin solid black lines represent the critical trajectories that form the stable manifold. The critical trajectory (bold solid line) divides the family of initial conditions into two classes: sub-threshold trajectories (blue lines) and super-threshold trajectories (red lines). Note that the filled circle is the intersection point of the initial condition and the stable manifold.

where $\xi = x - s(t)$, $\tau = t$, so $\tilde{\mathbf{u}}(\cdot, \tau)$ describes evolution of the shape of the wave profile in a frame of reference which moves according to the law defined by the shift $s(t)$, and the dynamics of the shift $s(t)$ is determined from an extra condition, such as

$$\Gamma(\mathbf{u}(s(t), t)) \equiv 0, \tag{3.31}$$

for an appropriately selected function $\Gamma(\cdot)$, which allows to choose a unique value of s for any given profile $\mathbf{u}(\cdot, t)$ at any given time t, perhaps with some inequalities to distinguish the front from the back. This extra condition is an essential step for the determination of the parameter s, and a popular and efficient choice of functional $\Gamma(\cdot)$ can be made when one considers perturbations of a relative equilibrium, as done *e.g.* in [13, 33, 78]. This choice is based on the following observation, adapted to our case of a one-parametric symmetry group. An infinitesimal increment of the shift s is equivalent, in this situation, to a corresponding infinitesimal change of coefficient a_j in an expansion like (3.19). Let $\mathbf{V}_j(\xi) = \hat{\mathbf{u}}'(\xi)$ be the "translational" mode, corresponding to $\lambda_j = 0$. Then a (locally) unique fixation of s can be achieved by requiring that $a_j = 0$. In our present situation, the index of the projector to the shift mode is $j = 2$. The resulting extra requirement is to be applied to the solution at all moments of time,

including the initial condition, for which it gives

$$\left\langle \mathbf{W}_2(\xi) \middle| \mathbf{u}_r + \mathbf{u}_\mathrm{s}(\xi+s) - \hat{\mathbf{u}}(\xi) \right\rangle = 0,$$

leading to

$$U_\mathrm{s} \left\langle \mathbf{W}_2(\xi) \middle| \mathbf{X}(\xi+s) \right\rangle = \left\langle \mathbf{W}_2(\xi) \middle| \hat{\mathbf{u}}(\xi) - \mathbf{u}_r \right\rangle. \tag{3.32}$$

Another interpretation of the same requirement is that the condition $a_2(0) = 0$, in addition to the already imposed condition of criticality $a_1(0) = 0$, makes sure that at least two first terms in the Fourier series (3.19) are zero, thus making $\mathbf{v}(\xi, 0)$ "smaller" in that sense.

The two conditions give a system of two similar equations,

$$\begin{cases} U_\mathrm{s} \mathscr{D}_1(s) & = \mathscr{N}_1, \\ U_\mathrm{s} \mathscr{D}_2(s) & = \mathscr{N}_2, \end{cases} \tag{3.33}$$

where

$$\mathscr{N}_\ell = \left\langle \mathbf{W}_\ell(\xi) \middle| \hat{\mathbf{u}}(\xi) - \mathbf{u}_r \right\rangle, \quad \ell = 1, 2, \tag{3.34}$$

and

$$\mathscr{D}_\ell(s) = \left\langle \mathbf{W}_\ell(\xi) \middle| \mathbf{X}(\xi+s) \right\rangle, \quad \ell = 1, 2. \tag{3.35}$$

The definitions of $\mathscr{N}_1$, $\mathscr{D}_1$ here agree with the ones given earlier in (3.26), (3.27). We note that, if $\hat{\mathbf{u}}_- \neq \mathbf{u}_r$, integrals (3.34) converge if $\mathbf{W}_\ell(\xi \to -\infty) \to 0$ sufficiently quickly.

System (3.33) is a nonlinear system of two equations for two unknowns, s and U_s. It is linear and over-determined with respect to U_s. The compatibility condition for the two equations for U_s is $\mathscr{N}_1 \mathscr{D}_2(s) - \mathscr{N}_2 \mathscr{D}_1(s) = 0$, or

$$\left\langle \Phi(\xi) \middle| \mathbf{X}(\xi+s) \right\rangle = 0$$

where

$$\Phi(\xi) = \mathscr{N}_1 \mathbf{W}_2(\xi) - \mathscr{N}_2 \mathbf{W}_1(\xi), \tag{3.36}$$

presenting a nonlinear equation for s. For a rectangular stimulus profile,

$$\mathbf{X}(x) = \mathrm{H}(x + x_\mathrm{s}) \mathrm{H}(x_\mathrm{s} - x) \mathbf{e},$$

the compatibility condition becomes

$$\int_{-s-x_\mathrm{s}}^{-s+x_\mathrm{s}} \Xi(\xi)\,\mathrm{d}\xi = 0$$

where

$$\Xi(\xi) = \mathbf{e}^\top \Phi(\xi). \tag{3.37}$$

This equation for s can be transformed into a more convenient form if we introduce the anti-derivative of $\Xi(\xi)$,

$$\Xi(\xi) = \eta'(\xi).$$

Then

$$\eta(-s+x_\mathrm{s}) - \eta(-s-x_\mathrm{s}) = 0, \tag{3.38}$$

that is, the two points $\xi^+ = -s+x_\mathrm{s}$ and $\xi^- = -s-x_\mathrm{s}$ are points of equal value of function $\eta(\cdot)$. If this function happens to be unimodal, then a unique solution of the compatibility condition is guaranteed to exist, and if its monotonic pieces $\eta^+(\cdot)$ and $\eta^-(\cdot)$ are effectively invertible with, say, $\mathrm{dom}\left(\eta^+\right) > \mathrm{dom}\left(\eta^-\right)$ pointwise, then (3.38) leads to a parametric equation for the critical curve $U_\mathrm{s}(x_\mathrm{s})$. If we denote the value of function $\eta(\cdot)$ in (3.38) by ζ and take it as the parameter, then we have

$$\begin{aligned}
\xi^\pm(\zeta) &= (\eta^\pm)^{-1}(\zeta),\\
x_\mathrm{s}(\zeta) &= \frac{1}{2}\left(\xi^+(\zeta) - \xi^-(\zeta)\right),\\
s(\zeta) &= -\frac{1}{2}\left(\xi^+(\zeta) + \xi^-(\zeta)\right),\\
U_\mathrm{s}(\zeta) &= \mathscr{N}_1/\mathscr{D}_1(s(\zeta)).
\end{aligned} \tag{3.39}$$

For reference, we also summarise here the definitions of the ingredients of (3.39) given earlier:

$$\eta(\xi) = \mathscr{N}_1\mathscr{I}_2(\xi) - \mathscr{N}_2\mathscr{I}_1(\xi), \tag{3.40}$$

$$\mathscr{I}_{1,2}(\xi) = \int^\xi \mathbf{e}^\top \mathbf{W}_{1,2}(\xi')\,\mathrm{d}\xi', \tag{3.41}$$

$$\mathscr{N}_{1,2} = \int_{-\infty}^{\infty} \mathbf{W}_{1,2}^\top(\xi)(\hat{\mathbf{u}}(\xi) - \mathbf{u}_r)\,\mathrm{d}\xi, \tag{3.42}$$

$$\mathscr{D}_1(s) = \mathscr{I}_1(\xi^+) - \mathscr{I}_1(\xi^-). \tag{3.43}$$

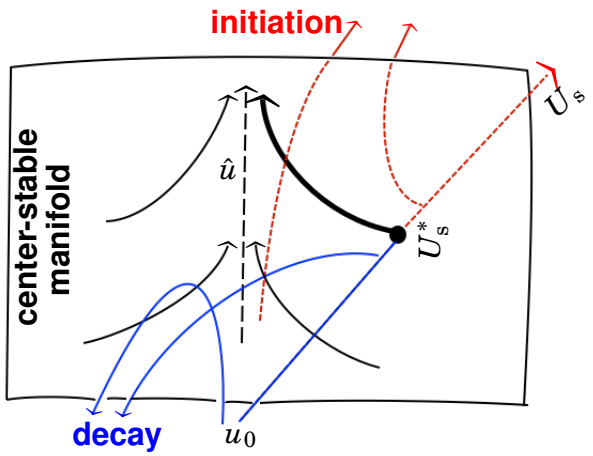

Figure 3.3: The sketch of a center-stable manifold of a moving critical solution. The dashed black line denotes the critical solution, while the solid black lines represent the critical trajectories that form the center-stable manifold. The bold solid black line is the critical trajectory that divides the family of initial conditions into two classes: sub-threshold trajectories (blue lines) and super-threshold trajectories (red lines). The point where the curve of initial conditions intersects the center-stable manifold is shown as the filled circle.

We note that for the case of critical nucleus, $c = 0$, $\hat{\mathbf{u}}$ is an even function, operators $\mathscr{L}$ and $\mathscr{L}^+$ commute with the operator of inversion $\xi \mapsto -\xi$, function $\mathbf{W}_1$ is even, function $\mathbf{W}_2$ is odd, $\mathscr{N}_2 = 0$, $\mathscr{I}_2$ is even, η is even, $\xi^+ = -\xi^-$, $s = 0$ and (3.39) formally recovers the result (3.25) obtained previously based on the choice $s = 0$ as "intuitive" and "natural".

3.3.2 Quadratic Approximation of the Stable Manifold

The use of a linear approximation around the critical solution for the situation when distance from it is not guaranteed to be very small is, admittedly, the weakest point of our approach. In this section, we consider the second-order approximation, in order to assess the limits of applicability of the linear approximation, and possibly to improve it. We restrict consideration to the case of critical nucleus, *i.e.* reaction-diffusion system is a scalar equation. We use the formulation on $x \in (-\infty, \infty)$ and space of even functions $u(\cdot, t)$. Even though we only consider the scalar equation, we intend our quadratic theory to be also applicable to the multicomponent systems.

Rather than using the matrix notation as in the linear approximation, we shall now proceed with explicit notation for the components of the reaction-diffusion systems,

use Greek letters for superscripts to enumerate them, and adopt Einstein's summation convention for those indices. In this way we start from the generic reaction-diffusion system

$$\frac{\partial u^\alpha}{\partial t} = D^{\alpha\beta}\frac{\partial^2 u^\beta}{\partial x^2} + f^\alpha(u^\beta),$$

then consider the deviation v^α of the solution u^α from the critical nucleus $\hat{u}^\alpha$,

$$u^\alpha(x,t) = \hat{u}^\alpha(x) + v^\alpha(x,t),$$

the equation defining the critical nucleus,

$$D^{\alpha\beta}\frac{\partial^2 \hat{u}^\beta}{\partial x^2} + f^\alpha(\hat{\mathbf{u}}) = 0, \tag{3.44}$$

and the Taylor expansion of the equation for the deviation,

$$\dot{v}^\alpha = D^{\alpha\beta}v^\beta{}_{xx} + f^\alpha{}_{,\beta}(\hat{\mathbf{u}})v^\beta + \frac{1}{2}f^\alpha{}_{,\beta\gamma}(\hat{\mathbf{u}})v^\beta v^\gamma + \ldots,$$

where overdot denotes differentiation with respect to time, subscripts $(\cdot)_x$ denote differentiation with respect to space and Greek subscripts after a comma designate a partial differentiation by the corresponding reactive components. The right and left eigenfunctions are defined respectively by

$$D^{\alpha\beta}\partial_{xx}V^\beta{}_j(x) + f^\alpha{}_{,\beta}(x)V^\beta{}_j(x) = \lambda_j V^\alpha{}_j(x)$$

and

$$D^{\beta\alpha}\partial_{xx}W^\beta{}_j(x) + f^\beta{}_{,\alpha}(x)W^\beta{}_j(x) = \lambda_j W^\alpha{}_j(x),$$

where $j \in \{1,2,3,\ldots\}$, and the biorthogonality condition is

$$\left\langle \mathbf{W}_j \middle| \mathbf{V}_k \right\rangle \triangleq \int_{-\infty}^{\infty} \overline{W^\alpha{}_j(x)}V^\alpha{}_k(x)\,\mathrm{d}x = \begin{cases} 1, & \text{if} \quad j = k, \\ 0, & \text{otherwise.} \end{cases}$$

We consider only even solutions, so in the subsequent sums only those j that correspond to even eigenfunctions are assumed. We seek solutions in the form of generalized Fourier series in terms of the right eigenfunctions,

$$v^\alpha(x,t) = \sum_j a_j(t)V^\alpha{}_j(x), \tag{3.45}$$

where the Fourier coefficients are defined by

$$a_j(t) = \left\langle \mathbf{W}_j(x) \middle| \mathbf{v}(x,t) \right\rangle \triangleq \int_{-\infty}^{\infty} \overline{W^\alpha{}_j(x)}\, v^\alpha(x,t)\,\mathrm{d}x. \tag{3.46}$$

Time-differentiation of this gives

$$\dot{a}_j = \lambda_j a_j + \sum_{m,n} Q^j_{m,n} a_m a_n, \tag{3.47}$$

where

$$Q^j_{m,n} = Q^j_{n,m} \triangleq \frac{1}{2} \int_{-\infty}^{\infty} \overline{W^\alpha{}_j(x)}\, f^\alpha{}_{,\beta\gamma}(\hat{\mathbf{u}}(x)) V^\beta{}_m(x) V^\gamma{}_n(x)\,\mathrm{d}x. \tag{3.48}$$

We assume that eigenvalues are real and ordered from larger to smaller, $\lambda_1 > 0$, $\lambda_2 = 0$ is of course the eigenvalue corresponding to the translational symmetry and an odd eigenfunction $\mathbf{V}_2 = \hat{\mathbf{u}}'$, and $\lambda_j < 0$ for all $j \geq 3$. Our task is to determine conditions on initial values of the Fourier coefficients

$$A_j \triangleq a_j(0) = \int_{-\infty}^{\infty} W^\alpha{}_j(x) v^\alpha(x,0)\,\mathrm{d}x$$

that would ensure that

$$a_1(\infty) = 0,$$

which means that the trajectory approaches the critical nucleus, so the initial condition is precisely at the threshold.

Let us rewrite the system (3.47) as an equivalent system of integral equations,

$$a_j(t) = \mathrm{e}^{\lambda_j t} \left(A_j + \int_0^t \mathrm{e}^{-\lambda_j t'} \sum_{m,n} Q^j_{m,n} a_m(t') a_n(t')\,\mathrm{d}t' \right).$$

Successive approximations to the solution can be obtained by direct iterations of this system,

$$a_j^{(i+1)}(t) = \mathrm{e}^{\lambda_j t} \left(A_j + \int_0^t \mathrm{e}^{-\lambda_j t'} \sum_{m,n} Q^j_{m,n} a_m^{(i)}(t') a_n^{(i)}(t')\,\mathrm{d}t' \right). \tag{3.49}$$

Taking $a_j^{(0)} = 0$ for all j, we have

$$a_j^{(1)} = A_j \mathrm{e}^{\lambda_j t}.$$

With account of $\lambda_1 > 0$, $\lambda_j < 0$, $j \geq 3$, and $a_j^{(1)}(t) \to 0$, this implies that

$$A_1 = 0, \qquad A_j \in \mathbb{R}, \quad j \geq 3,$$

which is the answer we have from the linear approximation. The next iteration produces

$$a_j^{(2)}(t) = \mathrm{e}^{\lambda_j t}\left(A_j + \sum_{m,n\geq 3} \frac{Q_{m,n}^j A_m A_n}{\lambda_j - \lambda_m - \lambda_n}\right) - \sum_{m,n\geq 3} \frac{Q_{m,n}^j A_m A_n}{\lambda_j - \lambda_m - \lambda_n} \mathrm{e}^{(\lambda_m+\lambda_n)t}.$$

Assuming that the sums converge, the last term always tends to zero as $t \to \infty$ because $\lambda_n \leq \lambda_3 < 0$ for all $n \geq 3$, and the first term tends to zero for all $j \geq 3$ for the same reason. So, the condition $a_1^{(2)}(t) \to 0$ implies that the first term vanishes for $j = 1$, that is,

$$A_1 = -\sum_{m,n\geq 3} \frac{Q_{m,n}^1 A_m A_n}{\lambda_1 - \lambda_m - \lambda_n}, \tag{3.50}$$

which is our second-order (quadratic) approximation for the critical condition, as opposed to the first-order (linear) approximation which states simply that $A_1 = 0$. We see that the linear approximation will be more accurate when A_n, $n \geq 3$ are smaller, and that for given magnitudes of A_n, the linear approximation will be better if $\lambda_1 - \lambda_m - \lambda_n$, the smallest of which is $\lambda_1 - 2\lambda_3$, are larger (remember we exclude all eigenpairs with odd eigenfunctions, including $n = 2$).

Further iterations of (3.49) lead to still higher-order approximations of the stable manifold of the critical nucleus, and possibly further improvement of the critical condition. This, however, is beyond the scope of this thesis.

Substitution into (3.50) of the definition of A_j in terms of the stimulation amplitude,

$$A_j = \int_{-\infty}^{\infty} \mathbf{W}_j(x)^\top \left(\mathbf{u}_r - \hat{\mathbf{u}}(x) + U_\mathrm{s}\mathbf{X}(x)\right) \mathrm{d}x,$$

leads to a quadratic equation for U_s,

$$A{U_\mathrm{s}}^2 + BU_\mathrm{s} + C = 0 \tag{3.51}$$

where

$$\begin{aligned} A &= \sum_{n,m\geq 3} R_{m,n}\mathscr{D}_m\mathscr{D}_n, \\ B &= \mathscr{D}_1 - 2\sum_{n,m\geq 3} R_{m,n}\mathscr{N}_m\mathscr{D}_n, \\ C &= -\mathscr{N}_1 + \sum_{n,m\geq 3} R_{m,n}\mathscr{N}_m\mathscr{N}_n, \end{aligned} \tag{3.52}$$

and

$$R_{m,n} = \frac{Q^1_{m,n}}{\lambda_1 - \lambda_m - \lambda_n} = R_{n,m},$$
$$\mathscr{N}_j = \int_{-\infty}^{\infty} \mathbf{W}_j(x)^\top (\hat{\mathbf{u}} - \mathbf{u}_r)\,\mathrm{d}x, \tag{3.53}$$
$$\mathscr{D}_j = \int_{-\infty}^{\infty} \mathbf{W}_j(x)^\top \mathbf{X}(x)\,\mathrm{d}x.$$

Note that the definitions of $\mathscr{N}_j$, $\mathscr{D}_j$ here are the same as in (3.34), (3.35), with account of $s = 0$.

An essential detail is the question of properties of the spectra of $\mathscr{L}$ and $\mathscr{L}^+$. In the above derivation, we assumed that these two spectra coincide, are discrete and all eigenvalues are simple. In the specific cases we consider in the following chapters, these assumptions will be tested numerically; in particular, we shall observe that the spectra can in fact be continuous, so the formulas should be generalized, to replace summation over eigenvalues to integrals with respect to the spectral measure, and convergence issue becomes even more complicated.

3.3.3 A Priori Bound in the Critical Nucleus Case

Finally, we comment on a simple *a priori* bound for the critical curve, which follows from considerations different from the analysis of the center-stable manifold of the critical solution, and therefore may provide useful extra information. It applies for the case of $k = 1$, when the critical solution is the critical nucleus:

$$\frac{\partial u}{\partial t} = \frac{\partial^2 u}{\partial x^2} + f(u), \tag{3.54}$$

with the assumptions that $f(u_j) = 0$, $j = 1,2,3$, $u_1 = u_r < u_2 < u_3$, $f(u) < 0$ for $u \in (u_1, u_2)$ and $f(u) > 0$ for $u \in (u_2, u_3)$. In these terms, successful initiation means that at large t solution $u(x,t)$ is a trigger wave from u_1 to u_3, and the failure of initiation means that $u(x,t) \to u_1$ as $t \to \infty$ uniformly in x.

It follows from the results by Fife and McLeod [43], that any initial conditions such that $u(x,0) \in [u_2, u_3]$ for $x \in (-\infty, x_1)$ and $u(x,0) \in [u_1, u_2]$ for $x \in (x_2, \infty)$ guarantee ignition, and for rectangular initial conditions (3.24) this means that even for the smallest excess of U_s over $u_2 - u_1$, this initial condition will produce ignition, provided that x_s is large enough, so we have

$$U^*_\mathrm{s}(x_\mathrm{s}) \searrow \underline{U^*_\mathrm{s}}, \qquad x_\mathrm{s} \to \infty, \tag{3.55}$$

where

$$\underline{U_{\mathrm{s}}^{*}} = u_2 - u_1. \tag{3.56}$$

3.4 Initiation by Current: Strength-Duration Curve

This section provides an analytical description of the threshold curve in the $(t_{\mathrm{s}}, I_{\mathrm{s}})$-plane that separates the boundary conditions leading to initiation from those leading to decay. To obtain explicit approximations to the strength-duration curves, we consider problem (3.9) with vanishing initial condition, *i.e.* initial condition is resting state, $\mathbf{u}_{\mathrm{s}} = \mathbf{u}_r$ and with the boundary condition given by (3.11) at $x = 0$.

3.4.1 Linear Approximation

Linear procedure for the strength-duration analysis is rather similar to the previous case, thus we omit some intermediate calculations. The linearized equation in this case is

$$\begin{aligned} \frac{\partial \mathbf{v}}{\partial \tau} &= \mathbf{D}\frac{\partial^2 \mathbf{v}}{\partial \xi^2} + c\frac{\partial \mathbf{v}}{\partial \xi} + \mathbf{F}(\xi)\mathbf{v} + \tilde{\mathbf{h}}(\xi,\tau), \\ \mathbf{v}(\xi,0) &= \mathbf{u}_r - \hat{\mathbf{u}}(\xi), \end{aligned} \tag{3.57}$$

where

$$\tilde{\mathbf{h}}(\xi,\tau) = \mathbf{h}(\xi + c\tau + s, \tau) \tag{3.58}$$

is the forcing term as measured in the moving frame of reference. The coefficients of the generalized Fourier series will now satisfy the following decoupled ODEs:

$$\begin{aligned} \frac{\mathrm{d}a_j}{\mathrm{d}\tau} &= \lambda_j a_j + h_j(\tau), \\ a_j(0) &= \left\langle \mathbf{W}_j(\xi) \middle| \mathbf{v}(\xi,0) \right\rangle, \end{aligned} \tag{3.59}$$

where

$$h_j(\tau) = \left\langle \mathbf{W}_j(\xi) \middle| \tilde{\mathbf{h}}(\xi,\tau) \right\rangle. \tag{3.60}$$

The solution of (3.59) is

$$a_j(\tau) = \mathrm{e}^{\lambda_j \tau}\left(a_j(0) + \int_0^{\tau} h_j(\tau')\mathrm{e}^{-\lambda_j \tau'}\,\mathrm{d}\tau' \right).$$

Since the stimulation is supposed to be finite in time, $h_j(\tau) \equiv 0$ for $\tau > t_\mathrm{s}$, then the condition of criticality is in turn

$$a_1(t_\mathrm{s}) = 0$$

which implies

$$a_1(0) + \int_0^{t_\mathrm{s}} h_1(\tau') e^{-\lambda_1 \tau'} \, \mathrm{d}\tau' = 0,$$

from which we seek to obtain the critical curve based on linear approximation.

General Setting

Using the definitions of $a_1(0)$ and $h_1(\tau')$, we have

$$\int_0^{t_\mathrm{s}} e^{-\lambda_1 \tau'} \left\langle \mathbf{W}_1(\xi) \middle| \mathbf{h}(\xi + c\tau' + s, \tau') \right\rangle \mathrm{d}\tau' = \left\langle \mathbf{W}_1(\xi) \middle| \hat{\mathbf{u}}(\xi) - \mathbf{u}_r \right\rangle. \tag{3.61}$$

Consider the boundary condition with a rectangular profile,

$$\mathbf{h}(x,t) = 2I_\mathrm{s} \mathbf{e} \, \mathrm{H}(t_\mathrm{s} - t) \delta(x). \tag{3.62}$$

Then (3.61) gives

$$2I_\mathrm{s} \int_0^{t_\mathrm{s}} e^{-\lambda_1 \tau'} \mathbf{W}_1(-c\tau' - s)^\top \mathbf{e} \, \mathrm{d}\tau' = \int_{-\infty}^{\infty} \mathbf{W}_1(\xi)^\top (\hat{\mathbf{u}}(\xi) - \mathbf{u}_r) \, \mathrm{d}\xi. \tag{3.63}$$

The Case of Critical Nucleus

This is the case when $c = 0$, and we again choose $s = 0$ due to symmetry considerations. Hence, (3.63) gives the classical Lapicque-Blair-Hill formula [21, 58, 79]

$$I_\mathrm{s} = \frac{I_\mathrm{rh}}{1 - e^{-\lambda_1 t_\mathrm{s}}}, \tag{3.64}$$

where the rheobase is

$$I_\mathrm{rh} = \frac{\lambda_1 \int_0^{\infty} \mathbf{W}_1(\xi)^\top \hat{\mathbf{u}}(\xi) \, \mathrm{d}\xi}{\mathbf{W}_1(0)^\top \mathbf{e}}. \tag{3.65}$$

The Case of Moving Critical Solution

In a similar fashion to the case of strength-extent curve, two criticality conditions $a_1(t_\mathrm{s}) = 0$ and $a_2(t_\mathrm{s}) = 0$ must be obeyed. Taking into account these two criticality conditions, we have

$$\begin{cases} 2I_\mathrm{s} \int_0^{t_\mathrm{s}} e^{-\lambda_1 \tau'} \mathbf{W}_1 \left(-c\tau' - s\right)^\top \mathbf{e} \, \mathrm{d}\tau' & = \mathscr{N}_1, \\ 2I_\mathrm{s} \int_0^{t_\mathrm{s}} e^{-\lambda_2 \tau'} \mathbf{W}_2 \left(-c\tau' - s\right)^\top \mathbf{e} \, \mathrm{d}\tau' & = \mathscr{N}_2. \end{cases} \tag{3.66}$$

System (3.66) is a nonlinear system of two equations for two unknown parameters, I_s and s. By eliminating the parameter I_s, we find the compatibility condition as follows:

$$\int_0^{t_\mathrm{s}} \left[\mathscr{N}_2 e^{-\lambda_1 \tau'} \mathbf{W}_1 \left(-c\tau' - s\right)^\top \mathbf{e} - \mathscr{N}_1 e^{-\lambda_2 \tau'} \mathbf{W}_2 \left(-c\tau' - s\right)^\top \mathbf{e} \right] \mathrm{d}\tau' = 0. \tag{3.67}$$

This can be further simplified by using the following change of variable,

$$\tau' = \frac{-(\zeta + s)}{c}$$

that leads to

$$\overline{\mu}(s) \triangleq \frac{\mathscr{N}_1 e^{\lambda_2 s/c}}{c} \int_{-s}^{-ct_\mathrm{s}-s} e^{\lambda_2 \zeta/c} \mathbf{W}_2(\zeta)^\top \mathbf{e} \, \mathrm{d}\zeta - \frac{\mathscr{N}_2 e^{\lambda_1 s/c}}{c} \int_{-s}^{-ct_\mathrm{s}-s} e^{\lambda_1 \zeta/c} \mathbf{W}_1(\zeta)^\top \mathbf{e} \, \mathrm{d}\zeta = 0. \tag{3.68}$$

Equation (3.68) defines the shift s for a given t_s (or vice versa). After finding the value of s, one only needs to employ this value in one of the compatibility conditions in (3.66) in order to find the amplitude I_s since both produce the same result. This completes the construction of the strength-duration curve $I_\mathrm{s}(t_\mathrm{s})$.

3.4.2 Quadratic Approximation of the Stable Manifold

As in Section 3.3, we adopt Einstein's summation convention for indices notation to find the quadratic approximation of the stable manifold of the critical nucleus solution. In this way, we start from the initiation problem as one posed on the whole real line $x \in \mathbb{R}$,

$$\frac{\partial u^\alpha}{\partial t} = D^{\alpha\beta} \frac{\partial^2 u^\beta}{\partial x^2} + f^\alpha(u^\beta) + 2I_\mathrm{s} e^\alpha \, \mathrm{H}(t_\mathrm{s} - t)\delta(x),$$

where $I_{\mathrm{s}} \neq 0$. Now, linearizing this equation around the critical nucleus $\hat{u}^{\alpha}$ using

$$u^{\alpha}(x,t) = \hat{u}^{\alpha}(x) + v^{\alpha}(x,t),$$

where the equation defining the critical nucleus is given by (3.44). Using Taylor expansion, we have

$$\dot{v}^{\alpha} = D^{\alpha\beta} v^{\beta}{}_{xx} + f^{\alpha}{}_{,\beta}(\hat{u}) v^{\beta} + f^{\alpha}{}_{,\beta\gamma}(\hat{u}) v^{\beta} v^{\gamma} + 2 I_{\mathrm{s}}\, e^{\alpha}\, \mathrm{H}(t_{\mathrm{s}} - t)\delta(x) + \ldots.$$

Here, yet again, we seek solutions in the form of generalized Fourier series given by (3.45) and its Fourier coefficients are defined by (3.46). But, in this case, the time differentiation of the Fourier coefficients yields,

$$\dot{a}_j(t) = \left\langle W^{\alpha}{}_j(x) \,\middle|\, \dot{v}^{\alpha}(x,t) \right\rangle = \lambda_j a_j + \sum_{m,n} Q^j_{m,n} a_m a_n + 2 I_{\mathrm{s}} E_j\, \mathrm{H}(t_{\mathrm{s}} - t), \tag{3.69}$$

where

$$E_j = W^{\alpha}{}_j(0) e^{\alpha} \tag{3.70}$$

and $Q^j_{m,n}$ is same as in (3.48). The system (3.69) can be written in an equivalent system of integral equations,

$$a_j(t) = \mathrm{e}^{\lambda_j t} \left[A_j + 2 I_{\mathrm{s}} E_j \frac{1}{\lambda_j} \left(1 - \mathrm{e}^{-\lambda_j \min(t, t_{\mathrm{s}})} \right) + \int_0^t \mathrm{e}^{-\lambda_j t'} \sum_{m,n} Q^j_{m,n} a_m(t') a_n(t')\, \mathrm{d}t' \right].$$

Once again, we use the direct iteration method to obtain the approximate solution

$$a_j^{(i+1)}(t) = \mathrm{e}^{\lambda_j t} \left[A_j + 2 I_{\mathrm{s}} E_j \frac{1}{\lambda_j} \left(1 - \mathrm{e}^{-\lambda_j \min(t, t_{\mathrm{s}})} \right) + \int_0^t \mathrm{e}^{-\lambda_j t'} \sum_{m,n} Q^j_{m,n} a_m^{(i)}(t') a_n^{(i)}(t')\, \mathrm{d}t' \right].$$

Taking $a_j^{(0)} = 0$ for all j, we have

$$a_j^{(1)}(t) = \mathrm{e}^{\lambda_j t} \left[A_j + I_{\mathrm{s}} \frac{2E_j}{\lambda_j} \left(1 - \mathrm{e}^{-\lambda_j \min(t, t_{\mathrm{s}})} \right) \right].$$

Considering $\lambda_1 > 0$ and $\lambda_j < 0$ for all $j \geq 3$, we have $a_1^{(1)} \to 0$ as $t \to \infty$, this corresponds to the linear approximation. The next iteration produces

$$\begin{aligned} a_j^{(2)}(t) &= \mathrm{e}^{\lambda_j t} \left[A_j + I_{\mathrm{s}} \frac{2E_j}{\lambda_j} \left(1 - \mathrm{e}^{-\lambda_j \min(t, t_{\mathrm{s}})} \right) + \int_0^t \mathrm{e}^{-\lambda_j t'} \sum_{m,n} Q^j_{m,n} a_m^{(1)}(t') a_n^{(1)}(t')\, \mathrm{d}t' \right] \\ &= \mathrm{e}^{\lambda_j t} \left(A_j + I_{\mathrm{s}} \frac{2E_j}{\lambda_j} \left(1 - \mathrm{e}^{-\lambda_j \min(t, t_{\mathrm{s}})} \right) + \int_0^t \left\{ \sum_{m,n} \mathrm{e}^{\lambda_m t'} \left[A_m + I_{\mathrm{s}} \frac{2E_m}{\lambda_m} \left(1 - \mathrm{e}^{-\lambda_m \min(t', t_{\mathrm{s}})} \right) \right] \right. \right. \\ &\quad \left. \left. \times \mathrm{e}^{\lambda_n t'} \left[A_n + I_{\mathrm{s}} \frac{2E_n}{\lambda_n} \left(1 - \mathrm{e}^{-\lambda_n \min(t', t_{\mathrm{s}})} \right) \right] \mathrm{e}^{-\lambda_j t'} Q^j_{m,n} \right\} \mathrm{d}t' \right). \end{aligned}$$

Note that $\mathrm{e}^{(\lambda_m+\lambda_n-\lambda_1)t} \to 0$ as $t \to \infty$ because $\lambda_k \le \lambda_3 < 0$ for $k = m, n$. By requiring that $a_1^{(2)}(t) \to 0$, we derive the following quadratic equation for I_s,

$$\zeta_1 {I_\mathrm{s}}^2 + \zeta_2 I_\mathrm{s} + \zeta_3 = 0, \tag{3.71}$$

where

$$\begin{aligned}
\zeta_1 &= 4 \sum_{m,n} Q^1_{m,n} \Big[\frac{E_m E_n}{\lambda_m \lambda_n} \Big\{ \frac{1-\mathrm{e}^{-\lambda_1 t_\mathrm{s}}}{\lambda_1} - \frac{\mathrm{e}^{(\lambda_n-\lambda_1)t_\mathrm{s}}-1}{\lambda_n-\lambda_1} \\
&\quad - \frac{\mathrm{e}^{(\lambda_m-\lambda_1)t_\mathrm{s}}-1}{\lambda_m-\lambda_1} - \frac{\mathrm{e}^{-\lambda_1 t_\mathrm{s}} - \mathrm{e}^{(\lambda_m-\lambda_1)t_\mathrm{s}} - \mathrm{e}^{(\lambda_n-\lambda_1)t_\mathrm{s}} + 1}{\lambda_m+\lambda_n-\lambda_1} \Big\} \Big], \\
\zeta_2 &= 2 \sum_{m,n} Q^1_{m,n} \Big[\frac{A_m E_n}{\lambda_n} \Big\{ \frac{\mathrm{e}^{(\lambda_m-\lambda_1)t_\mathrm{s}}-1}{\lambda_m+\lambda_n-\lambda_1} - \frac{\mathrm{e}^{(\lambda_m-\lambda_1)t_\mathrm{s}}-1}{\lambda_m-\lambda_1} \Big\} \\
&\quad + \frac{A_n E_m}{\lambda_m} \Big\{ \frac{\mathrm{e}^{(\lambda_n-\lambda_1)t_\mathrm{s}}-1}{\lambda_m+\lambda_n-\lambda_1} - \frac{\mathrm{e}^{(\lambda_n-\lambda_1)t_\mathrm{s}}-1}{\lambda_n-\lambda_1} \Big\} \Big] - \frac{2E_1\left(\mathrm{e}^{-\lambda_1 t_\mathrm{s}}-1\right)}{\lambda_1}, \\
\zeta_3 &= -\sum_{m,n} Q^1_{m,n} \frac{A_m A_n}{\lambda_m+\lambda_n-\lambda_1} + A_1.
\end{aligned}$$

Note that, in the case of strength-duration curve, the definitions of A_j are slightly different from those of defined in the strength-extent curve analysis. It is basically due to the initial condition being the unperturbed resting state, *i.e.* $U_\mathrm{s} = 0$. Overall, these coefficients are to be determined as

$$A_j \triangleq a_j(0) = \int_{-\infty}^{\infty} {W^\alpha}_j(x) v^\alpha(x,0)\,\mathrm{d}x = \int_{-\infty}^{\infty} \mathbf{W}_j(x)^\top (\mathbf{u}_r - \hat{\mathbf{u}}(x))\,\mathrm{d}x. \tag{3.72}$$

3.4.3 A Priori Bound in the Critical Nucleus Case

We conclude this section with a simple *a priori* bound for the threshold curve, which is applicable to scalar equations. For $U_\mathrm{s} = 0$ and boundary conditions (3.4,3.62), an appropriate *a priori* bound has been obtained by Mornev [95]. In our notations, it implies that

$$I^*_\mathrm{s}(t_\mathrm{s}) \searrow \underline{I^*_\mathrm{s}}, \qquad t_\mathrm{s} \to \infty, \tag{3.73}$$

where

$$\underline{I^*_\mathrm{s}} = \max|\hat{u}'(x)| = |\hat{u}'(x_*)| = \left(-2 \int_{u_1}^{u_2} f(u)\,\mathrm{d}u \right)^{1/2}, \tag{3.74}$$

and x_* is the coordinate point where $\hat{u}(x_*) = u_2$.

3.5 Chapter Summary

In this chapter, we provided analytical formulations of strength-extent and strength-duration relationships for the problems of initiation of propagating waves in one spatial dimension. These formulations are based on an approximation of the (center-)stable manifold of a certain critical solution. The structure of each of these formulations is similar.

Firstly, we have proposed a method of obtaining the linear approximation analytical criterion for ignition of excitation waves, under the assumption of the existence of a critical solution. For scalar equation, the critical solution is the critical nucleus, unstable time-independent solution with one positive eigenvalue whose stable manifold has codimension one that partitions the phase space separating ignition solutions from decay solutions. Moreover, in multicomponent reaction-diffusion systems, the critical solution is called either critical front or critical pulse (both moving) whose stable manifold has codimension two and its center-stable manifold has codimension one that also partitions the phase space separating the two outcomes.

In the case of the critical nucleus, we have also considered the second-order approximation for each critical curve analysis. This allowed us to assess the limits of applicability of the linear approximation and to further improve it. Another practical finding for the critical nucleus case is the existence of an a priori bound for the critical curve. This criterion provides a necessary condition to have ignition.

CHAPTER 4

NUMERICAL METHODS

4.1 Chapter Introduction

This chapter is devoted to numerical techniques for approximating the expressions for the critical curves and all the ingredients of the analytical critical curves. Direct numerical simulations are needed to compare and/or to validate the analytical solution. In Section 4.2, numerical strength-extent threshold curve based on finite difference and finite element simulations is given in detail. In Section 4.3, a similar analysis for numerical strength-duration threshold curve is provided. The analytical initiation criteria proposed in the previous chapter provided both the linear and quadratic approximation of the threshold curves. However, it is not always possible to derive the analytical formula for the ingredients of these curves. The essential ingredients of the linear approximation are the critical solution and the leading eigenpair for the one-component systems while two leading eigenpairs are needed for the multicomponent systems. In addition, for the quadratic approximation in the critical nucleus solution case, we need as many eigenpairs as possible to achieve better accuracy. In Section 4.4, we propose a hybrid approach, where these key ingredients are determined numerically. The chapter is then concluded with a summary in Section 4.5.

4.2 Direct Numerical Simulation of the Strength-Extent Curve

Numerical methods especially play an important role when partial or ordinary differential equations cannot be solved analytically and/or it can be used as a verification of the analytical result as stated earlier. In this section, we introduce both finite difference and finite element discretization formula for the following generic initial and boundary value problem:

$$\begin{aligned} &\mathbf{u}_t = \mathbf{D}\mathbf{u}_{xx} + \mathbf{f}(\mathbf{u}), \\ &\mathbf{u}(x,0) = \mathbf{u}_r + U_{\mathrm{s}}\,\mathrm{H}(x_{\mathrm{s}} - x)\mathbf{e}, \qquad x > 0, \\ &\mathbf{D}\mathbf{u}_x(0,t) = \mathbf{D}\mathbf{u}_x(L,t) = 0, \qquad t > 0, \end{aligned} \tag{4.1}$$

where a finite interval $x \in [0, L]$ is considered as an approximation of $x \in [0, \infty)$.

4.2.1 Finite Difference Discretization Formula

The finite difference discretization formula for the above problem (4.1) can be obtained using explicit forward Euler differencing in time and explicit central differencing in space

$$\hat{\mathbf{u}}_i^{n+1} = \hat{\mathbf{u}}_i^n + \frac{\mathbf{D}\Delta_t}{{\Delta_x}^2}\left(\hat{\mathbf{u}}_{i-1}^n - 2\hat{\mathbf{u}}_i^n + \hat{\mathbf{u}}_{i+1}^n\right) + \Delta_t \mathbf{f}\left(\hat{\mathbf{u}}_i^n\right), \tag{4.2}$$

in conjunction with its initial condition and no-flux Neumann boundary condition at $x = 0$ and $x = L$

$$\begin{aligned} &\hat{\mathbf{u}}_i^0 = \mathbf{u}_r + U_{\mathrm{s}}\,\mathrm{H}(x_{\mathrm{s}} - x_i)\mathbf{e}, \\ &\hat{\mathbf{u}}_0^0 = \hat{\mathbf{u}}_2^0, \quad \hat{\mathbf{u}}_{N+1}^0 = \hat{\mathbf{u}}_{N-1}^0, \\ &\hat{\mathbf{u}}_0^{n+1} = \hat{\mathbf{u}}_2^{n+1}, \quad \hat{\mathbf{u}}_{N+1}^{n+1} = \hat{\mathbf{u}}_{N-1}^{n+1}. \end{aligned} \tag{4.3}$$

In (4.3), points with subscripts 0 and $N+1$ are known as "ghost points" since they reside outside of the grid, which the solution is defined. We thus respectively replace them by the values with subscripts 2 and $N-1$ using no-flux Neumann boundary conditions.

4.2.2 Finite Element Discretization Formula

To solve the initial value problem (4.1) using a finite element discretization, we find it more convenient to perform the numerical computation of a single component, and

then we repeat the same procedure for any other remaining component's equation in the system. Apparently, the diffusion term of such considered equation becomes scalar, *i.e.* $\hat{D} = \mathbf{D}(m,m)$ for $m-th$ component, and hence, its finite element discretization formula becomes

$$\left[\mathbf{A} + \Delta_t \theta \hat{D} \mathbf{B}\right] \hat{u}^{n+1} = \mathbf{F}\left(\hat{u}^{n+\theta}\right) + \left[\mathbf{A} - \Delta_t (1-\theta) \hat{D} \mathbf{B}\right] \hat{u}^{n}, \tag{4.4}$$

where $\mathbf{F}\left(\hat{u}^{n+\theta}\right) = \theta \mathbf{F}\left(\hat{u}^{n+1}\right) + (1-\theta)\mathbf{F}(\hat{u}^{n})$ and $0 \leq \theta \leq 1$ is a real parameter. The initial condition is same as in the case of finite difference discretization formula and the boundary conditions are implemented when constructing the mass and stiffness matrices $\mathbf{A}$ and $\mathbf{B}$, both of which are defined in Section 2.6.

4.2.3 Threshold Curve

We solve a sequence of the "stimulation by voltage" initial-value problem (4.1) in order to obtain the threshold curve in the stimulus strength-extent plane. This is achieved by fixing stimulation extent x_{s} and varying amplitude U_{s}. We use a standard bisection method to determine the threshold value for U_{s} which we denote as U_{s}^{*}. In essence, the idea is to start from an upper estimate $\overline{U_{\mathrm{s}}}$ (superthreshold), known to be sufficient for ignition, and a lower estimate $\underline{U_{\mathrm{s}}}$ (subthreshold), known to fail to ignite, and take the average of these two values to be used as the new amplitude of the initial condition. Then, we solve (4.1) for this initial condition, and update the amplitude according to the solution giving rise to excitation or not. This procedure leads to the following bisection loop (Algorithm 3).

This bisection loop is repeated until the absolute difference between $\overline{U_{\mathrm{s}}}$ and $\underline{U_{\mathrm{s}}}$ is less than a user-defined $\mathrm{tolerance}$ value. In fact, to achieve the best result, we typically use zero tolerance, *i.e.* repeat the bisection loop as long as ${U_{\mathrm{s}}}^{\#}$ remains distinct from both $\overline{U_{\mathrm{s}}}$ and $\underline{U_{\mathrm{s}}}$ given the processor precision. The critical amplitude U_{s}^{*} for the given x_{s} is determined by the final value of ${U_{\mathrm{s}}}^{\#}$. From a computational viewpoint, the zero tolerance, in this algorithm, refers to the number of significant digits desired for the approximation of $|\overline{U_{\mathrm{s}}} - \underline{U_{\mathrm{s}}}|$. Hence, it could conceivably be said that the last value of $\overline{U_{\mathrm{s}}}$ and $\underline{U_{\mathrm{s}}}$ are equally likely approximations ${U_{\mathrm{s}}}^{\#}$ of U_{s}^{*}, as either of them may happen to be equal to $(\overline{U_{\mathrm{s}}} + \underline{U_{\mathrm{s}}})/2$ in computer arithmetics.

This procedure will be repeated as many times as necessary to obtain the strength-extent threshold curve.

Input: x_{s}, $\overline{U_{\mathrm{s}}}$, $\underline{U_{\mathrm{s}}}$
Output: U_{s}^{*}
Set ${U_{\mathrm{s}}}^{\#} := \frac{1}{2}\left(\overline{U_{\mathrm{s}}} + \underline{U_{\mathrm{s}}}\right)$;
while $\left(|\overline{U_{\mathrm{s}}} - \underline{U_{\mathrm{s}}}| \geq \mathrm{tolerance}\right)$ **do**
  Solve (4.1) with $U_{\mathrm{s}} = {U_{\mathrm{s}}}^{\#}$ via FD (4.2) & (4.3) or FE (4.4) ;
  if *ignition* **then**
    $\overline{U_{\mathrm{s}}} := {U_{\mathrm{s}}}^{\#}$;
  else
    $\underline{U_{\mathrm{s}}} := {U_{\mathrm{s}}}^{\#}$;
  end
end
$U_{\mathrm{s}}^{*} := {U_{\mathrm{s}}}^{\#}$

Algorithm 3: Bisection loop for finding amplitude U_{s}^{*} for a fixed parameter x_{s}.

4.3 Direct Numerical Simulation of the Strength-Duration Curve

Now, we consider the second case where the initial condition is the unperturbed resting state and there is a constant current injected through the left boundary of the interval,

$$\begin{aligned} &\mathbf{u}_t = \mathbf{D}\mathbf{u}_{xx} + \mathbf{f}(\mathbf{u}), \\ &\mathbf{u}(x,0) = \mathbf{u}_r, \qquad x > 0, \\ &\mathbf{D}\mathbf{u}_x(0,t) = -I_{\mathrm{s}}\,\mathrm{H}(t_{\mathrm{s}} - t)\mathbf{e}, \;\; \mathbf{D}\mathbf{u}_x(L,t) = 0, \qquad t > 0. \end{aligned} \tag{4.5}$$

4.3.1 Finite Difference Discretization Formula

In the case of initiation by current, the finite difference discretization formula remains the same as (4.2), while we now have the following initial and boundary conditions

$$\begin{aligned} &\hat{\mathbf{u}}_i^0 = \mathbf{u}_r, \\ &\hat{\mathbf{u}}_0^0 = \hat{\mathbf{u}}_2^0 + 2\Delta_x I_{\mathrm{s}}\,\mathrm{H}(t_{\mathrm{s}} - t_0)\mathbf{D}^{-1}\mathbf{e}, \quad \hat{\mathbf{u}}_{N+1}^0 = \hat{\mathbf{u}}_{N-1}^0, \\ &\hat{\mathbf{u}}_0^{n+1} = \hat{\mathbf{u}}_2^{n+1} + 2\Delta_x I_{\mathrm{s}}\,\mathrm{H}(t_{\mathrm{s}} - t_{n+1})\mathbf{D}^{-1}\mathbf{e}, \quad \hat{\mathbf{u}}_{N+1}^{n+1} = \hat{\mathbf{u}}_{N-1}^{n+1}, \end{aligned} \tag{4.6}$$

where no-flux Neumann boundary condition is applied at $x = L$.

4.3.2 Finite Element Discretization Formula

For the sake of simplicity, here we find it more convenient to consider the initiation problem defined on the whole line $x \in \mathbb{R}$, as given by equation (3.9). Once again, we aim to solve the one-component version of (3.9), *i.e.* the transmembrane voltage equation

$$\frac{\partial u}{\partial t} = \hat{D}\frac{\partial^2 u}{\partial x^2} + f(u) + 2I_{\mathrm{s}}\,\mathrm{H}(t_{\mathrm{s}} - t)\delta(x), \quad u(x,0) = u_r, \quad (x,t) \in \mathbb{R} \times \mathbb{R}_+. \tag{4.7}$$

The discretization formula based on the finite element method is

$$\mathbf{A}\frac{\mathrm{d}\hat{u}}{\mathrm{d}t} + \hat{D}\mathbf{B}\hat{u} = \mathbf{F}(\hat{u}) + 2I_{\mathrm{s}}\,\mathrm{H}(t_{\mathrm{s}} - t)\mathbf{G}, \tag{4.8}$$

where the entries of the load vector $\mathbf{G}$ are given by

$$G_i = \int_0^L \delta(x)\Phi_i(x)\,\mathrm{d}x, \tag{4.9}$$

which has only one nonzero entry, $G_1 = 1$ by definition of Dirac Delta function. Finally, we apply the generalized trapezoidal rule to (4.8) to get

$$\left[\mathbf{A} + \Delta_t\theta\hat{D}\mathbf{B}\right]\hat{\mathbf{u}}^{n+1} = \mathbf{F}\left(\hat{u}^{n+\theta}\right) + \left[\mathbf{A} - \Delta_t(1-\theta)\hat{D}\mathbf{B}\right]\hat{\mathbf{u}}^{n} + 2I_{\mathrm{s}}\,\mathrm{H}(t_{\mathrm{s}} - t)\mathbf{G}. \tag{4.10}$$

One should bear in mind here that this discretization formula is only for transmembrane equation of (3.9), and the discretization formula for the remaining equations can be obtained in a similar way, except that the last term in (4.10) is removed and that the diffusion coefficient and kinetic term, of course, differ from component to component.

4.3.3 Threshold Curve

Numerical strength-duration threshold curve can be obtained in a similar fashion to the case of the strength-extent curve. We solve (4.5) using the finite difference discretization, or (3.9) using the finite element discretization, for fixed stimulation time duration t_{s} and varying the strength of the current I_{s}. For any initial upper estimate $\overline{I_{\mathrm{s}}}$ (superthreshold), known to be sufficient for ignition, and lower estimate $\underline{I_{\mathrm{s}}}$, known to

fail to ignite, the following bisection algorithm gives the threshold value I_{s}^*:

Input: t_{s}, $\overline{I_{\mathrm{s}}}$, $\underline{I_{\mathrm{s}}}$
Output: I_{s}^*
Set ${I_{\mathrm{s}}}^{\#} := \frac{1}{2}\left(\overline{I_{\mathrm{s}}} + \underline{I_{\mathrm{s}}}\right)$;
while $\left(|\overline{I_{\mathrm{s}}} - \underline{I_{\mathrm{s}}}| \geq \mathrm{tolerance}\right)$ **do**
  Solve (4.1) with $I_{\mathrm{s}} = {I_{\mathrm{s}}}^{\#}$ via FD (4.2) & (4.6) or (4.7) via FE (4.10) ;
  if *ignition* **then**
    $\overline{I_{\mathrm{s}}} := {I_{\mathrm{s}}}^{\#}$;
  else
    $\underline{I_{\mathrm{s}}} := {I_{\mathrm{s}}}^{\#}$;
  end
end
$I_{\mathrm{s}}^* := {I_{\mathrm{s}}}^{\#}$

Algorithm 4: Bisection loop for finding the strength of the current I_{s}^* for a fixed parameter t_{s}.

This procedure is repeated as many times for different t_{s} as necessary to obtain the strength-duration curve.

4.4 Hybrid Approach

4.4.1 Rationale

As outlined in the previous chapter, the linear approximation of the strength-extent threshold curves requires the knowledge of $\hat{\mathbf{u}}(x)$, $\mathbf{W}_1(x)$, and, for the non-self-adjoint cases, also $\mathbf{W}_2(x)$, whereas for the strength-duration threshold curves, we also need the first leading eigenvalue λ_1 as $\lambda_2 = 0$ due to the translational symmetry. In the critical nucleus case, we have also proposed the quadratic approximation of both strength-extent and strength-duration critical curves, in which ideally the whole spectrum of λ_ℓ, $\mathbf{W}_\ell$, $\mathbf{V}_\ell$, $\ell = 1,3,5,\ldots$ is needed. As will be discussed in the following chapters, these can be calculated explicitly only in a few special cases. Therefore, for the purpose of determining these key factors numerically, we present a hybrid approach, after which the analytical expressions (3.30), (3.39), (3.64) or (3.66) can be applied. In the following, we describe in detail how to numerically compute each of these key factors.

4.4.2 The Case of Critical Nucleus

Shooting: The numerical approximation of the critical nucleus is determined by solving a nonlinear boundary-value problem. The first essential step is to provide a good initial guess for the solution, and this can be done by using the bisection loop described in the previous sections. The idea of having initial or boundary conditions very close to the threshold values is based on the behaviour of the generated solutions that approach the saddle point $\hat{u}(x)$ to within a small distance and will remain in its vicinity for a long time. Keeping in mind similar derivations can be made concerning "initiation by current", here we propose the numerical procedure for finding the critical nucleus according to the initial condition. Using an initial condition with its amplitude ${U_\mathrm{s}}^\#$ very close to the exact threshold $U_\mathrm{s}^*(x_\mathrm{s})$, we can approximate the critical nucleus. The first step is to find the speed of the change of the voltage profile over time, which is measured by computing

$$S(t) = ||\dot{u}||_{L^2}^2 = \int_0^L u_t^2(x,t)\,\mathrm{d}x. \tag{4.11}$$

We observe that when the voltage profile is the slowest, it is also the closest profile to the critical nucleus, and therefore, we can take this voltage profile as an approximation of the critical nucleus. Thus, we find the time moment at which the minimum value of $S(t)$ is achieved,

$$t^\# = \mathrm{argmin}(S(t)), \tag{4.12}$$

so that the numerical solution at $t = t^\#$ is taken as an estimate of the critical nucleus $\hat{u}(x)$. This can be immediately used for the next step, or serve as an initial guess for a more advanced boundary-value solver if a higher accuracy is required. This process can be accomplished by the following algorithm:

Input: Pre-found value of ${U_\mathrm{s}}^\#$ for an arbitrarily chosen initial width x_s
Output: $\hat{u}$
Solve nonlinear problem: $\dfrac{\partial u}{\partial t} = D\dfrac{\partial^2 u}{\partial x^2} + f(u)$ for $u(x,0) = u_r + {U_\mathrm{s}}^\#\mathrm{H}(x_\mathrm{s} - x)$;
Find: $S(t) = ||\dot{u}||_{L^2}^2 = \int\limits_0^L u_t^2(x,t)\,\mathrm{d}x$, $t^\# = \mathrm{argmin}(S(t))$;
Solve nonlinear problem till $t = t^\#$: $\dfrac{\partial u}{\partial t} = D\dfrac{\partial^2 u}{\partial x^2} + f(u)$ and set $\hat{u} = u$.

Algorithm 5: Numerical computation of the critical nucleus.

Note that the center-stable manifold of the unique critical nucleus solution corresponds to the threshold curve that separates ignition initial conditions from decay initial conditions. Hence, the above procedure should produce (nearly) the same $\hat{u}(x)$ for any choice of x_{s}. To verify the validity of this key assumption, and to assess the accuracy of the found critical nucleus, we used the procedure for different values of x_{s}.

Marching: With the numerical approximation of the critical nucleus $\hat{u}^{\#}(x)$, we next describe the algorithm used to calculate the principal eigenvalue λ_1 and the corresponding eigenfunction $\mathbf{W}_1$. Since λ_1 by definition is the eigenvalue with the largest real part, we should expect that the solution of the differential equation

$$\frac{\partial \mathbf{w}}{\partial t} = \mathscr{L}^{+}\mathbf{w} \triangleq \mathbf{D}^{\top}\frac{\partial^2 \mathbf{w}}{\partial x^2} + \mathbf{F}^{\top}(x)\mathbf{w}, \tag{4.13}$$

for almost any initial conditions, should satisfy

$$\mathbf{w}(t,x) = C\,\mathrm{e}^{\lambda_1 t}\mathbf{W}_1(x)(1+\mathscr{O}(1)), \qquad t\to\infty, \tag{4.14}$$

for some constant C.

The numerical estimate of λ_1 can be found fitting the linear part of the graph of $\ln|\mathbf{w}(0,t)|$ to a straight line by least squares such that the slope gives this leading eigenvalue. We have also verified that the profile $\mathbf{w}(t,x)/\mathbf{w}(t,0)$ remained virtually unchanged during this linear part, and took the most recent profile as the ignition mode $\mathbf{W}_1(x)$. An equivalent (and more general) procedure of estimating the eigenvalue λ_1 for a time interval from t to $t+\delta t$ is

$$\frac{\ln\left(\left\langle \mathbf{w}(x,t+\delta t)\,\middle|\,\mathbf{w}(x,t)\right\rangle\right)}{\delta t\left\langle \mathbf{w}(x,t)\,\middle|\,\mathbf{w}(x,t)\right\rangle},$$

under the assumption that this estimate converges as $t\to\infty$. Again, the results of these obtained λ_1 and $\mathbf{W}_1(x)$ can be immediately used or serve as an initial approximation for a more sophisticated eigenvalue problem solver if a better accuracy is required.

So far, we have numerically derived all key ingredients needed for the linear approximation of the critical curves. However, we have also proposed the quadratic approximation, which requires the whole spectrum, as emphasised before. From a numerical point of view, we must consider a limited number of eigenpairs, not the whole infinite spectrum. Thus, we extend this method to calculate a number of eigenpairs

with largest eigenvalues as long as they are real. For a one-component excitable medium, the critical solution is the critical nucleus, and hence $\mathscr{L} = \mathscr{L}^+$. To obtain the desired number of eigenpairs, we need to numerically solve (4.13) for a number of linearly independent initial conditions, then use the Gram-Schmidt procedure to extract a solution that is orthogonal to $\mathbf{W}_1$, which will give the λ_2 and $\mathbf{W}_2$ pair, then solution orthogonal both to $\mathbf{W}_1$ and $\mathbf{W}_2$ to obtain λ_3 and $\mathbf{W}_3$ and so on.

Now, we turn our attention to calculation of the eigenpairs based on a modified power iteration method in an algorithmic form. To preserve stability and computational efficiency, we use random number generator to assign an initial guess of $\mathbf{W}_1$, and then we set $\mathbf{W}_2$ as the spatial derivative of $\mathbf{W}_1$, $\mathbf{W}_3$ as the spatial derivative of $\mathbf{W}_2$, and so on. This guarantees that the initial estimation of the eigenfunctions is linearly independent, as required, while the initial guess for the eigenvalues is set to be zero. If we choose a time domain $t \in (0, T)$, then, the following algorithm is applied until the desired convergence criterion is fulfilled:

Input: Any linearly independent initial estimation of $\left(\mathbf{W}_1^0, \mathbf{W}_2^0, \cdots, \mathbf{W}_n^0\right)$
Output: $(\lambda_1, \mathbf{W}_1), (\lambda_2, \mathbf{W}_2), \cdots, (\lambda_n, \mathbf{W}_n)$
Set: $\lambda_1^0, \lambda_2^0, \cdots, \lambda_n^0 \leftarrow 0$;
for $i = 1, 2, \ldots$ **do**
  for $k = 1, 2, \ldots, n$ **do**
    Solve: $\mathbf{W}_k^i \leftarrow \exp\left(\mathscr{L}^+ T\right) \mathbf{W}_k^{i-1}$;
    Orthogonality: $\mathbf{W}_k^i \leftarrow \mathbf{W}_k^i - \sum_{m=1}^{k-1} \left\langle \mathbf{W}_k^i \middle| \mathbf{W}_m^i \right\rangle \times \mathbf{W}_m^i$;
    Normalization: $\mathbf{W}_k^i \leftarrow \frac{\mathbf{W}_k^i}{\left\| \mathbf{W}_k^i \right\|}$;
    Eigenvalue : $\lambda_k^i \leftarrow \frac{\ln\left(\left\langle \mathbf{W}_k^i \middle| \mathbf{W}_k^{i-1} \right\rangle\right)}{T}$;
  end
  if $|\lambda_k^i - \lambda_k^{i-1}| \leq \text{tolerance}$ *for all* k **then**
    break;
  end
end

Algorithm 6: Numerical computation of n principal eigenpairs of a self-adjoint operator by "marching".

We have chosen the stopping criterion according to the absolute change in each eigenvalue, and such convergence criterion can also be stated in terms of the change

in the eigenfunctions.

4.4.3 The Case of Moving Critical Solution

Co-moving Frame of Reference: As in Section 3.3.1, the idea of symmetry reduction can be here used in numerical simulations to replace the problem of moving critical solution by the problem of a stationary critical solution. For that purpose, we consider the unperturbed nonlinear equation

$$\frac{\partial \mathbf{u}}{\partial t} = \mathbf{D}\frac{\partial^2 \mathbf{u}}{\partial x^2} + \mathbf{f}(\mathbf{u}), \tag{4.15}$$

where the position of the front, s, is defined implicitly by

$$\Gamma(\mathbf{u}(s,t)) = 0,$$

and some extra inequalities may be also needed so that the front is distinguishable from the back. Then, in the comoving frame of reference $\xi = x - s(t)$, $\tau = t$, we have an unknown function of time and space,

$$\tilde{\mathbf{u}}(\xi,\tau) = \mathbf{u}(x,t),$$

and an unknown function of time, $s(t)$, the system of PDEs and a finite constraint

$$\begin{aligned} \frac{\partial \tilde{\mathbf{u}}}{\partial \tau} &= \mathbf{D}\frac{\partial^2 \tilde{\mathbf{u}}}{\partial \xi^2} + \frac{\mathrm{d}s}{\mathrm{d}\tau}\frac{\partial \tilde{\mathbf{u}}}{\partial \xi} + \mathbf{f}(\tilde{\mathbf{u}}), \\ \Gamma(\tilde{\mathbf{u}}(0,\tau)) &= 0. \end{aligned} \tag{4.16}$$

A relative equilibrium, including the moving critical solution, in the system (4.15), corresponds to an equilibrium in (4.16). This allows us to solve the comoving system (4.16) in a similar technique as the one described for the case of stationary critical solution.

Shooting: The moving critical solutions can be found solving initial value problems for (4.16). The amplitude of the initial condition is chosen close to the initiation threshold with high precision to improve the accuracy of the numerical computation of the moving critical solutions. In the computation of the solutions of (4.16), we use Lie operator splitting, known to be the simplest splitting method, to divide the equation (4.16) into four subsystems, each of which is to be assigned as follows:

1. updating $\tilde{\mathbf{u}}$ by an explicit first-order (forward Euler) scheme, for the nonlinear kinetics term $\mathbf{f}(\tilde{\mathbf{u}})$;

2. updating $\tilde{\mathbf{u}}$ by a scheme semi-implicit (Crank-Nicholson) in time, and central difference in space, for the diffusion term $\mathbf{D}\dfrac{\partial^2\tilde{\mathbf{u}}}{\partial\xi^2}$;

3. finding the convection speed $\dfrac{\mathrm{d}s}{\mathrm{d}\tau}$ based on a "virtual" or "predictor" convection substep, that would update $\tilde{\mathbf{u}}$ by an explicit in time, two-point upwind scheme without smoothing;

4. the actual updating of $\tilde{\mathbf{u}}$ by an implicit in time, 3-point upwind scheme with smoothing (Beam-Warming, [11]) for the convection term $\dfrac{\mathrm{d}s}{\mathrm{d}\tau}\dfrac{\partial\tilde{\mathbf{u}}}{\partial\xi}$, using the value of $\dfrac{\mathrm{d}s}{\mathrm{d}\tau}$ found in the previous substep.

Continuation: The accuracy of the moving critical solution found by the shooting method described above is not always sufficient. Hence, alternatively, we can find the non-stationary critical solution as a solution of boundary-value problem (3.12), an autonomous system for $\hat{\mathbf{u}}(\xi)$, with parameter c. We aim to calculate conduction velocity restitution curve [125] that can be found from the following periodic boundary-value problem using popular continuation software AUTO [34]:

$$\begin{aligned} \mathbf{0} &= \mathbf{D}\frac{\mathrm{d}^2\mathbf{u}_P}{\mathrm{d}\xi^2} + c_P\frac{\mathrm{d}\mathbf{u}_P}{\mathrm{d}\xi} + \mathbf{f}(\mathbf{u}_P), \\ \mathbf{u}_P(\xi+P) &\equiv \mathbf{u}_P(\xi), \end{aligned} \tag{4.17}$$

where P is the spatial period of the waves. When the problem is well posed, (4.17) defines a curve in the $(P, c_P, \mathbf{u}_P(\xi))$ space. In the limit $P\to\infty$, this curve splits into two branches, the upper branch with stable propagating pulse solution, $(c_\mathrm{w}, \mathbf{u}_\mathrm{w}(\xi))$ and the lower branch with the unstable critical pulse solution, $(c, \hat{\mathbf{u}}(\xi))$, which is of interest to us.

To determine the unstable speed and the critical pulse, we proceed as follows. We consider (4.17), with an extra parameter corresponding to "stimulation current" added to the transmembrane voltage equation. Starting from an initial guess of c_w, the numerical derivation is performed by following Algorithm 7 below.

AUTO uses collocation to discretize the solutions, we, therefore, use piecewise Hermite interpolation [92] to interpolate the solution obtained by AUTO to the regular grid (for further details, see the related part in Section 2.6).

Marching: The shooting and continuation procedures described above let us determine the critical solution, which includes both $\hat{\mathbf{u}}^\#(\xi)$ and $c^\# = \mathrm{d}s/\mathrm{d}\tau$. We here seek to

Input: An initial guess of c_{w} and $I_{ext} = 0$
Output: c_P, $\hat{\mathbf{u}}(\xi)$

$$\mathbf{D}\frac{\mathrm{d}^2\mathbf{u}_P}{\mathrm{d}\xi^2} + c_P\frac{\mathrm{d}\mathbf{u}_P}{\mathrm{d}\xi} + \mathbf{f}(\mathbf{u}_P) + I_{ext}\mathbf{e} = 0, \quad \mathbf{u}_P(\xi + P) \equiv \mathbf{u}_P(\xi).$$

- Start from the equilibrium of the system and increase the continuation parameter I_{ext} until a Hopf bifurcation point is located. This is an essential step to compute the homoclinic orbit.
- Continue the cycle from the Hopf in the (c_P, P)-plane, down by c_P until the locus of the fold is depicted.
- By using (I_{ext}, c_P, P) as the principal continuation parameters, decrease the value of I_{ext} to be smaller than a predefined $\mathrm{tolerance}$ value. AUTO stores the variables with 12 digits of precision. Hence, we set this $\mathrm{tolerance}$ value very close to machine precision $\mathscr{O}\left(10^{-12}\right)$.
- Trace the periodic orbit in the (P, c_P)-plane both ways,

where lower branch gives the unstable speed c_P along with the corresponding critical pulse $\hat{\mathbf{u}}(\xi)$.

Algorithm 7: Numerical critical pulse obtained using the continuation software AUTO.

determine the right and left eigenfunctions, which are found by calculating solutions of

$$\frac{\partial\mathbf{v}}{\partial\tau} = \mathscr{L}\mathbf{v} \triangleq \mathbf{D}\frac{\partial^2\mathbf{v}}{\partial\xi^2} + c^{\#}\frac{\partial\mathbf{v}}{\partial\xi} + \mathbf{F}(\xi)\mathbf{v}, \tag{4.18}$$

and

$$\frac{\partial\mathbf{w}}{\partial\tau} = \mathscr{L}^{+}\mathbf{w} \triangleq \mathbf{D}^{\top}\frac{\partial^2\mathbf{w}}{\partial\xi^2} - c^{\#}\frac{\partial\mathbf{w}}{\partial\xi} + \mathbf{F}^{\top}(\xi)\mathbf{w}. \tag{4.19}$$

The leading eigenvalue λ_1 and corresponding right eigenfunctions $\mathbf{V}_1$ and left eigenfunctions $\mathbf{W}_1$ are obtained in the $\tau \to \infty$ limit for almost any initial conditions in (4.18) and (4.19). The second eigenvalue λ_2 and the corresponding eigenfunctions $\mathbf{V}_2$ and $\mathbf{W}_2$ are obtained as linearly independent solutions of the same equations, satisfying the constraints

$$\left\langle \mathbf{W}_2 \middle| \mathbf{V}_1 \right\rangle = \left\langle \mathbf{W}_1 \middle| \mathbf{V}_2 \right\rangle = 0, \tag{4.20}$$

using a Gram-Schmidt style process, adopted for our non-self-adjoint situation. Overall, following Algorithm 8 can be written for obtaining a number of eigenvalues and corresponding left and right eigenfunctions.

Input: Any linearly independent initial estimation of $(\mathbf{V}_1^0, \mathbf{W}_1^0)$, $(\mathbf{V}_2^0, \mathbf{W}_2^0), \cdots, (\mathbf{V}_n^0, \mathbf{W}_n^0)$
Output: $(\lambda_1, \mathbf{V}_1, \mathbf{W}_1), (\lambda_2, \mathbf{V}_2, \mathbf{W}_2), \cdots, (\lambda_n, \mathbf{V}_n, \mathbf{W}_n)$
Set: $\lambda_1^0, \lambda_2^0, \cdots, \lambda_n^0 \leftarrow 0$;
for $i = 1, 2, \ldots$ **do**
  for $k = 1, 2, \ldots, n$ **do**
    Solve: $\mathbf{V}_k^i \leftarrow \exp(\mathscr{L}T)\mathbf{V}_k^{i-1}$, $\mathbf{W}_k^i \leftarrow \exp\left(\mathscr{L}^+T\right)\mathbf{W}_k^{i-1}$;
    Biorthogonality: $\mathbf{V}_k^i \leftarrow \mathbf{V}_k^i - \sum_{m=1}^{k-1} \langle \mathbf{V}_k^i \,|\mathbf{W}_m^i\, \rangle \times \mathbf{V}_m^i$,
    $\mathbf{W}_k^i \leftarrow \mathbf{W}_k^i - \sum_{m=1}^{k-1} \langle \mathbf{W}_k^i \,|\mathbf{V}_m^i\, \rangle \times \mathbf{W}_m^i$;
    Normalization: $\mathbf{V}_k^i \leftarrow \frac{\mathbf{V}_k^i}{\left\|\mathbf{V}_k^i\right\|}$, $\mathbf{W}_k^i \leftarrow \frac{\mathbf{W}_k^i}{\left\|\mathbf{W}_k^i\right\|}$;
    Eigenvalue : $\lambda_k^i \leftarrow \frac{\ln\left(\left\langle \mathbf{W}_k^i \middle| \mathbf{W}_k^{i-1} \right\rangle\right)}{T}$;
  end
  if $|\lambda_k^i - \lambda_k^{i-1}| \leq \text{tolerance}$ *for all* k **then**
    break;
  end
end

Algorithm 8: Numerical computation of n principal eigenpairs of a non-self-adjoint operator by "marching".

Arnoldi Iterations: Using the marching method discussed above to compute the required eigenvalues and eigenfunctions with the required accuracy sometimes causes higher computational costs. In this case, we use the standard implicitly restarted Arnoldi iterations as explained in Section 2.6, using the implementation described in [107]. The eigenvalues with the biggest real parts and corresponding left and right eigenfunctions are found by considering the matrix representation of the right-hand side of (4.18) and (4.19). The Arnoldi iterative method can also be, of course, implemented to determine the eigenpairs of the self-adjoint problem (4.13). Figure 4.1 show the matrix representation of discretized version of the one-component equation, which is a tridiagonal matrix with all other entries are zero. This leads us to the Arnoldi method so that the computational cost can be reduced.

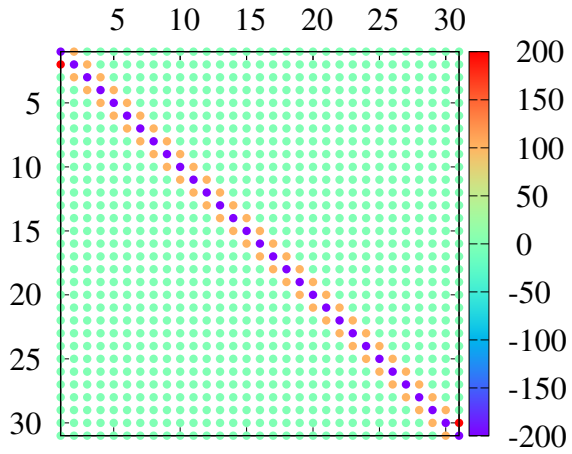

Figure 4.1: A matrix representation of the discretized $\mathscr{L}$ operator for one-component reaction-diffusion system.

We now turn our attention to one of the main advantages of the hybrid approach. All essential ingredients required for the theory are independent of the choices of the initial and boundary profiles. Thus, the hybrid method is computationally efficient, as opposed to direct numerical simulations, which naturally require a complete rerun when a different family of initial or boundary profile is considered.

4.5 Chapter Summary

This chapter reviewed the direct numerical simulation of the threshold curves and the numerical methods required to approximate the key ingredients of the analytical threshold curves. Initially, two numerical methods for solving initial and boundary value problem were introduced. These standard approaches are finite difference method and finite element method and the choice of the numerical method to use depends on the specific model considered. A numerical procedure for identifying the critical curve has been developed using the bisection method, an algorithm for finding the threshold values by means of some upper and lower estimates which are respectively known to be sufficient for ignition and to fail to ignite.

The ingredients of the analytical expressions for the threshold curves are not always explicitly found, except for a few specific ones. For the purpose of finding them numerically, we proceeded to employ a hybrid approach. A numerical estimate of the critical nucleus has been given by the fact that for any initial (or boundary) condition near to the threshold, the solution of the problem approaches to the critical nucleus to

within a small distance and remains in its vicinity for a long time. In the case of moving critical solution, we have provided two different techniques for numerically evaluating the critical solution, one of which is devoted to an operator splitting method for semi-implicit time-stepping in which the critical solution is estimated as the slowest point of the trajectory, and the other is based on the conduction velocity restitution curve requiring solving periodic boundary value problem with the aid of the continuation software AUTO.

Other essential ingredients of the analytical threshold curves are the eigenpairs. To find as many eigenvalues and eigenfunctions as desired, we used a modified power iteration method combined with the Gram-Schmidt orthogonalization procedure. This method, however, may be too expensive computationally, especially when the discrete matrix representation of the right-hand side of the problem is very large. Therefore, we have used the standard implicitly restarted Arnoldi iterations as well for the same purpose.

CHAPTER 5

ONE-COMPONENT SYSTEMS

5.1 Chapter Introduction

The two previous chapters have covered the analytical formulation of the ignition criteria for the initiation problem and the hybrid approach that aims to find the essential ingredients of the analytical theory numerically along with how to obtain the threshold curves by direct numerical simulations. In this chapter, we demonstrate the applicability of the approach on two one-component test problems, both of which have unique, unstable, time-independent critical nucleus solution, whose center-stable manifold is the boundary between ignition and decay. In Section 5.2, we analyse the initiation problem in the Zeldovich-Frank-Kamenetsky (ZFK) equation, one-component reaction-diffusion equation with cubic nonlinearity. The second test problem we consider is the piecewise linear analogue of the ZFK equation, known as the McKean equation and its detailed analysis is provided in Section 5.3. For both model types, two different initiation protocols, namely, initiation by current and initiation by voltage are addressed, and the linear and quadratic approximation of the stable manifold are compared with numerical results. Finally, a brief summary of the chapter given in Section 5.4.

5.2 Zeldovich-Frank-Kamenetsky Equation

In this section, we demonstrate the ignition criteria on one-component bistable reaction-diffusion equation, Zeldovich and Frank-Kamenetsky (ZFK) equation [138]. This equation is also known as "Nagumo equation" [89] and "Schlögl model" [119]. We consider the equation in the following form:

$$\begin{aligned} &k=1, \quad \mathbf{D}=\Big(1\Big), \quad \mathbf{u}=\Big(u\Big), \\ &\mathbf{f}(\mathbf{u})=\Big(f(u)\Big), \quad f(u)=u(u-\theta)(1-u), \end{aligned} \tag{5.1}$$

where θ is the threshold parameter satisfying $\theta \in (0,1/2)$. The critical nucleus solution $\hat{\mathbf{u}}=\Big(\hat{u}\Big)$ for this equation is known exactly [48, 68] [1]

$$\hat{u}(x)=\frac{3\theta\sqrt{2}}{(1+\theta)\sqrt{2}+\cosh(x\sqrt{\theta})\sqrt{2-5\theta+2\theta^2}}. \tag{5.2}$$

The critical curve based on the linear approximation of the critical manifold also requires the first leading eigenvalue λ_1 and corresponding eigenfunction $\mathbf{W}_1=\mathbf{V}_1=\Big(V_1\Big)$ which are solutions of

$$\begin{aligned} &\frac{\mathrm{d}^2V_1}{\mathrm{d}x^2}+\left(-3\hat{u}^2+2(\theta+1)\hat{u}-\theta\right)V_1=\lambda_1 V_1, \\ &\lambda_1>0, \quad V_1(\pm\infty)=0. \end{aligned} \tag{5.3}$$

We have been unable to solve this eigenvalue problem analytically. As stated in reference [68], the critical nucleus given by (5.2) is an even function, therefore $\hat{u}'$ is the eigenfunction of $\mathscr{L}$ corresponding to $\lambda=0$. By Sturm's oscillation theorem, $\hat{u}'=V_2$ and $\lambda_2=0$, and therefore, there is indeed exactly one simple eigenvalue $\lambda_1>0$.

For $\theta \ll 1$, the nonlinear kinetic term can be approximated by $f(u)\approx u(u-\theta)$. Then, the critical nucleus (5.2) is $\mathscr{O}(\theta)$ uniformly in x, and is approximately

$$\hat{u}(x)\approx\frac{3\theta}{1+\cosh(x\sqrt{\theta})}=\frac{3}{2}\theta\,\mathrm{sech}^2(x\sqrt{\theta}/2), \tag{5.4}$$

as in [101]. In the same limit, the eigenvalue problem (5.3) has the solution

$$\lambda_1\approx\frac{5}{4}\theta, \qquad V_1\approx\mathrm{sech}^3(x\sqrt{\theta}/2). \tag{5.5}$$

[1] As pointed out before, expressions given in both of these works contain typos.

5.2.1 Hybrid Approach

Numerical computation of the essential ingredients needed for the linear approximation of the critical curves is carried out using the "shooting" algorithm described in Section 4.4.2. Figure 5.1 illustrates the processes involved in obtaining the critical nucleus (a) and ignition mode (b) in ZFK model numerically. The stimulation is done by fixing the threshold parameter and the excitation width at the values $\theta = 0.15$ and $x_{\rm s} = 0.6$. The left panel of the figure shows how typical functions $S(t)$ are evolved at near-threshold initial conditions. As seen, the minimum value of $S(t)$ is achieved at about $t^{\#} \approx 50$, and therefore the solution $u(x, t^{\#})$ of the nonlinear problem (3.1) provides an estimate of the critical nucleus. Meanwhile, the right panel of the figure is the graph of $\ln|\mathbf{w}(0,t)|$, the solution of the linear problem (4.13) at $x = 0$ in the semilogarithmic coordinates. We observe that the solution after an initial transient, mostly expiring before $t = 10$, grows exponentially. The estimate of the ignition eigenvalue λ_1 is given by the increment of this exponential growth. We also find the numerical estimate of the ignition mode $V_1(x) = W_1(x)$ given by the most recent profile $\mathbf{w}(x,t)/\mathbf{w}(0,t)$ such that it remains almost unchanged, *i.e.* after $t = 10$.

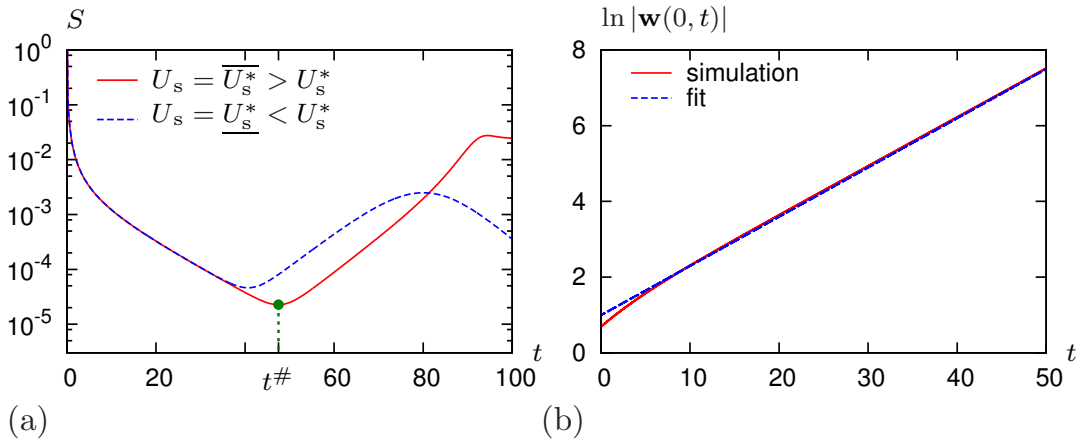

Figure 5.1: Illustration of numerical computation of critical nucleus and ignition mode by "shooting" and "marching" in ZFK. (a) Typical functions $S(t)$ at near-threshold initial conditions in (3.1), (3.4), (3.5), (3.6), (5.1). Parameters: $\theta = 0.15$, $x_{\rm s} = 0.6$, $U_{\rm s}^* \approx 1.1676\ldots$, $|\overline{U_{\rm s}^*} - \underline{U_{\rm s}^*}| < 10^{-5}$, $L = 20$, $\Delta_x = 0.02$, $\Delta_t = 4{\Delta_x}^2/9$. (b) Growth of the numerical solution of (4.13) in semilogarithmic coordinates, and its linear fit, defining the numerical value of λ_1.

The results of these numerical procedures are shown in Figures 5.2 and 5.3. From the plots given in Figure 5.2(a), we can see that the numerical predictions of the critical nuclei obtained using the shooting procedure agree very well with those

derived analytically (5.2) for all threshold parameters θ ranging from 0.05 to 0.45 with increment 0.1, whereas the accuracy of the approximation obtained for $\theta \ll 1$, unsurprisingly, is not good for larger θ. The eigenvalues and corresponding eigenfunctions of the adjoint linearized problem are sketched in Figure 5.2(b) and 5.3. Comparing both analytical formula for the first eigenvalue (5.5) obtained in the limit of small θ and the numerically found first eigenvalue, we see that the two start deviating noticeably already for $\theta \approx 0.1$, and the further increase in θ leads to a monotonic increase for the ignition eigenvalue $\lambda_1(\theta)$ until it approximately reaches to 0.3. From this value on, $\lambda_1(\theta)$ stops increasing and starts decreasing, and the ignition mode V_1 stops shrinking and starts expanding, and later even loses the unimodal shape and becomes bimodal (see $\theta = 0.45$ curve in the top left panel of Figure 5.3).

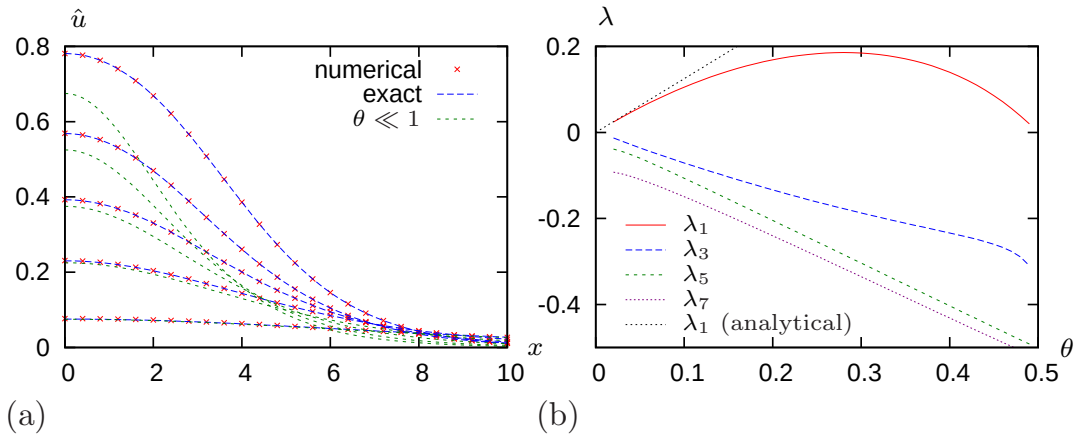

Figure 5.2: Numerical computation of the components of the hybrid approach in ZFK. (a) Critical nucleus solutions for a θ from 0.05 (bottom) to 0.45 (top) with step 0.1: numerical found by shooting, $\hat{u}^{\#}(x)$; exact analytical given by (5.2); approximate analytical for $\theta \ll 1$ given by (5.4). (b) First four eigenvalues, found by marching based on numerical nucleus as functions of θ. Parameters used for numerical computation: $\theta = 0.05, 0.15, 0.25, 0.35, 0.45$, $x_s = 3$, $L = 30$, $\Delta_x = 0.02$, $\Delta_t = 4{\Delta_x}^2/9$.

Figure 5.2(b) also provides insight into the behaviour of λ_j, $j > 1$. The first immediate observation from this figure is that all these eigenvalues are negative, as assumed by the theory. Moreover, the distance $|\lambda_3 - \lambda_5|$ grows with θ, while the distance $|\lambda_5 - \lambda_7|$ remains approximately the same and relatively small. This suggests that the eigenvalue λ_3 lies in the discrete spectrum, while the remaining eigenvalues in the figure λ_5 and λ_7 are located within the continuous spectrum. This is due to the finite length L of the computational interval, and at increasing values of L, the distance $|\lambda_5 - \lambda_7|$ decreases. This is further confirmed by the study of the corresponding eigenfunctions: the eigenfunctions V_1 and V_3 corresponding to the discrete eigenvalues λ_1 and λ_3 are

well localised towards the left end of the interval $x \in [0, L]$, whereas those corresponding to the continuous eigenvalues are evidently non-localised, *i.e.* vary significantly throughout $x \in [0, L]$, as shown in Figure 5.3.

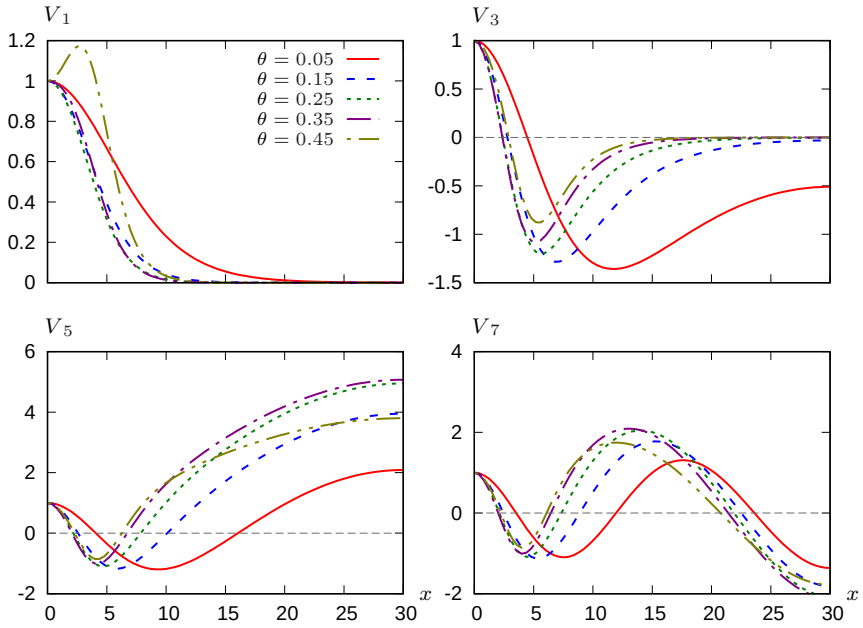

Figure 5.3: Numerical computation of the first four ignition mode of the ZFK equation for a selection of values of θ. Parameters used are same as in Figure 5.2.

5.2.2 Linear Approximation of the Strength-Extent Curve

In the small-threshold limit $\theta \ll 1$, both critical nucleus and the leading eigenpair are exactly known. Substituting them into (3.30) gives an explicit expression for the strength-extent curve in the form [68]

$$U_{\mathrm{s}}^{*} \approx \frac{9\pi\theta}{8\left[4\arctan\left(\mathrm{e}^{\tilde{x_{\mathrm{s}}}}\right) + 2\tanh(\tilde{x_{\mathrm{s}}})\operatorname{sech}(\tilde{x_{\mathrm{s}}}) - \pi\right]}, \tag{5.6}$$

where $\tilde{x_{\mathrm{s}}} = \frac{1}{2} x_{\mathrm{s}} \sqrt{\theta}$.

In particular, if the amplitude of the initial condition is below the threshold parameter, then the ignition is impossible. In other words, the strength-extent curve approximation remains above the *a priori* lower bound (3.56), $\underline{U_{\mathrm{s}}^{*}} = \theta$, for all x_{s}.

Comparison of this approximation with the direct numerical simulations is shown in Figure 5.4(a). Result obtained for small threshold parameter is in close agreement with numerical results, whereas it gets worse when the values of θ get bigger but this

is totally expected as the analytical expressions used are only valid in the limit of small θ.

Comparison of the resulting hybrid numeric-asymptotic prediction with the direct numerical simulations is shown in Figure 5.4(b). As can be seen from the plots, better agreement is observed over the entire parameter range of θ, as opposed the results of the left panel. There are, however, still some large deviations, which are observed when U_{s}^* gets large. The reason for this is that the theory involves a linear approximation, and for large U_{s}^* all A_j are large. We also note that for $U_{\mathrm{s}}^* \lesssim 1$, the hybrid approximation achieves a better accuracy for larger θ. This is because the spectral gap, which is related to the accuracy of the linear approximation, $\lambda_1 - 2\lambda_3$ grows with θ. Please refer to the discussion after equation (3.50) for more detailed explanation.

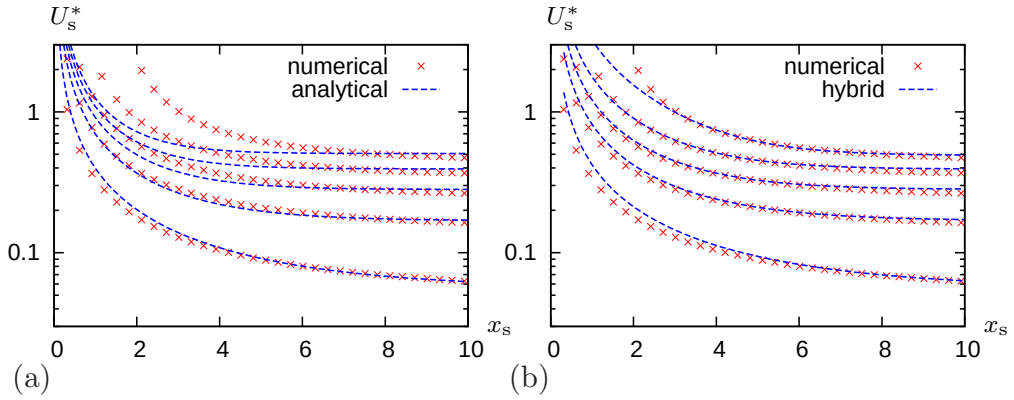

Figure 5.4: Strength-extent curves for the ZFK model, for $\theta = 0.05,\ 0.15,\ 0.25,\ 0.35,\ 0.45$ (bottom to top), comparison of direct numerical simulations (lines with symbols) with theoretical predictions (dashed lines), (a) for the exact analytical answers in the $\theta \ll 1$ limit; (b) for the hybrid method, using the numerically found ignition eigenpairs. Discretization parameters: $\Delta_x = 0.03$, $\Delta_t = 4{\Delta_x}^2/9$, $L = 100$.

5.2.3 Quadratic Approximation of the Strength-Extent Curve

The second-order approximation of the strength-extent curve is characterized by a quadratic equation given by (3.51) whose coefficients involve double infinite sums over stable modes of the linearized problems, and in practice, we cannot evaluate these infinite sums analytically. There is, however, particularly useful information buried within these coefficients, which simplifies the quadratic approximation. This is that these expressions have denominators increasing with the stable mode indices, so one may expect that depending on the properties of the spectrum, the terms in the

series may quickly decay and one can get a sufficiently accurate result by retaining only a few principal terms.

As discussed in the previous subsection, the linearized problem has one discrete stable eigenvalue and the subsequent eigenvalues are part of the continuous spectrum. For convenience, we thus retain only discrete eigenvalues and discard the rest, which gives $n = m = 3$ in (3.51). Therefore, we get a closed expression for the critical curve,

$$U_{\mathrm{s}}^{*} \approx \frac{2R_{3,3}\mathscr{N}_3\mathscr{D}_3 - \mathscr{D}_1 + \sqrt{\mathscr{D}_1^2 + 4R_{3,3}\mathscr{D}_3(\mathscr{N}_1\mathscr{D}_3 - \mathscr{D}_1\mathscr{N}_3)}}{2R_{3,3}\mathscr{D}_3^2} \tag{5.7}$$

or by expanding the square root,

$$U_{\mathrm{s}}^{*} \approx \frac{\mathscr{N}_1}{\mathscr{D}_1} - \frac{Q_{3,3}^{1}(\mathscr{N}_1\mathscr{D}_3 - \mathscr{D}_1\mathscr{N}_3)^2}{\mathscr{D}_1^3(\lambda_1 - 2\lambda_3)}, \tag{5.8}$$

the coefficients in which are defined by (3.48) and (3.53).

The resulting approximations of the critical curves are shown in Figure 5.5. It can be seen from these figures that the quadratic correction term in (5.7) gives noticeably better results for $\theta = 0.05$ and $\theta = 0.15$ when compared with the linear approximation due to the relatively small denominator $(\lambda_1 - 2\lambda_3)$, whereas the results for other threshold parameters are less improved because the linear approximation for those are already reasonably good.

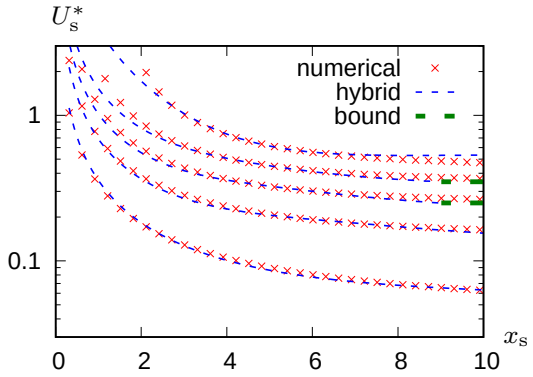

Figure 5.5: Quadratic approximation of the strength-extent curve for ZFK model for $\theta = 0.05,\ 0.15,\ 0.25,\ 0.35,\ 0.45$ (bottom to top) compared with direct numerical simulations (lines with symbols). The lower bound $U_{\mathrm{s}} = \theta$ is indicated by green dashed lines. Parameters: $\Delta_x = 0.03$, $\Delta_t = 4{\Delta_x}^2/9$, $L = 100$.

5.2.4 Linear Approximation of the Strength-Duration Curve

In the small-threshold limit $\theta \ll 1$, the classical Lapicque-Blair-Hill formula (3.64)

$$I_{\mathrm{s}}^{*} = \frac{I_{\mathrm{rh}}}{1 - e^{-\lambda_1 t_{\mathrm{s}}}}, \tag{5.9}$$

has the following rheobase and eigenvalue forms [68]:

$$I_{\mathrm{rh}} = \frac{45}{64}\pi\theta^{3/2}, \quad \lambda_1 = \frac{5\theta}{4}. \tag{5.10}$$

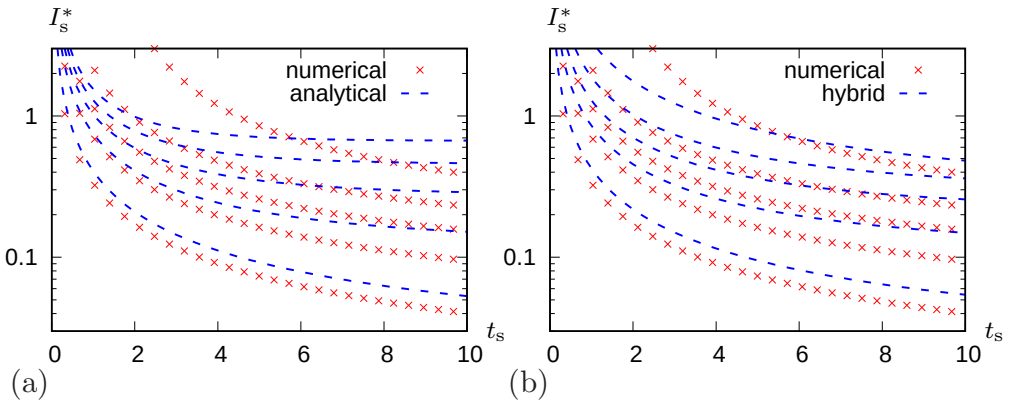

Figure 5.6: Strength-duration curves for the ZFK model, for $\theta = 0.05,\ 0.15,\ 0.25,\ 0.35,\ 0.45$ (bottom to top), comparison of direct numerical simulations (lines with symbols) with theoretical predictions (dashed lines), (a) for the exact analytical answers in the $\theta \ll 1$ limit; (b) for the hybrid method, using the numerically found ignition eigenpairs. Discretization parameters: $\Delta_x = 0.03$, $\Delta_t = 4{\Delta_x}^2/9$, $L = 30$.

Figure 5.6(a) illustrates this approximate strength-duration curve, compared to the direct numerical simulations. For chosen parameter values, the comparison is, yet again, significantly better with smaller values of θ, as expected.

Remark that the performance of the resulting approximation based on the analytical expression for the strength-duration curve (5.9) and (5.10) can be further improved by obtaining the essential ingredients numerically. This is done considering (5.9), in which the rheobase is, instead, defined according to (3.65), as

$$I_{\mathrm{rh}} = \frac{\lambda_1 \int_0^{\infty} V_1(x)\hat{u}(x)\,\mathrm{d}x}{V_1(0)}. \tag{5.11}$$

The plot of the hybrid numeric-asymptotic prediction is compared with the direct numerical simulations as shown in Figure 5.6(b). As depicted in the figure, reasonable

agreement between the two data sets is observed when the threshold parameter is small.

It should be noted that the strength-duration curve approximation remains above the *a priori* lower bound (3.74)

$$\underline{I_{\mathrm{s}}^*} = \left(-2 \int_0^\theta u(u-\theta)(1-u)\,\mathrm{d}u \right)^{1/2} = \frac{\theta^{3/2}\sqrt{(2-\theta)}}{\sqrt{6}},$$

for all t_{s}. However, this bound lies outside of the domain of interest.

5.2.5 Quadratic Approximation of the Strength-Duration Curve

For the quadratic approximation, once again, we retain in (3.71) only the leading term, using the same reasoning as in strength-extent threshold curve analysis. Setting $n = m = 3$ gives a closed expression for the critical curve in the strength-duration plane,

$$\zeta_1 I_{\mathrm{s}}^{*2} + \zeta_2 I_{\mathrm{s}}^* + \zeta_3 = 0, \tag{5.12}$$

where

$$\begin{aligned}
\zeta_1 &= \frac{4Q_{3,3}^1 E_3^2}{\lambda_3^2}\left\{ \frac{1-\mathrm{e}^{-\lambda_1 t_{\mathrm{s}}}}{\lambda_1} - 2\frac{\mathrm{e}^{(\lambda_3-\lambda_1)t_{\mathrm{s}}}-1}{\lambda_3-\lambda_1} - \frac{\mathrm{e}^{-\lambda_1 t_{\mathrm{s}}} - 2\mathrm{e}^{(\lambda_3-\lambda_1)t_{\mathrm{s}}}+1}{2\lambda_3-\lambda_1} \right\}, \\
\zeta_2 &= \frac{4Q_{3,3}^1 A_3 E_3 \left(1-\mathrm{e}^{(\lambda_3-\lambda_1)t_{\mathrm{s}}}\right)}{(2\lambda_3-\lambda_1)(\lambda_3-\lambda_1)} - \frac{2E_1\left(\mathrm{e}^{-\lambda_1 t_{\mathrm{s}}}-1\right)}{\lambda_1}, \\
\zeta_3 &= -\frac{Q_{3,3}^1 A_3^2}{2\lambda_3-\lambda_1} + A_1,
\end{aligned}$$

the coefficients in which are defined by (3.48), (3.70) and (3.72). Figure 5.7 shows the comparison between the quadratic approximation of the critical curves and the numerical curves. Compared to the linear approximation, one can see some significant improvement for $\theta = 0.05,\ 0.15,\ 0.25,\ 0.35$, while the discrepancy between analytical and numerical results continues for $\theta = 0.45$.

5.3 McKean Equation

Our second example is a piecewise-linear representation of the ZFK equation, considered first by McKean in [89] and then also in [111]:

$$\begin{aligned}
&k = 1, \quad \mathbf{D} = \Big(1\Big), \quad \mathbf{u} = \Big(u\Big), \\
&\mathbf{f}(\mathbf{u}) = \Big(f(u)\Big), \quad f(u) = -u + \mathrm{H}(u-a),
\end{aligned} \tag{5.13}$$

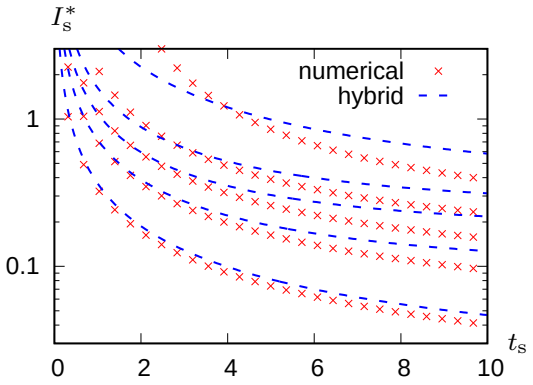

Figure 5.7: Quadratic approximation of the strength-extent curve for ZFK model for $\theta = 0.05, 0.15, 0.25, 0.35, 0.45$ (bottom to top) compared with direct numerical simulations (lines with symbols). Parameters: $\Delta_x = 0.03$, $\Delta_t = 4{\Delta_x}^2/9$, $L = 100$.

where we assume that $a \in (0, 1/2)$, and $\mathrm{H}(\cdot)$ is the Heaviside step function. In contrast to the ZFK equation with smooth right-hand side, this model has a discontinuous right-hand side, similar to the front model we consider in the following chapter. Using direct numerical simulations based on finite differences leads to qualitatively different behaviour from expected due to this discontinuity: the discretized critical nucleus solution is not unique and is stable, although it is expected to be an even, ***unique***, ***unstable***, nontrivial time-independent solution of the discretized equation. This phenomenon is somehow similar to "propagation block" or "propagation failure" observed in several different forms of discrete reaction-diffusion system (see *e.g.* [37, 62, 65, 72]), with the exception is that here we are dealing with even solutions and spatially localised solutions. It has been established that the generic system with a smooth cubic nonlinearity has "frozen solutions" for sufficiently large discretization steps [72]. For the McKean model with its discontinuous right-hand side, the frozen solutions, however, exist for *all* discretization steps. The details of the non-uniqueness and stability of the discrete critical nucleus are contained in Appendix B. This motivates us to use the finite-element approach to the numerical computation of the essential ingredients of the theory, the critical nucleus and the ignition mode, as well as the critical curves. The finite-element approach is discussed in detail in Appendix A.

The critical nucleus solution in this equation is found exactly in a closed form,

$$\hat{u}(x) = \begin{cases} 1 - (1-a)\dfrac{\cosh(x)}{\cosh(x_*)}, & x \le x_*, \\ a\,\exp(x_* - x), & x \ge x_*, \end{cases} \tag{5.14}$$

where

$$x_* = \frac{1}{2}\ln\left(\frac{1}{1-2a}\right) \tag{5.15}$$

obtained by the fact that $\hat{u}(x)$ and its derivative are continuous at this point. This solution is illustrated in Figure 5.9(a).

5.3.1 Analytical Derivation of the Eigenvalue Problem

In this subsection, we turn our attention to the solution to the eigenvalue problem of the McKean equation. As the right-hand side of this equation includes the discontinuous Heaviside step function, its linearization contains the Dirac delta function, and thus the linearized equation becomes singular. We present a precise formulation of eigenvalue problem and solution of it below.

To begin with, we linearize (5.13) around critical nucleus using

$$u = \hat{u}(x) + \epsilon u_1(x,t),$$

where ϵu_1 is a small perturbation, $\epsilon \ll 1$. Then, (5.13) becomes

$$\epsilon\frac{\partial u_1}{\partial t} = \frac{\mathrm{d}^2\hat{u}}{\mathrm{d}x^2} + \epsilon\frac{\partial^2 u_1}{\partial x^2} + f(\hat{u}+\epsilon u_1). \tag{5.16}$$

Taking a linear Taylor series expansion to express $f(\hat{u}+\epsilon u_1)$ in the form

$$f(\hat{u}+\epsilon u_1) = f(\hat{u}) + \epsilon\frac{\partial f}{\partial u}(\hat{u})\,u_1 + \mathcal{O}\left(\epsilon^2\right).$$

Using the definition of Dirac delta function $\delta(u) = \frac{\mathrm{dH}(u)}{\mathrm{d}u}$ and the chain rule, we have

$$\left[\frac{\partial f}{\partial u}\right]_{u=\hat{u}} = -1 + \left[\frac{\partial \mathrm{H}(u-a)}{\partial u}\right]_{u=\hat{u}} = -1 + \frac{\partial \mathrm{H}(x_*-x)}{\partial x}\Big/\frac{\partial \hat{u}}{\partial x}\Big|_{x=x_*} = -1 - \frac{1}{\hat{u}'(x_*)}\delta(x-x_*).$$

By neglecting higher order terms, equation (5.16) thus reduces to

$$\frac{\partial u_1}{\partial t} = \frac{\partial^2 u_1}{\partial x^2} + \left(-1 + \frac{1}{a}\delta(x-x_*)\right)u_1. \tag{5.17}$$

Consider the solution of the linearized equation (5.17) of the form $u_1(x,t) = \mathrm{e}^{\lambda t}V(x)$ which leads to the following eigenvalue problem

$$\lambda V = \frac{\mathrm{d}^2 V}{\mathrm{d}x^2} + \left(-1 + \frac{1}{a}\delta(x-x_*)\right)V, \tag{5.18}$$

where $V(x)$ are some eigenfunctions. This eigenvalue problem can also be expressed as

$$\lambda V = \mathscr{L} V, \tag{5.19}$$

where the linearization operator is

$$\mathscr{L} \triangleq \frac{\partial^2}{\partial x^2} - 1 - \frac{1}{a}\delta(x - x_*). \tag{5.20}$$

Due to the singular term in the eigenvalue problem (5.18), it is not straightforward to obtain the solution. To tackle this singularity, we integrate (5.18) from $x_* - \rho$ to $x_* + \rho$

$$\int_{x_*-\rho}^{x_*+\rho} \lambda V(x)\,\mathrm{d}x = \int_{x_*-\rho}^{x_*+\rho} V''(x)\,\mathrm{d}x - \int_{x_*-\rho}^{x_*+\rho} V(x)\,\mathrm{d}x + \frac{1}{a}\int_{x_*-\rho}^{x_*+\rho} \delta(x - x_*)V(x)\,\mathrm{d}x,$$

for an arbitrary constant ρ. Taking the limit as $\rho \to 0$, we obtain the following condition

$$V'(x_* + 0) - V'(x_* - 0) + \frac{1}{a}V(x_*) = 0. \tag{5.21}$$

Using this condition along with assumption that we are looking for an even function V which is bounded as $x \to \infty$, we can conclude that the eigenvalue problem (5.18) is equivalently written as

$$\frac{\mathrm{d}^2 V(x)}{\mathrm{d}x^2} - (\lambda + 1)V(x) = 0, \tag{5.22a}$$

$$V(\infty) = 0, \quad V'(0) = 0, \quad V'(x_* + 0) - V'(x_* - 0) + \frac{1}{a}V(x_*) = 0. \tag{5.22b}$$

This problem has one positive eigenvalue. This eigenvalue and the corresponding eigenfunction can be written in the form

$$\begin{aligned} \lambda_1 &= -1 + \kappa^2, \\ V_1 &= \begin{cases} \dfrac{\cosh(\kappa x)}{\cosh(\kappa x_*)}, & x \le x_*, \\ \exp(\kappa(x_* - x)), & x \ge x_*, \end{cases} \end{aligned} \tag{5.23}$$

where

$$\kappa = \frac{1}{2a} + \frac{1}{2x_*}\mathrm{W}_0\left(\frac{x_*}{a}\,\mathrm{e}^{-x_*/a}\right) \tag{5.24}$$

and $\mathrm{W}_0(\cdot)$ is the principal branch of the Lambert W-function as defined *e.g.* in [29]. Remark that in the eigenvalue formulation, Lambert W-function always returns a positive real value for all values of a in the range $(0, 1/2)$ and therefore, it is guaranteed that λ_1 is a positive definite function of a.

5.3.1.1 Asymptotic Analysis of the Eigenvalue

Alternatively, the leading eigenvalue can be asymptotically obtained. Employing the condition (5.21) and the continuity property of V_1 at x_*, we have

$$\tanh(\nu) = -1 + \frac{\theta}{\nu}, \tag{5.25}$$

or equivalently,

$$\mathrm{e}^{2\nu}(2\nu - \theta) = \theta, \tag{5.26}$$

where $\nu = \kappa x_* = \frac{\kappa}{2}\ln\left(\frac{1}{1-2\alpha}\right) > 0$ and $\theta = x_*/\alpha > 0$. The domain of the threshold parameter α can be redefined as $\alpha = 1/2 - \alpha$ where $\alpha \in (0, 1/2)$. First, we examine asymptotic estimation of eigenvalue when $\alpha \to 0$. In this case,

$$\theta = \frac{\beta}{1-\mathrm{e}^{-\beta}}, \quad x_* = \frac{\beta}{2},$$

where $\beta = -\ln(2\alpha)$ and $\beta \to \infty$ as $\alpha \to 0$. In the limit of small α, we derive the following expressions:

$$\mathrm{e}^{-\theta} = \exp\left[-\beta\left(1-\mathrm{e}^{-\beta}\right)^{-1}\right] = \exp\left[-\beta + \mathcal{O}\left(\beta\mathrm{e}^{-\beta}\right)\right] = \mathrm{e}^{-\beta}\left[1 + \mathcal{O}\left(\beta\mathrm{e}^{-\beta}\right)\right],$$

$$\theta\mathrm{e}^{-\theta} = \frac{\beta\mathrm{e}^{-\beta}\left[1 + \mathcal{O}\left(\beta\mathrm{e}^{-\beta}\right)\right]}{1 + \mathcal{O}\left(\mathrm{e}^{-\beta}\right)} \approx \beta\mathrm{e}^{-\beta}\left[1 + \mathcal{O}\left(\beta e^{-\beta}\right) - \mathcal{O}\left(\mathrm{e}^{-\beta}\right)\right] \approx \beta\mathrm{e}^{-\beta}\left[1 + \mathcal{O}\left(\beta\mathrm{e}^{-\beta}\right)\right],$$

where we have used L'Hôpital's rule and the fact that $\mathcal{O}\left(\mathrm{e}^{-\beta}\right) \ll \mathcal{O}\left(\beta\mathrm{e}^{-\beta}\right)$. Hence, $\theta\mathrm{e}^{-\theta} \to 0$ as $\beta \to \infty$ which is why Taylor series of the Lambert W-function around 0 can be used

$$\mathrm{W}_0\left(\theta\mathrm{e}^{-\theta}\right) \approx \theta e^{-\theta} + \mathcal{O}\left(\theta^2\right).$$

Therefore, κ can in turn be written as

$$\begin{aligned}\kappa = \frac{\theta + \mathrm{W}_0\left(\theta\mathrm{e}^{-\theta}\right)}{2x_*} &\approx \frac{\theta + \theta e^{-\theta}}{\beta} = \frac{1}{1-\mathrm{e}^{-\beta}} + \mathrm{e}^{-\beta}\left[1 + \mathcal{O}\left(\beta\mathrm{e}^{-\beta}\right)\right] \\ &\approx 1 + 2\mathrm{e}^{-\beta} + \mathcal{O}\left(\beta\mathrm{e}^{-2\beta}\right) = 1 + 4\alpha + O\left(\alpha^2\ln(\alpha)\right)\end{aligned} \tag{5.27}$$

and corresponding asymptotic formula for λ_1 in terms of α is

$$\lambda_1^{(1/2)} = 8\alpha + \mathcal{O}\left(\alpha^2\ln(\alpha)\right). \tag{5.28}$$

The above expression is plausible when $\alpha \to 1/2$. For the case $\alpha \to 0$, we have $x_* \approx \alpha$, $\theta \approx 1$ and assume that $\lim_{\alpha\to 0}\nu = \nu_*$. The value of ν_* is obtained from the transcendental equation (5.25) as

$$\nu_* = \frac{1}{2}\mathrm{W}_0\left(e^{-1}\right) + \frac{1}{2} \approx 0.6392,$$

from which the asymptotic approximate eigenvalue can be written as a function of a

$$\lambda_1^{(0)} \approx \frac{\nu_*^2}{a^2} \approx \frac{0.4086}{a^2}. \tag{5.29}$$

The behaviour of the analytical and asymptotic eigenvalue analysis at different values of a is illustrated in Figure 5.8.

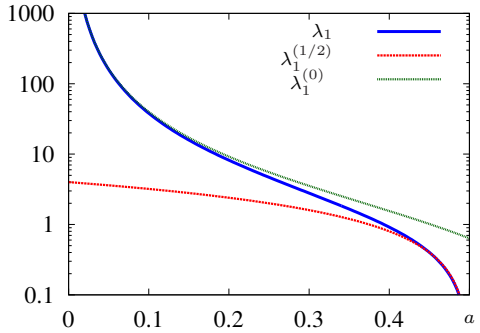

Figure 5.8: The sketch of the asymptotic behaviour of the principal eigenvalue compared with analytically found ignition eigenvalue.

5.3.2 Hybrid Approach

In this model, since the exact analytical solution for the critical nucleus and the ignition eigenpair are known for an arbitrary $a \in (0, 1/2)$, the "hybrid approach" is not necessary. However, for technical purposes, we address it here as well, to show when the approach used with finite-element discretization it works satisfactorily.

Figure 5.9 illustrates the processes of numerical computation of the critical nucleus and the ignition mode in McKean model for a range of threshold parameter varying from 0.05 to 0.45 with increment 0.1. As seen in the top panel of this figure, the minimum of $S(t)$ decreases when a increases. To obtain the minimum of $S(t)$ and $t^{\#} = \mathrm{argmin}(S(t))$, the bisection loop is terminated as long as the absolute difference between upper and lower estimate for the threshold is sufficiently small, *i.e.* $|\overline{U_{\mathrm{s}}^*} - \underline{U_{\mathrm{s}}^*}| < 10^{-7}$. The numerical estimate of the critical nucleus is then found taking $\hat{u}^{\#}(x) = u(x, t^{\#})$. The sketch of these numerical critical nuclei compared with corresponding exact solutions is shown in the left bottom panel of Figure 5.9.

We now proceed to calculate the principal eigenpair numerically. Equation (5.17) has solution in the form

$$u_1 = \sum_{j=1}^{\infty} a_j \mathrm{e}^{\lambda_j t} V_j(x), \quad a_1 \neq 0,$$

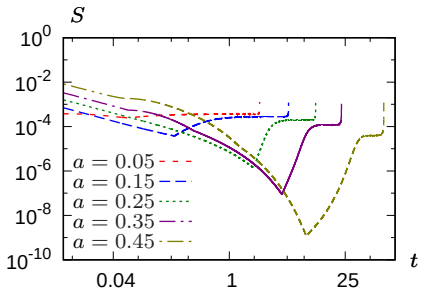

a	$t^{\#}$	U_{s}^{*}
0.05	0.06	0.0500011
0.15	0.21	0.1500153
0.25	1.98	0.3395199
0.35	4.33	0.7057082
0.45	8.53	1.7306417

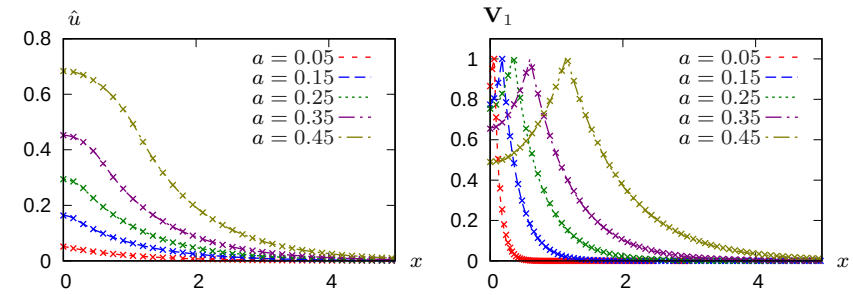

Figure 5.9: Critical nucleus solutions and ignition modes of the McKean model (5.13) for various values of the parameter a varying from 0.05 to 0.45 with increment 0.1. In the bottom panel, the dashed lines and lines with symbols represent the analytical and numerical approximations, respectively. Parameters used: $x_{\mathrm{s}} = 0.6$, $\Delta_x = 0.03$, $\Delta_t = 4{\Delta_x}^2/9$, $|\overline{U_{\mathrm{s}}^{*}} - \underline{U_{\mathrm{s}}^{*}}| < 10^{-7}$, $L = 10$.

which yields

$$u_1(x,t) \approx a_1 \mathrm{e}^{\lambda_1 t} V_1(x), \tag{5.30}$$

as $t \to \infty$ since $a_2 = 0$ because the critical nucleus is an even function and its derivative corresponds to the second eigenfunction, and $\lambda_j < 0$ for all $j \geq 3$. Fixing a_1 using the fact that the ignition mode is normalized with its maximum at $x = 0$, *i.e.* $V_1(0) = 1$ results in

$$V_1(x) \approx \frac{u_1(x,t)}{u_1(0,t)}.$$

The comparison between this numerical eigenfunction and exact analytical eigenfunction is depicted in the right bottom panel of Figure 5.9. As seen, the numerical solution produces a good approximation of the analytical one for every threshold parameter considered.

As an alternative approach to the standard marching procedure of identifying the ignition eigenvalue discussed in Section 4.4, we use the least-square method. From (5.30), we have the following condition for the principal eigenvalue

$$\ln(u_1(0,t)) \approx \ln(a_1) + \lambda_1 t,$$

for all $t > 0$.For a given data set $\{(t_s, \ln[u_1(0,t_s)]), \ldots, (t_n, \ln[u_1(0,t_n)])\}$, we obtain the following expression for leading eigenvalue λ_1 using the least-square method

$$\lambda_1 = \frac{\left(\sum\limits_{j=s}^{n} \ln\left(u_1\left(0,t_j\right)\right)\right) \times \left(\sum\limits_{j=s}^{n} t_j\right) - \left(\sum\limits_{j=s}^{n} t_j \ln\left(u_1\left(0,t_j\right)\right)\right) \times (n-s+1)}{\left(\sum_{j=s}^{n} t_j\right)^2 - \left(\sum\limits_{j=s}^{n} t_j^2\right) \times (n-s+1)}. \tag{5.31}$$

The computation of this eigenvalue expression for two different discretization steps

Discretization step	$\Delta_x = 0.03$	$\Delta_x = 0.01$
Analytical eigenvalue	2.2714	2.2714
Standard marching	2.2453	2.2627
Least-square	2.3391	2.2852

Table 5.1: The comparison between exact analytical eigenvalue and numerical ones obtained by the standard marching procedure and least-square method. Parameters: $t_s = 0.8$, $t_n = 25$, $a = 0.32$, $L = 15$.

compared with the numerical prediction based on the standard marching procedure and corresponding exact eigenvalue is given in Table 5.1. As seen, using the marching method to compute the leading eigenvalue gives a more accurate result.

5.3.3 Linear Approximation of the Strength-Extent Curve

Substituting (5.14), (5.15), (5.23), (5.24) into (3.25), we obtain the analytical expression for the strength-extent curve,

$$U_{\mathrm{s}}^*(x_{\mathrm{s}}) = \begin{cases} \dfrac{\kappa \mathcal{N}}{\sinh(\kappa x_{\mathrm{s}})}, & x_{\mathrm{s}} < x_*, \\ \dfrac{\kappa \mathcal{N}}{\sinh(\kappa x_{\mathrm{s}}) - \cosh(\kappa x_{\mathrm{s}})\left(\mathrm{e}^{\kappa(x_* - x_{\mathrm{s}})} - 1\right)}, & x_{\mathrm{s}} > x_*, \end{cases} \tag{5.32}$$

where

$$\mathcal{N} = \frac{\sinh(\kappa x_*)}{\kappa} + \frac{a}{\kappa+1}\cosh(\kappa x_*) - \frac{1-a}{2\cosh(x_*)}\left(\frac{\sinh((\kappa+1)x_*)}{\kappa+1} + \frac{\sinh((\kappa-1)x_*)}{\kappa-1}\right).$$

Figure 5.10(a) shows this theoretical prediction compared with the direct numerical simulations. As in ZFK equation, the ignition is impossible if the amplitude of the initial condition is below the threshold parameter. Hence, we require to apply the *a priori* bound $U_{\mathrm{s}}^* = a$ to improve the theoretical prediction. This is also shown in the figure.

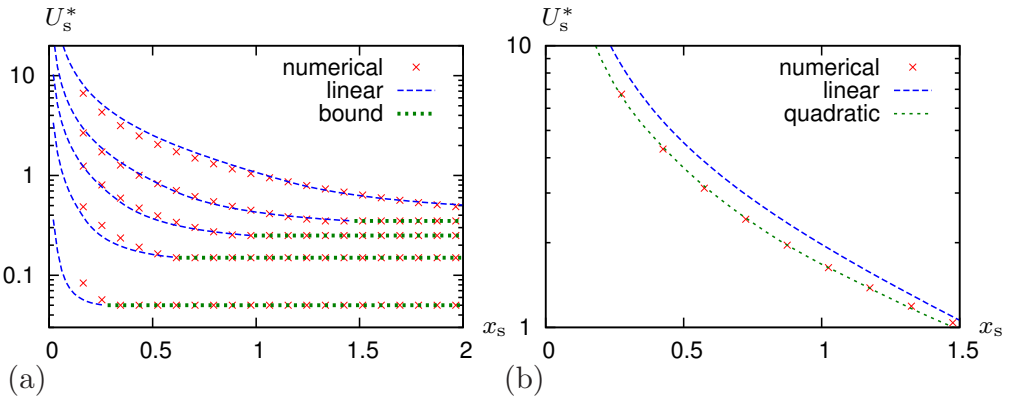

Figure 5.10: Strength-extent curves in McKean model: direct numerical simulations (red circles) vs (a) linear theory, for $a = 0.05$ at the bottom increased by 0.1 to $a = 0.45$ at the top, and (b) linear and quadratic theories, for $a = 0.48$. Blue long-dashed lines: analytical dependencies given by (5.32). Green short-dashed lines: the lower bound $U_s = a$ in (a) and the predictions given by quadratic theory in (b). Discretization: $\Delta_x = 0.01$, $\Delta_t = 4{\Delta_x}^2/9$, $L = 10$.

5.3.4 Quadratic Approximation of the Strength-Extent Curve

The linear approximation of the strength-extent curve can be improved by considering the second-order approximation. This is particularly needed when obtaining the threshold curve for the parameter a close to $1/2$ in which case the analytical strength-extent curves move away from its numerical predictions.

To obtain the quadratic approximation of the critical curve, we adopt the method described in Section 3.3.2. For our scalar McKean model, we have $f^{\alpha}{}_{,\beta\gamma} = f''$ and $\overline{W^{\alpha}{}_1(x)} = V_1(x)$. Further, we define the expressions of $Q^1_{m,n}$ and A_j as

$$Q^1_{m,n} = Q^1_{n,m} \triangleq \frac{1}{2}\int_{-\infty}^{\infty} \overline{W^{\alpha}{}_1(x)}\, f^{\alpha}{}_{,\beta\gamma}(\hat{\mathbf{u}}(x)) V^{\beta}{}_m(x) V^{\gamma}{}_n(x)\,\mathrm{d}x$$
$$= \frac{\int_{-\infty}^{\infty} V_1(x) f''(\hat{u}(x)) V_m(x) V_n(x)\,\mathrm{d}x}{2\,\|V_1\|\cdot\|V_m\|\cdot\|V_n\|}, \tag{5.33}$$

$$A_j \triangleq a_j(0) = \int_{-\infty}^{\infty} W^{\alpha}{}_j(x) v^{\alpha}(x,0)\,\mathrm{d}x = \frac{\int_{-\infty}^{\infty} [u(x,0) - \hat{u}(x)] V_j(x)\,\mathrm{d}x}{\|V_j\|}, \tag{5.34}$$

where the eigenfunctions are normalized.

For the quadratic approximation, the knowledge of the whole spectrum is ideally required. We know that the linearization spectrum of the critical nucleus has only one unstable eigenvalue $\lambda_1 > 0$, and due to translational symmetry, $\lambda_2 = 0$, and the rest of

the spectrum lies entirely in the left half-plane. The first aim of this part of the section is to find these remaining stable eigenvalues and corresponding eigenfunctions. To obtain these eigenpairs, we replace the infinite interval $[0,\infty)$ by a finite interval $[0,L]$ with a homogeneous Dirichlet boundary condition at $x=L$, aiming to consider the limit $L\to\infty$.

The solution of eigenvalue problem (5.22) in this case is the linear combination of the pair of trigonometric functions $\{\cos(\mu x),\sin(\mu x)\}$ with μ being a positive constant where $\lambda=-1-\mu^2$. For each case $x<x_*$ and $x>x_*$, the solution has the same form

$$V_\mu(x)=\begin{cases} c_1\cos(\mu x)+c_2\sin(\mu x), & x<x_*,\\ c_3\cos(\mu x)+c_4\sin(\mu x), & x_*<x,\end{cases} \tag{5.35}$$

where c_i, $i=1,2,3,4$ are constants to be determined. Employing the homogeneous Dirichlet boundary condition at $x=L$, the continuity condition at $x=x_*$ and the equality (5.21) gives the following relations between these four unknown coefficients:

$$\begin{aligned} &c_2=0,\\ &(c_1-c_3)\cos\left(\mu x_*\right)=c_4\sin\left(\mu x_*\right),\\ &c_3\sin\left(\mu x_*\right)-c_4\cos\left(\mu x_*\right)=c_1\left(\sin\left(\mu x_*\right)+\frac{1}{a\mu}\cos\left(\mu x_*\right)\right),\\ &c_3\cos\left(\mu L\right)=-c_4\sin\left(\mu L\right). \end{aligned} \tag{5.36}$$

This enables us to deduce the following transcendental equation for μ in terms of a, x_* and L,

$$h\left(\mu\right)\triangleq\tan\left(\mu L\right)-\tan\left(\mu x_*\right)-\frac{a\mu}{\cos^2\left(\mu x_*\right)}=0, \tag{5.37}$$

and the corresponding generalized eigenfunction in the form

$$V_\mu(x)=\begin{cases} -a\mu\cos\left(\mu x\right), & x<x_*,\\ -\left[a\mu+\sin\left(\mu x_*\right)\cos\left(\mu x_*\right)\right]\cos\left(\mu x\right)+\cos^2\left(\mu x_*\right)\sin\left(\mu x\right), & x_*<x.\end{cases} \tag{5.38}$$

Now, we investigate the asymptotic behaviour of the transcendental equation (5.37). When $\mu\to 0$ and $L\to\infty$ we have $\mu\sim L^{-1}$ such that $\mu x_*\to 0$, $\cos\left(\mu x_*\right)\approx 1$, $\sin\left(\mu x_*\right)\approx \mu x_*$. Hence the transcendental equation reduces to

$$\tan\left(\eta\right)=\frac{a+x_*}{L}\eta, \tag{5.39}$$

where $\eta=\mu L$. For any positive integer k, we define $\eta=k\pi+\epsilon_k$ for $|\epsilon_k|\ll 1$. Thus, the left-hand side of the last equality simplifies to

$$\tan(k\pi+\epsilon_k)=\tan(\epsilon_k)\approx\epsilon_k,$$

and the right-hand side of which becomes

$$\frac{a+x_*}{L}(k\pi+\epsilon_k)\approx\frac{a+x_*}{L}k\pi.$$

Hence η is in turn

$$\eta\approx k\pi\left(1+\frac{a+x_*}{L}\right)$$

and finally μ can be obtained explicitly as

$$\mu=\frac{\eta}{L}=\frac{k\pi}{L}\left(1+\frac{a+x_*}{L}\right)\approx\frac{k\pi}{L}. \tag{5.40}$$

For these asymptotic values, the eigenfunction expression also simplifies to

$$V_k(x)=\begin{cases}\tan\left(\frac{k\pi}{L}x_*\right)\cos\left(\frac{k\pi}{L}x\right), & x<x_*,\\ \sin\left(\frac{k\pi}{L}x\right), & x_*<x.\end{cases} \tag{5.41}$$

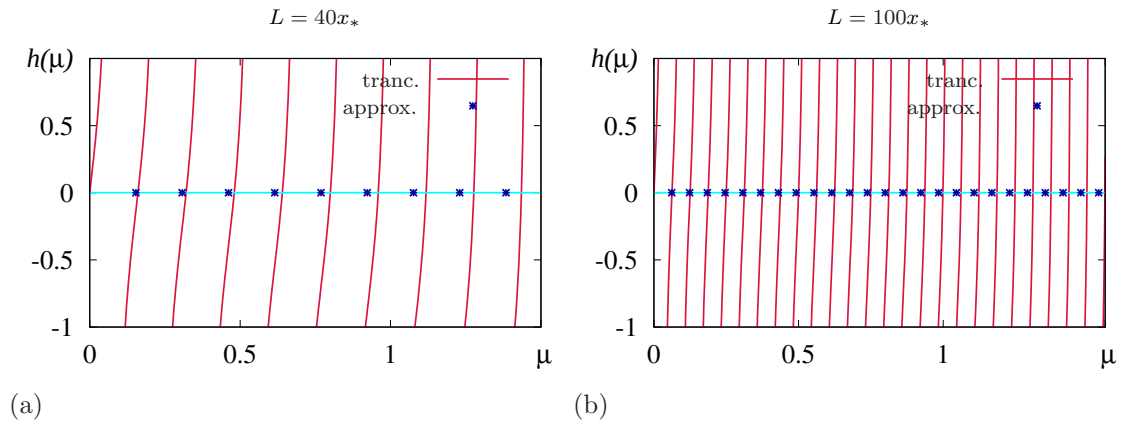

Figure 5.11: The sketch of the roots of the transcendental eigenvalue equation compared with the approximate eigenvalue for two different choices of the domain length (a) $L=40x_*$ and (b) $L=100x_*$ where the threshold parameter is set to $a=0.32$.

Figure 5.11 illustrates the comparison between the roots of the transcendental equation (5.37) and explicit asymptotic form of μ given by (5.40) within two bounded domains $L=40x_*$ and $L=100x_*$. As seen from the figure, it is no surprising that the asymptotic estimations get closer to their analytical counterparts when the considered domain L is increased. However, the larger L results in high computational cost due to the number of eigenvalues and eigenfunctions growing with the domain size. For this reason, we stick to the transcendental equation (5.37) in order to obtain the values of μ and hence, the stable eigenvalues via $\lambda=-1-\mu^2$ and their associated eigenfunctions. Note that the stable spectrum of the linearized problem is entirely continuous.

After finding analytical expressions for the eigenpairs, the next step is to calculate $Q^1_{m,n}$, A_j and A_1. When calculating $Q^1_{m,n}$ (5.33) there occurs a discontinuity at $x = x_*$ that can be removed by modifying the Heaviside step function as

$$\hat{\mathrm{H}}(x) = \frac{1}{2} + \frac{1}{\pi}\arctan(x/\epsilon), \tag{5.42}$$

for a small parameter ϵ. Hence, $f''(\hat{u}(x))$ becomes

$$f''(\hat{u}(x)) = -\frac{2(x_* - x)\epsilon}{a^2\pi\left[(x_* - x)^2 + \epsilon^2\right]^2}. \tag{5.43}$$

For reducing the size of the equations, we introduce the following short notations:

$$\begin{aligned} &C_\eta^{x_*} = \cos\left(\mu_\eta x_*\right), \quad C_\eta^{x_s} = \cos\left(\mu_\eta x_s\right), \quad S_\eta^{x_*} = \sin\left(\mu_\eta x_*\right), \quad S_\eta^{x_s} = \sin\left(\mu_\eta x_s\right), \\ &T_\eta^{x_*} = \tan\left(\mu_\eta x_*\right), \quad H_c^{x_*} = \cosh(k x_*), \quad H_s^{x_*} = \sinh(k x_*), \text{ for } \quad \eta = m, n. \end{aligned}$$

the expression for $Q^1_{m,n}$ can thus be rewritten as

$$Q^1_{m,n} = \frac{\int_0^L V_1(x) f''(\hat{u}(x)) V_m(x) V_n(x)\,\mathrm{d}x}{\|V_1\| \cdot \|V_m\| \cdot \|V_n\|} = \frac{2a^2\epsilon\mu_m\mu_n I_1 + 2\epsilon H_c^{x_*} I_2}{a^2\pi\,\|V_1\| \cdot \|V_m\| \cdot \|V_n\|},$$

where

$$\begin{aligned} I_1 &= -\int_0^{x_*} \cosh(\kappa x)\frac{(x_* - x)\cos\left(\mu_m x\right)\cos\left(\mu_n x\right)}{\left[\epsilon^2 + (x_* - x)^2\right]^2}\,\mathrm{d}x, \\ I_2 &= -\int_{x_*}^{L} \mathrm{e}^{\kappa(x_* - x)}\frac{(x_* - x)\left(-\left[a\mu_m + S_m^{x_*}C_m^{x_*}\right]\cos\left(\mu_m x\right) + \left(C_m^{x_*}\right)^2\sin\left(\mu_m x\right)\right)}{\left[\epsilon^2 + (x_* - x)^2\right]^2} \\ &\quad \times \left(-\left[a\mu_n + S_n^{x_*}C_n^{x_*}\right]\cos\left(\mu_n x\right) + \left(C_n^{x_*}\right)^2\sin\left(\mu_n x\right)\right)\mathrm{d}x. \end{aligned}$$

Now, we first perform the change of variable $y = \frac{x_* - x}{\epsilon}$ and use the following second-order Taylor series to approximate these two definite integrals

$$\begin{aligned} &\sin(\gamma(x_* - \epsilon y)) = \sin\left(\gamma x_*\right) - \gamma\epsilon y\cos\left(\gamma x_*\right) + \mathcal{O}\left(\epsilon^2\right), \\ &\cos(\gamma(x_* - \epsilon y)) = \cos\left(\gamma x_*\right) + \gamma\epsilon y\sin\left(\gamma x_*\right) + \mathcal{O}\left(\epsilon^2\right), \\ &\exp(\epsilon y) = 1 + \epsilon y + \mathcal{O}\left(\epsilon^2\right), \end{aligned}$$

for any scalar γ. Thus, I_1 and I_2 are evaluated as

$$
\begin{aligned}
I_1 =& -\frac{1}{\epsilon^2}\int_0^{x_*/\epsilon}\left[H_c^{x_*}-\kappa\epsilon y H_s^{x_*}\right]\cdot\left[C_m^{x_*}+\mu_m\epsilon y S_m^{x_*}\right]\cdot\left[C_n^{x_*}+\mu_n\epsilon y S_n^{x_*}\right]\cdot\frac{y}{\left(1+y^2\right)^2}\,\mathrm{d}y,\\
=& -\left(\frac{H_c^{x_*}C_m^{x_*}S_n^{x_*}\mu_n+H_c^{x_*}C_n^{x_*}S_m^{x_*}\mu_m-kH_s^{x_*}C_m^{x_*}C_n^{x_*}}{2\epsilon}\right)\times\left(\arctan\left(\frac{x_*}{\epsilon}\right)-\frac{\epsilon x_*}{\epsilon^2+{x_*}^2}\right)\\
&-\frac{H_c^{x_*}C_m^{x_*}C_n^{x_*}}{2\epsilon^2}\left(1-\frac{\epsilon^2}{\epsilon^2+{x_*}^2}\right)+\mathcal{O}(1),\\
I_2 =& -\frac{1}{\epsilon^2}\int_{-(L-x_*)/\epsilon}^{0}\left[-\left(a\mu_m+S_m^{x_*}C_m^{x_*}\right)\left(C_m^{x_*}+\mu_m\epsilon y S_m^{x_*}\right)+\left(C_m^{x_*}\right)^2\left(S_m^{x_*}-\mu_m\epsilon y C_m^{x_*}\right)\right]\times\\
&\left[-\left(a\mu_n+S_n^{x_*}C_n^{x_*}\right)\left(C_n^{x_*}+\mu_n\epsilon y S_n^{x_*}\right)+\left(C_n^{x_*}\right)^2\left(S_n^{x_*}-\mu_n\epsilon y C_n^{x_*}\right)\right]\cdot\frac{(1+\kappa\epsilon y)\,y}{\left(1+y^2\right)^2}\,\mathrm{d}y\\
=&\frac{a}{2\epsilon}\left[\mu_m\mu_n C_n^{x_*}\left(a\mu_m S_m^{x_*}+C_m^{x_*}\right)+\mu_n\mu_m C_m^{x_*}\left(a\mu_n S_n^{x_*}+C_n^{x_*}\right)+\kappa a\mu_m\mu_n C_m^{x_*}C_n^{x_*}\right]\\
&\times\left(\arctan\left(-\frac{L-x_*}{\epsilon}\right)+\frac{(L-x_*)\epsilon}{(L-x_*)^2+\epsilon^2}\right)-\frac{a^2\mu_m\mu_n C_m^{x_*}C_n^{x_*}}{2\epsilon^2}\left(\frac{\epsilon^2}{\epsilon^2+(L-x_*)^2}-1\right)+\mathcal{O}(1).
\end{aligned}
$$

By taking the limit $\epsilon\to 0$, we obtain

$$
\begin{aligned}
Q_{m,n}^1 =& -\frac{1}{\|V_1\|\cdot\|V_m\|\cdot\|V_n\|}\left\{H_c^{x_*}\left[\mu_m\mu_n\left(C_m^{x_*}S_n^{x_*}\mu_n+C_n^{x_*}S_m^{x_*}\mu_m\right)+\frac{\mu_m\mu_n C_m^{x_*}C_n^{x_*}}{a}\right]\right.\\
&\left.+\frac{\mu_m\mu_n C_m^{x_*}C_n^{x_*}\mathrm{e}^{-\kappa x_*}}{2}\right\},
\end{aligned}
\tag{5.44}
$$

where the L^2-norm of the eigenfunctions are

$$
\begin{aligned}
\|V_1\| &= \sqrt{2}\left\{\frac{1}{2\kappa}\left[\cosh(\kappa x_*)\sinh(\kappa x_*)+\kappa x_*-\cosh^2(\kappa x_*)\left(\mathrm{e}^{-2\kappa(L-x_*)}-1\right)\right]\right\}^{1/2},\\
\|V_m\| &= \sqrt{2}\left[\frac{a^2\mu_m}{2}\left(C_m^{x_*}S_m^{x_*}+\mu_m x_*\right)+\frac{\left(a\mu_m+C_m^{x_*}S_m^{x_*}\right)^2}{2\mu_m}\left(C_m^L S_m^L+\mu_m L-C_m^{x_*}S_m^{x_*}-\mu_m x_*\right)\right.\\
&\left.-\frac{\left(a\mu_m+S_m^{x_*}C_m^{x_*}\right)\left(C_m^{x_*}\right)^2}{\mu_m}\left(\left(C_m^{x_*}\right)^2-\left(C_m^L\right)^2\right)+\frac{\left(C_m^{x_*}\right)^4}{2\mu_m}\left(C_m^{x_*}S_m^{x_*}-\mu_m x_*-C_m^L S_m^L+\mu_m L\right)\right]^{1/2}.
\end{aligned}
$$

Meanwhile, initial values of the Fourier coefficients can be determined as

$$
A_m=\frac{2\int_0^L\left[u(x,0)-\hat{u}(x)\right]V_m(x)\,\mathrm{d}x}{\|V_m\|}=\frac{2}{\|V_m\|}\begin{cases}U_{\mathrm{s}}h_1\left(\mu_m;x_{\mathrm{s}}\right)-h_3\left(\mu_m\right), & x_{\mathrm{s}}<x_*,\\ U_{\mathrm{s}}h_2\left(\mu_m;x_{\mathrm{s}}\right)-h_3\left(\mu_m\right), & x_*<x_{\mathrm{s}},\end{cases}
\tag{5.45}
$$

where

$$h_1(\mu_m;x_\mathrm{s}) = -aS_m^{x_\mathrm{s}}, \quad h_2(\mu_m;x_\mathrm{s}) = -aS_m^{x_*} - \left(\frac{a\mu_m + S_m^{x_*}C_m^{x_*}}{\mu_m}\right)\left(S_m^{x_\mathrm{s}} - S_m^{x_*}\right) - \frac{\left(C_m^{x_*}\right)^2\left(C_m^{x_\mathrm{s}} - C_m^{x_*}\right)}{\mu_m},$$

$$h_3(\mu_m) = \frac{a\mu_m(1-a)}{1+{\mu_m}^2}\left[C_m^{x_*}\tanh(x_*) + \mu_m S_m^{x_*}\right] + \frac{a\left(C_m^{x_*}\right)^2}{1+{\mu_m}^2}\left[\mu_m C_m^{x_*} + S_m^{x_*} - \mu_m \mathrm{e}^{x_*-L}C_m^L - \mathrm{e}^{x_*-L}S_m^L\right]$$
$$- aS_m^{x_*} - \frac{a^2\mu_m + aS_m^{x_*}C_m^{x_*}}{1+{\mu_m}^2}\left[C_m^{x_*} - \mu_m S_m^{x_*} - \mathrm{e}^{x_*-L}C_m^L + \mu_m \mathrm{e}^{x_*-L}S_m^L\right].$$

Similarly, $\|V_n\|$ and A_n can be found replacing subscript m by n. The initial value of the first Fourier coefficient can be expressed in a similar manner using the leading eigenfunction,

$$A_1 = \frac{2\int_0^L [u(x,0) - \hat{u}(x)]V_1(x)\,\mathrm{d}x}{\|V_1\|} = \frac{2}{\|V_1\|}\begin{cases} U_\mathrm{s}g_1(\kappa;x_\mathrm{s}) - g_3(\kappa), & x_\mathrm{s} < x_*, \\ U_\mathrm{s}g_2(\kappa;x_\mathrm{s}) - g_3(\kappa), & x_* < x_\mathrm{s}, \end{cases} \tag{5.46}$$

where

$$g_1(\kappa;x_\mathrm{s}) = \frac{H_s^{x_\mathrm{s}}}{\kappa}, \quad g_2(\kappa;x_\mathrm{s}) = \frac{H_s^{x_*} - H_c^{x_*}\left(\mathrm{e}^{\kappa(\tilde{x}-x_\mathrm{s})} - 1\right)}{\kappa},$$

$$g_3(\kappa) = \frac{H_s^{x_*}}{\kappa} - \frac{1-a}{2\cosh(x_*)}\left[\frac{\sinh((\kappa+1)x_*)}{\kappa+1} + \frac{\sinh((\kappa-1)x_*)}{\kappa-1}\right] + \frac{aH_c^{x_*}}{\kappa+1}\left(1 - \mathrm{e}^{(\kappa+1)(x_*-L)}\right).$$

Before we formulate the quadratic approximation, it is helpful to introduce the following quantity

$$\overline{R_{m,n}} = \overline{R_{n,m}} = \frac{2\|V_1\|Q_{m,n}^1}{\|V_m\|\|V_n\|(\lambda_1 - \lambda_m - \lambda_n)} = \frac{2\|V_1\|Q_{m,n}^1}{\|V_m\|\|V_n\|\left(\lambda_1 + 2 + {\mu_m}^2 + {\mu_n}^2\right)}. \tag{5.47}$$

Substituting (5.45), (5.46) and (5.47) into (3.50), we obtain the quadratic equation for U_s

$$\begin{cases} \overline{A}{U_\mathrm{s}}^2 + \overline{B}U_\mathrm{s} + \overline{C} = 0, & x_\mathrm{s} < x_*, \\ \underline{A}{U_\mathrm{s}}^2 + \underline{B}U_\mathrm{s} + \underline{C} = 0, & x_* < x_\mathrm{s}, \end{cases} \tag{5.48}$$

where

$$\overline{A} = \sum_{n,m\geq 3}\overline{R_{m,n}}h_1(\mu_m;x_\mathrm{s})\,h_1(\mu_n;x_\mathrm{s}), \tag{5.49a}$$

$$\overline{B} = g_1(\kappa;x_\mathrm{s}) - \sum_{n,m\geq 3}\overline{R_{m,n}}\left[h_1(\mu_m;x_\mathrm{s})\,h_3(\mu_n) + h_3(\mu_m)\,h_1(\mu_n;x_\mathrm{s})\right], \tag{5.49b}$$

$$\overline{C} = \sum_{n,m\geq 3}\overline{R_{m,n}}h_3(\mu_m)\,h_3(\mu_n) - g_3(\kappa) = \underline{C}, \tag{5.49c}$$

$$\underline{A} = \sum_{n,m\geq 3}\overline{R_{m,n}}h_2(\mu_n;x_\mathrm{s})\,h_2(\mu_m;x_\mathrm{s}), \tag{5.49d}$$

$$\underline{B} = g_2(\kappa;x_\mathrm{s}) - \sum_{n,m\geq 3}\overline{R_{m,n}}\left[h_2(\mu_m;x_\mathrm{s})\,h_3(\mu_n) + h_3(\mu_m)\,h_2(\mu_n;x_\mathrm{s})\right]. \tag{5.49e}$$

A representative result is shown in Figure 5.10(b). This was obtained for $L = 10$ and 287 eigenvalues. As seen, the quadratic approximation agrees well with direct numerical simulation, considerably better than the linear approximation, for the selected a.

5.3.5 Linear Approximation of the Strength-Duration Curve

The linear approximation of the strength-duration curve can be found using the analytically derived expression given by (5.9). However, it must be noted that in this case, the rheobase is found as

$$I_{\mathrm{rh}} = \frac{\lambda_1 \int_0^\infty V_1(x)^\top \hat{u}(x)\,\mathrm{d}x}{V_1(0)} = \lambda_1 \cosh(\kappa x_*) \left\{ \int_0^{x_*} \frac{\cosh(\kappa x)}{\cosh(\kappa x_*)} \left(1 - (1-a)\frac{\cosh(x)}{\cosh(x_*)}\right) \mathrm{d}x \right.$$
$$\left. + \int_{x_*}^\infty \exp(\kappa(x_* - x))\, a\, \exp(x_* - x)\,\mathrm{d}x \right\} = \lambda_1 \mathscr{N},$$

where $\mathscr{N}$ is same as used in the strength-extent curve formula.

This linear prediction formalism compared with the direct numerical simulations is depicted in Figure 5.12(a). As in ZFK equation, the *a priori* bound for these chosen threshold parameters is outside of the duration domain. As shown in the figure, the linear approximation of large parameter value close to $1/2$ better fits to the numerical simulation than that of small parameter value. This is due to the fact that the leading eigenvalue is inversely proportional to the threshold parameter a. Even for larger a, there are still some deviations between the linear theory and numerical simulations, which can be reduced by considering the second-order approximation that will be outlined in the following subsection.

5.3.6 Quadratic Approximation of the Strength-Duration Curve

By substituting (5.44), (5.45) and (5.46) in the coefficients of the quadratic equation for I_{s} (3.71), the second-order approximation of the strength-duration curve can be immediately generated.

Figure 5.12(b) shows graphs of the linear and quadratic approximation of the strength-duration curves along with its numerical result for $a = 0.4$. As in the strength-extent curve analysis, the quadratic approximation was obtained for $L = 10$ and 287

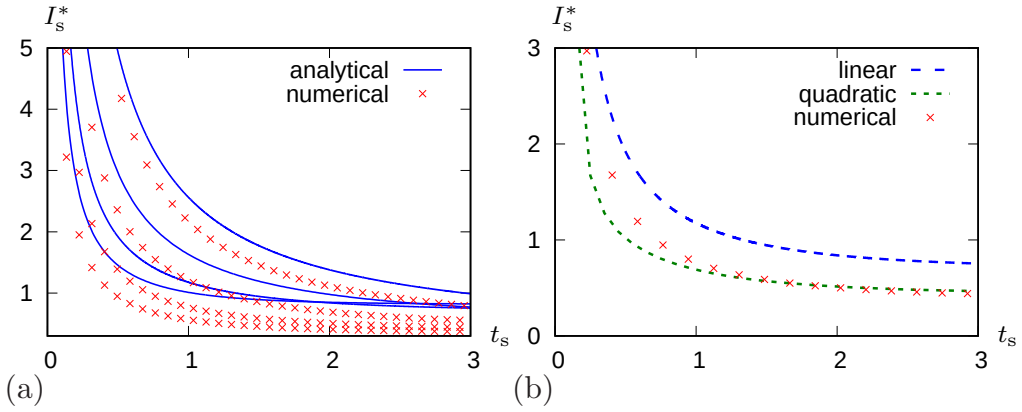

Figure 5.12: Strength-duration curves in McKean model: direct numerical simulations (red circles) vs (a) linear theory (blue lines), for $a = 0.35$ at the bottom , $a = 0.4$, $a = 0.45$ to $a = 0.48$ at the top, and (b) linear and quadratic theories, for $a = 0.4$. Blue long-dashed lines: analytical dependencies. Green short-dashed line: the predictions given by quadratic theory. Discretization: $\Delta_x = 0.01$, $\Delta_t = 4{\Delta_x}^2/9$, $L = 10$.

eigenvalues. Confirming the hypothesis, the accuracy of the second-order approximation is much closer to the direct numerical simulation compared to the first-order approximation.

5.4 Chapter Summary

In this chapter, the applicability of the ignition criterion has been tested on two one-component reaction-diffusion systems, both of which have the same type of time-independent critical solution, which corresponds to the critical nucleus. The importance of this critical nucleus solution is that its center-stable manifold has codimension one and separates the basins of attraction of propagation front solutions and decaying solutions.

We have firstly reviewed Zeldovich-Frank-Kamenetsky (ZFK) equation for which closed analytical formulas for the leading eigenpair is known only for $\theta \ll 1$. Therefore, the hybrid approach has been implemented to provide numerical estimation of the ingredients of the linearized theory and their performance has been assessed as satisfactory since hybrid numeric-asymptotic prediction is somewhat better than the explicit expression for the threshold curves given in the small threshold limit.

For ZFK equation, the linearized problem has only one discrete stable eigenvalue and thus, the quadratic theory result of the threshold curves has been estimated by means of only first two principal eigenpairs. The resulting quadratic approximations

of the critical curves has led to further improvement in accuracy as opposed to the linear approximation. We also gave the explicit forms of *a priori* lower bound for the ignition threshold.

The second test problem we considered in this chapter is McKean equation for which both the critical nucleus and leading eigenpair is known exactly. However, we have used the hybrid approach method here as well in order to validate the efficiency of the method as the right-hand of the equation has discontinuous term, which directs us towards the finite element numerical treatment. In some cases, the linear predictions do not match well with the direct numerical simulations. This is the case especially for the strength-duration threshold curve analysis. For this reason, the quadratic approximation of the threshold curves have been employed in order to perform the discrepancy reduction.

Figure	**Parameter(s)** & **Discretization** & L
Fig. 5.1	$\theta = 0.15, x_{\mathrm{s}} = 0.6, \lvert\overline{U_{\mathrm{s}}^*} - \underline{U_{\mathrm{s}}^*}\rvert < 10^{-5}, \Delta_x = 0.02, \Delta_t = 4{\Delta_x}^2/9, L = 20$
Fig. 5.2 & 5.3	$\theta = 0.05, 0.15, 0.25, 0.\overline{35}, 0.45, \Delta_x = 0.02, \Delta_t = 4{\Delta_x}^2/9, L = 30$
Fig. 5.4	$\theta = 0.05, 0.15, 0.25, 0.35, 0.45, \Delta_x = 0.03, \Delta_t = 4{\Delta_x}^2/9, L = 100$
Fig. 5.5	$\theta = 0.05, \Delta_x = 0.03, \Delta_t = 4{\Delta_x}^2/9, L = 100$
Fig. 5.6	$\theta = 0.05, 0.15, 0.25, 0.35, 0.45, \Delta_x = 0.03, \Delta_t = 4{\Delta_x}^2/9, L = 30$
Fig. 5.7	$\theta = 0.05, 0.15, 0.25, 0.35, 0.45, \Delta_x = 0.03, \Delta_t = 4{\Delta_x}^2/9, L = 100$
Fig. 5.9	$a = 0.05, 0.15, 0.25, 0.35, 0.45, x_{\mathrm{s}} = 0.6, \Delta_x = 0.01, \Delta_t = 4{\Delta_x}^2/9, L = 10$
Fig. 5.10 (a)	$a = 0.05, 0.15, 0.25, 0.35, 0.45, \Delta_x = 0.01, \Delta_t = 4{\Delta_x}^2/9, L = 10$
Fig. 5.10 (b)	$a = 0.48, \Delta_x = 0.01, \Delta_t = 4{\Delta_x}^2/9, L = 10$
Fig. 5.11	$a = 0.32, L = 40x_*$(a), $L = 100x_*$(b)
Fig. 5.12	$a = 0.35, 0.4, 0.45, 0.48$(a), $a = 0.4$(b), $\Delta_x = 0.01, \Delta_t = 4{\Delta_x}^2/9, L = 10$

Table 5.2: The complete set of parameters and discretization values used in the figures.

CHAPTER 6

MULTICOMPONENT SYSTEMS

6.1 Chapter Introduction

In the previous chapter, we have demonstrated the applicability of the approach on one-component test problems. This chapter is focused on the multicomponent reaction-diffusion systems with moving critical solutions. In Section 6.2, we provide a brief introduction to a caricature model of cardiac excitation propagating fronts, Biktashev model, in which hybrid method is proposed and implemented to calculate the exact analytical closed-form solution of its critical front and leading eigenpair, followed by the derivation of the linear approximation of the strength-duration curve. Section 6.3 and Section 6.4 are dedicated to the systems that have critical pulse solutions. In Section 6.3, we consider FitzHugh-Nagumo system serving as a prototype of an excitable system and in Section 6.4, we present the results of a modified Beeler-Reuter model. For the modified Beeler-Reuter model, the ingredients of the analytical ignition criterion are exclusively numerically obtainable. For FitzHugh-Nagumo system, on the other hand, there is a well-known alternative approach called perturbation theory that can be used to find approximate solutions of the critical pulse and the first two leading eigenvalues along with corresponding left and right eigenfunctions by using the exact solution of the one-component version of the model, Zeldovich-Frank-Kamenetsky equation. This perturbation method is also given in detail as well as the strength-duration and the strength-extent curve analysis of these two models. Finally, a brief summary of the chapter is offered in Section 6.5.

6.2 Biktashev Model

The first example of this chapter is the Biktashev model [16], simplified cardiac excitation front model. As described in more detail in Subsection 2.4.3.3, this is a two-component reaction-diffusion system (3.1) with $\mathbf{u} = (E,h)^\top$, $\mathbf{D} = \begin{pmatrix} 1 & 0 \\ 0 & 0 \end{pmatrix}$ and $\mathbf{f} = (f_E, f_h)^\top$, where

$$\begin{aligned} f_E(E,h) &= \mathrm{H}(E-1)h, \\ f_h(E,h) &= \frac{1}{\tau_*}(\mathrm{H}(-E)-h), \end{aligned} \tag{6.1}$$

and $\mathrm{H}(\cdot)$ is the Heaviside step function. The component E corresponds to the transmembrane voltage, the component h describes the inactivation gate of the fast sodium current, and τ_* is the dimensionless parameter.

The critical front solution $\hat{\mathbf{u}} = (\hat{E},\hat{h})^\top$ is described by [16]

$$\hat{E}(\xi) = \begin{cases} \omega - \dfrac{{\tau_*}^2 c^2}{1+\tau_* c^2}\,\mathrm{e}^{\xi/(\tau_* c)}, & \xi \le -\Delta, \\ -\alpha + \alpha \mathrm{e}^{-c\xi}, & \xi \ge -\Delta, \end{cases}$$

$$\hat{h}(\xi) = \begin{cases} \mathrm{e}^{\xi/(\tau_* c)}, & \xi \le 0, \\ 1, & \xi \ge 0, \end{cases} \tag{6.2}$$

where

$$\omega = 1 + \tau_* c^2(1+\alpha), \quad \Delta = \frac{1}{c}\ln\left(\frac{1+\alpha}{\alpha}\right), \tag{6.3}$$

and the front speed c is defined by an implicit equation

$$\tau_* c^2 \ln\left(\frac{(1+\alpha)(1+\tau_* c^2)}{\tau_*}\right) + \ln\left(\frac{\alpha+1}{\alpha}\right) = 0, \tag{6.4}$$

or equivalently

$$\tau_* = g(\beta,\sigma) \triangleq \frac{1+\sigma}{1-\beta}\,\beta^{-1/\sigma}, \tag{6.5}$$

where

$$\sigma = \tau_* c^2,\ \beta = \alpha/(\alpha+1). \tag{6.6}$$

In terms of (3.3), this front solution has $u \equiv E$, $u_r = -\alpha$ and $u_- = \omega$.

6.2.1 Hybrid Approach

This section aims at providing a numerical scheme for computing the critical front and the first two leading eigenpairs of the Biktashev model even though we know the explicit form of them. The hybrid approach is needed not only because it helps to validate the analytical result but also because, in some cases, it is the only option as the analytical derivation is not always possible.

In the comoving frame of reference $\xi = x - s(\tau)$, $\tau = t$, we have

$$\tilde{E}(\xi,\tau) = E(x,t), \quad \tilde{h}(\xi,\tau) = h(x,t),$$

such that (6.1) reads,

$$\begin{aligned} \frac{\partial \tilde{E}}{\partial \tau} &= \frac{\partial^2 \tilde{E}}{\partial \xi^2} + \frac{\mathrm{d}s}{\mathrm{d}\tau}\frac{\partial \tilde{E}}{\partial \xi} + \mathrm{H}(\tilde{E}-1)\tilde{h}, \\ \frac{\partial \tilde{h}}{\partial \tau} &= \frac{\mathrm{d}s}{\mathrm{d}\tau}\frac{\partial \tilde{h}}{\partial \xi} + \frac{1}{\tau_*}\left(\mathrm{H}(-\tilde{E}) - \tilde{h}\right), \end{aligned} \tag{6.7}$$

with the initial condition

$$\tilde{E}(\xi,0) = E_{\mathrm{s}}\mathrm{H}(-\xi)\mathrm{H}(\xi + 2x_{\mathrm{s}}) - \alpha. \tag{6.8}$$

To find the critical solutions, we use shooting procedure and adjust the initial condition by employing the bisection method, as described in Section 4.4. The idea behind this shooting procedure is to solve initial value problem (6.7) and (6.8) using operator splitting method (see, for example [50]). This can be achieved by splitting (6.7) into four subsystems. Due to the discontinuous right-hand sides, it is essential to use the standard finite element method, at least when dealing with these discontinuous terms. The complete discretization formula for the critical front of the model is presented in Appendix C.

Figure 6.1 gives the comparison of the numerical critical front obtained using operator splitting method and its analytical closed-form solution given by (6.2). We can see that the shooting procedure provides a good approximation of the critical front for the selected parameters. For two initial conditions, Figure 6.2 shows the evolution of E component in the comoving frame of reference. For each case, the solution approaches the critical front, *i.e.* the solution at $\tau = 120$ in the figure and then gives rise to the stable propagating wave if the initial condition is above the threshold or decays back to the resting state otherwise.

Numerical experiments suggest that there are two values of the speed c satisfying $0 < c_{slow} < c_{fast} < \infty$ such that the faster front is stable, and the slower front is

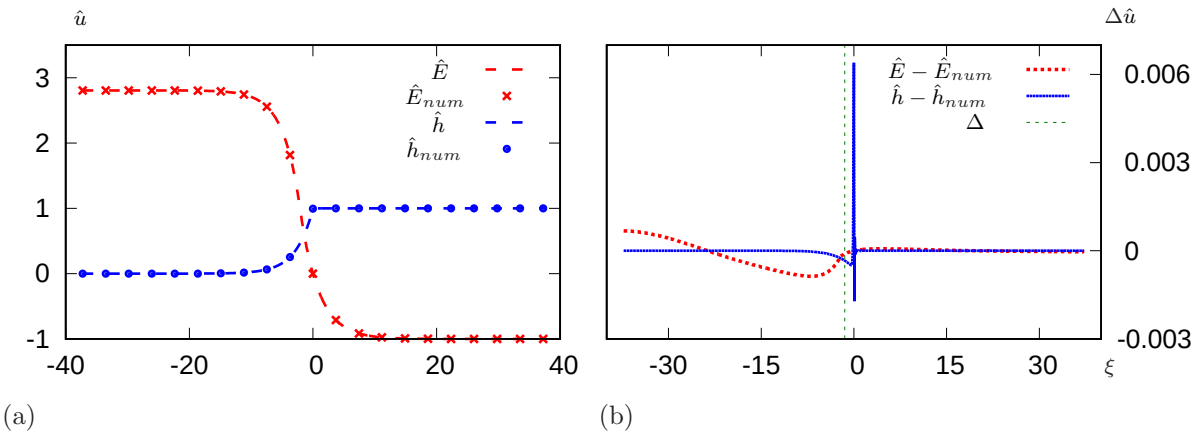

Figure 6.1: Comparison between analytical and numerical critical fronts of the Biktashev model (a), and error analysis (b). Parameters: $\alpha = 1$, $\tau_* = 8.2$, $x_s = 1.5$, $|\overline{E_s} - \underline{E_s}| < 10^{-6}$, $\Delta_\xi = 0.05$, $\Delta_\tau = 4\Delta_\xi{}^2/9$, $L = 20$.

unstable, hence a slower front either dissipates or increases in the speed to the fast branch solution depending on the initial condition being below- and above-threshold, respectively [16, 60]. This can be seen in the right panel of Figure 6.2 where the blue circle and green square symbols represent fast and slow front speeds for the selected pair of $\alpha = 1$, $\tau_* = 8.2$, and the red line indicates how the speed of the front changes over the time interval $\tau \in (0, 1000)$. For initial conditions slightly above threshold, the front speed gets closer to the slow speed and stays in the vicinity of it for a long time before developing into the fast speed while the initial condition slightly below threshold results in the front speed to drop to zero eventually. Concerning the behaviour of the Biktashev model near-threshold initial conditions, a different numerical scheme was presented in [66, 67]. However, the method used here provides additional reliability and validity in a discontinuity eliminating manner.

The next step after finding the critical front of the Biktashev model is the determination of the right and left eigenfunctions along with the corresponding eigenvalues employing the marching procedure detailed in Section 4.4. To begin with, we linearize (6.7) about the critical front $(\hat{E}, \hat{h})$ using

$$\begin{aligned} \tilde{E}(\xi,\tau) &= \hat{E}(\xi) + \epsilon\overline{E}(\xi,\tau), \\ \tilde{h}(\xi,\tau) &= \hat{h}(\xi) + \epsilon\overline{h}(\xi,\tau), \end{aligned} \tag{6.9}$$

where $\epsilon \ll 1$, $|\overline{E}(\xi,\tau)| \ll 1$, $|\overline{h}(\xi,\tau)| \ll 1$. This results in the following linearized equa-

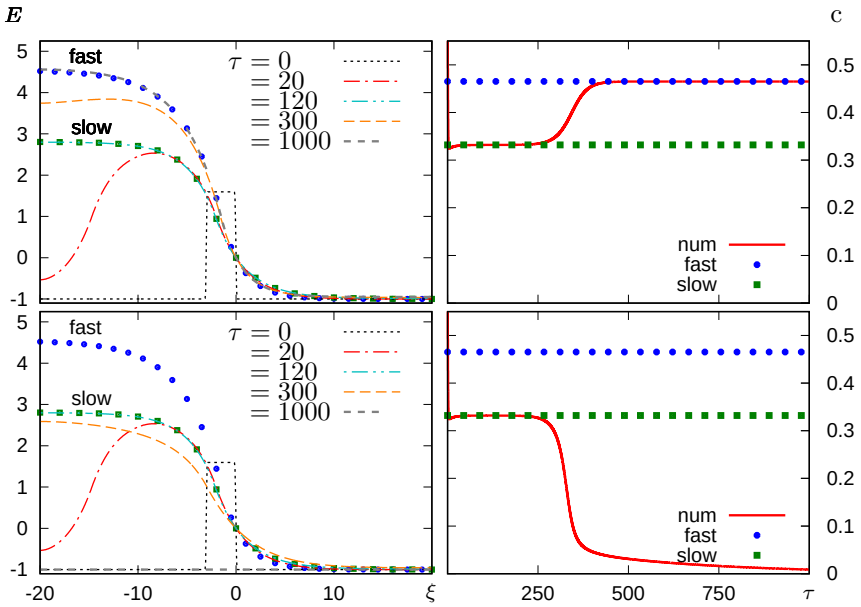

Figure 6.2: Response to below- and above-threshold initial conditions in the Biktashev model. Evolution of E component in the comoving frame of reference and the speed of the front for sub-threshold $\underline{E_{\rm s}} = 2.59403$ (bottom panel) and super-threshold $\overline{E_{\rm s}} = 2.59404$ (top panel) initial conditions. Parameters used: $\Delta_n = 20$, $\Delta_\xi = \Delta/\Delta_n$, $\Delta_\tau = 4\Delta_\xi{}^2/9$, $L = 25\Delta$, $\alpha = 1$, $\tau_* = 8.2$, $x_{\rm s} = 1.5$.

tion:

$$\begin{aligned}
\frac{\partial \overline{E}}{\partial \tau} &= \frac{\partial^2 \overline{E}}{\partial \xi^2} + c\frac{\partial \overline{E}}{\partial \xi} - \frac{1}{\hat{E}'(-\Delta)}\delta(\xi+\Delta)\hat{h}\overline{E} + \mathrm{H}(-\Delta-\xi)\overline{h}, \\
\frac{\partial \overline{h}}{\partial \tau} &= c\frac{\partial \overline{h}}{\partial \xi} + \left(\frac{1}{\hat{E}'(0)}\delta(\xi)\overline{E} - \overline{h}\right)/\tau_*,
\end{aligned} \tag{6.10}$$

while the adjoint linearized problem is

$$\begin{aligned}
\frac{\partial \bar{E}}{\partial \tau} &= \frac{\partial^2 \bar{E}}{\partial \xi^2} - c\frac{\partial \bar{E}}{\partial \xi} - \frac{1}{\hat{E}'(-\Delta)}\delta(\xi+\Delta)\hat{h}\bar{E} + \frac{\delta(\xi)}{\tau_*\hat{E}'(0)}\bar{h}, \\
\frac{\partial \bar{h}}{\partial \tau} &= -c\frac{\partial \bar{h}}{\partial \xi} + \mathrm{H}(-\Delta-\xi)\bar{E} - \frac{\bar{h}}{\tau_*},
\end{aligned} \tag{6.11}$$

where $c = \dfrac{\mathrm{d}s}{\mathrm{d}\tau}$.

The eigenfunctions of the linearized and adjoint linearized problems are respectively called as the right and left eigenfunctions. The numerical scheme aiming for determining the first two left and right eigenfunctions and the corresponding eigenvalues of Biktashev model is presented in Appendices C.2 and C.3, and these are compared with their exact analytical counterparts explicitly given in Appendix C.4. In

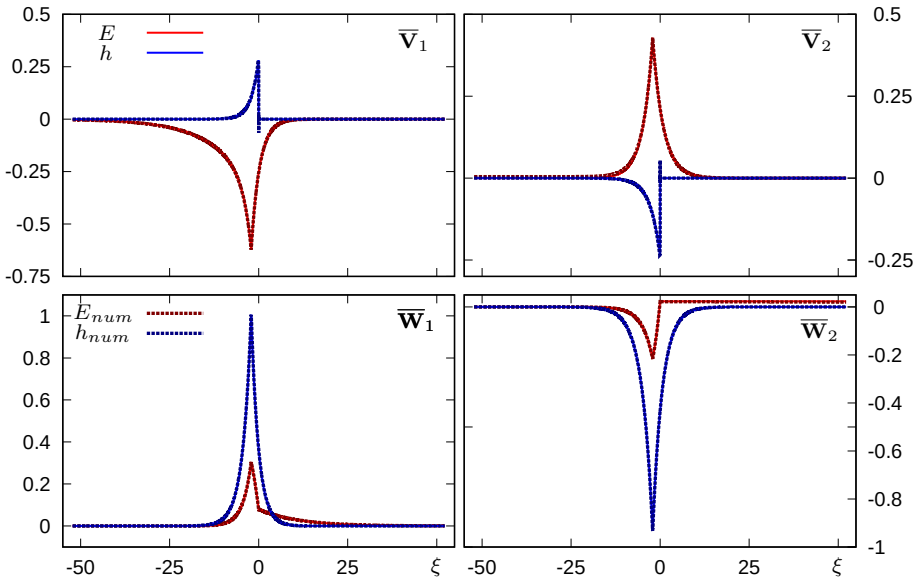

Figure 6.3: Comparison between first two right and left eigenfunctions of Biktashev model. Parameters: $\alpha = 1$, $\tau_* = 8.2$, $\Delta_n = 100$, $\Delta_\xi = \Delta/\Delta_n$, $\Delta_\tau = 4{\Delta_\xi}^2/9$, $L = 25\Delta$.

Figure 6.3, the eigenfunctions obtained using hybrid method fairly resemble exact analytical eigenfunctions. The largest difference between the numerical and analytical eigenfunctions is observed in the vicinity of the discontinuous values, $\xi = 0$ and $\xi = -\Delta$. This is totally expected as the numerical scheme used to calculate the eigenfunctions is the second-order accurate, except near discontinuities, where it reduces to the first-order accuracy and introduces spurious oscillations due to Beam-Warming method [39].

In the operator splitting method, as we have chosen the time step Δ_τ proportional to the second power of the spatial step, $\Delta_\tau = 4{\Delta_\xi}^2/9$, any error raised by the splitting procedure is negligibly small (see, for example [63]) compared to the highest error associated with one of the subsystems. The truncation error in the numerical scheme is therefore approximately proportional to $\mathcal{O}\left({\Delta_\xi}^2\right)$. This can be verified by looking at how the absolute error between analytical and numerical leading eigenvalues changes with the discretization step Δ_ξ, as shown in Figure 6.4.

6.2.2 Linear Approximation of the Strength-Duration Curve

The result of the calculation of the strength-duration curve for Biktashev model is visualized in Figure 6.5 on which the linear approximation is based on the formulas (3.66) and (3.68). For every chosen duration of stimulus t_s, we calculate the zeros

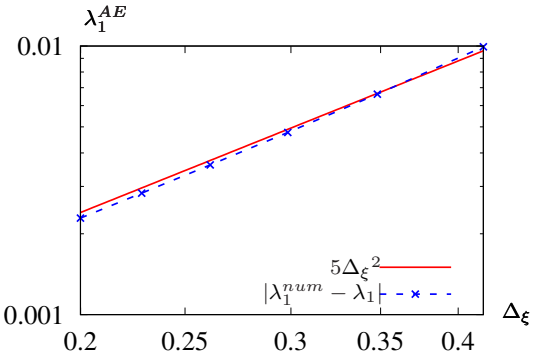

Figure 6.4: The absolute error between analytical and numerical first eigenvalues of the Biktashev model for different choices of discretization steps. As seen the absolute error is the second-order as the scheme promises.

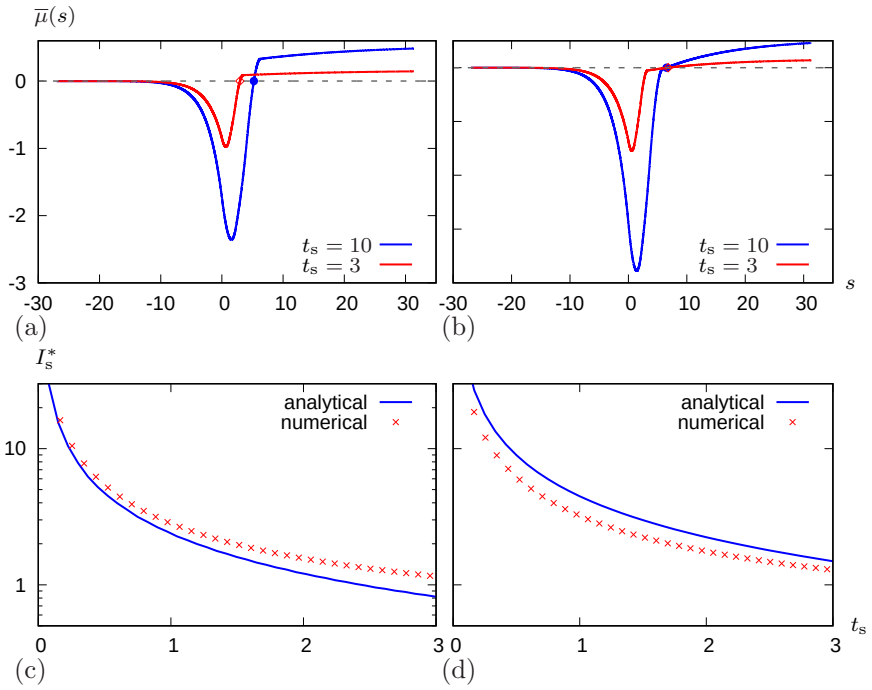

Figure 6.5: Equation (3.68) that defines the shift s in terms of t_s and comparison of analytical and numerical strength-duration curve for the Biktashev model for the following choice of parameters: $\Delta_\xi = 0.03$, $\Delta_\tau = 4\Delta_\xi{}^2/9$, $L = 30$, $\tau_* = 7.8$, $\alpha = 2/3$ (a,c) and $\tau_* = 8$, $\alpha = 9/11$ (b,d).

of (3.68) in order to find the value of the shift s. We then substitute this value of s into one of the equation in (3.66) (since both produce the same result) to get the corresponding value of I_{s}. In the simulations, we choose two different set of the model parameters, $\tau_* = 7.8$, $\alpha = 2/3$ and $\tau_* = 8$, $\alpha = 9/11$ from which the resulting curves are respectively shown in Figure 6.5(a,c) and Figure 6.5(b,d). The shape of $\overline{\mu}(s)$ is rather similar for both cases and the main difference between the two is the closeness of the s values for two different duration of stimulus values, $t_{\mathrm{s}} = 3$ and $t_{\mathrm{s}} = 10$. We observe that the theoretical critical curve for the first set of parameter values is well adapted to the direct numerical simulation threshold curve for smaller values of t_{s}, and then bends down dramatically as the value of t_{s} increases. The theoretical prediction for the second set of parameters values, however, gets better with t_{s}.

6.3 FitzHugh-Nagumo System

Our second test problem in this chapter is another example of two-component reaction-diffusion system with critical pulse solution rather than front, namely, the FitzHugh-Nagumo (FHN) system, which is considered as a ZFK equation extended by a slow variable, describing inhibition of excitation. This model is considered as a prototype for excitable systems, and hence has been extensively studied. As mentioned before, there are many different forms of the kinetics terms of the FHN system and we consider the model in the form

$$\begin{aligned} &k = 2, \quad \mathbf{D} = \mathrm{diag}(1,0), \quad \mathbf{u} = \Big(u, v\Big)^\top, \\ &\mathbf{f}(\mathbf{u}) = \Big(f_u(u,v), f_v(u,v)\Big)^\top, \\ &f_u(u,v) = u(u-\beta)(1-u) - v, \\ &f_v(u,v) = \gamma(\alpha u - v), \end{aligned} \tag{6.12}$$

for fixed values of the slow dynamics parameters, $\gamma = 0.01$ and $\alpha = 0.37$, and two values of the excitation threshold for the fast dynamics, $\beta = 0.05$ and $\beta = 0.13$.

6.3.1 Hybrid Approach

System (6.12) has an unstable propagating pulse solution as opposed to its reduced form, the ZFK equation with nontrivial stationary solution. It is known (see *e.g.* [49] and references therein) that in the limit $\gamma \searrow 0$, v-component of the critical pulse is very small compared to u-component of it which is close to the critical nucleus of the

β	c	λ_1	λ_2
0.05	0.2561	0.17204	$\pm 1 \cdot 10^{-5}$
0.13	0.2328	0.18619	$\pm 1 \cdot 10^{-5}$

Table 6.1: Nonlinear and linear eigenvalues for the FitzHugh-Nagumo system.

corresponding ZFK equation. However, this by itself does not provide a well enough approximation for the linearized theory (see, however, Section 6.3.4) and we used only the hybrid approach. As discussed in Section 4.4.3, we have obtained the critical pulse using numerical continuation software AUTO and Figure 6.6 shows the corresponding conduction velocity (CV) restitution curves such that the lower branches at $P > 7.5 \cdot 10^3$ give the critical pulses and the upper branches estimate the stable propagating pulse solution, which is not the case of interest to us in this thesis. The corresponding unstable propagation pulse speeds are given in Table 6.1.

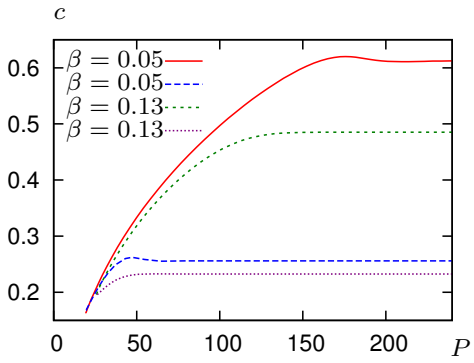

Figure 6.6: CV restitution curves for the FHN model for two selected values of the model parameter.

6.3.2 Linear Approximation of the Strength-Extent Curve

The result of the linear approximation of the strength-extent curve based on the formulas (3.39)–(3.43) is shown in Figure 6.8. The "pre-compatibility" function $\eta(\xi)$ defined by (3.40) in both cases is not unimodal, and has two local maxima and one local minimum, at least for $\beta = 0.05$. Hence, the implementation of the algorithm (3.39)–(3.43) requires investigation of the local extrema. We find that in both cases the local maximum nearest to $\xi = 0$ provides the adequate answer. The corresponding theoretical critical curves, as shown in the bottom panel of Figure 6.8, are compared with the curves obtained by direct numerical simulation. Although the eigenfunctions for the

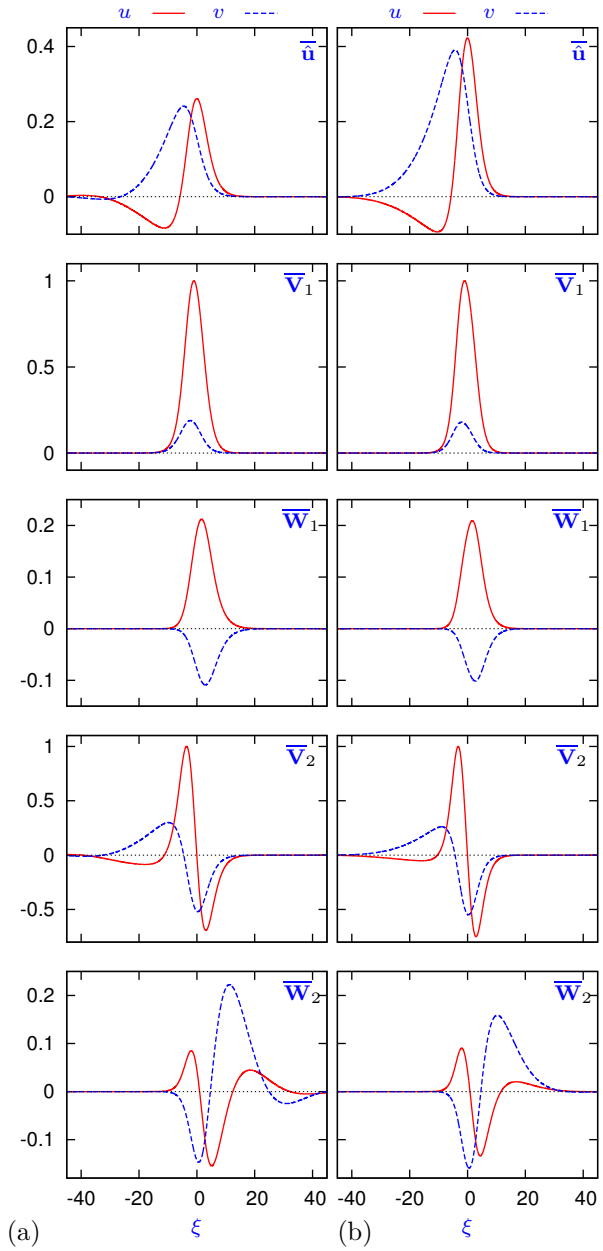

Figure 6.7: FHN theory ingredients for (a) $\beta = 0.05$ and (b) $\beta = 0.13$. Shown are components of scaled vector functions, indicated in top right corner of each panel, where $\overline{\hat{\mathbf{u}}} = \mathbf{S}\hat{\mathbf{u}}$, $\overline{\mathbf{W}}_j = \mathbf{S}^{-1}\mathbf{W}_j$, and $\mathbf{S} = \mathrm{diag}(1, 10)$. The space coordinate is chosen so that $\xi = 0$ at the maximum of $\hat{u}$. Correspondence of lines with components is according to the legends at the top. Other parameters: $\gamma = 0.01$, $\alpha = 0.37$, $\Delta_\xi = 0.03$, $\Delta_\tau = 4\Delta_\xi{}^2/9$.

two cases look rather similar, as is illustrated in Figure 6.7, the theory works somewhat better for $\beta = 0.05$ than for $\beta = 0.13$ and better accuracy is associated with smaller value of λ_1.

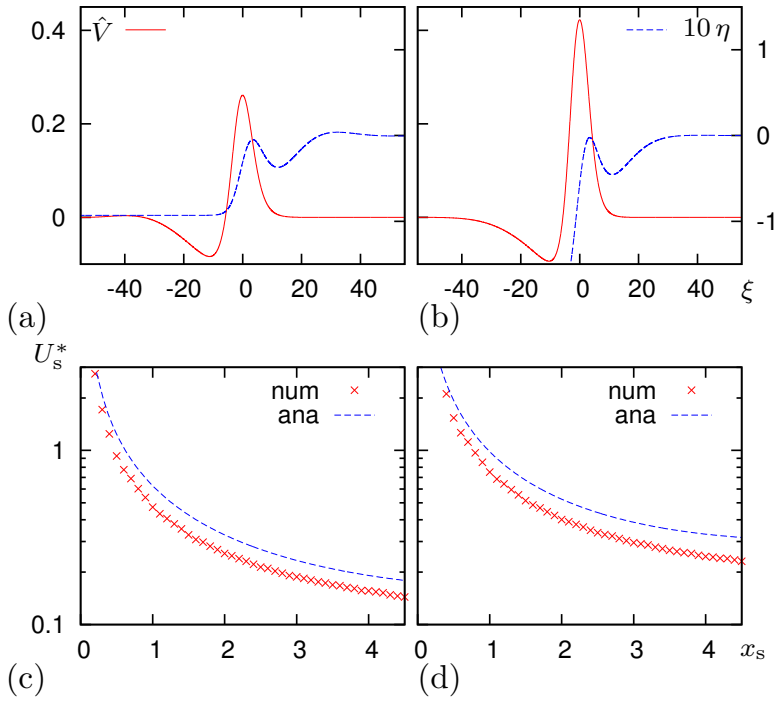

Figure 6.8: Results of linearized FitzHugh-Nagumo theory for (a,c) $\beta = 0.05$ and (b,d) $\beta = 0.13$. (a,b): The pre-compatibility function $\eta(\xi)$, used to compute the theoretical critical curve. The $u(\xi)$ component of the critical solution $\hat{u}$ is also shown for positioning purposes. (c,d): Comparison of the theoretical critical curves obtained in the linear approximation, and the critical curves obtained by direct numerical simulations. Parameters same as Fig. 6.7.

6.3.3 Linear Approximation of the Strength-Duration Curve

Figure 6.9 illustrates the calculation of the strength-duration curve for FHN model for $\beta = 0.05$ and $\beta = 0.13$ according to the formulas (3.66) and (3.68). The equation (3.68) has two roots, one of them is negative close to zero and the other is positive. We find that in both cases the smaller root denoted by blue circle and red square points in Figure 6.9(a,b) gives the corresponding value of s. The critical curves compared with those obtained from direct numerical simulation are sketched in Figure 6.9(c,d). From this plot, it can be seen that the theoretical prediction for both values of parameter is almost equally close to the numerical prediction.

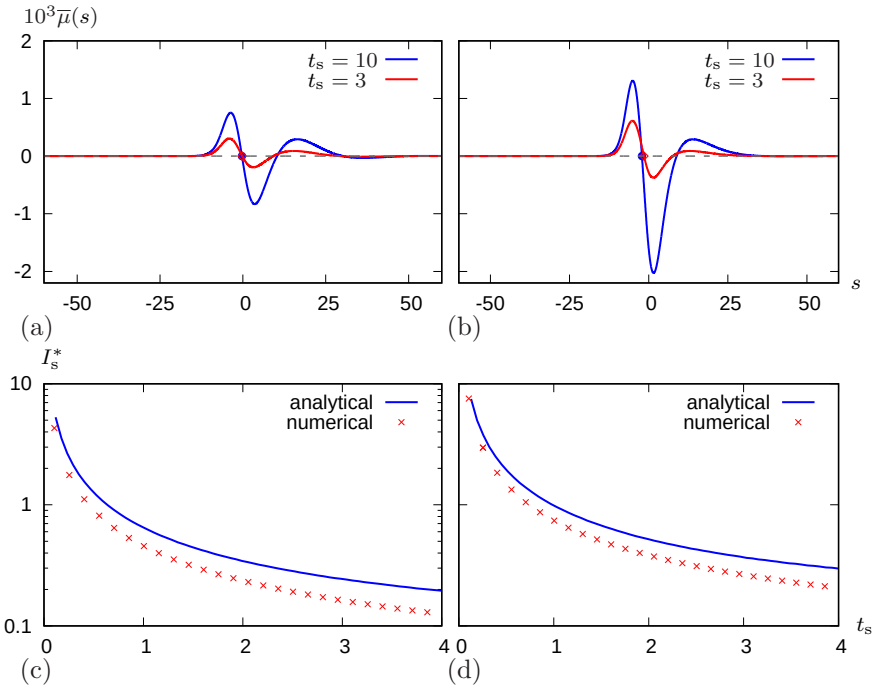

Figure 6.9: Equation (3.68) that defines the shift s in terms of t_s and comparison of analytical and numerical strength duration-curve for the FHN model for $\beta = 0.05$ and $\beta = 0.13$. Other parameters: $\gamma = 0.01$, $\alpha = 0.37$, $\Delta_\xi = 0.03$, $\Delta_\tau = 4\Delta_\xi{}^2/9$, $L = 60$.

6.3.4 Perturbation Theory Analysis of the Model

Perturbation theory is one of the most reliable and popular method for finding an approximate solution to a problem by reducing the problem to a related, relatively easy problem with the exact analytical solution. In this section, we will present how the perturbation theory can be employed to obtain the critical pulse, and even the leading eigenfunctions and corresponding eigenvalues of FHN system using the exact solution of its fast subsystem, ZFK equation. Clearly, when we set $\gamma = 0$ and $v \equiv 0$, FHN system transforms into ZFK equation and formally, we use a series in γ and the solution of ZFK equation to have the approximation to the full solution of FHN system.

Finding the Unstable Pulse

To find the critical pulse, we start with the usual procedure looking for solutions of the form $u(x,t) = \tilde{u}(\xi,\tau)$, $v(x,t) = \tilde{v}(\xi,\tau)$ where $\xi = x - c\tau$, $\tau = t$ and the positive constant c is the propagation speed of the rightward traveling wave, yet to be determined. Then, FHN system can be converted into the following system of first-order ordinary

differential equations:

$$\begin{aligned}\tilde{u}_\xi &= \tilde{w},\\ \tilde{w}_\xi &= c\tilde{w} - f(\tilde{u}) + \tilde{v},\\ \tilde{v}_\xi &= \frac{\gamma(\alpha\tilde{u} - \tilde{v})}{c}.\end{aligned} \tag{6.13}$$

The traveling wave solution vanishes at infinity along with its first derivative

$$\lim_{|\xi|\to\infty} \tilde{u} = \lim_{|\xi|\to\infty} \tilde{v} = \lim_{|\xi|\to\infty} \tilde{w} = 0.$$

Hastings has proven that for a sufficiently small γ, there are at least two distinct positive numbers c such that the above system has a homoclinic orbit [56]. It has been also proven that the pulse with higher speed is stable, while the slower wave is unstable with the speed values $c(\gamma) \approx \sqrt{2}\left(\frac{1}{2} - \gamma\right)$ and $c(\gamma) \approx \mathcal{O}\left(\sqrt{\gamma}\right)$ [49, 57]. Since the critical pulse corresponds to the pulse with slower speed, we restrict our analysis to the slow-wave case. In this case, the basic idea of the perturbation method analysis is to divide the domain of the problem into two subdomains such that the small positive parameter of the problem, being γ for FHN system, causes the rapid change in the solution in one region while the solution varies slowly in the other region. These two regions are called as inner and outer regions while the solutions obtained in these regions are called as inner and outer solutions, respectively. As a final step, the inner and outer solutions are then matched together to ensure that the approximate solution is uniformly valid in the whole domain. This is achieved by using transition zone, in which the two solutions are asymptotically equal.

Inner Solution: Even though there are various possibilities, we find the following inner expansion proposed first by [27] more convenient:

$$\begin{aligned}\tilde{u}_{inner} &= \tilde{u}_0 + \gamma^{1/2}\tilde{u}_1 + \gamma\tilde{u}_2 + \ldots,\\ \tilde{v}_{inner} &= \gamma^{1/2}\tilde{v}_1 + \gamma\tilde{v}_2 + \ldots,\\ c &= \gamma^{1/2}c_1 + \ldots,\end{aligned} \tag{6.14}$$

where $\tilde{v}_0 \equiv 0$ and $c_0 = 0$ as ZFK equation is one-component and its critical nucleus solution has zero velocity. Substituting this into equation (6.13) and collecting the

terms according to the order of $\gamma^{1/2}$, we have

$$\frac{\mathrm{d}^2\tilde{u}_0}{\mathrm{d}\xi^2} + f(\tilde{u}_0) = 0, \tag{6.15}$$

$$\frac{\mathrm{d}^2\tilde{u}_1}{\mathrm{d}\xi^2} + f'(\tilde{u}_0)\tilde{u}_1 - c_1\frac{\mathrm{d}\tilde{u}_0}{\mathrm{d}\xi} - \tilde{v}_1 = 0, \tag{6.16}$$

$$\frac{\mathrm{d}\tilde{v}_1}{\mathrm{d}\xi} - \frac{\alpha\tilde{u}_0}{c_1} = 0. \tag{6.17}$$

Coefficient c_1 can be determined by multiplying (6.16) by $\mathrm{d}\tilde{u}_0/\mathrm{d}\xi$ throughout and then integrating the result using the equations (6.15) and (6.17) therein,

$$c_1 = \left(\frac{\alpha \oint \tilde{u}_0^2 \mathrm{d}\xi}{\oint \left(\frac{\mathrm{d}\tilde{u}_0}{\mathrm{d}\xi}\right)^2 \mathrm{d}\xi}\right)^{1/2}, \tag{6.18}$$

where the integration is performed over the domain of $\tilde{u}_0$. As we aim to obtain explicit analytical expressions if possible, we consider the limit of small β. For $u \lesssim \beta$ we can estimate $f(u) \approx u\left(u-\beta\right)$ for which the critical nucleus of ZFK is equal to,

$$\tilde{u}_0 = 3\beta\,\mathrm{sech}^2\left(\xi\sqrt{\beta}/2\right)/2,$$

so that the coefficient c_1 can be found as $c_1 = \sqrt{\frac{5\alpha}{\beta}}$. Equation for $\tilde{v}_1$ (6.17) is a first-order separable differential equation with solution,

$$\tilde{v}_1 = \frac{3\beta\sqrt{\alpha}\left(\sinh\left(\xi\sqrt{\beta}/2\right) + \cosh\left(\xi\sqrt{\beta}/2\right)\right)}{\sqrt{5}\cosh\left(\xi\sqrt{\beta}/2\right)}. \tag{6.19}$$

We can write the solution of (6.16) in the form,

$$\tilde{u}_1 = g(\xi)\frac{\mathrm{d}\tilde{u}_0}{\mathrm{d}\xi},$$

as $\frac{\mathrm{d}\tilde{u}_0}{\mathrm{d}\xi}$ is the eigensolution of the governing equation (6.16). This transformation leads to

$$c_1\frac{\mathrm{d}\tilde{u}_0}{\mathrm{d}\xi} + \tilde{v}_1 = \frac{\mathrm{d}^2 g}{\mathrm{d}\xi^2}\frac{\mathrm{d}\tilde{u}_0}{\mathrm{d}\xi} + 2\frac{\mathrm{d}g}{\mathrm{d}\xi}\frac{\mathrm{d}^2\tilde{u}_0}{\mathrm{d}\xi^2}$$

Integrating twice and using equation (6.17), we get

$$\left(\tilde{u}_0'\right)^2\frac{\mathrm{d}g}{\mathrm{d}z} = \tilde{v}_1(z)\tilde{u}_0(z) + c_1\int_{-\infty}^{z}\left(\tilde{u}_0'(z)\right)^2\mathrm{d}z - \frac{1}{c_1}\int_{-\infty}^{z}\left(\tilde{u}_0(z)\right)^2\mathrm{d}z.$$

By defining the right-hand side of above equation as $F(z)$, we obtain

$$\tilde{u}_1 = \tilde{u}_0'\int_{-\infty}^{\xi}\frac{F(z)}{\left(\tilde{u}_0'\right)^2}\mathrm{d}z,$$

which has an analytical solution in the following closed form,

$$\tilde{u}_1 = \frac{-6\sqrt{\alpha}\,\mathrm{e}^{\xi\sqrt{\beta}}\left(\mathrm{e}^{2\xi\sqrt{\beta}}\sqrt{\beta}+3\,\mathrm{e}^{\xi\sqrt{\beta}}\beta\xi-4\,\mathrm{e}^{\xi\sqrt{\beta}}\sqrt{\beta}-3\beta\xi-5\sqrt{\beta}\right)}{\sqrt{5\beta}\left(\mathrm{e}^{\xi\sqrt{\beta}}+1\right)^3}. \tag{6.20}$$

Outer Solution: As outer variables, we use ζ defined by $\zeta = \gamma^{1/2}\xi$, and assume that the outer expansion is proceeded in powers of $\gamma^{1/2}$ as

$$\begin{aligned}\tilde{u}_{outer} &= \gamma^{1/2}\hat{u}_1(\zeta)+\ldots,\\ \tilde{v}_{outer} &= \gamma^{1/2}\hat{v}_1(\zeta)+\ldots.\end{aligned} \tag{6.21}$$

Substituting these into (6.13) and collecting the terms according to the order of $\gamma^{1/2}$, we get

$$\beta\hat{u}_1+\hat{v}_1 = 0, \tag{6.22}$$

$$c_1\frac{\mathrm{d}\hat{v}_1}{\mathrm{d}\zeta} = \alpha\hat{u}_1-\hat{v}_1, \tag{6.23}$$

which have the following nontrivial solutions

$$\hat{v}_1(\zeta) = A\,\mathrm{e}^{-\zeta\left(\frac{\alpha+\beta}{\sqrt{5\alpha\beta}}\right)}, \tag{6.24}$$

$$\hat{u}_1(\zeta) = -\frac{A}{\beta}\,\mathrm{e}^{-\zeta\left(\frac{\alpha+\beta}{\sqrt{5\alpha\beta}}\right)}, \tag{6.25}$$

where the constant A is to be determined by the condition that the inner and outer expansions give the same result in the transition zone. This can be achieved by requiring that the inner solution at the boundary layer (*i.e.* as $\xi\to\infty$) is equal to the outer solution at the boundary layer (*i.e.* as $\zeta\to 0$). In other words, we require that

$$\lim_{\xi\to\infty}\tilde{v}_1 = \lim_{\zeta\to 0}\hat{v}_1, \tag{6.26}$$

which gives

$$A = \frac{6\beta\sqrt{\alpha}}{\sqrt{5}}.$$

In the literature, the condition (6.26) is known as Van Dyke's matching principle [133]. So, we have derived all the terms of the inner and outer approximations of the critical pulse of the FHN system. Figure 6.10 shows the inner and outer solutions of u and v components of FHN system for the parameter values, $\gamma = 0.01$, $\beta = 0.05$, $\alpha = 0.37$. In the negative ξ region, the inner solution is wholly valid. In the positive ξ region, on

the other hand, neither the inner nor the outer solutions alone can be the solution and it is desired to combine these two solutions in a way that this so-called "composite solution" is to be valid. This is done by adding the inner and outer approximations and subtracting the common part, the overlap term, which would take into account twice, otherwise. Thus, our final critical pulse solution based on perturbation theory, valid in the whole domain, is in the following form,

$$\hat{u} = \begin{cases} \tilde{u}_{inner}(\xi), & \xi < 0, \\ \tilde{u}_{inner}(\xi) + \tilde{u}_{outer}(\xi) - \tilde{u}^{overlap}, & \xi > 0, \end{cases} \tag{6.27}$$

$$\hat{v} = \begin{cases} \tilde{v}_{inner}(\xi), & \xi < 0, \\ \tilde{v}_{inner}(\xi) + \tilde{v}_{outer}(\xi) - \tilde{v}^{overlap}, & \xi > 0, \end{cases} \tag{6.28}$$

where the overlapping parts are

$$\tilde{u}^{overlap} = \lim_{\xi \to \infty} \tilde{u}_{inner}, \quad \tilde{v}^{overlap} = \lim_{\xi \to \infty} \tilde{v}_{inner}.$$

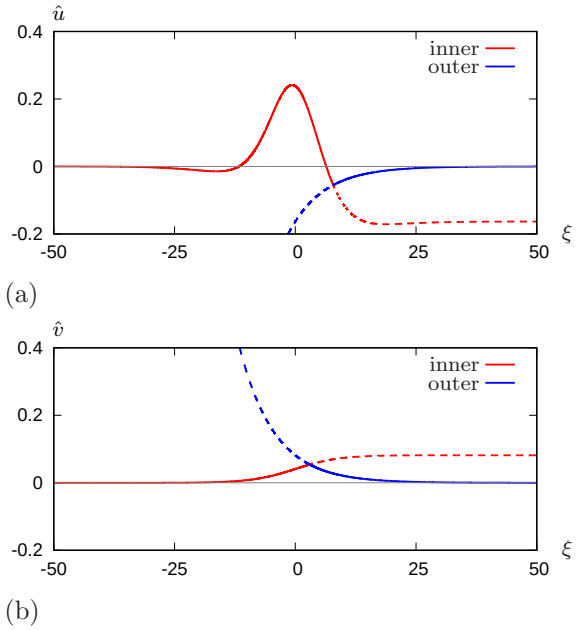

Figure 6.10: Inner and outer solutions of (a) $\hat{u}$ and (b) $\hat{v}$ components of the perturbed critical pulse. Parameters used: $\gamma = 0.01$, $\beta = 0.05$, $\alpha = 0.37$.

Figure 6.11 shows the critical pulse solutions of FHN system based on the asymptotic perturbation theory analysis compared with the ones obtained using hybrid approach for two selected set of parameters $\gamma = 0.001$, $\beta = 0.05$, $\alpha = 0.37$ (top panel)

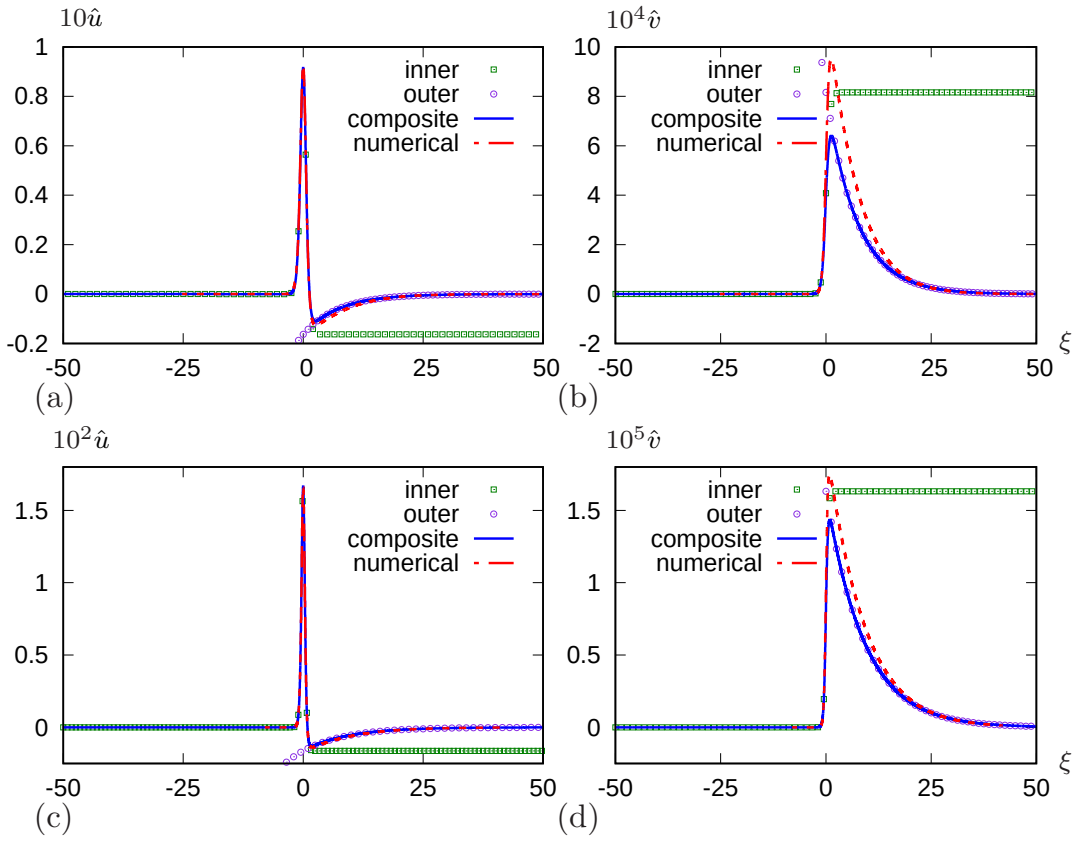

Figure 6.11: The plot of the perturbed critical pulse compared with the one obtained numerically. Two set of parameter values are chosen: $\gamma = 0.001$, $\beta = 0.05$, $\alpha = 0.37$ (a,b) and $\gamma = 0.00001$, $\beta = 0.01$, $\alpha = 0.37$(c,d).

and $\gamma = 0.00001$, $\beta = 0.01$, $\alpha = 0.37$ (bottom panel). As seen, the asymptotic result gets closer to the numerical critical pulse when the parameters β and γ both become smaller, which is indeed expected.

Finding the Leading Eigenfunctions and Corresponding Eigenvalues

In a similar fashion, perturbation theory can be applied to approximate the eigenfunctions and eigenvalues of FHN system. For the purpose of demonstration of the method, the eigenvalue problem is, generally speaking, to be solved as a two-stage process for which the inner and outer approximations are taken into account separately. However, in this model, we only need to look at the inner approximate solution due to its validity almost in the whole domain as the outer approximations would make a very small contribution to the composite solution, which is neglected. So, the composite solution simply encompasses the inner approximations. To begin with, we

linearize the FHN system around the critical pulse,

$$u(t,\xi) = \tilde{u}(\xi) + U(t,\xi), \quad v(t,\xi) = \tilde{v}(\xi) + V(t,\xi),$$

such that FHN system with the quadratic nonlinearity becomes

$$\frac{\partial U}{\partial t} = \frac{\partial^2 U}{\partial \xi^2} - c\frac{\partial U}{\partial \xi} + \big(2\tilde{u} - \beta\big)U - V, \tag{6.29}$$

$$\frac{\partial V}{\partial t} = -c\frac{\partial V}{\partial \xi} + \gamma(\alpha U - V). \tag{6.30}$$

Let the above linearized equation support solution of the form $U(t,\xi) = \mathrm{e}^{\lambda t}\phi(\xi)$ and $V(t,\xi) = \mathrm{e}^{\lambda t}\psi(\xi)$, which leads to the following eigenvalue problem,

$$\lambda\phi = \frac{\mathrm{d}^2\phi}{\mathrm{d}\xi^2} - c\frac{\mathrm{d}\phi}{\mathrm{d}\xi} + \big(2\tilde{u} - \beta\big)\phi - \psi,$$

$$\lambda\psi = -c\frac{\mathrm{d}\psi}{\mathrm{d}\xi} + \gamma\big(\alpha\phi - \psi\big),$$

where $\phi(\xi)$ and $\psi(\xi)$ are some eigenfunctions. This eigenvalue problem can be written in the form,

$$\lambda V = \mathscr{L}V, \tag{6.31}$$

where

$$\mathscr{L} = \begin{pmatrix} \partial_\xi^2 - c\partial_\xi + 2\tilde{u} - \beta & -1 \\ \gamma\alpha & -c\partial_\xi - \gamma \end{pmatrix}, \quad V = \begin{pmatrix} \phi \\ \psi \end{pmatrix}.$$

Inserting the speed and critical pulse defined in the inner expansion analysis into the operator $\mathscr{L}$, we have

$$\mathscr{L} = \begin{pmatrix} \partial_\xi^2 - \gamma^{1/2}c_1\partial_\xi + 2\big(\tilde{u}_0 + \gamma^{1/2}\tilde{u}_1\big) - \beta + \mathscr{O}(\gamma) & -1 \\ \mathscr{O}(\gamma) & -\gamma^{1/2}c_1\partial_\xi + \mathscr{O}(\gamma) \end{pmatrix},$$

which can be considered as a combination of two linear operators,

$$\mathscr{L} = \mathscr{L}_0 + \gamma^{1/2}\mathscr{L}_1 + \mathscr{O}(\gamma),$$

where

$$\mathscr{L}_0 = \begin{pmatrix} \partial_\xi^2 + 2\tilde{u}_0 - \beta & -1 \\ 0 & 0 \end{pmatrix}, \quad \mathscr{L}_1 = \begin{pmatrix} -c_1\partial_\xi + 2\tilde{u}_1 & 0 \\ 0 & -c_1\partial_\xi \end{pmatrix}.$$

Now, we expand the eigenvalues and eigenfunctions in a power series in terms of $\gamma^{1/2}$,

$$\lambda = \widetilde{\lambda} + \gamma^{1/2}\widehat{\lambda} + \mathcal{O}(\gamma),$$
$$V = \widetilde{V} + \gamma^{1/2}\widehat{V} + \mathcal{O}(\gamma).$$

This kind of expansion has been widely used in the field of quantum mechanics, see for example [117]. Implementing this eigenpair expansion into the original eigenvalue problem (6.31), we have

$$\left(\widetilde{\lambda} + \gamma^{1/2}\widehat{\lambda}\right)\left(\widetilde{V} + \gamma^{1/2}\widehat{V}\right) = \left(\mathscr{L}_0 + \gamma^{1/2}\mathscr{L}_1\right)\left(\widetilde{V} + \gamma^{1/2}\widehat{V}\right) + \mathcal{O}(\gamma).$$

Equating this in terms of the coefficients of the powers of $\gamma^{1/2}$, we get

$$\widetilde{\lambda}_j\widetilde{V}_j = \mathscr{L}_0\widetilde{V}_j, \tag{6.32}$$
$$\widetilde{\lambda}_j\widehat{V}_j + \widehat{\lambda}_j\widetilde{V}_j = \mathscr{L}_1\widetilde{V}_j + \mathscr{L}_0\widehat{V}_j, \tag{6.33}$$

for $j = 1, 2, \ldots$. At order γ^0, we have (6.32) which refers to the eigenvalue problem of the unperturbed problem, ZFK equation. The leading eigenvalue and corresponding eigenfunction of the ZFK equation are known explicitly as [68]

$$\widetilde{V}_1 = \begin{pmatrix}\widetilde{\phi}_1\\ \widetilde{\psi}_1\end{pmatrix} = \begin{pmatrix}\operatorname{sech}^3\left(\xi\sqrt{\beta}/2\right)\\ 0\end{pmatrix}, \quad \widetilde{\lambda}_1 = \frac{5\beta}{4}.$$

Also note that the derivative of the critical nucleus of ZFK equation corresponds to the second eigenfunction with zero eigenvalue

$$\widetilde{V}_2 = \begin{pmatrix}\widetilde{\phi}_2\\ \widetilde{\psi}_2\end{pmatrix} = \begin{pmatrix}\dfrac{\mathrm{d}\tilde{u}_0}{\mathrm{d}\xi}\\ 0\end{pmatrix}, \quad \widetilde{\lambda}_2 = 0.$$

Our first goal is to find an analytical expression for the perturbed eigenvalue that can be obtained using the identity of self-adjoint problems. We can rewrite (6.33) as

$$\left(\widetilde{\lambda}_j - \mathscr{L}_0\right)\widehat{V}_j = \left(\mathscr{L}_1 - \widehat{\lambda}_j\right)\widetilde{V}_j. \tag{6.34}$$

As we already know the first two leading eigenvalues of the linearized eigenvalue problem of ZFK equation, we take the inner product between the left-hand side of (6.33) and $\widetilde{V}_j$ to get,

$$\left\langle \widetilde{V}_j \middle| \left(\widetilde{\lambda}_j - \mathscr{L}_0\right)\widehat{V}_j \right\rangle = \widetilde{\lambda}_j\left\langle \widetilde{V}_j \middle| \widehat{V}_j \right\rangle - \left\langle \mathscr{L}_0^{+}\widetilde{V}_j \middle| \widehat{V}_j \right\rangle = \widetilde{\lambda}_j\left\langle \widetilde{V}_j \middle| \widehat{V}_j \right\rangle - \widetilde{\lambda}_j\left\langle \widetilde{V}_j \middle| \widehat{V}_j \right\rangle = 0,$$

since $\mathscr{L}_0^+ = \mathscr{L}_0$ and $\mathscr{L}_0\widetilde{V}_j = \widetilde{\lambda}_j\widetilde{V}_j$. Using this result in (6.33), we obtain a simple expression for the perturbed eigenvalues,

$$\widehat{\lambda}_j = \frac{\left\langle \widetilde{V}_j \middle| \mathscr{L}_1\widetilde{V}_j \right\rangle}{\left\langle \widetilde{V}_j \middle| \widetilde{V}_j \right\rangle}, \tag{6.35}$$

where we have used the fact that all eigenvalues of the unperturbed system are real. For example, for $j = 1$, we find the leading eigenvalue as

$$\widehat{\lambda}_1 = \frac{\int_{-\infty}^{\infty} \widetilde{\phi}_1\left(-c_1\partial_\xi + 2\tilde{u}_1\right)\widetilde{\phi}_1 \,\mathrm{d}\xi}{\int_{-\infty}^{\infty} \widetilde{\phi}_1^2 \,\mathrm{d}\xi} = \frac{3\sqrt{5\alpha}}{2}, \tag{6.36}$$

and for $j = 2$, $\widehat{\lambda}_2 = 0$ due to the translational symmetry.

The linear approximations of the critical curves require the knowledge of the left eigenfunctions, *i.e.* the eigenfunctions of the adjoint linearized equation. Hence, we skip the details of the analytical construction of the right eigenfunctions. For the adjoint-linearized problem for FHN system, we have

$$\lambda W = \mathscr{L}^+ W, \tag{6.37}$$

where

$$\mathscr{L}^+ = \begin{pmatrix} \partial_\xi^2 + c\partial_\xi + 2\tilde{u} - \beta & \gamma\alpha \\ -1 & c\partial_\xi - \gamma \end{pmatrix}, \quad W = \begin{pmatrix} \phi^* \\ \psi^* \end{pmatrix}.$$

This can be written using the inner expansions of the critical pulse and the speed as

$$\mathscr{L}^+ = \begin{pmatrix} \partial_\xi^2 + \gamma^{1/2}c_1\partial_\xi + 2\left(\tilde{u}_0 + \gamma^{1/2}\tilde{u}_1\right) - \beta + \mathscr{O}(\gamma) & \mathscr{O}(\gamma) \\ -1 & \gamma^{1/2}c_1\partial_\xi + \mathscr{O}(\gamma) \end{pmatrix},$$

which can be simplified as a combination of two adjoint linear operators

$$\mathscr{L}^+ = \mathscr{L}^+{}_0 + \gamma^{1/2}\mathscr{L}^+{}_1 + \mathscr{O}(\gamma),$$

where

$$\mathscr{L}^+{}_0 = \begin{pmatrix} \partial_\xi^2 + 2\tilde{u}_0 - \beta & 0 \\ -1 & 0 \end{pmatrix}, \quad \mathscr{L}^+{}_1 = \begin{pmatrix} c_1\partial_\xi + 2\tilde{u}_1 & 0 \\ 0 & c_1\partial_\xi \end{pmatrix}.$$

Since γ is a small parameter, we expand the left eigenfunctions in series as

$$W = \widetilde{W} + \gamma^{1/2}\widehat{W} + \mathscr{O}(\gamma).$$

The expansion of the eigenvalue is same as in the case of the linearized problem. Inserting this expansion into (6.37) and equating the system up to the order of $\gamma^{1/2}$, we have

$$\widetilde{\lambda}_j \widetilde{W}_j = \mathscr{L}^+{}_0 \widetilde{W}_j, \tag{6.38}$$

$$\widetilde{\lambda}_j \widehat{W}_j + \widehat{\lambda}_j \widetilde{W}_j = \mathscr{L}^+{}_1 \widetilde{W}_j + \mathscr{L}^+{}_0 \widehat{W}_j. \tag{6.39}$$

It must be emphasized that the eigenvalues of the linearized and adjoint-linearized systems must be same and from above two equations we can obtain first two perturbed eigenvalues as

$$\widehat{\lambda}_1 = \frac{3\sqrt{5\alpha}}{2}, \quad \widehat{\lambda}_2 = 0,$$

as expected. Now, we look for the eigenfunctions of the perturbed adjoint problem. For $j = 1$, we begin with the first component of the first left eigenfunction satisfying the following partial differential equation

$$\left(\partial_\xi^2 + 2\tilde{u}_0 - \beta - \widetilde{\lambda}_1\right)\widehat{\phi}_1^* = \left(\widehat{\lambda}_1 - c_1\partial_\xi - 2\tilde{u}_1\right)\widetilde{\phi}_1^*. \tag{6.40}$$

In other words, we need to solve an equation in the form of $\partial_\xi^2\widehat{\phi}_1^* + P(\xi)\widehat{\phi}_1^* = R(\xi)$ where $P(\xi) = 2\tilde{u}_0 - \beta - \widetilde{\lambda}_1$, $R(\xi) = \left(\widehat{\lambda}_1 - c_1\partial_\xi - 2\tilde{u}_1\right)\widetilde{\phi}_1^*$ with all ingredients known. The solution of the homogeneous equation ($R(\xi) = 0$) is $\widetilde{\phi}_1^* = \operatorname{sech}^3\left(\xi\sqrt{\beta}/2\right)$ and for the solution of the full non-homogeneous equation, we introduce

$$\widehat{\phi}_1^*(\xi) = \widetilde{\phi}_1^*(\xi)v(\xi),$$

motivated by the reduction of order approach so we can reduce the equation (6.40) to

$$v'' + \frac{2\widetilde{\phi}_1^{*\prime}}{\widetilde{\phi}_1^*}v' = \frac{R}{\widetilde{\phi}_1^*}$$

which has the solution in the form

$$v(\xi) = \int_{-\infty}^{\xi} \frac{\int_{-\infty}^{\xi} \widetilde{\phi}_1^*(\xi)R(\xi)\,\mathrm{d}\xi + C_1}{\left(\widetilde{\phi}_1^*(\xi)\right)^2}\,\mathrm{d}\xi + C_2,$$

where C_1 and C_2 are the constants of the integration. The explicit expression for $\widehat{\phi}_1^*$ is

$$\widehat{\phi}_1^*(\xi) = \widetilde{\phi}_1^*(\xi)v(\xi) = \frac{8}{\left(\mathrm{e}^{\xi\sqrt{\beta}/2} + \mathrm{e}^{-\xi\sqrt{\beta}/2}\right)^3} \times (C_2 + I_1 + C_1 I_2) \tag{6.41}$$

where

$$I_1 = -\frac{9\sqrt{\alpha}\xi e^{\xi\sqrt{\beta}}}{\sqrt{5\beta}\left(e^{\xi\sqrt{\beta}}+1\right)},$$
$$I_2 = \frac{\left(e^{6\xi\sqrt{\beta}}+9e^{5\xi\sqrt{\beta}}+60\xi\sqrt{\beta}e^{3\xi\sqrt{\beta}}+45e^{4\xi\sqrt{\beta}}-45e^{2\xi\sqrt{\beta}}-9e^{\xi\sqrt{\beta}}-1\right)e^{-3\xi\sqrt{\beta}}}{192\sqrt{\beta}}.$$

This eigenfunction expansion must be bounded at $\xi = -\infty$ since the composite eigenfunction is exactly equal to inner expansion in the left half plane, and also in the limit $\xi \to -\infty$, we have

$$\lim_{x\to-\infty}\frac{8}{\left(e^{\xi\sqrt{\beta}/2}+e^{-\xi\sqrt{\beta}/2}\right)^3}=0,$$
$$\lim_{x\to-\infty}\frac{8I_1}{\left(e^{\xi\sqrt{\beta}/2}+e^{-\xi\sqrt{\beta}/2}\right)^3}=0,$$
$$\lim_{x\to-\infty}\frac{8I_2}{\left(e^{\xi\sqrt{\beta}/2}+e^{-\xi\sqrt{\beta}/2}\right)^3}=-\infty,$$

and consequently, the constant C_1 must be zero. Then (6.41) simplifies to

$$\widehat{\phi}_1^* = \frac{8}{\left(e^{\xi\sqrt{\beta}/2}+e^{-\xi\sqrt{\beta}/2}\right)^3}(C_2+I_1). \tag{6.42}$$

In order to determine the coefficient C_2, we first find the ingredients of the second components of the first adjoint eigenfunction as

$$\widetilde{\psi}_1^* = -\frac{\widetilde{\phi}_1^*}{\widetilde{\lambda}_1} = \frac{-4\mathrm{sech}^3\left(\xi\sqrt{\beta}/2\right)}{5\beta}, \tag{6.43}$$
$$\widehat{\psi}_1^* = \frac{c_1\widetilde{\psi}_1^{*\prime}-\widehat{\phi}_1^*-\widetilde{\lambda}_1\widetilde{\phi}_1^*}{\widehat{\lambda}_1}. \tag{6.44}$$

The value of the coefficient C_2 can then be found from orthogonality condition $\left\langle W_1 \middle| V_2 \right\rangle = 0$. In the expanded form, this can be written as

$$\left\langle \begin{pmatrix} u_0' \\ 0 \end{pmatrix} \middle| \begin{pmatrix} \widetilde{\phi}_1^* \\ \widetilde{\psi}_1^* \end{pmatrix} \right\rangle + \gamma^{1/2}\left\{ \left\langle \begin{pmatrix} u_0' \\ 0 \end{pmatrix} \middle| \begin{pmatrix} \widehat{\phi}_1^* \\ \widehat{\psi}_1^* \end{pmatrix} \right\rangle + \left\langle \begin{pmatrix} u_1' \\ v_1' \end{pmatrix} \middle| \begin{pmatrix} \widetilde{\phi}_1^* \\ \widetilde{\psi}_1^* \end{pmatrix} \right\rangle \right\} + \gamma \left\langle \begin{pmatrix} u_1' \\ v_1' \end{pmatrix} \middle| \begin{pmatrix} \widehat{\phi}_1^* \\ \widehat{\psi}_1^* \end{pmatrix} \right\rangle = 0,$$

where the first term is actually equal to zero as the derivative of the critical nucleus of ZFK equation, u_0', is an eigenfunction corresponding to zero eigenvalue and $\widetilde{\phi}_1^*$

refers another eigenfunction of ZFK equation with biggest real eigenvalue so their inner product is equal to zero. Similarly, the second term in the above formula also vanishes since the sum of all three definite integrals is equal to zero as calculated below,

$$\int_{-\infty}^{\infty} u_0' \widehat{\phi}_1^* \,\mathrm{d}\xi = C_2 \int_{-\infty}^{\infty} u_0' \widetilde{\phi}_1^* \,\mathrm{d}\xi + \int_{-\infty}^{\infty} u_0' \widetilde{\phi}_1^* I_1 \,\mathrm{d}\xi = \frac{81\pi\sqrt{5\alpha}}{200},$$
$$\int_{-\infty}^{\infty} u_1' \widetilde{\phi}_1^* \,\mathrm{d}\xi = -\frac{9\pi\sqrt{5\alpha}}{40},$$
$$\int_{-\infty}^{\infty} v_1' \widetilde{\psi}_1^* \,\mathrm{d}\xi = -\frac{1}{\widetilde{\lambda}_1} \int_{-\infty}^{\infty} v_1' \widetilde{\phi}_1^* \,\mathrm{d}\xi = -\frac{9\pi\sqrt{5\alpha}}{50}.$$

Therefore, the coefficient C_2 can be found from the third term as,

$$C_2 = \frac{\int_{-\infty}^{\infty} \left(v_1' \widetilde{\phi}_1^* I_1 + \widetilde{\lambda}_1 v_1' \widetilde{\phi}_1^* - c_1 v_1' \widetilde{\psi}_1^{*\prime} - \widehat{\lambda}_1 u_1' \widetilde{\phi}_1^* I_1 \right) \mathrm{d}\xi}{\int_{-\infty}^{\infty} \left(\widehat{\lambda}_1 u_1' \widetilde{\phi}_1^* - v_1' \widetilde{\phi}_1^* \right) \mathrm{d}\xi},$$

in which the integrals seem to be too complicated for an explicit analytical answer, but these integrals can be evaluated using some numerical integration techniques such as trapezoidal rule. Finding this constant C_2 completes the derivation of the first left eigenfunction. For the second left eigenfunction, the formulas (6.43) and (6.44) above do not work as $\lambda_2 = 0$, we use the following eigenfunction expansion instead

$$\phi_2^* = \gamma^{1/2} \widehat{\phi}_2^*, \quad \psi_2^* = \widetilde{\psi}_2^* + \gamma^{1/2} \widehat{\psi}_2^*.$$

Substituting this expansion into adjoint linearized equation (6.37) and equating coefficients of powers of $\gamma^{1/2}$, we have

$$\widehat{\phi}_2^{*\prime\prime} + \left(2u_0 - \beta\right) \widehat{\phi}_2^* = 0, \quad -\widehat{\phi}_2^* + c_1 \widetilde{\psi}_2^{*\prime} = 0,$$

with solutions

$$\widehat{\phi}_2^* = -3\beta^{3/2} \mathrm{sech}^2\left(\xi\sqrt{\beta}/2\right) \tanh\left(\xi\sqrt{\beta}/2\right)/2,$$
$$\widetilde{\psi}_2^* = \frac{3\sqrt{5}\beta^{3/2} \mathrm{sech}^2\left(\xi\sqrt{\beta}/2\right)}{10\sqrt{\alpha}}. \tag{6.45}$$

Figure 6.12 shows the first two estimated perturbed eigenfunctions of FHN system for the parameters $\beta = 0.05$, $\alpha = 0.37$. Since we have employed the inner expansion

here, it is expected to have the perturbed eigenfunctions bounded at $\xi = -\infty$. What is surprising is that they are also vanishing at $\xi = \infty$. The reason for this is not clear but we assume it is related to the outer eigenfunction solution which likely has a very small contribution to the composite eigenfunction solution and hence, we do not consider the outer expansion here.

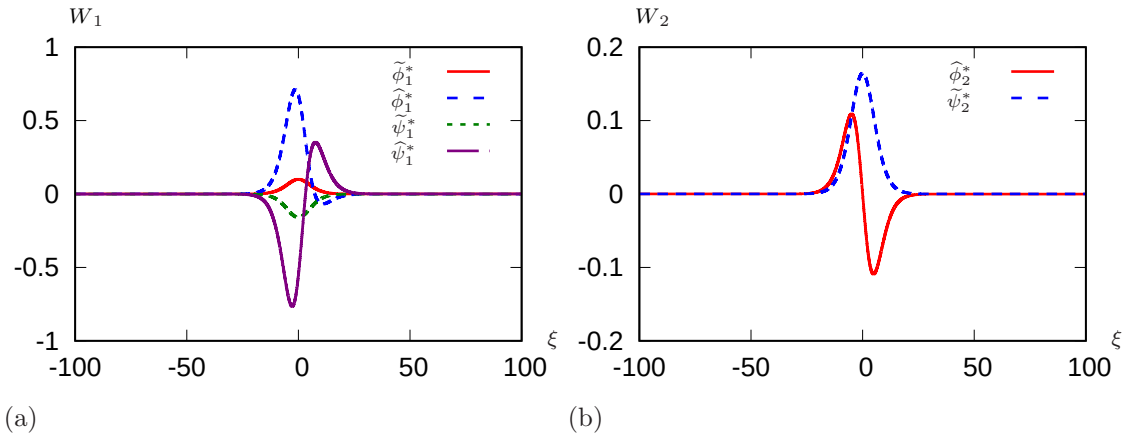

Figure 6.12: Plot of the two components of first (a) and second (b) eigenfunctions of FHN system. Parameters used: $\beta = 0.05$, $\alpha = 0.37$.

Strength-Duration Curve

After finding the eigenfunctions of the model in closed forms, the next primary aim of this section is to assess the critical curves by means of the formulas obtained through the use of perturbation theory. We exclusively attempt to investigate the strength-duration curve.

In our proposed procedure, the value of s is given by the transcendental equation (3.68). Employing the first component of the first two left eigenfunctions in the equation, we are left with

$$f(\beta,\gamma,s,t_s) \triangleq 2\mathcal{N}_2 e^{\lambda_1 s/c}\left[(1+\sqrt{\gamma}C_2)I_3(\beta,s,t_s) - \frac{9\sqrt{\gamma\alpha}}{\sqrt{5\beta}}I_4(\beta,s,t_s)\right] + 3\mathcal{N}_1\sqrt{\gamma}\beta I_5(\beta,s,t_s) = 0. \tag{6.46}$$

The integral I_3 in this equation is calculated as

$$I_3(\beta,s,t_s) = \int_{-s}^{-ct_s-s} e^{\lambda_1\xi/c}\operatorname{sech}^3\left(\xi\sqrt{\beta}/2\right)\mathrm{d}\xi = \frac{1}{\sqrt{\beta}}\left(\Upsilon_1\left(e^{-(ct_s+s)\sqrt{\beta}}\right) - \Upsilon_1\left(e^{-s\sqrt{\beta}}\right)\right),$$

where

$$\Upsilon_1(\rho) = \frac{2\rho^{(a+1)/2}(a\rho + a + \rho - 1)}{(\rho+1)^2} - \rho^{(a+1)/2}(a^2-1)\,\Omega(-\rho, 1, (a+1)/2),\ a = \frac{2\lambda_1}{c\sqrt{\beta}}$$

and Ω is the Lerch transcendent as defined *e.g.* in [10] given by

$$\Omega(z,k,q) = \sum_{n=0}^{\infty} \frac{z^n}{(q+n)^k}, \tag{6.47}$$

provided that $|z| < 1$ and $q \neq 0, -1, \ldots$. The integral I_3 is also calculated as a function of Lerch transcendent as

$$I_4(\beta, s, t_s) = \int_{-s}^{-ct_s - s} e^{\lambda_1 \xi/c} \frac{\xi e^{\xi\sqrt{\beta}} \operatorname{sech}^3(\xi\sqrt{\beta}/2)}{e^{\xi\sqrt{\beta}} + 1}\, d\xi = \frac{2}{\beta}\left(\Upsilon_2\left(e^{-(ct_s+s)\sqrt{\beta}}\right) - \Upsilon_2\left(e^{-s\sqrt{\beta}}\right)\right),$$

where

$$\begin{aligned}\Upsilon_2(\rho) = {} & \frac{\rho^{(b+1)/2}}{6(\rho+1)^3}\left[\left(\left(-b^2+2b+3\right)\rho^2 + \left(-2b^2+6b+8\right)\rho - b^2 + 4b - 3\right)\ln(\rho)\right. \\ & \left. -4b\rho^2 - 8b\rho + 4\rho^2 - 4b + 12\rho + 8\right] - \frac{\rho^{(b+1)/2}(b+1)\left(b^2-4b+3\right)}{12}\Omega(-\rho, 2, (b+1)/2) \\ & + \frac{\left(\ln(\rho)\, b^3 - 3b^2\ln(\rho) - b\ln(\rho) + 6b^2 + 3\ln(\rho) - 12b - 2\right)\rho^{(b+1)/2}}{12}\Omega(-\rho, 1, (b+1)/2),\end{aligned}$$

$$b = 2\left(\frac{\lambda_1}{c\sqrt{\beta}} + 1\right)$$

and finally the integral I_5 is calculated as

$$\begin{aligned} I_5(\beta, s, t_s) &= \int_{-s}^{-ct_s - s} \operatorname{sech}^2\left(\xi\sqrt{\beta}/2\right)\tanh\left(\xi\sqrt{\beta}/2\right) d\xi \\ &= \frac{\operatorname{sech}^2\left(s\sqrt{\beta}/2\right) - \operatorname{sech}^2\left((ct_s + s)\sqrt{\beta}/2\right)}{\sqrt{\beta}}. \end{aligned}$$

Moreover, one of the FHN system parameters, namely, β has been assumed to be small. A further simplification of these integrals can be made using this smallness assumption by employing the change of variable, $\rho = e^{\xi\sqrt{\beta}}$, so that the limits of all three integrals become close to 1. Hence, these integrals can be evaluated as the Taylor expansion around 1 and they become regular functions,

$$\begin{aligned} I_3(\beta, s, t_s) &= \frac{8}{\sqrt{\beta}} \int_{e^{-s\sqrt{\beta}}}^{e^{-(ct_s+s)\sqrt{\beta}}} \frac{\rho^{(a+1)/2}}{(\rho+1)^3}\, d\rho \approx \frac{1}{\sqrt{\beta}} \int_{1-s\sqrt{\beta}}^{1-(ct_s+s)\sqrt{\beta}} \left(1 + (\rho-1)(a/2-1)\right) d\rho \\ &= \lambda_1 t_s s + \gamma^{1/2} c_1 t_s \left(\lambda_1 t_s/2 - s\sqrt{\beta} - 1\right) - \gamma c_1^2 {t_s}^2 \sqrt{\beta}/2, \end{aligned}$$

$$I_4(\beta,s,t_s) = \frac{16}{\beta}\int_{e^{-s\sqrt{\beta}}}^{e^{-(ct_s+s)\sqrt{\beta}}} \frac{\ln(\sqrt{\rho})\,\rho^{(b+1)/2}}{(\rho+1)^4}\,d\rho \approx \frac{1}{\beta}\int_{1-s\sqrt{\beta}}^{1-(ct_s+s)\sqrt{\beta}} (\rho-1)\,d\rho$$
$$= \gamma^{1/2}c_1 t_s s + \gamma c_1^2 {t_s}^2/2,$$

$$I_5(\beta,s,t_s) = \frac{4}{\sqrt{\beta}}\int_{e^{-s\sqrt{\beta}}}^{e^{-(ct_s+s)\sqrt{\beta}}} \frac{\rho-1}{(\rho+1)^3}\,d\rho \approx \frac{1}{2\sqrt{\beta}}\int_{1-s\sqrt{\beta}}^{1-(ct_s+s)\sqrt{\beta}} (\rho-1)\,d\rho$$
$$= \gamma^{1/2}c_1 t_s s\sqrt{\beta}/2 + \gamma c_1^2 {t_s}^2\sqrt{\beta}/4.$$

Plugging these back into the transcendental equation (6.46), we have

$$\mathcal{N}_2 e^{\lambda_1 s/c}\left(1+\gamma^{1/2}C_2\right)\left(\lambda_1 t_s s + \gamma^{1/2}c_1 t_s\,\left(\lambda_1 t_s/2 - s\sqrt{\beta}-1\right) - \gamma c_1^2 {t_s}^2\sqrt{\beta}/2\right)$$
$$-\frac{9\sqrt{\alpha}\mathcal{N}_2 e^{\lambda_1 s/c}}{\sqrt{5\beta}}\left(\gamma c_1 t_s s + \gamma^{3/2}c_1^2 {t_s}^2/2\right) + \frac{3\mathcal{N}_1\beta^{3/2}}{2}\left(\gamma c_1 t_s s\sqrt{\beta}/2 + \gamma^{3/2}c_1^2 {t_s}^2\sqrt{\beta}/4\right) = 0,$$

and equating this up to the order of $\gamma^{1/2}$ gives the value of s as

$$s = \frac{c_1(2-\lambda_1 t_s)}{2\left(\lambda_1 C_2 - c_1\sqrt{\beta}\right)} + \mathcal{O}(\gamma). \tag{6.48}$$

Having demonstrated how to obtain a closed expression for s for small parameter β, the final step is to substitute the value of s into one of the equations in (3.33), *i.e.*

$$I_s = \frac{\mathcal{N}_1}{2\int_0^{t_s} e^{-\lambda_1\tau'}\mathbf{W}_1(-c\tau'-s)^\top e\,d\tau'} = \frac{-c\mathcal{N}_1}{2e^{\lambda_1 s/c}\left[\left(1+\sqrt{\gamma}C_2\right)I_3(\beta,s,t_s) - \frac{9\sqrt{\gamma\alpha}}{\sqrt{5\beta}}I_4(\beta,s,t_s)\right]}. \tag{6.49}$$

The plots of the asymptotic threshold curves given by equation (6.49), compared against the direct numerical simulations, are shown in Figure 6.13. In the left panel of the figure, since the value of slow dynamics parameter γ is fixed to 10^{-5}, the numerical curve for ZFK equation is also sketched, and it can be observed that there is a good agreement between the two numerical curves. In the right panel of the figure, the values of both γ and β are increased compared to the figure on the left panel which is why the hybrid numeric-asymptotic prediction is presented instead of the numerical result of ZFK. Expectedly, the asymptotic threshold curve, in this case, is not better than the hybrid prediction. For each figure, we also plot the classical Lapicque-Blair-Hill formula (3.64), where the values of the chronaxie and rheobase are obtained

using the Levenberg-Marquardt nonlinear, least-squares fitting algorithm described in Section 2.6. The asymptotic threshold curve at larger t_s performs slightly better than the formula (3.64) for much smaller value of γ. As evident from both figures, the classical Lapicque-Blair-Hill formula does not always fit the numerical data well. We believe that the fully analytical linear approximation and/or the second-order approximation of the strength-duration curve would presumably surpass this formula (3.64).

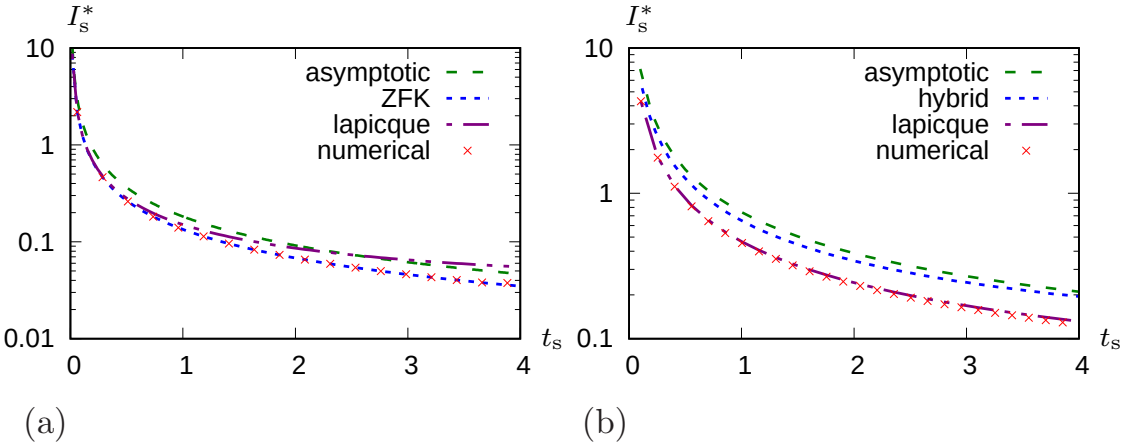

Figure 6.13: (a) Sketch of the comparison between analytical and numerical strength-duration curve where we used the perturbation analysis for analytical derivation and Lapicque and ZFK curves also plotted for the parameters $\beta = 0.01$, $\alpha = 0.37$, $\gamma = 10^{-5}$. (b) Same for $\beta = 0.05$, $\alpha = 0.37$, $\gamma = 10^{-2}$, apart from we do not include ZFK result and add hybrid approach analytical derivation instead.

6.4 The Modified Beeler-Reuter Model

In this section, we apply the theory to a variant of the classical Beeler-Reuter (BR) model [12], modified to describe phenomenologically the dynamics of neonatal cardiac cells [4, 18, 19, 106]:

$$k = 7, \quad \mathbf{D} = \mathrm{diag}(1,0,0,0,0,0,0), \tag{6.50}$$

$$\mathbf{u} = \left(V, h, j, x_1, d, f, \mathrm{Ca}\right)^\top \tag{6.51}$$

$$\mathbf{f} : (V, h, j, x_1, d, f, \mathrm{Ca})^\top \mapsto \left(f_V, f_h, f_j, f_{x_1}, f_d, f_f, f_{\mathrm{Ca}}\right) \tag{6.52}$$

where

$$\begin{aligned}
f_V &= -I_{K_1}(V) - I_{x1}(V,x_1) - I_{Na}(V,h,j) - I_s(V,d,f,\mathrm{Ca}),\\
f_h &= \alpha_h(V)(1-h) - \beta_h(V)h,\\
f_j &= \alpha_j(V)(1-j) - \beta_j(V)j,\\
f_{x_1} &= \alpha_{x1}(V)(1-x_1) - \beta_{x1}(V)x_1,\\
f_d &= \alpha_d(V)(1-d) - \beta_d(V)d,\\
f_f &= \alpha_f(V)(1-f) - \beta_f(V)f,\\
f_{\mathrm{Ca}} &= -10^{-7} I_s + 0.07(10^{-7} - \mathrm{Ca}),
\end{aligned}$$

where the ionic currents are given by

$$\begin{aligned}
&I_{K_1}(V) = 0.35\,(0.3-\alpha)\,\overline{I_{K_1}}(V),\\
&\overline{I_{K_1}}(V) = \frac{4\left(\mathrm{e}^{0.04(V+85)}-1\right)}{\mathrm{e}^{0.08(V+53)}+\mathrm{e}^{0.04(V+53)}} + \frac{0.2(V+23)}{1-\mathrm{e}^{-0.04(V+23)}},\\
&I_{x1}(V,x_1) = g_{ix}(V)x_1,\\
&g_{ix}(V) = 0.8\frac{\mathrm{e}^{0.04(V+77)}-1}{\mathrm{e}^{0.04(V+35)}},\\
&I_{Na}(V,h,j) = (g_{Na}\,(m(V))^3\,h\,j + g_{Na_c})(V-E_{Na}),\\
&I_s(V,d,f,\mathrm{Ca}) = g_s\,d\,f(V-E_s(\mathrm{Ca})).
\end{aligned}$$

The dynamic variable m is fixed at its quasi-stationary state,

$$m(V) = \alpha_m(V)/(\alpha_m(V)+\beta_m(V)),$$

the gate opening and closing transition rates are described as the following:

$$\begin{aligned}
&\alpha_{x1}(V) = \frac{0.0005\,\mathrm{e}^{0.083(V+50)}}{\mathrm{e}^{0.057(V+50)}+1}, \quad \beta_{x1}(V) = \frac{0.0013\,\mathrm{e}^{-0.06(V+20)}}{\mathrm{e}^{-0.04(V+20)}+1},\\
&\alpha_m(V) = \frac{V+47}{1-\mathrm{e}^{-0.1(V+47)}}, \quad \beta_m(V) = 40\,\mathrm{e}^{-0.056(V+72)},\\
&\alpha_h(V) = 0.126\,\mathrm{e}^{-0.25(V+77)}, \quad \beta_h(V) = \frac{1.7}{\mathrm{e}^{-0.082(V+22.5)}+1},\\
&\alpha_j(V) = \frac{0.055\,\mathrm{e}^{-0.25(V+78)}}{\mathrm{e}^{-0.2(V+78)}+1}, \quad \beta_j(V) = \frac{0.3}{\mathrm{e}^{-0.1(V+32)}+1},\\
&\alpha_d(V) = \frac{0.095\,\mathrm{e}^{-0.01(V-5)}}{\mathrm{e}^{-0.072(V-5)}+1}, \quad \beta_d(V) = \frac{0.07\,\mathrm{e}^{-0.017(V+44)}}{\mathrm{e}^{0.05(V+44)}+1},\\
&\alpha_f(V) = \frac{0.012\,\mathrm{e}^{-0.008(V+28)}}{\mathrm{e}^{0.15(V+28)}+1}, \quad \beta_f(V) = \frac{0.0065\,\mathrm{e}^{-0.02(V+30)}}{\mathrm{e}^{-0.2(V+30)}+1},
\end{aligned}$$

α_f	c	λ_1	λ_2
0.105	0.04232	0.01578	$\pm 2 \cdot 10^{-8}$
0.115	0.04497	0.01515	$\pm 1 \cdot 10^{-8}$

Table 6.2: Nonlinear and linear eigenvalues for the modified Beeler-Reuter model.

and the calcium reversal potential is defined by the Nernst law,

$$E_s(\mathrm{Ca}) = -82.3 - 13.0287 \ln(\mathrm{Ca}).$$

Here α is the excitability parameter and special attention was given to $\alpha = 0.105$ and $\alpha = 0.115$, as in [19]. The other parameters of the model are fixed as follows:

$$g_{Na} = 2.4,\ g_s = 0.45,\ g_{Na_c} = 0.003,\ E_{Na} = 50,$$

the default parameter values as used in [4, 18, 19, 106].

6.4.1 Hybrid Approach

As in the FitzHugh-Nagumo system, the critical solution is a moving pulse, and thus, we obtain the CV restitution curves and the critical pulse in a similar way. The CV restitution curves for the modified Beeler-Reuter model is sketched in Figure 6.14 and the corresponding unstable propagation pulse speeds are given in Table 6.2. Apart from the critical pulse, the solution at lower branches, the knowledge of the first two left eigenfunctions and the corresponding eigenvalues is also required. These ingredients have been found by the straightforward marching method and then verified by Arnoldi iterations.

6.4.2 Linear Approximation of the Strength-Extent Curve

Figure 6.16 shows the results of the semi-analytical prediction of the strength-extent curves according to the formulas (3.39)–(3.43). The pre-compatibility functions $\eta(\xi)$ are this time nearly unimodal compared to those of FHN system, but the shape of the $\eta(\xi)$ graphs is considerably different even though the eigenfunctions for the two cases, as seen in Figure 6.15, look quite similar. The resulting theoretical critical curves, shown in Figure 6.16(c,d), are much better for $\alpha = 0.105$ than for $\alpha = 0.115$.

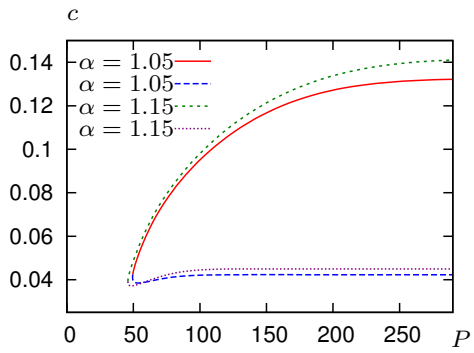

Figure 6.14: CV restitution curves for the BR model for two selected values of the model parameter. Stable (upper) and unstable (lower) branches are shown by different line types.

6.4.3 Linear Approximation of the Strength-Duration Curve

Figure 6.17 exhibits the strength-duration threshold curve analysis for BR model for two different excitability parameters, $\alpha = 0.105$ and $\alpha = 0.115$. The resulting theoretical critical curves are derived according to the formulas (3.66) and (3.68). Firstly, the values of s are determined by the transcendental equation (3.68) and compared to FHN system, it is easier to detect the zeros of this equation, two of which are shown in the top panel of the figure for $t_{\mathrm{s}} = 3$ and $t_{\mathrm{s}} = 10$. Then, the remaining part is to insert the found value of s back into theoretical threshold curve generated by (3.66). The bottom panel of the figure shows these threshold curves being compared with numerical critical curves. As can be seen from the figure, the analytical estimate for $\alpha = 0.115$ provides a somewhat better approximation than that for $\alpha = 0.105$.

6.5 Chapter Summary

In this chapter, we have successfully tested the initiation of excitation waves on multicomponent reaction-diffusion test problems. Two different initiation protocols have been reported for the models considered, except for the Biktashev model, in which only the linear approximation of the strength-duration curve analysis has been performed as the critical curve in the strength-extent plane is covered in [66]. For this model, the analytical expression for the critical front and first two left and right eigenpairs are explicitly known. We have proposed a hybrid approach based on operator splitting as a combination of the finite element and finite difference methods to calculate these ingredients numerically. This hybrid procedure for such a model having

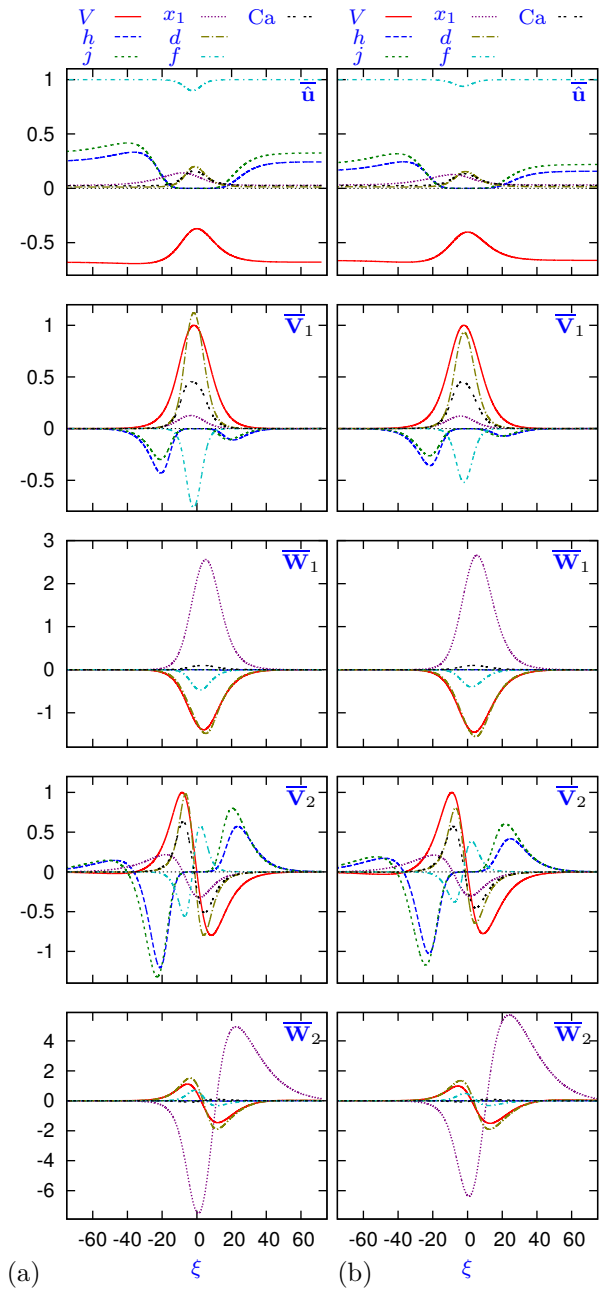

Figure 6.15: BR theory ingredients for (a) $\alpha = 0.105$ and (b) $\alpha = 0.115$. Shown are components of scaled vector functions, indicated in top right corner of each panel, where $\ldots\ \overline{\mathbf{u}} = \mathbf{S}\hat{\mathbf{u}}$, $\overline{\mathbf{W}}_j = 10^4\mathbf{S}^{-1}\mathbf{W}_j$, and $\mathbf{S} = \mathrm{diag}(10^{-2}, 1, 1, 1, 1, 1, 10^5)$. The space coordinate is chosen so that $\xi = 0$ at the maximum of $\hat{V}$. Correspondence of lines with components is according to the legends at the top.

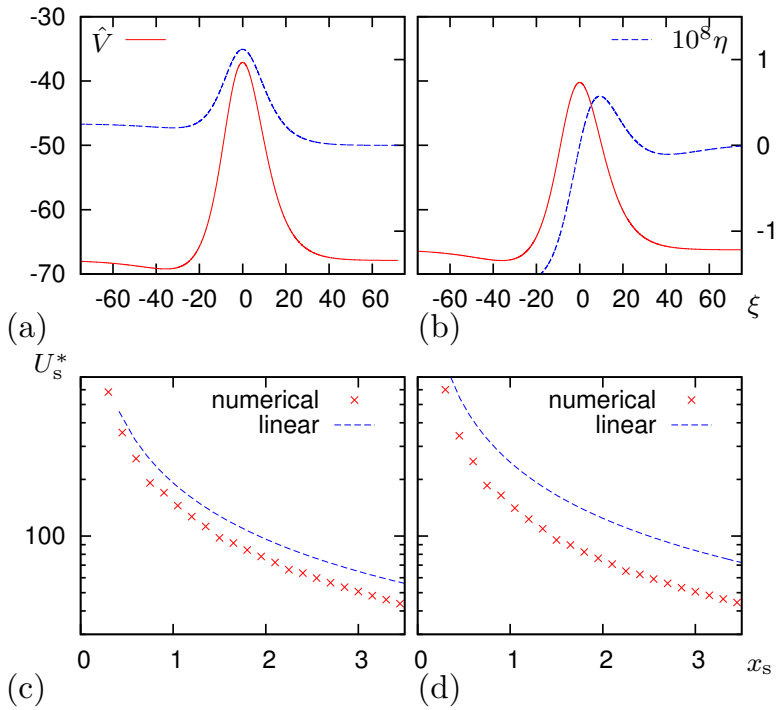

Figure 6.16: Results of BR theory for (a,c) $\alpha = 0.105$ and (b,d) $\alpha = 0.115$. (a,b): The pre-compatibility function $\eta(\xi)$, used to compute the theoretical critical curve. The $V(\xi)$ component of the critical solution $\hat{u}$ is also shown for positioning purposes. (c,d): Comparison of the theoretical critical curves obtained in the linear approximation, and the critical curves obtained by direct numerical simulations.

discontinuous right-hand side is essential, especially when there are no existing analytical closed forms of the ingredients, which is the case for most of the realistic cardiac excitation models.

Apart from the case of moving critical front, we have also considered two test problems with moving critical pulse, FihzHugh-Nagumo and Beeler-Reuter models. The critical pulse and eigenpairs for both models have been respectively obtained by using AUTO continuation package and the marching method. These ingredients have been then employed in the analytical description of the threshold curves.

To compare the performance of the proposed approach with direct numerical threshold curves, the results of two set of parameter values for each model has been presented. These results have indicated that the described method perform well, but differently according to the parameters values and possible explanations given in the text.

The FHN system is considered as a ZFK equation extended by a slow variable. It is possible, therefore, that the perturbation theory can be applied in a straightforward

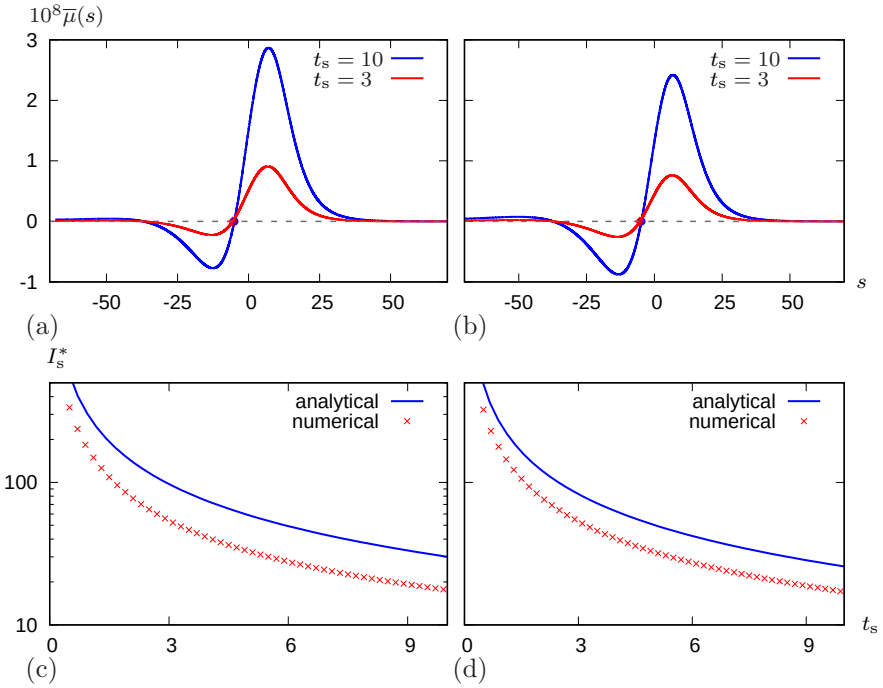

Figure 6.17: Equation (3.68) that defines the shift s in terms of t_s and comparison of analytical and numerical strength-duration curve for the BR model for $\alpha = 0.105$ and $\alpha = 0.115$.

way to determine the critical pulse and the first two eigenfunctions corresponding to the first two leading eigenvalues of FHN system, and even hence the critical curve itself analytically. This alternative approach has also been given in details in this chapter.

Figure	**Parameter(s)** & **Discretization** & L
Fig. 6.1	$\alpha = 1, \tau_* = 8.2, x_\mathrm{s} = 0.6, \Delta_\xi = 0.05, U_\mathrm{s} = 2.59404, \Delta_\tau = 4\Delta_\xi{}^2/9, L = 30$
Fig. 6.2 (top)	$\alpha = 1, \tau_* = 8.2, x_\mathrm{s} = 1.5, U_\mathrm{s} = 2.59403, \Delta_\xi = 0.05, \Delta_\tau = 4\Delta_\xi{}^2/9, L = 20$
Fig. 6.2 (bottom)	$\alpha = 1, \tau_* = 8.2, x_\mathrm{s} = 1.5, U_\mathrm{s} = 2.59404, \Delta_\xi = 0.05, \Delta_\tau = 4\Delta_\xi{}^2/9, L = 20$
Fig. 6.3	$\alpha = 1, \tau_* = 8.2, \Delta_n = 7, \Delta_\xi = \Delta/\Delta_n, \Delta_\tau = 4\Delta_\xi{}^2/9, L = 40\Delta$
Fig. 6.4	$\alpha = 1, \tau_* = 8.2, \Delta_n = 5,6,7,8,9,10, \Delta_\xi = \Delta/\Delta_n, \Delta_\tau = 4\Delta_\xi{}^2/9, L = 40\Delta$
Fig. 6.5 (a,c)	$\tau_* = 7.8, \alpha = 2/3, \Delta_\xi = 0.03, \Delta_\tau = 4\Delta_\xi{}^2/9, L = 30$
Fig. 6.5 (b,d)	$\tau_* = 8, \alpha = 9/11, \Delta_\xi = 0.03, \Delta_\tau = 4\Delta_\xi{}^2/9, L = 30$
Fig. 6.6	$\gamma = 0.01, \alpha = 0.37, \beta = 0.05$(red,blue), $\beta = 0.13$(green,violet)
Fig. 6.7 & 6.8	$\gamma = 0.01, \alpha = 0.37, \beta = 0.05$(a), $\beta = 0.13$(b), $\Delta_\xi = 0.03, \Delta_\tau = 4\Delta_\xi{}^2/9$
Fig. 6.9(a,c)	$\gamma = 0.01, \alpha = 0.37, \beta = 0.05, \Delta_\xi = 0.03, \Delta_\tau = 4\Delta_\xi{}^2/9, L = 60$
Fig. 6.9(b,d)	$\gamma = 0.01, \alpha = 0.37, \beta = 0.13, \Delta_\xi = 0.03, \Delta_\tau = 4\Delta_\xi{}^2/9, L = 60$
Fig. 6.10 & 6.12	$\gamma = 0.01, \alpha = 0.37, \beta = 0.05$
Fig. 6.11(a,b)	$\gamma = 0.001, \beta = 0.05, \alpha = 0.37$
Fig. 6.11(c,d)	$\gamma = 10^{-6}, \beta = 0.01, \alpha = 0.37$
Fig. 6.13(a)	$\beta = 0.01, \alpha = 0.37, \gamma = 10^{-5}$
Fig. 6.13(b)	$\beta = 0.05, \alpha = 0.37, \gamma = 10^{-2}$
Fig. 6.14	$\alpha = 0.105$(red,blue), $\alpha = 0.115$ (green,violet)
Fig. 6.15	$\alpha = 0.105$(a), $\alpha = 0.115$(b), $\Delta_\xi = 0.03, \Delta_\tau = 4\Delta_\xi{}^2/9$
Fig. 6.16	$\alpha = 0.105$(a,c), $\alpha = 0.115$(b,d), $\Delta_\xi = 0.03, \Delta_\tau = 4\Delta_\xi{}^2/9$
Fig. 6.17	$\alpha = 0.105$(a,c), $\alpha = 0.115$(b,d), $\Delta_\xi = 0.03, \Delta_\tau = 4\Delta_\xi{}^2/9$

Table 6.3: The complete set of parameters and discretization values used in the figures.

CHAPTER 7

CONCLUSION AND FUTURE WORK

In this final chapter, we shall summarise the results we have obtained in this thesis, and then discuss the implications and limitations of the research. We finally conclude the chapter with an outline of further directions.

7.1 Summary and Main Results

The main aim of this thesis was to substantially extend the method proposed in [68] for analytical description of the threshold curves that separate the basins of attraction of propagating wave solutions and of decaying solutions of certain reaction-diffusion models of spatially-extended excitable media. The specific aims of this thesis were:

- Extending the proposed theory to analysis of a wider class of excitable systems, including multicomponent reaction-diffusion systems, systems with non-self-adjoint linearized operators and in particular, systems with moving critical solutions (critical fronts and critical pulses).
- Building an extension of this method from a linear to a quadratic approximation of the (center-)stable manifold of the critical solution to demonstrate the discrepancy between the analytical based on the linear approximation and numerical threshold curves encountered when considering this quadratic approximation.

The mathematical structure of the theory of these main aims listed above has been outlined in Chapter 3. The essential ingredients of the theory are the critical solution

itself, and the eigenfunctions of the corresponding linearized operator. For the linear approximation in the critical nucleus case, we need the leading left (adjoint) eigenfunction; in the moving critical solution case, we need two leading left eigenfunctions; and for the quadratic approximations we require as many eigenvalues and left and right eigenfunctions as possible to achieve better accuracy. Of course, closed analytical formulas for these ingredients can only be obtained in exceptional cases, and in a more typical situation a "hybrid" approach is required, where these ingredients are obtained numerically. In Chapter 4, we have provided insight into how the numerical computation of these essential ingredients and the direct numerical simulation of the threshold curves can be carried out. Specifically, the following has been covered in Chapter 4:

- The finite difference and finite element numerical simulations of the strength-extent and strength-duration curves generated using the bisection algorithm.
- A numerical procedure for the determination of the critical nucleus that is a unique, time-independent solution of one-component reaction-diffusion equation.
- A shooting technique for the numerical solution of the initial value problem with the initial condition very close to initiation threshold in order to identify the moving critical solution, in particular the critical front, by means of the operator splitting method.
- Providing insight into how the conduction velocity restitution curves are computed with the help of the continuation software AUTO [34] as a solution of the periodic boundary value problem such that one end of this curve (lower branch) defines the critical pulse solution.
- Numerical computation of the eigenvalues, and left and right eigenfunctions using modified power iteration method that solves the linearized and adjoint linearized eigenvalue problems.
- Proposing the standard implicitly restarted Arnoldi iterative method to approximately determine the eigenpairs as an alternative and usually less time-consuming technique compared to the power iteration.

The analytical theory and hybrid procedure have been demonstrated on five different test problems given in Chapter 5 and Chapter 6. Chapter 5 is dedicated to

the one-component reaction-diffusion test problems where the critical solution is the critical nucleus and Chapter 6 contains the multicomponent test problems with either critical front or critical pulse solution. Some results that we have presented in these chapters are as follows:

- The hybrid numerical method of calculating the essential ingredients of the theory has been applied in a simple, generic manner as described in Chapter 4 even when we have the closed analytical formulas for some of these ingredients so that the hybrid method is effectively validated.
- In all models, the analytical threshold curves are compared with the ones obtained from direct numerical simulations. We have applied both the linear and quadratic approximations for one-component test problems, ZFK and McKean models. The quadratic approximation agreed very well with numerical threshold curves compared to the linear approximations' results, as would be expected.
- For the models with discontinuous right hand sides, the standard finite difference discretization leads to the "frozen solution" phenomenon, which directs us to a finite-element approximation instead and this approach prevented this frozen solution as in explained in more detail in the appendices at the end of this thesis.
- For the multicomponent test problems, one is unlikely to obtain the analytical description of the ingredients of the threshold curves, so we have invoked the hybrid numerical-asymptotic method to deal with these ingredients. Nevertheless, we have presented a reasonable approach for FHN system to provide a full analytical treatment by the use of the perturbation theory that benefits from the exact analytical solutions of its primitive version, ZFK equation.
- We have also developed a numerical procedure based on an operator splitting procedure for obtaining the critical front in a comoving frame of reference and the first two leading left and right eigenfunctions along with corresponding eigenvalues for Biktashev model, as described in detail in Appendix C.

7.2 Research Implications and Limitations

As is emphasised in this thesis, the essential ingredients of the theory can not always be analytically calculated, and therefore we have presented the hybrid approach, which describes how to obtain these ingredients numerically. The main disadvantages

of such approach are that it naturally causes some error in the prediction of any considered ingredient(s), and also increases the computational expense of the theory. For example, when performing the quadratic approximation in McKean equation, we have considered a limited number of eigenpairs instead of the whole spectrum, and a finite interval $x \in [0, L)$ as an approximation of $x \in [0, \infty)$. With this in mind, the choice of the parameter L is directly related to the required computation time and considering the performance of the quadratic approximation related to L, a large amount of computational effort is usually required.

The accuracy and efficiency of the hybrid computation of the essential ingredients are dependent on the numerical scheme and mesh resolution. In general, we have chosen the spatial and temporal discretizations in the way that we keep the numerical error under control and the computation time as small as possible. It is obvious that some of the numerical schemes discussed in this thesis do not outperform other long-running and mathematically more complicated numerical schemes. In particular, the numerical study of Biktashev model has introduced the spurious oscillations and first-order accurate result near the discontinuities due to Beam-Warming method, which can be tackled using some advanced shape-preserving advection schemes (see, for example, [114]). However, these approaches demand high computational cost, which is why they are beyond the scope of this thesis.

Obviously, we have considered stepwise rectangular initial and boundary profiles throughout the thesis. However, the theory can be easily generalized to any kind of shape. Note that the hybrid approach determining the essential ingredients of the theory is actually independent of the choice of both initial and boundary profiles.

As the results of the theory pointed out, our method provides more accurate results for some parameter values than the others, especially in the linear analysis. Even though the quadratic approximation offered for one-component test problems with the critical nucleus solutions provides more accurate estimates, still it is not fully understood why the choice of parameter values significantly matters. We can, however, point several possible likely explanations for this disagreement based on empirical evidences. As can be observed from the related figures, the linear approximation works better if the correction induced by the quadratic approximation is small. Yet again, this has been verified only for the scalar equations since we have not investigated the quadratic approximation for the cases of moving critical solutions. Another possible explanation for such discrepancy would be linked to the behaviour of the discrete and continuous spectra, and hence corresponding eigenfunctions. We also believe

that the absolute difference between the first (for the case of the critical nucleus) or second (for the case of the moving critical solutions) leading eigenvalue and the next eigenvalues with biggest real part has the effect of making the linear approximation better or worse.

7.3 Future Work

- The theory established in this thesis is limited to one spatial dimension. Therefore, it could be of interest for further researches to adopt the theory to two and three dimensions.
- The proposed theory based on the moving critical solutions involves only the linear approximation. As an additional consideration, the quadratic approximation for the cases of moving critical solutions can also be carried out. This could lead us to understand why the performance of the theory varies according to the choices of the parameters.
- Another extension of the work worth considering would be to investigate the theory on some up-to-date realistic cardiac excitation models [28], simplified cardiac models with unusual properties [36, 59], and other excitable media such as combustible media [64, 83, 121], pipe flow [8, 9] *etc.*
- Throughout the theory, we have made the assumption that the spectrum is real. This is, however, not necessarily the case for the non-self-adjoint problems, which remains an interesting direction for future research.
- Although it is rather hard to obtain, development of new procedure to provide closed analytical formulas for essential ingredients could also be another interesting line of research. This is needed especially when we compare our theory with some other well-known approaches. For instance, it is known that the classical Lapicque-Blair-Hill formula does not always work well. We have shown that this is indeed the case for the FHN system by means of the asymptotic perturbation theory analysis.

APPENDIX A

FINITE ELEMENT DISCRETIZATION FOR THE MCKEAN MODEL

Here, we present the finite element discretization formula for the McKean model to solve initial-value problems both for the nonlinear equation,

$$\frac{\partial u}{\partial t} = \frac{\partial^2 u}{\partial x^2} - u + \mathrm{H}(u-a),$$

and its linearization,

$$\frac{\partial v}{\partial t} = \frac{\partial^2 v}{\partial x^2} - v + \delta(u-a)v.$$

These are equivalent (for u decreasing in x) to

$$\frac{\partial u}{\partial t} = \frac{\partial^2 u}{\partial x^2} - u + \mathrm{H}(x_* - x),$$
$$\frac{\partial v}{\partial t} = \frac{\partial^2 v}{\partial x^2} - v + \frac{1}{u'(x_*)}\delta(x-x_*)v,$$

where $x_* = x_*(t)$ is defined by

$$u(x_*(t),t) = a.$$

As the right-hand sides of each equation include Heaviside step and Dirac delta functions, the finite-element treatment is required for both cases, and we present the details for both cases together, by writing both as

$$\frac{\partial w}{\partial t} = \frac{\partial^2 w}{\partial x^2} + f(w,x), \tag{A.1}$$

where $w = u$, $f = -u + \mathrm{H}(u-a) = -u + \mathrm{H}(x_* - x)$ in one case, and $w = v$, $f = -v + \delta(u-a)v = -v + (1/u'(x_*))\delta(x-x_*)v$ in the other case.

Multiplying (A.1) by any "test function" $\Phi(x)$, and integrating over the domain gives the weak formulation of the problem,

$$\int_0^L \Phi(x)\left\{\frac{\partial w}{\partial t} - \frac{\partial^2 w}{\partial x^2} - f(w,x)\right\}\mathrm{d}x = 0.$$

As is known and stated in Section 2.6, the solution of the weak formulation is also the solution of the original equation. After integration by parts and taking into account Neumann boundary conditions for w, the weak formulation can be formally re-written as

$$\int_0^L \left[\Phi(x)\left(\frac{\partial w}{\partial t} - f(w,x)\right) + \frac{\partial \Phi}{\partial x}\frac{\partial w}{\partial x}\right]\mathrm{d}x = 0. \tag{A.2}$$

The difference is, of course, that whereas the original formulation requires that w is twice differentiable in x, the weak formulation (A.2) uses only first derivatives of w, and can be applied as long as the test functions Φ are once differentiable.

The standard finite element method is the Galerkin method applied to (A.2). It uses a set of linearly independent functions,$\Phi_j(x)$, $j = 1,\ldots,N$, called the finite elements, as the test functions, and seeks the approximation of the solution in the span of this same set:

$$w(x,t) \approx \breve{w}(x,t) = \sum_{j=0}^{N} \breve{w}_j(t)\Phi_j(x). \tag{A.3}$$

Substitution of (A.3) into (A.2) for $\Phi = \Phi_i$, $i = 1,\ldots,N$, leads to the system of equations

$$\sum_{j=0}^{N} A_{i,j}\frac{\mathrm{d}\breve{w}_j}{\mathrm{d}t} + \sum_{j=0}^{N} B_{i,j}\breve{w}_j = C_i\left(\breve{w}_j\right), \quad i = 1,\ldots,N,$$

or in the vector form, for $\breve{\mathbf{w}}(t) = \left(\breve{w}_j\right)$,

$$\mathbf{A}\frac{\mathrm{d}\breve{\mathbf{w}}}{\mathrm{d}t} + \mathbf{B}\breve{\mathbf{w}} = \mathbf{C}, \tag{A.4}$$

where the coefficients are given by

$$A_{i,j} = \int_0^L \Phi_i(x)\Phi_j(x)\,\mathrm{d}x, \tag{A.5a}$$

$$B_{i,j} = \int_0^L \Phi_i'(x)\Phi_j'(x)\,\mathrm{d}x, \tag{A.5b}$$

$$C_i\left(\breve{w}_j\right) = \int_0^L \Phi_i(x) f\left(\sum_{j=0}^{N}\breve{w}_j\Phi_j(x), x\right)\mathrm{d}x. \tag{A.5c}$$

Throughout the thesis, we stick to the same simple and popular choice of the test function, the piecewise linear *tent functions*:

$$\Phi_i(x) = \begin{cases} (x - x_{i-1})/\Delta_x, & x \in [x_{i-1}, x_i], \\ (x_{i+1} - x)/\Delta_x, & x \in [x_i, x_{i+1}], \\ 0, & \text{otherwise} \end{cases} \tag{A.6}$$

for a regular grid of (x_i),

$$x_i = (i-1)\,\Delta_x, \quad i = 1, \ldots, N, \qquad \Delta_x = L/(N-1). \tag{A.7}$$

Obviously, in this case

$$\Phi_j(x_i) = \begin{cases} 1, & \text{if} \quad i = j, \\ 0, & \text{otherwise} \end{cases}$$

and therefore $\check{w}(x_i) = \check{w}_i$. For these test functions, the mass matrix $\mathbf{A} = \left(A_{i,j}\right)$ and the stiffness matrix $\mathbf{B} = \left(B_{i,j}\right)$ are tridiagonal matrices as respectively given in (2.73) and (2.74) whereas the load vector $\mathbf{C} = \left(C_i\right)$ is expressed as

$$\mathbf{C}(\check{\mathbf{w}}) = -\mathbf{A}\check{\mathbf{w}} + \mathbf{F}, \tag{A.8}$$

where $\mathbf{F} = \left(F_i\right)$ and differs for the nonlinear problem and for the linearized problem.

For the nonlinear problem, $\check{\mathbf{w}} = \check{\mathbf{u}}$, we get $\mathbf{F} = \mathbf{F}^{(1)} + \mathbf{F}^{(2)}$, where

$$F_i^{(1)} = \frac{1}{2\Delta_x} \begin{cases} {\Delta_x}^2, & \check{u}_{i-1} > a,\ \check{u}_i > a, \\ (x_* - x_{i-1})^2, & \check{u}_{i-1} > a,\ \check{u}_i < a, \\ {\Delta_x}^2 - (x_* - x_{i-1})^2, & \check{u}_{i-1} < a,\ \check{u}_i > a, \\ 0, & \text{otherwise}, \end{cases} \tag{A.9}$$

and

$$F_i^{(2)} = \frac{1}{2\Delta_x} \begin{cases} {\Delta_x}^2, & \check{u}_{i+1} > a,\ \check{u}_i > a, \\ (x_* - x_{i+1})^2, & \check{u}_{i+1} > a,\ \check{u}_i < a, \\ {\Delta_x}^2 - (x_* - x_{i+1})^2, & \check{u}_{i+1} < a,\ \check{u}_i > a, \\ 0, & \text{otherwise} \end{cases} \tag{A.10}$$

for $i = 2, \ldots, N-1$, and

$$F_1 = \frac{1}{4\Delta_x} \begin{cases} 2{\Delta_x}^2, & \check{u}_1 > a,\ \check{u}_2 > a, \\ (x_* - x_0)^2 + (x_2 - x_*)^2, & \check{u}_1 < a,\ \check{u}_2 > a, \\ 2{\Delta_x}^2 - (x_* - x_0)^2 - (x_2 - x_*)^2, & \check{u}_1 > a,\ \check{u}_2 < a, \\ 0, & \text{otherwise}, \end{cases} \tag{A.11}$$

and

$$F_N = \frac{1}{4\Delta_x} \begin{cases} 2{\Delta_x}^2, & \check{u}_{N-1} > a,\ \check{u}_N > a, \\ (x_* - x_{N+1})^2 + (x_{N-1} - x_*)^2, & \check{u}_{N-1} > a,\ \check{u}_N < a, \\ 2{\Delta_x}^2 - (x_* - x_{N+1})^2 - (x_{N-1} - x_*)^2, & \check{u}_{N-1} < a,\ \check{u}_N > a, \\ 0, & \text{otherwise} \end{cases} \tag{A.12}$$

for the boundary points. In these formulas, where x_* is the point such that $\check{u}(x_*, t) = a$ by linear interpolation, i.e. for m such that $(\check{u}_m - a)(\check{u}_{m+1} - a) \le 0$, we have $x_* = ((\check{u}_{m+1} - a)x_m + (a - \check{u}_m)x_{m+1})/(\check{u}_{m+1} - \check{u}_m)$, and the definition (A.7) is extended to $i = 0$ and $i = N+1$.

For the linear problem, $\check{\mathbf{w}} = \check{\mathbf{v}}$, we get

$$F_m = \frac{1}{a{\Delta_x}^2} \left[(x_{m+1} - x_*)^2 \check{v}_m + (x_{m+1} - x_*)(x_* - x_m)\check{v}_{m+1} \right], \tag{A.13}$$

$$F_{m+1} = \frac{1}{a{\Delta_x}^2} \left[(x_{m+1} - x_*)(x_* - x_m)\check{v}_m + (x_* = -x_m)^2 \check{v}_{m+1} \right], \tag{A.14}$$

$$F_j = 0, \qquad j \neq m, m+1, \tag{A.15}$$

where m and x_* are defined based on the nonlinear solution $\check{\mathbf{u}}$ based on the same rule as above.

After forming the mass and stiffness matrices, and the load vector, we are left to apply the generalized trapezoidal rule [110] to approximate the time derivative in the residual of (A.4), which results in

$$(\mathbf{A} + \Delta_t \theta \mathbf{B})\check{\mathbf{w}}^{n+1} = (\mathbf{A} - \Delta_t (1-\theta)\mathbf{B})\check{\mathbf{w}}^n + \mathbf{C}, \tag{A.16}$$

for the regular discretization of time

$$t_n = n\Delta_t, \quad n = 0, 1\ldots, \qquad \Delta_t = t_1 - t_0. \tag{A.17}$$

and the parameter θ is fixed to $1/2$ so that we have a second-order neutrally stable scheme.

APPENDIX B

ON "FROZEN NUCLEI" IN THE MCKEAN EQUATION

As already mentioned in the previous chapters, the critical nucleus solution, which is even, unstable, nontrivial time-independent solution of one-dimensional one-component reaction-diffusion system (3.1) (with k=1) plays a crucial role in understanding initiation of propagating waves in ZFK and McKean equations. In addition, such solution is unique as shown *e.g.* in [101]. For the sake of completeness and generality, we have presented the general technique approximating this critical nucleus as outlined in Section 4.4 but without describing specific numerical integration. The choice of the numerical method solving the discretized version of McKean equation is particularly important, we have considered the standard finite difference discretization at first. The numerical results based on this discretization, however, are not promising and convincing since the numerical critical nucleus as defined by the standard difference scheme is not actually unique and is stable. This scenario is similar to "propagation block" or "propagation failure" observed in several different forms of discrete reaction-diffusion system (see *e.g.* [37, 62, 65, 72]). Keener [72] established that the generic system with a smooth cubic nonlinearity has "frozen solutions" for sufficiently large discretization steps. Roughly speaking, for McKean model, however, the frozen solution exists for *all* discretization steps due to the discontinuous right-hand side, as will be explained in more details below.

For the regular grid discretization,

$$u_j = u(x_j), \qquad x_j = j\Delta_x, \qquad j \in \mathbb{Z}, \qquad u_{-j} \equiv u_j,$$

the "discrete critical nucleus" is the nontrivial solution of

$$\frac{u_{j-1}-2u_j+u_{j+1}}{{\Delta_x}^2}-u_j+\mathrm{H}(u_j-a)=0. \tag{B.1}$$

Since the critical nucleus is even in x and strictly monotonically decreasing in $0\le x<\infty$, we let $u_j>a$ for $j\in\overline{0,m}$ and $u_j<a$ otherwise. Then, we set $v_j=u_j-\mathrm{H}(u_j-a)$ so that (B.1) takes the same form on the each of the intervals

$$v_{j-1}-2v_j+v_{j+1}-{\Delta_x}^2 v_j=0. \tag{B.2}$$

For $v_j\propto\sigma^j$, this gives

$$\sigma^2-\left(2+{\Delta_x}^2\right)\sigma+1=0,$$

and so $\sigma=\mu$ or $\sigma=1/\mu$, where

$$\mu\triangleq\frac{2+{\Delta_x}^2+\Delta_x\sqrt{4+{\Delta_x}^2}}{2}. \tag{B.3}$$

The general solution of equation (B.2) satisfying the boundary condition $\lim_{j\to\infty}v_j=0$ is

$$v_j=\begin{cases}A\mu^{-j}, & j\ge m,\\ B\left(\mu^j+\mu^{-j}\right), & j\le m+1,\end{cases} \tag{B.4}$$

for some constants A and B, and these are specified by the matching conditions implying that the two solutions should coincide at $j=m$ and $j=m+1$

$$A=\frac{\left(\mu^{2m+1}-1\right)}{\mu^m\left(\mu+1\right)},\quad B=-\frac{1}{\mu^m\left(\mu+1\right)}. \tag{B.5}$$

The critical nucleus solution is then obtained by substituting these coefficients into (B.4) and then v_j back into $u_j=v_j+\mathrm{H}(u_j-a)$

$$\hat{u}_j=\begin{cases}1-\dfrac{\mu^j+\mu^{-j}}{\mu^m\left(\mu+1\right)}, & j\in\overline{0,m+1},\\ \dfrac{\left(\mu^{2m+1}-1\right)\mu^{-j}}{\mu^m\left(\mu+1\right)}, & j\in\overline{m,\infty},\end{cases} \tag{B.6}$$

where we have considered $a\in(\hat{u}_{m+1},\hat{u}_m)$, *i.e.* there is no corresponding value of the discretized solution exactly equal to a. The parameter a can be written as

$$a\in\left(\frac{\mu^m-\mu^{-m-1}}{\mu^{m+1}+\mu^m},\frac{\mu^{m+1}-\mu^{-m}}{\mu^{m+1}+\mu^m}\right)=\left(\underline{a}_m,\overline{a}_m\right).$$

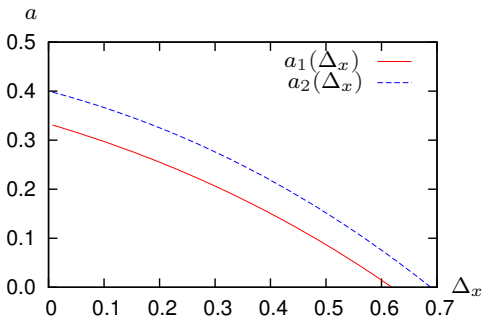

Figure B.1: Non-uniqueness of the discrete critical nucleus solutions is observed for some $a > a_1(\Delta_x)$, and for all $a > a_2(\Delta_x)$.

This verifies that there is a range of possible values of a for a given m. Hence, at a fixed discretization step Δ_x, the critical nucleus solution discontinuously depends on the parameter a, and it is possible to obtain more than one solution for some combinations of Δ_x and a, as opposed to the uniqueness property of the critical nucleus. Indeed, this can be shown by solving the inequality

$$\underline{a}_{m+1} < \overline{a}_m,$$

we find the following relation

$$m > m_1 \triangleq \frac{\ln\left(\mu^2+\mu+1\right)}{2\ln\mu} - \frac{3}{2}. \tag{B.7}$$

Considering that the discrete critical nucleus solution (B.6) approximates the exact critical nucleus solution (5.14), we have the corresponding matching point coordinate

$$x_* > x_1^* \approx \Delta_x m_1, \tag{B.8}$$

and then from (5.15)

$$a > a_1 \approx \frac{1}{2}\left(1-\mathrm{e}^{-2x_1^*}\right) = \frac{1}{2}\left[1-\exp\left(-\Delta_x\left(\frac{\ln\left(\mu^2+\mu+1\right)}{\ln\mu}-3\right)\right)\right]. \tag{B.9}$$

Equations (B.3), (B.7), (B.8) and (B.9) define a_1 as a function of Δ_x, such that for $a > a_1(\Delta_x)$ there can be more than one discrete solution corresponding to the same a. Similarly, by solving the inequality

$$\underline{a}_{m+2} < \overline{a}_m,$$

we obtain

$$m > m_2 \triangleq \frac{\ln\left(\mu^4+\mu^3+\mu^2+\mu+1\right)}{2\ln\mu} - \frac{5}{2}. \tag{B.10}$$

In this case, the matching point coordinate is $x_2^* \approx \Delta_x m_2$ and we have the following relation derived from (5.15)

$$a > a_2 \approx \frac{1}{2}\left(1 - \mathrm{e}^{-2x_2^*}\right) = \frac{1}{2}\left[1 - \exp\left(-\Delta_x\left(\frac{\ln\left(\mu^4+\mu^3+\mu^2+\mu+1\right)}{\ln\mu} - 5\right)\right)\right]. \tag{B.11}$$

Figure B.1 shows the graph of functions $a_1(\Delta_x)$ and $a_2(\Delta_x)$, which characterizes the non-uniqueness of the discrete critical nucleus solutions.

Moreover, to investigate the *stability* of the discrete critical nucleus solution, we consider the linearized system around the critical nucleus

$$\frac{\mathrm{d}v_j}{\mathrm{d}t} = \frac{v_{j-1} - 2v_j + v_{j+1}}{{\Delta_x}^2} - v_j, \qquad j \in \mathbb{Z}. \tag{B.12}$$

The spectrum of the system (B.12) in $\ell^2(\mathbb{Z})$ is $[-1-4/{\Delta_x}^2, -1]$, with eigenpairs

$$W_j = \exp(i\kappa j) + \exp(-i\kappa j), \quad \lambda = -1 - 2(1-\cos\kappa)/{\Delta_x}^2, \quad \kappa \in \mathbb{R}.$$

Thus, the discretized critical nuclei are almost surely asymptotically stable in the linear approximation. Contrary to the expectation that any initial condition with amplitude U_s either ignites or decays (likewise for I_s), the result of the direct numerical simulation encounters time-independent solutions behaving like these “critical nucleus” solutions. Generally speaking, these “frozen” solutions are to be observed for all discretization steps and the region where “frozen” solutions occur is inversely proportional to the discretization step. This “frozen” region is illustrated in Figure B.2.

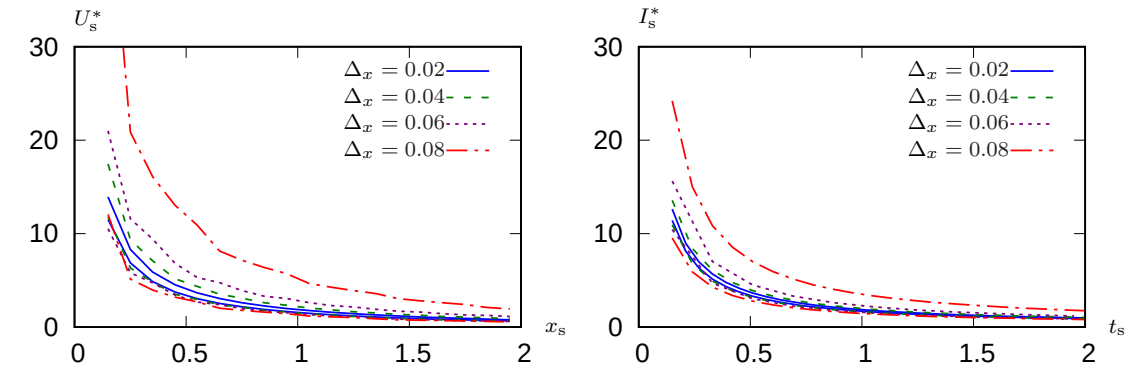

Figure B.2: The "frozen" nuclei solution of the McKean model obtained by direct numerical simulations for different discretization steps where panel (a) corresponds to the strength-extent curve analysis and panel (b) is for the strength-duration curve. Parameters: $a = 0.48$, $L = 10$, $\Delta_t = 4{\Delta_x}^2/9$.

APPENDIX C

NUMERICAL APPROACHES TO THE BIKTASHEV MODEL

This appendix contains the discretization formula for the Biktashev model. Specifically, we aim to provide the numerical procedure for finding the critical front and first two leading eigenvalues and the corresponding left and right eigenfunctions accordingly. To begin with, we consider an even extension of the model,

$$\begin{aligned} \frac{\partial E}{\partial t} &= \frac{\partial^2 E}{\partial x^2} + \mathrm{H}(E-1)h, \\ \frac{\partial h}{\partial t} &= \frac{1}{\tau_*}(\mathrm{H}(-E)-h), \quad x \in (-\infty,\infty), t \in (0,\infty), \\ E(x,0) &= E_\mathrm{s}\mathrm{H}(x_\mathrm{s}-x)\mathrm{H}(x_\mathrm{s}+x)-\alpha. \end{aligned} \tag{C.1}$$

In the co-moving frame of reference $\xi = x - s(\tau)$, $\tau = t$, (C.1) becomes

$$\begin{aligned} \frac{\partial E}{\partial \tau} &= \frac{\partial^2 E}{\partial \xi^2} + s'(\tau)\frac{\partial E}{\partial \xi} + \mathrm{H}(E-1)h, \\ \frac{\partial h}{\partial \tau} &= s'(\tau)\frac{\partial h}{\partial \xi} + \frac{1}{\tau_*}(\mathrm{H}(-E)-h), \quad \xi \in (-\infty,\infty), \tau \in (0,\infty), \\ E(\xi,0) &= E_\mathrm{s}\mathrm{H}(-\xi)\mathrm{H}(\xi+2x_\mathrm{s})-\alpha. \end{aligned} \tag{C.2}$$

We also need to impose a pinning condition in order to find the value of s' which varies at each time step. This can be achieved by considering the shape of E component of the critical front solution. A common way to define such condition is to choose a constant E^* represented once in the front profile for every time step,

$$E(s(\tau),\tau) = E^*. \tag{C.3}$$

For simplicity, we take $E^* = 0$.

C.1 Discretization Formula for the Critical Front

Numerical analysis of the critical front for Biktashev model is based on a combination of finite element and finite difference methods by using the operator splitting method (see *e.g.* [50]). Finite element method is used to handle the right-hand sides of the equations with discontinuous terms involving the Heaviside step function. For the standard finite difference discretization, we use the Beam-Warming scheme for the first spatial derivatives of both E and h. We set the domain of ξ and τ coordinates to be $-L \le \xi \le L$, $0 \le \tau \le \tau_f$ so that the grid points ξ_i, τ_n are

$$\xi_i = -L + i\Delta_\xi, \quad \tau_n = n\Delta_\tau,$$

where $\Delta_\xi > 0$ and $\Delta_\tau > 0$ are fixed space and time steps, and $i = 1,2,\cdots,N$, $n = 0,1,\cdots,M$ for $N,M > 0$. For convenience, we use the following shorthand notations: E_i^n, h_i^n as the numerical approximation of $E(\xi_i,\tau_n)$ and $h(\xi_i,\tau_n)$, $E_{i_*}^n = 0$ as our pinning condition which will be further explained later, and finally $c^n = s'(\tau_n)$ as the speed at $n-th$ time step. Using these representations, we solve (C.2) numerically using operator splitting method approach in the following seven steps:

Step 1(Finite element method): As a first step, we solve E equation without the advection term as it is multiplied by the speed which is not determined yet

$$\frac{\partial E}{\partial \tau} = \frac{\partial^2 E}{\partial \xi^2} + \mathrm{H}(E-1)h. \tag{C.4}$$

We have to employ the finite element method due to the discontinuous Heaviside step function which gives

$$[\mathbf{A} + \Delta_\tau \mathbf{B}\theta]E_i^{n+1/2} = [\mathbf{A} - \Delta_\tau \mathbf{B}(1-\theta)]E_i^n + \Delta_\tau \mathbf{D}h_i^n, \tag{C.5}$$

where we set $\theta = 0.5$. The matrices $\mathbf{A}$ and $\mathbf{B}$ are the mass and stiffness matrices as defined in (2.73) and (2.74), while the matrix $\mathbf{D}$ is the matrix obtained from the kinetics term

$$\mathbf{D} = \left[d_{i,j}\right] = \int_{-L}^{L} \mathrm{H}(E-1)\Phi_i(\xi)\Phi_j(\xi)\,\mathrm{d}\xi, \tag{C.6}$$

which is a tridiagonal matrix with following diagonal elements,

$$\begin{aligned} d_{i,i} = \int_{-L}^{L} \mathrm{H}(E-1)\Phi_i^2(\xi)\,\mathrm{d}\xi = \frac{1}{{\Delta_\xi}^2}\left(\int_{\xi_{i-1}}^{\xi_i} \mathrm{H}(E-1)(\xi-\xi_{i-1})^2\,\mathrm{d}\xi \right. \\ \left. + \int_{\xi_i}^{\xi_{i+1}} \mathrm{H}(E-1)(\xi_{i+1}-\xi)^2\,\mathrm{d}\xi\right) = {I_3}^i + {I_4}^i, \qquad \text{for} \quad i = 2,3,\cdots,N-1 \end{aligned} \tag{C.7}$$

where

$$I_3{}^i = \frac{1}{3\Delta_\xi{}^2}\begin{cases}\Delta_\xi{}^3, & E_{i-1}>1, E_i>1,\\ \left(\xi^*_{i-1}-\xi_{i-1}\right)^3, & E_{i-1}>1, E_i<1,\\ \Delta_\xi{}^3-\left(\xi^*_{i-1}-\xi_{i-1}\right)^3, & E_{i-1}<1, E_i>1,\\ 0, & \text{otherwise,}\end{cases} \tag{C.8}$$

$$I_4{}^i = \frac{1}{3\Delta_\xi{}^2}\begin{cases}\Delta_\xi{}^3, & E_i>1, E_{i+1}>1,\\ \Delta_\xi{}^3-\left(\xi_{i+1}-\xi^*_{i+1}\right)^3, & E_i>1, E_{i+1}<1,\\ \left(\xi_{i+1}-\xi^*_{i+1}\right)^3, & E_i<1, E_{i+1}>1,\\ 0, & \text{otherwise.}\end{cases} \tag{C.9}$$

The supradiagonal elements of $\mathbf{D}$ are evaluated as

$$d_{i,i+1} = \int_{-L}^{L} \mathrm{H}(E-1)\,\Phi_i(\xi)\Phi_{i+1}(\xi)\,\mathrm{d}\xi = \frac{1}{\Delta_\xi}\int_{\xi_i}^{\xi_{i+1}} \mathrm{H}(E-1)(\xi_{i+1}-\xi)(\xi-\xi_i)\,\mathrm{d}\xi$$

$$= \frac{1}{6\Delta_\xi{}^2}\begin{cases}\Delta_\xi{}^3, & E_i>1, E_{i+1}>1,\\ 3\xi_{i+1}\xi^*_{i+1}{}^2+3\xi_{i+1}\xi_i^2-2\xi^*_{i+1}{}^3-\xi_i^3 & \\ \quad -6\xi_{i+1}\xi_i\xi^*_{i+1}+3\xi_i\xi^*_{i+1}{}^2, & E_i>1, E_{i+1}<1,\\ \xi_{i+1}^3-3\xi_{i+1}\xi^*_{i+1}{}^2+2\xi^*_{i+1}{}^3-3\xi_i\xi^*_{i+1}{}^2 & \\ \quad -3\xi_i\xi^*_{i+1}{}^2+6\xi_i\xi_{i+1}\xi^*_{i+1}, & E_i<1, E_{i+1}>1,\\ 0, & \text{otherwise,}\end{cases} \tag{C.10}$$

and finally the subdiagoanal elements are

$$d_{i-1,i} = \int_{-L}^{L} \mathrm{H}(E-1)\,\Phi_i(\xi)\Phi_{i-1}(\xi)\,\mathrm{d}\xi = \frac{1}{\Delta_\xi{}^2}\int_{\xi_{-1}}^{\xi_i} \mathrm{H}(E-1)(\xi-\xi_{i-1})(\xi_i-\xi)\,\mathrm{d}\xi$$

$$= \frac{1}{6\Delta_\xi{}^2}\begin{cases}\Delta_\xi{}^3, & E_{i-1}>1, E_i>1,\\ 3\xi_i\xi^*_{i-1}{}^2+3\xi_{i-1}\xi^*_{i-1}{}^2+3\xi_i\xi_{i-1}^2-\xi_{i-1}^3 & \\ \quad -6\xi_{i-1}\xi_i\xi^*_{i-1}-2\xi^*_{i-1}{}^3, & E_{i-1}>1, E_i<1,\\ \xi_i^3+6\xi_i\xi_{i-1}\xi^*_{i-1}+2\xi^*_{i-1}{}^3-3\xi_{i-1}\xi_i^2 & \\ \quad -3\xi_i\xi^*_{i-1}{}^2-3\xi_{i-1}\xi^*_{i-1}{}^2, & E_{i-1}<1, E_i>1,\\ 0, & \text{otherwise.}\end{cases} \tag{C.11}$$

Inserting the no-flux boundary conditions at each end gives

$$d_{1,1}=\frac{1}{3{\Delta_\xi}^2}\begin{cases}2{\Delta_\xi}^3, & E_1>1, E_2>1,\\ 2{\Delta_\xi}^3-\left(\xi_2-\xi_2^*\right)^3-\left(\xi_2^*-\xi_2+2\Delta_\xi\right)^3, & E_1>1, E_2<1,\\ \left(\xi_2^*-\xi_2+2\Delta_\xi\right)^3+\left(\xi_2-\xi_2^*\right)^3, & E_1<1, E_2>1,\\ 0, & \text{otherwise},\end{cases} \tag{C.12}$$

$$d_{N,N}=\frac{1}{3{\Delta_\xi}^2}\begin{cases}2{\Delta_\xi}^3, & E_{N-1}>1, E_N>1,\\ \left(\xi_{N-1}+2\Delta_\xi-\xi_{N-1}^*\right)^3+\left(\xi_{N-1}^*-\xi_{N-1}\right)^3, & E_{N-1}>1, E_N<1,\\ -\left(\xi_{N-1}+2\Delta_\xi-\xi_{N-1}^*\right)^3+2{\Delta_\xi}^3-\left(\xi_{N-1}^*-\xi_{N-1}\right)^3, & E_{N-1}<1, E_N>1,\\ 0, & \text{otherwise}.\end{cases} \tag{C.13}$$

Having in mind that the tent functions we have chosen are piecewise linear, the points ξ_{i-1}^*, ξ_{i+1}^*, ξ_2^* and ξ_{N-1}^* are then obtained from the linear interpolation method

$$\xi_{k+1}^*=\frac{[E(\xi_{k+1})-1]\xi_k+[1-E(\xi_k)]\xi_{k+1}}{E(\xi_{k+1})-E(\xi_k)},$$

for $k=1,i-2,i,N-2$.

Step 2(Thomas algorithm): Inserting the elements of the matrices **A**, **B** and **D** into (C.5) yields

$$\begin{bmatrix}\beta_1 & \gamma_1 & 0 & & 0\\ \alpha_2 & \beta_2 & \gamma_2 & & \\ & \alpha_3 & \beta_3 & \ddots & \\ & & \ddots & \ddots & \gamma_{N-1}\\ 0 & & & \alpha_N & \beta_N\end{bmatrix}\begin{pmatrix}E_1^{n+1/2}\\ \vdots\\ \vdots\\ \vdots\\ E_N^{n+1/2}\end{pmatrix}=\begin{pmatrix}\delta_1\\ \vdots\\ \vdots\\ \vdots\\ \delta_N\end{pmatrix}, \tag{C.14}$$

where

$\beta_k=a_{k,k}+\Delta_\tau(1-\theta)b_{k,k}$, for $k=1,2,\cdots,N$,

$\alpha_{m+1}=\gamma_m=a_{m,m+1}+\Delta_\tau(1-\theta)b_{m,m+1}$, for $m=2,\cdots,N-1$,

$\delta_1=\left[a_{1,1}+\Delta_\tau(1-\theta)b_{1,1}\right]E_1^n+\left[a_{1,2}+\Delta_\tau(1-\theta)b_{1,2}\right]E_2^n+\Delta_\tau\left[d_{1,1}h_1^n+d_{1,2}h_2^n\right]$,

$\delta_i=\left[a_{i,i-1}+\Delta_\tau(1-\theta)b_{i,i-1}\right]E_{i-1}^n+\left[a_{i,i}+\Delta_\tau(1-\theta)b_{i,i}\right]E_i^n+\left[a_{i,i+1}+\Delta_\tau(1-\theta)b_{i,i+1}\right]E_{i+1}^n$
$+\Delta_\tau\left[d_{i,i-1}h_{i-1}^n+d_{i,i}h_i^n+d_{i,i+1}h_{i+1}^n\right]$, for $i=2,\cdots,N-1$,

$\delta_N=\left[a_{N,N-1}+\Delta_\tau(1-\theta)b_{N,N-1}\right]E_{N-1}^n+\left[a_{N,N}+\Delta_\tau(1-\theta)b_{N,N}\right]E_N^n$
$+\Delta_\tau\left[d_{N,N-1}h_{N-1}^n+d_{N,N}h_N^n\right]$.

System (C.14) is a tridiagonal system of N equations that can be solved using a standard Gaussian elimination method such as Thomas algorithm and using such algorithm is sometimes crucial as it leads to a reduced computational cost. The back substitution procedure (see *e.g.* [134] for more detailed explanation) generates the solution as

$$\gamma_i' = \begin{cases} \frac{\gamma_i}{\beta_i}, & i = 1, \\ \frac{\gamma_i}{\beta_i - \alpha_i \gamma_{i-1}'}, & i = 2,3,\cdots,N-1, \end{cases} \tag{C.15}$$

$$\delta_i' = \begin{cases} \frac{\delta_i}{\beta_i}, & i = 1, \\ \frac{\delta_i - \alpha_i \delta_{i-1}'}{\beta_i - \alpha_i - \gamma_{i-1}'}, & i = 2,3,\cdots,N-1, \end{cases} \tag{C.16}$$

$$E_N^{n+1/2} = \delta_N',$$

$$E_i^{n+1/2} = \delta_i' - \gamma_i' E_{i+1}^{n+1/2}, \qquad i = N-1, N-2, \cdots, 1. \tag{C.17}$$

Step 3(Finding the value of the speed): We have divided E equation in (C.2) into two parts and it remains to find the solution of the advection step in the splitted scheme. Before we update the solution, it is necessary to find the value of the speed according to the pinning condition $E_{i_*}^{n+1/2} = 0$, where the index i_* corresponds to an integer value, indicating the spatial position at which the solution is equal to zero initially, *i.e.* $\xi_{i_*} = 0$. As the Beam-Warming method is a second-order accurate scheme, we find the speed value using the Beam-Warming scheme by means of the discretized solution found in the previous step as,

$$c = -\frac{\Delta_\xi \left(3E_{i_*}^{n+1/2} - 4E_{i_*-1}^{n+1/2} + E_{i_*-2}^{n+1/2}\right)}{2\Delta_\tau \left(E_{i_*}^{n+1/2} - 2E_{i_*-1}^{n+1/2} + E_{i_*-2}^{n+1/2}\right)} \tag{C.18}$$
$$- \frac{\sqrt{\left[\frac{\Delta_\tau}{2\Delta_\xi}\left(3E_{i_*}^{n+1/2} - 4E_{i_*-1}^{n+1/2} + E_{i_*-2}^{n+1/2}\right)\right]^2 - \frac{2{\Delta_\tau}^2}{{\Delta_\xi}^2}\left(E_{i_*}^{n+1/2} - 2E_{i_*-1}^{n+1/2} + E_{i_*-2}^{n+1/2}\right)\left(E_{i_*}^{n+1/2} - E_*\right)}}{\frac{{\Delta_\tau}^2}{{\Delta_\xi}^2}\left(E_{i_*}^{n+1/2} - 2E_{i_*-1}^{n+1/2} + E_{i_*-2}^{n+1/2}\right)}.$$

This formula is actually derived from the following standard Beam-Warming discretization, which is quadratic in c.

Step 4(Beam-Warming scheme): The next step is to use the Beam-Warming scheme to update the solution of advection term of E component at step $n+1$,

$$E_i^{n+1} = E_i^{n+1/2} + \frac{c\Delta_\tau}{2\Delta_\xi}\left(3E_i^{n+1/2} - 4E_{i-1}^{n+1/2} + E_{i-2}^{n+1/2}\right) + \left(\frac{c\Delta_\tau}{\sqrt{2}\Delta_\xi}\right)^2 \left(E_i^{n+1/2} - 2E_{i-1}^{n+1/2} + E_{i-2}^{n+1/2}\right). \tag{C.19}$$

Step 5(Finite element method): In a similar manner, the equation of h component can be divided into two parts and once again, we use finite element method to solve h equation with the advection term removed

$$\frac{\partial h}{\partial \tau} = \frac{1}{\tau_*}(\mathrm{H}(-E) - h), \tag{C.20}$$

which gives

$$\mathbf{A}\left[1 + \frac{\Delta_\tau \theta}{\tau_*}\right] h_i^{n+1/2} = \mathbf{A}\left[1 - \frac{\Delta_\tau (1-\theta)}{\tau_*}\right] h_i^n + \frac{\Delta_\tau G}{\tau_*}, \tag{C.21}$$

where the load vector G is

$$G = [g_i] = \int_{-L}^{L} \Phi_i(\xi)\mathrm{H}(-E)\,\mathrm{d}\xi, \tag{C.22}$$

with entries

$$g_i = \frac{1}{\Delta_\xi}\left(\int_{\xi_{i-1}}^{\xi_i} \mathrm{H}(-E)(\xi - \xi_{i-1})\,\mathrm{d}\xi + \int_{\xi_i}^{\xi_{i+1}} \mathrm{H}(-E)(\xi_{i+1} - \xi)\,\mathrm{d}\xi\right) = {I_5}^i + {I_6}^i,$$

where

$${I_5}^i = \frac{1}{2\Delta_\xi}\begin{cases} {\Delta_\xi}^2, & E_{i-1} < 0, E_i < 0, \\ \left(\xi^*_{i-1} - \xi_{i-1}\right)^2, & E_{i-1} < 0, E_i > 0, \\ {\Delta_\xi}^2 - \left(\xi^*_{i-1} - \xi_{i-1}\right)^2, & E_{i-1} > 0, E_i < 0, \\ 0, & \text{otherwise}, \end{cases} \tag{C.23}$$

and

$${I_6}^i = \frac{1}{2\Delta_\xi}\begin{cases} {\Delta_\xi}^2, & E_i < 0, E_{i+1} < 0, \\ {\Delta_\xi}^2 - \left(\xi_{i+1} - \xi^*_{i+1}\right)^2, & E_i < 0, E_{i+1} > 0, \\ \left(\xi_{i+1} - \xi^*_{i+1}\right)^2, & E_i > 0, E_{i+1} < 0, \\ 0, & \text{otherwise}, \end{cases} \tag{C.24}$$

for $i = 2, 3, \cdots, N-1$. On the boundaries, we have

$$g_1 = \frac{1}{2\Delta_\xi}\begin{cases} 2{\Delta_x}^2, & E_1 < 0, E_2 < 0, \\ 2{\Delta_\xi}^2 - \left(\xi^*_2 - \xi_2 + 2\Delta_\xi\right)^2 - \left(\xi_2 - \xi^*_2\right)^2, & E_1 < 0, E_2 > 0, \\ \left(\xi^*_2 - \xi_2 + 2\Delta_\xi\right)^2 + \left(\xi_2 - \xi^*_2\right)^2, & E_1 > 0, E_2 < 0, \\ 0, & \text{otherwise}, \end{cases} \tag{C.25}$$

$$g_N = \frac{1}{2\Delta_\xi}\begin{cases} 2{\Delta_x}^2, & E_{N-1}<0,\, E_N<0, \\ \left(\xi_{N-1}+2\Delta_\xi-\xi^*_{N-1}\right)^2+\left(\xi^*_{N-1}-\xi_{N-1}\right)^2, & E_{N-1}<0,\, E_N>0, \\ 2{\Delta_\xi}^2-\left(\xi^*_{N-1}-\xi_{N-1}\right)^2-\left(\xi_{N-1}+2\Delta_\xi-\xi^*_{N-1}\right)^2, & E_{N-1}>0,\, E_N<0, \\ 0, & \text{otherwise.} \end{cases} \tag{C.26}$$

The spatial points that are not actually on the grid can be found using the linear interpolation method,

$$\xi^*_{k+1} = \frac{E(\xi_{k+1})\xi_k - E(\xi_k)\xi_{k+1}}{E(\xi_{k+1})-E(\xi_k)}, \tag{C.27}$$

for $k = 1, i-2, i, N-2$.

Step 6(Thomas algorithm): Yet again, we would like to make our computation less expensive. The equation (C.21) can be written as a tridiagonal matrix system,

$$\begin{bmatrix} \hat\beta_1 & \hat\gamma_1 & 0 & & 0 \\ \hat\alpha_2 & \hat\beta_2 & \hat\gamma_2 & & \\ & \hat\alpha_3 & \hat\beta_3 & \ddots & \\ & & \ddots & \ddots & \hat\gamma_{N-1} \\ 0 & & & \hat\alpha_N & \hat\beta_N \end{bmatrix} \begin{pmatrix} h_1^{n+1/2} \\ \vdots \\ \vdots \\ \vdots \\ h_N^{n+1/2} \end{pmatrix} = \begin{pmatrix} \hat\delta_1 \\ \vdots \\ \vdots \\ \vdots \\ \hat\delta_N \end{pmatrix}, \tag{C.28}$$

where

$$\hat{\beta_k} = \left[1+\frac{\theta\Delta_\tau}{\tau_*}\right] a_{k,k}, \text{for } k = 1,2,\cdots,N,$$
$$\hat\alpha_{m+1} = \hat\gamma_m = \left[1+\frac{\theta\Delta_\tau}{\tau_*}\right] a_{m,m+1}, \text{for } m = 2,\cdots,N-1,$$
$$\hat\delta_1 = a_{1,1}\left[1-\frac{\Delta_\tau(1-\theta)}{\tau_*}\right] h_1^n + a_{1,2}\left[1-\frac{\Delta_\tau(1-\theta)}{\tau_*}\right] h_2^n + \frac{\Delta_\tau g_1}{\tau_*},$$
$$\hat\delta_i = \left[1-\frac{\Delta_\tau(1-\theta)}{\tau_*}\right]\left(a_{i,i-1}h_{i-1}^n + a_{i,i}h_i^n + a_{i,i+1}h_{i+1}^n\right) + \frac{\Delta_\tau g_i}{\tau_*} \quad \text{for} \quad i = 2,3,\cdots,N-1,$$
$$\hat\delta_N = a_{N,N-1}\left[1-\frac{\Delta_\tau(1-\theta)}{\tau_*}\right] h_{N-1}^n + a_{N,N}\left[1-\frac{\Delta_\tau(1-\theta)}{\tau_*}\right] h_N^n + \frac{\Delta_\tau g_N}{\tau_*},$$

so that the Thomas algorithm results in

$$\hat{\gamma}'_i = \begin{cases} \frac{\hat{\gamma}_i}{\hat{\beta}_i}, & i = 1, \\ \frac{\hat{\gamma}_i}{\hat{\beta}_i - \hat{\alpha}_i \hat{\gamma}'_{i-1}}, & i = 2,3,\cdots,N-1, \end{cases} \tag{C.29}$$

$$\hat{\delta}'_i = \begin{cases} \frac{\hat{\delta}_i}{\hat{\beta}_i}, & i = 1, \\ \frac{\hat{\delta}_i - \hat{\alpha}_i \hat{\delta}'_{i-1}}{\hat{\beta}_i - \hat{\alpha}_i - \hat{\gamma}'_{i-1}}, & i = 2,3,\cdots,N-1, \end{cases} \tag{C.30}$$

$$h_N^{n+1/2} = \hat{\delta}'_N,$$

$$h_i^{n+1/2} = \hat{\delta}'_i - \hat{\gamma}'_i h_{i+1}^{n+1/2}, \qquad i = N-1, N-2, \cdots, 1. \tag{C.31}$$

Step 7(Beam-Warming scheme): Once again, we use the second-order accurate Beam-Warming scheme with truncation error $\mathcal{O}\left({\Delta_\tau}^2, {\Delta_\xi}^2\right)$ for the advection term of the h component

$$h_i^{n+1} = h_i^{n+1/2} + \frac{c\Delta_\tau}{2\Delta_\xi}\left(3h_i^{n+1/2} - 4h_{i-1}^{n+1/2} + h_{i-2}^{n+1/2}\right) + \left(\frac{c\Delta_\tau}{\sqrt{2}\Delta_\xi}\right)^2 \left(h_i^{n+1/2} - 2h_{i-1}^{n+1/2} + h_{i-2}^{n+1/2}\right). \tag{C.32}$$

The numerical computation of the critical front is achieved by solving (C.2) according to above seven-step procedure using the "shooting" technique as described in Section 4.4. As the Biktashev model is a two-component system, to find the numerical estimation of the critical front, we calculate $S(\tau)$ as

$$S(\tau) = \int_{-L}^{L} \left(E_\tau^2(\xi,\tau) + h_\tau^2(\xi,\tau)\right) \mathrm{d}\xi. \tag{C.33}$$

C.2 Discretization Formula for the Linearized Problem

We linearize the system (C.2) about the critical front $\left(\hat{E}, \hat{h}\right)$ using

$$\begin{aligned} E(\xi,\tau) &= \hat{E}(\xi) + \epsilon\overline{E}(\xi,\tau), \\ h(\xi,\tau) &= \hat{h}(\xi) + \epsilon\overline{h}(\xi,\tau), \end{aligned} \tag{C.34}$$

where $\epsilon\overline{E}$ and $\epsilon\overline{h}$ are small perturbations, $\epsilon \ll 1$. Hence, we have the following system of equations:

$$\begin{aligned}\frac{\partial\overline{E}}{\partial\tau} &= \frac{\partial^2\overline{E}}{\partial\xi^2} + c\frac{\partial\overline{E}}{\partial\xi} - \frac{1}{\hat{E}'(-\Delta)}\delta(\xi+\Delta)\hat{h}\overline{E} + \mathrm{H}(-\Delta-\xi)\overline{h},\\ \frac{\partial\overline{h}}{\partial\tau} &= c\frac{\partial\overline{h}}{\partial\xi} + \left(\frac{1}{\hat{E}'(0)}\delta(\xi)\overline{E} - \overline{h}\right)/\tau_*.\end{aligned} \tag{C.35}$$

We solve this linearized equation with the operator splitting technique by splitting the system into four equations. We use either the finite element or finite difference methods to obtain the solution of each of these four equations as follows:

Step 1(Finite element method): First of all, we solve

$$\frac{\partial\overline{E}}{\partial\tau} = \frac{\partial^2\overline{E}}{\partial\xi^2} - \frac{1}{\hat{E}'(-\Delta)}\delta(\xi+\Delta)\hat{h}\overline{E} + \mathrm{H}(-\Delta-\xi)\overline{h},$$

using the finite element method this yields

$$\left[\mathbf{A} + \Delta_\tau\theta\left(\mathbf{B} + \frac{\mathbf{L}}{\hat{E}'(-\Delta)}\right)\right]\overline{E}_i^{n+1/2} = \left[\mathbf{A} - \Delta_\tau(1-\theta)\left(\mathbf{B} + \frac{\mathbf{L}}{\hat{E}'(-\Delta)}\right)\right]\overline{E}_i^n + \Delta_\tau\mathbf{K}\overline{h}_i^n, \tag{C.36}$$

where the matrices $\mathbf{K}$ and $\mathbf{L}$ are

$$\begin{aligned}\mathbf{K} &= \left[k_{i,j}\right] = \int_{-L}^{L}\mathrm{H}(-\Delta-\xi)\Phi_i(\xi)\Phi_j(\xi)\,\mathrm{d}\xi,\\ \mathbf{L} &= \left[l_{i,j}\right] = \int_{-L}^{L}\delta(\xi+\Delta)\hat{h}(\xi)\Phi_i(x)\Phi_j(\xi)\,\mathrm{d}\xi = \hat{h}(-\Delta)\Phi_i(-\Delta)\Phi_j(-\Delta).\end{aligned}$$

The matrix $\mathbf{L}$ has exactly 4 non-zero elements and these are

$$l_{i,j} = \frac{\hat{h}(-\Delta)}{{\Delta_\xi}^2}\begin{cases}(\xi_{m+1}+\Delta)^2, & i=j=m,\\ -(\xi_{m+1}+\Delta)(\Delta+\xi_m), & i=m, j=m+1,\\ -(\Delta+\xi_m)(\xi_{m+1}+\Delta), & i=m+1, j=m,\\ (\Delta+\xi_m)^2, & i=j=m+1,\\ 0, & \text{otherwise},\end{cases} \tag{C.37}$$

where $\xi_m \le \Delta \le \xi_{m+1}$. Actually, this can be further simplified by discretizing the spatial domain in the way that Δ is situated exactly on the grid that makes $\mathbf{L}$ with only one non-zero element. On the other hand, the diagonal entries of the matrix $\mathbf{K}$ are found as

$$\begin{aligned}k_{i,i} &= \int_{-L}^{L}\mathrm{H}(-\Delta-\xi)\Phi_i^2(\xi)\,\mathrm{d}\xi\\ &= \frac{1}{{\Delta_\xi}^2}\left(\int_{\xi_{i-1}}^{\xi_i}\mathrm{H}(-\Delta-\xi)(\xi-\xi_{i-1})^2\,\mathrm{d}\xi + \int_{\xi_i}^{\xi_{i+1}}\mathrm{H}(-\Delta-\xi)(\xi_{i+1}-\xi)^2\,\mathrm{d}\xi\right) = {I_7}^i + {I_8}^i,\end{aligned}$$

where

$$I_7{}^i = \frac{1}{3\Delta_\xi{}^2}\begin{cases}\Delta_\xi{}^3, & E_{i-1}<-\Delta,\, E_i<-\Delta,\\ -(\Delta+\xi_{i-1})^3, & E_{i-1}<-\Delta,\, E_i>-\Delta,\\ \Delta_\xi{}^3+(\Delta+\xi_{i-1})^3, & E_{i-1}>-\Delta,\, E_i<-\Delta,\\ 0, & \text{otherwise,}\end{cases} \tag{C.38}$$

and

$$I_8{}^i = \frac{1}{3\Delta_\xi{}^2}\begin{cases}\Delta_\xi{}^3, & E_i<-\Delta,\, E_{i+1}<-\Delta,\\ \Delta_\xi{}^3-(\xi_{i+1}+\Delta)^3, & E_i<-\Delta,\, E_{i+1}>-\Delta,\\ (\xi_{i+1}+\Delta)^3, & E_i>-\Delta,\, E_{i+1}<-\Delta,\\ 0, & \text{otherwise.}\end{cases} \tag{C.39}$$

The supradiagonal elements of $\mathbf{K}$ are evaluated as

$$k_{i,i+1} = \int_{-L}^{L} \mathrm{H}(-\Delta-\xi)\,\Phi_i(\xi)\Phi_{i+1}(\xi)\,\mathrm{d}\xi = \frac{1}{\Delta_\xi{}^2}\int_{\xi_i}^{\xi_{i+1}} \mathrm{H}(-\Delta-\xi)(\xi_{i+1}-\xi)(\xi-\xi_i)\,\mathrm{d}\xi$$

$$= \frac{1}{6\Delta_\xi{}^2}\begin{cases}\Delta_\xi{}^3, & E_i<-\Delta,\, E_{i+1}<-\Delta,\\ 3\xi_{i+1}\Delta^2+6\xi_{i+1}\xi_i\Delta+2\Delta^3+3\xi_i\Delta^2+3\xi_{i+1}\xi_i^2-\Delta^3, & E_i<-\Delta,\, E_{i+1}>-\Delta,\\ \xi_{i+1}^3-3\xi_i\xi_{i+1}^2-2\Delta^3-3\xi_i\Delta^2-3\xi_{i+1}\Delta^2-6\xi_i\xi_{i+1}\Delta, & E_i>-\Delta,\, E_{i+1}<-\Delta,\\ 0, & \text{otherwise.}\end{cases} \tag{C.40}$$

The subdiagonal elements of $\mathbf{K}$ are also found as

$$k_{i-1,i} = \int_{-L}^{L} \mathrm{H}(-\Delta-\xi)\,\Phi_i(\xi)\Phi_{i-1}(\xi)\,\mathrm{d}\xi = \frac{1}{\Delta_\xi{}^2}\int_{\xi_{i-1}}^{\xi_i} \mathrm{H}(-\Delta-\xi)(\xi-\xi_{i-1})(\xi_i-\xi)\,\mathrm{d}\xi$$

$$= \frac{1}{6\Delta_\xi{}^2}\begin{cases}\Delta_\xi{}^3, & E_{i-1}<-\Delta,\, E_i<-\Delta,\\ 3\xi_i\Delta^2+2\Delta^3+3\xi_i\xi_{i-1}^2-\xi_{i-1}^3+6\xi_{i-1}\xi_i\Delta+3\xi_{i-1}\Delta^2, & E_{i-1}<-\Delta,\, E_i>-\Delta,\\ \xi_i^3-3\xi_{i-1}\xi_i^2-6\xi_i\xi_{i-1}\Delta-2\Delta^3-3\xi_i\Delta^2-3\xi_{i-1}\Delta^2, & E_{i-1}>-\Delta,\, E_i<-\Delta,\\ 0, & \text{otherwise,}\end{cases} \tag{C.41}$$

and on the boundaries, we have

$$k_{1,1}=\frac{1}{3{\Delta_\xi}^2}\begin{cases}2{\Delta_\xi}^3, & E_1<-\Delta,\ E_2<-\Delta,\\ 2{\Delta_\xi}^3-\left(2\Delta_\xi-\Delta-\xi_2\right)^3-(\xi_2+\Delta)^3, & E_1<-\Delta,\ E_2>-\Delta,\\ \left(2\Delta_\xi-\Delta-\xi_2\right)^3+{\Delta_\xi}^3, & E_1>-\Delta,\ E_2<-\Delta,\\ 0, & \text{otherwise},\end{cases} \tag{C.42}$$

$$k_{N,N}=\frac{1}{3{\Delta_\xi}^2}\begin{cases}2{\Delta_\xi}^3, & E_{N-1}<-\Delta,\ E_N<-\Delta,\\ \left(\xi_{N-1}+2\Delta_\xi+\Delta\right)^3-(\Delta+\xi_{N-1})^3, & E_{N-1}<-\Delta,\ E_N>-\Delta,\\ 2{\Delta_\xi}^3+(\Delta-\xi_{N-1})^3-\left(\xi_{N-1}+2\Delta_\xi+\Delta\right)^3, & E_{N-1}>-\Delta,\ E_N<-\Delta,\\ 0, & \text{otherwise}.\end{cases} \tag{C.43}$$

Step 2(Beam-Warming scheme): The second step is to solve the pure advection equation using the Beam-Warming scheme giving

$$\overline{E}_i^{n+1}=\overline{E}_i^{n+1/2}+\frac{c\Delta_\tau}{2\Delta_\xi}\left(4\overline{E}_{i+1}^{n+1/2}-3\overline{E}_i^{n+1/2}-\overline{E}_{i+2}^{n+1/2}\right)+\left(\frac{c\Delta_\tau}{\sqrt{2}\Delta_\xi}\right)^2\left(\overline{E}_i^{n+1/2}-2\overline{E}_{i+1}^{n+1/2}+\overline{E}_{i+2}^{n+1/2}\right), \tag{C.44}$$

that finishes the numerical scheme of $\overline{E}$ component of the linearized problem.

Step 3(Finite element method): Again the finite element method is conveniently employed to numerically solve the first equation of $\overline{h}$ component,

$$\frac{\partial\overline{h}}{\partial\tau}=\left(\frac{1}{\hat{E}'(0)}\delta(\xi)\overline{E}-\overline{h}\right)/\tau_*,$$

that results in

$$\left[\mathbf{A}+\frac{\Delta_\tau\theta\mathbf{A}}{\tau_*}\right]\overline{h}_i^{n+1/2}=\left[\mathbf{A}-\frac{\Delta_\tau(1-\theta)\mathbf{A}}{\tau_*}\right]\overline{h}_i^n+\frac{\Delta_\tau\mathbf{M}}{\tau_*\hat{E}'(0)}\overline{E}_i^n, \tag{C.45}$$

where

$$\begin{aligned}\mathbf{M}=\left[m_{i,j}\right]&=\int_{-L}^{L}\delta(\xi)\Phi_i(\xi)\Phi_j(\xi)\,\mathrm{d}\xi=\Phi_i(0)\Phi_j(0)\\ &=\frac{1}{{\Delta_\xi}^2}\begin{cases}\xi_{r+1}^2, & i=j=r,\\ -\xi_{r+1}\xi_r, & i=r, j=r+1,\\ -\xi_r\xi_{r+1}, & i=r+1, j=r,\\ \xi_r^2, & i=j=r+1,\\ 0, & \text{otherwise},\end{cases}\end{aligned} \tag{C.46}$$

such that $\xi_r \le 0 \le \xi_{r+1}$.

Step 4(Beam-Warming scheme): Similar to $\overline{E}$ equation, we employ the Beam-Warming scheme for pure advection equation of $\overline{h}$ component,

$$\overline{h}_i^{n+1} = \overline{h}_i^{n+1/2} + \frac{c\Delta_\tau}{2\Delta_\xi}\left(4\overline{h}_{i+1}^{n+1/2} - 3\overline{h}_i^{n+1/2} - \overline{h}_{i+2}^{n+1/2}\right) + \left(\frac{c\Delta_\tau}{\sqrt{2}\Delta_\xi}\right)^2\left(\overline{h}_i^{n+1/2} - 2\overline{h}_{i+1}^{n+1/2} + \overline{h}_{i+2}^{n+1/2}\right), \tag{C.47}$$

that completes the numerical solution of the linearized equation.

C.3 Discretization Formula for the Adjoint Linearized Problem

The adjoint linearized problem Biktashev model is

$$\begin{aligned}\frac{\partial \bar{E}}{\partial \tau} &= \frac{\partial^2 \bar{E}}{\partial \xi^2} - c\frac{\partial \bar{E}}{\partial \xi} - \frac{1}{\hat{E}'(-\Delta)}\delta(\xi+\Delta)\hat{h}\bar{E} + \frac{\delta(\xi)}{\tau_* \hat{E}'(0)}\bar{h},\\ \frac{\partial \bar{h}}{\partial \tau} &= -c\frac{\partial \bar{h}}{\partial \xi} + \mathrm{H}(-\Delta-\xi)\bar{E} - \frac{\bar{h}}{\tau_*}.\end{aligned} \tag{C.48}$$

This problem can also be solved in 4-steps as follows:

Step 1(Finite element method): We begin with the equation of $\bar{E}$ component and solve first the following,

$$\frac{\partial \bar{E}}{\partial \tau} = \frac{\partial^2 \bar{E}}{\partial \xi^2} - \frac{1}{\hat{E}'(-\Delta)}\delta(\xi+\Delta)\hat{h}\bar{E} + \frac{\delta(\xi)}{\tau_* \hat{E}'(0)}\bar{h},$$

with the solution based on the finite element method,

$$\left[\mathbf{A} + \Delta_\tau\theta\left(\mathbf{B} + \frac{\mathbf{L}}{\hat{E}'(-\Delta)}\right)\right]\bar{E}_i^{n+1/2} = \left[\mathbf{A} - \Delta_\tau(1-\theta)\left(\mathbf{B} + \frac{\mathbf{L}}{\hat{E}'(-\Delta)}\right)\right]\bar{E}_i^n + \frac{\Delta_\tau \mathbf{M}}{\tau_* \hat{E}'(0)}\bar{h}_i^n. \tag{C.49}$$

Step 2(Beam-Warming scheme): As the advection term has a negative sign in the front, the Beam-Warming numerical scheme is in this case,

$$\bar{E}_i^{n+1} = \bar{E}_i^{n+1/2} - \frac{c\Delta_\tau}{2\Delta_\xi}\left(3\bar{E}_i^{n+1/2} - 4\bar{E}_{i-1}^{n+1/2} + \bar{E}_{i-2}^{n+1/2}\right) + \left(\frac{c\Delta_\tau}{\sqrt{2}\Delta_\xi}\right)^2\left(\bar{E}_i^{n+1/2} - 2\bar{E}_{i-1}^{n+1/2} + \bar{E}_{i-2}^{n+1/2}\right). \tag{C.50}$$

Step 3(Finite element method): Using the finite element method to solve

$$\frac{\partial \bar{h}}{\partial \tau} = \mathrm{H}(-\xi-\Delta)\bar{E} - \frac{\bar{h}}{\tau_*},$$

let us obtain,

$$\left[\mathbf{A}+\frac{\mathbf{A}\Delta_\tau\theta}{\tau_*}\right]\bar{h}_i^{n+1/2}=\left[\mathbf{A}-\frac{\Delta_\tau\mathbf{A}(1-\theta)}{\tau_*}\right]\bar{h}_i^{n}+\Delta_\tau\mathbf{M}\bar{E}_i^{n}. \tag{C.51}$$

Step 4(Beam-Warming scheme): We conclude the numerical solution of the adjoint problem by solving the pure advection equation for $\bar{h}$ component,

$$\bar{h}_i^{n+1}=\bar{h}_i^{n+1/2}-\frac{c\Delta_\tau}{2\Delta_\xi}\left(3\bar{h}_i^{n+1/2}-4\bar{h}_{i-1}^{n+1/2}+\bar{h}_{i-2}^{n+1/2}\right)+\left(\frac{c\Delta_\tau}{\sqrt{2}\Delta_\xi}\right)^2\left(\bar{h}_i^{n+1/2}-2\bar{h}_{i-1}^{n+1/2}+\bar{h}_{i-2}^{n+1/2}\right). \tag{C.52}$$

We note that the Thomas algorithm can also be applied to the diagonal systems (C.36), (C.45), (C.49) and (C.51) in a similar manner to the earlier calculation steps in Section C.1. Hence, we skip the similar derivations here.

For this model, the linear approximation of the critical curves requires the knowledge of the critical front as well as the first two leading eigenvalues and corresponding left and right eigenfunctions. The numerical calculating of the eigenpairs are determined by the modified power iteration method discussed in Section 4.4 using the numerical solutions of the linearized and adjoint linearized problems, and these two last sections are dedicated to how to derive such numerical solution of these problems by means of the operator splitting method. Alternatively, the implicitly restarted Arnoldi method can be used to estimate these essential ingredients, in which case we use the matrix representations of the discretized versions of the equations (C.35) and (C.48).

C.4 Analytical Eigenfunctions

The numerical estimation of the first two leading eigenvalues and corresponding left and right eigenfunctions must agree with the analytical results found in [66]. We briefly provide the analytical expressions of the eigenfunctions with the aim of comparing them with their numerical versions (please refer to [66] for more details). Equation (C.35) support solutions of the form $\overline{E}=\mathrm{e}^{\lambda\tau}\phi(\xi)$ and $\overline{h}=\mathrm{e}^{\lambda\tau}\psi(\xi)$ and inserting this into

(C.35) leads to a temporal eigenvalue problem with the general solution,

$$\begin{aligned}
\begin{pmatrix}\phi_a\\ \psi_a\end{pmatrix} &= a_1\begin{pmatrix}1\\ -\nu_q\end{pmatrix}\mathrm{e}^{\nu_1\xi} + a_3\begin{pmatrix}1\\ 0\end{pmatrix}\mathrm{e}^{-\bar{\nu}_2\xi},\\
\begin{pmatrix}\phi_b\\ \psi_b\end{pmatrix} &= b_1\begin{pmatrix}0\\ 1\end{pmatrix}\mathrm{e}^{\nu_1\xi} + b_2\begin{pmatrix}1\\ 0\end{pmatrix}\mathrm{e}^{-\nu_2\xi} + b_3\begin{pmatrix}1\\ 0\end{pmatrix}\mathrm{e}^{-\bar{\nu}_2\xi},\\
\begin{pmatrix}\phi_c\\ \psi_c\end{pmatrix} &= c_2\begin{pmatrix}1\\ 0\end{pmatrix}\mathrm{e}^{-\nu_2\xi},
\end{aligned} \tag{C.53}$$

where

$$\nu = \frac{1+\tau_* c^2}{c\tau_*}, \quad \nu_1 = \frac{1+\lambda\tau_*}{c\tau_*}, \quad \nu_2 = \frac{c+\sqrt{c^2+4\lambda}}{2}, \quad \bar{\nu}_2 = \frac{c-\sqrt{c^2+4\lambda}}{2}, \tag{C.54}$$

and the three intervals are defined based on the discontinuous Heaviside and Dirac delta functions as $\xi\in(-\infty,-\Delta)(a)$, $\xi\in(-\Delta,0)(b)$ and $\xi\in(0,\infty)(c)$. The arbitrary constants are determined from matching conditions of the solutions in these three intervals, which gives a system of six equations,

$$\begin{aligned}
&a_1\alpha c\nu_1\mathrm{e}^{-\nu_1\Delta} - a_3\alpha c\bar{\nu}_1\mathrm{e}^{\bar{\nu}_2\Delta} + b_2\mathrm{e}^{\nu_2\Delta}\left(\alpha c\nu_2 - \mathrm{e}^{-\nu\Delta}\right) + b_3\mathrm{e}^{\bar{\nu}_2\Delta}\left(\alpha c\bar{\nu}_2 - \mathrm{e}^{-\nu\Delta}\right) = 0,\\
&a_1\mathrm{e}^{-\nu_1\Delta} + a_3\mathrm{e}^{\bar{\nu}_2\Delta} - b_2\mathrm{e}^{\nu_2\Delta} - b_3\mathrm{e}^{\bar{\nu}_2\Delta} = 0,\\
&a_1\nu_q + b_1 = 0,\\
&b_1\alpha\tau_* c^2 + c_2 = 0,\\
&b_2 + b_3 - c_2 = 0,\\
&b_2\nu_2 + b_3\bar{\nu}_2 - c_2\nu_2 = 0.
\end{aligned} \tag{C.55}$$

The solvability condition for this system gives a characteristic equation

$$f(\lambda;c,\alpha,\tau_*) \triangleq \alpha c(\nu_2-\bar{\nu}_2)\mathrm{e}^{\nu\Delta} - 1 + \frac{\tau_* c(\nu_1+\bar{\nu}_2)}{(1+\lambda\tau_*)^2+\tau_* c^2}\mathrm{e}^{-(\nu_1+\nu_2-\nu)\Delta} = 0, \tag{C.56}$$

from which the leading eigenvalue can be identified. On the other hand, the eigenpairs of adjoint linearized problem (C.48) support the solutions in the form $\bar{E} = \mathrm{e}^{\lambda\tau}\phi^*(\xi)$ and $\bar{h} = \mathrm{e}^{\lambda\tau}\psi^*(\xi)$ with the solution,

$$\begin{aligned}
\begin{pmatrix}\phi_a^*\\ \psi_a^*\end{pmatrix} &= a_2^*\begin{pmatrix}1\\ \gamma_3\end{pmatrix}\mathrm{e}^{\gamma_2\xi},\\
\begin{pmatrix}\phi_b^*\\ \psi_b^*\end{pmatrix} &= b_1^*\begin{pmatrix}0\\ 1\end{pmatrix}\mathrm{e}^{-\gamma_1\xi} + b_2^*\begin{pmatrix}1\\ 0\end{pmatrix}\mathrm{e}^{\gamma_2\xi} + b_3^*\begin{pmatrix}1\\ 0\end{pmatrix}\mathrm{e}^{\bar{\gamma}_2\xi},\\
\begin{pmatrix}\phi_c^*\\ \psi_c^*\end{pmatrix} &= c_1^*\begin{pmatrix}0\\ 1\end{pmatrix}\mathrm{e}^{-\gamma_1\xi} + c_3^*\begin{pmatrix}1\\ 0\end{pmatrix}\mathrm{e}^{\bar{\gamma}_2\xi},
\end{aligned} \tag{C.57}$$

where

$$\gamma = \frac{1+\tau_* c^2}{\tau_* c}, \quad \gamma_1 = \frac{1+\lambda\tau_*}{\tau_* c}, \quad \gamma_2 = \frac{c+\sqrt{c^2+4\lambda}}{2},$$
$$\bar{\gamma}_2 = \frac{c-\sqrt{c^2+4\lambda}}{2}, \quad \gamma_3 = \frac{1}{c\left(\gamma_1+\gamma_2\right)}, \quad \Delta = \frac{1}{c}\ln\left(\frac{1+\alpha}{\alpha}\right). \tag{C.58}$$

Similarly, the arbitrary constants are determined from the matching conditions which give a system of six equations

$$\begin{aligned}
&a_2^* \alpha c \gamma_2 \mathrm{e}^{-\gamma_2\Delta} - b_2^* \mathrm{e}^{-\gamma_2\Delta}\left(\alpha c\gamma_2 + \mathrm{e}^{-\gamma\Delta}\right) - b_3^* \mathrm{e}^{-\bar{\gamma}_2\Delta}\left(\alpha c\bar{\gamma}_2 + \mathrm{e}^{-\gamma\Delta}\right) = 0,\\
&a_2^* \mathrm{e}^{-\gamma_2\Delta} - b_2^* \mathrm{e}^{-\gamma_2\Delta} - b_3^* \mathrm{e}^{-\bar{\gamma}_2\Delta} = 0,\\
&a_2^* \gamma_3 \mathrm{e}^{-\gamma_2\Delta} - b_1^* \mathrm{e}^{\gamma_1\Delta} = 0,\\
&b_2^* \alpha\tau_* c\gamma_2 + b_3^* \alpha\tau_* c\bar{\gamma}_2 + c_1^* - c_3^* \alpha\tau_* c\bar{\gamma}_2 = 0,\\
&b_2^* + b_3^* - c_3^* = 0,\\
&b_1^* - c_1^* = 0,
\end{aligned} \tag{C.59}$$

with the same solvability condition (C.56).

BIBLIOGRAPHY

[1] T. ARENDT AND V. BIGL, *Alzheimer's disease as a presumptive threshold phenomenon*, Neurobiology of Aging, 8 (1987), pp. 552–554.

[2] W. E. ARNOLDI, *The principle of minimized iteration in the solution of the matrix eigenvalue problem*, Quarterly of Applied Mathematics, 9 (1951), pp. 17–29.

[3] D. G. ARONSON AND H. F. WEINBERGER, *Nonlinear diffusion in population genetics, combustion, and nerve pulse propagation*, in Partial differential equations and related topics, Springer, 1975, pp. 5–49.

[4] A. ARUTUNYAN, A. PUMIR, V. KRINSKY, L. SWIFT, AND N. SARVAZYAN, *Behavior of ectopic surface: effects of β-adrenergic stimulation and uncoupling*, American Journal of Physiology-Heart and Circulatory Physiology, 285 (2003), pp. H2531–H2542.

[5] R. ASTUDILLO AND Z. CASTILLO, *Computing pseudospectra using block implicitly restarted Arnoldi iteration*, Mathematical and Computer Modelling, 57 (2013), pp. 2149–2157.

[6] P. BAK, K. CHEN, AND C. TANG, *A forest-fire model and some thoughts on turbulence*, Physics Letters A, 147 (1990), pp. 297–300.

[7] D. BARKLEY, *A model for fast computer simulation of waves in excitable media*, Physica D: Nonlinear Phenomena, 49 (1991), pp. 61–70.

[8] D. BARKLEY, *Modeling the transition to turbulence in shear flows*, in Journal of Physics: Conference Series, vol. 318, IOP Publishing, 2011, p. 032001.

[9] D. BARKLEY, B. SONG, V. MUKUND, G. LEMOULT, M. AVILA, AND B. HOF, *The rise of fully turbulent flow*, Nature, 526 (2015), pp. 550–553.

[10] H. BATEMAN, A. ERDÉLYI, W. MAGNUS, F. OBERHETTINGER, AND F. G. TRICOMI, *Higher transcendental functions*, vol. 3, McGraw-Hill New York, 1955.

[11] R. M. BEAM AND R. F. WARMING, *An implicit finite-difference algorithm for hyperbolic systems in conservation-law form*, Journal of Computational Physics, 22 (1976), pp. 87–110.

[12] G. W. BEELER AND H. REUTER, *Reconstruction of the action potential of ventricular myocardial fibres*, The Journal of Physiology, 268 (1977), pp. 177–210.

[13] V. BIKTASHEV, *Diffusion of autowaves: Evolution equation for slowly varying autowaves*, Physica D: Nonlinear Phenomena, 40 (1989), pp. 83–90.

[14] V. BIKTASHEV AND A. HOLDEN, *Deterministic brownian motion in the hypermeander of spiral waves*, Physica D: Nonlinear Phenomena, 116 (1998), pp. 342–354.

[15] V. BIKTASHEV, A. HOLDEN, AND E. NIKOLAEV, *Spiral wave meander and symmetry of the plane*, International Journal of Bifurcation and Chaos in Applied Sciences and Engineering, 6 (1996), pp. 2433–2440.

[16] V. N. BIKTASHEV, *Dissipation of the excitation wave fronts*, Physical Review Letters, 89 (2002), p. 168102.

[17] V. N. BIKTASHEV, *A simplified model of propagation and dissipation of excitation fronts*, International Journal of Bifurcation and Chaos, 13 (2003), pp. 3605–3619.

[18] V. N. BIKTASHEV, A. ARUTUNYAN, AND N. A. SARVAZYAN, *Generation and escape of local waves from the boundary of uncoupled cardiac tissue*, Biophysical Journal, 94 (2008), pp. 3726–3738.

[19] V. N. BIKTASHEV, I. V. BIKTASHEVA, AND N. A. SARVAZYAN, *Evolution of spiral and scroll waves of excitation in a mathematical model of ischaemic border zone*, PLoS One, 6 (2011), p. e24388.

[20] H. BLAIR, *On the intensity-time relations for stimulation by electric currents. ii*, The Journal of General Physiology, 15 (1932), pp. 731–755.

[21] H. A. BLAIR, *On the intensity-time relations for stimulation by electric currents. i*, The Journal of General Physiology, 15 (1932), pp. 709–729.

[22] M. BLAUSTEIN, J. KAO, AND D. MATTESON, *Cellular Physiology and Neurophysiology*, Elsevier, 2012.

[23] P. B. BOCHEV, M. D. GUNZBURGER, AND J. N. SHADID, *Stability of the SUPG finite element method for transient advection–diffusion problems*, Computer Methods in Applied Mechanics and Engineering, 193 (2004), pp. 2301–2323.

[24] H. BOSTOCK, *The strength-duration relationship for excitation of myelinated nerve: computed dependence on membrane parameters.*, The Journal of Physiology, 341 (1983), pp. 59–74.

[25] N. BRUNEL AND M. C. VAN ROSSUM, *Quantitative investigations of electrical nerve excitation treated as polarization*, Biological Cybernetics, 97 (2007), pp. 341–349.

[26] G. A. CARPENTER, *A geometric approach to singular perturbation problems with applications to nerve impulse equations*, Journal of Differential Equations, 23 (1977), pp. 335–367.

[27] R. G. CASTEN, H. COHEN, AND P. A. LAGERSTROM, *Perturbation analysis of an approximation to the Hodgkin-Huxley theory*, Quarterly of Applied Mathematics, 32 (1975), pp. 365–402.

[28] R. CLAYTON, O. BERNUS, E. CHERRY, H. DIERCKX, F. FENTON, L. MIRABELLA, A. PANFILOV, F. B. SACHSE, G. SEEMANN, AND H. ZHANG, *Models of cardiac tissue electrophysiology: progress, challenges and open questions*, Progress in Biophysics and Molecular Biology, 104 (2011), pp. 22–48.

[29] R. M. CORLESS, G. H. GONNET, D. E. HARE, D. J. JEFFREY, AND D. E. KNUTH, *On the Lambert W function*, Advances in Computational Mathematics, 5 (1996), pp. 329–359.

[30] M. COSTABEL, *Principles of boundary element methods*, Computer Physics Reports, 6 (1987), pp. 243–274.

[31] M. COURTEMANCHE, L. GLASS, AND J. P. KEENER, *Instabilities of a propagating pulse in a ring of excitable media*, Physical Review Letters, 70 (1993), pp. 2182–2185.

[32] M. C. CROSS AND P. C. HOHENBERG, *Pattern formation outside of equilibrium*, Reviews of Modern Physics, 65 (1993), pp. 851–1112.

[33] H. DIERCKX, O. BERNUS, AND H. VERSCHELDE, *Accurate eikonal-curvature relation for wave fronts in locally anisotropic reaction-diffusion systems*, Physical Review Letters, 107 (2011), p. 108101.

[34] E. DOEDEL AND J. P. KERNEVEZ, *AUTO, software for continuation and bifurcation problems in ordinary differential equations*, California Institute of Technology, 1986.

[35] B. DROSSEL AND F. SCHWABL, *Self-organized critical forest-fire model*, Physical Review Letters, 69 (1992), pp. 1629–1632.

[36] G. DUCKETT AND D. BARKLEY, *Modeling the dynamics of cardiac action potentials*, Physical Review Letters, 85 (2000), pp. 884–887.

[37] T. ERNEUX AND G. NICOLIS, *Propagating waves in discrete bistable reaction-diffusion systems*, Physica D: Nonlinear Phenomena, 67 (1993), pp. 237–244.

[38] J. W. EVANS, *The stable and the unstable impulse*, Indiana University Mathematics Journal, 24 (1975), pp. 1169–1190.

[39] R. E. EWING AND H. WANG, *A summary of numerical methods for time-dependent advection-dominated partial differential equations*, Journal of Computational and Applied Mathematics, 128 (2001), pp. 423–445.

[40] I. FARKAS, D. HELBING, AND T. VICSEK, *Social behaviour: Mexican waves in an excitable medium*, Nature, 419 (2002), pp. 131–132.

[41] F. H. FENTON, E. M. CHERRY, H. M. HASTINGS, AND S. J. EVANS, *Real-time computer simulations of excitable media: Java as a scientific language and as a wrapper for C and Fortran programs*, Biosystems, 64 (2002), pp. 73–96.

[42] P. C. FIFE, *Asymptotic states for equations of reaction and diffusion*, Bulletin of the American Mathematical Society, 84 (1978), pp. 693–726.

[43] P. C. FIFE AND J. B. MCLEOD, *The approach of solutions of nonlinear diffusion equations to travelling front solutions*, Archive for Rational Mechanics and Analysis, 65 (1977), pp. 335–361.

[44] R. A. FISHER, *The wave of advance of advantageous genes*, Annals of Eugenics, 7 (1937), pp. 355–369.

[45] R. FITZHUGH, *Mathematical models of threshold phenomena in the nerve membrane*, The Bulletin of Mathematical Biophysics, 17 (1955), pp. 257–278.

[46] R. FITZHUGH, *Thresholds and plateaus in the Hodgkin-Huxley nerve equations*, The Journal of General Physiology, 43 (1960), pp. 867–896.

[47] R. FITZHUGH, *Impulses and physiological states in theoretical models of nerve membrane*, Biophysical Journal, 1 (1961), pp. 445–466.

[48] G. FLORES, *The stable manifold of the standing wave of the Nagumo equation*, Journal of Differential Equations, 80 (1989), pp. 306–314.

[49] G. FLORES, *Stability analysis for the slow travelling pulse of the FitzHugh-Nagumo system*, SIAM Journal on Mathematical Analysis, 22 (1991), pp. 392–399.

[50] A. FOULKES AND V. BIKTASHEV, *Riding a spiral wave: Numerical simulation of spiral waves in a comoving frame of reference*, Physical Review E, 81 (2010), p. 046702.

[51] J. G. FRANCIS, *The QR transformation a unitary analogue to the LR transformation—part 1*, The Computer Journal, 4 (1961), pp. 265–271.

[52] L. A. GEDDES, *Accuracy limitations of chronaxie values*, IEEE Transactions Biomedical Engineering, 51 (2004), pp. 176–181.

[53] B. H. GILDING AND R. KERSNER, *Travelling waves in nonlinear diffusion-convection reaction*, vol. 60, Birkhäuser, 2012.

[54] G. H. GOLUB AND C. F. VAN LOAN, *Matrix computations*, vol. 3, JHU Press, 2012.

[55] Y. GUO, Y. ZHAO, S. A. BILLINGS, D. COCA, R. I. RISTIC, AND L. DEMATOS, *Identification ofexcitable media using a scalar coupled mapped lattice model*, International Journal of Bifurcation and Chaos, 20 (2010), pp. 2137–2150.

[56] S. HASTINGS, *On the existence of homoclinic and periodic orbits for the FitzHugh-Nagumo equations*, The Quarterly Journal of Mathematics, 27 (1976), pp. 123–134.

[57] S. P. HASTINGS, *Single and multiple pulse waves for the FitzHugh-Nagumo*, SIAM Journal on Applied Mathematics, 42 (1982), pp. 247–260.

[58] A. HILL, *Excitation and accommodation in nerve*, Proceedings of the Royal Society of London. Series B, Biological Sciences, 119 (1936), pp. 305–355.

[59] R. HINCH, *An analytical study of the physiology and pathology of the propagation of cardiac action potentials*, Progress in Biophysics and Molecular Biology, 78 (2002), pp. 45–81.

[60] R. HINCH, *Stability of cardiac waves*, Bulletin of Mathematical Biology, 66 (2004), pp. 1887–1908.

[61] A. L. HODGKIN AND A. F. HUXLEY, *A quantitative description of membrane current and its application to conduction and excitation in nerve*, The Journal of Physiology, 117 (1952), pp. 500–544.

[62] A. HOFFMAN AND J. MALLET-PARET, *Universality of crystallographic pinning*, Journal of Dynamics and Differential Equations, 22 (2010), pp. 79–119.

[63] M. HOLT, *Numerical methods in fluid dynamics*, Springer Science & Business Media, 2012.

[64] K. J. HUGHES, J. BRINDLEY, AND A. C. MCINTOSH, *Initiation and propagation of combustion waves with competitive reactions and water evaporation*, in Proc. R. Soc. A, vol. 469, The Royal Society, 2013, p. 20130506.

[65] H. HUPKES, D. PELINOVSKY, AND B. SANDSTEDE, *Propagation failure in the discrete Nagumo equation*, Proceedings of the American Mathematical Society, 139 (2011), pp. 3537–3551.

[66] I. IDRIS, *Initiation Of Excitation Waves*, PhD thesis, 2008.

[67] I. IDRIS AND V. BIKTASHEV, *Critical fronts in initiation of excitation waves*, Physical Review E, 76 (2007), p. 021906.

[68] I. IDRIS AND V. N. BIKTASHEV, *An analytical approach to initiation of propagating fronts*, Physical Review Letters, 101 (2008), p. 244101.

[69] C. K. JONES, *Stability of the travelling wave solution of the FitzHugh-Nagumo system*, Transactions of the American Mathematical Society, 286 (1984), pp. 431–469.

[70] E. R. KANDEL, J. H. SCHWARTZ, T. M. JESSELL, S. A. SIEGELBAUM, AND A. HUDSPETH, *Principles of neural science*, vol. 4, McGraw-Hill New York, 2000.

[71] D. T. KAPLAN, J. R. CLAY, T. MANNING, L. GLASS, M. R. GUEVARA, AND A. SHRIER, *Subthreshold dynamics in periodically stimulated squid giant axons*, Physical Review Letters, 76 (1996), pp. 4074–4077.

[72] J. P. KEENER, *Propagation and its failure in coupled systems of discrete excitable cells*, SIAM Journal on Applied Mathematics, 47 (1987), pp. 556–572.

[73] J. P. KEENER, *The dynamics of excitability*, April 2016.

[74] J. P. KEENER AND J. SNEYD, *Mathematical physiology*, vol. 1, Springer, 1998.

[75] H. KOKUBU, Y. NISHIURA, AND H. OKA, *Heteroclinic and homoclinic bifurcations in bistable reaction diffusion systems*, Journal of Differential Equations, 86 (1990), pp. 260–341.

[76] A. KOLMOGOROV, I. PETROVSKY, AND N. PISKUNOV, *Investigation of the equation of diffusion combined with increasing of the substance and its application to a biology problem*, Bull. Moscow State Univ. Ser. A: Math. Mech, 1 (1937), pp. 1–25.

[77] A. N. KOLMOGOROV, I. PETROVSKY, AND N. PISKUNOV, *Etude de l'équation de la diffusion avec croissance de la quantité de matiere et son applicationa un probleme biologique*, Moscow Univ. Math. Bull, 1 (1937), pp. 1–25.

[78] Y. KURAMOTO, *Instability and turbulence of wavefronts in reaction-diffusion systems*, Progress of Theoretical Physics, 63 (1980), pp. 1885–1903.

[79] L. LAPICQUE, *Recherches quantitatives sur l'excitation électrique des nerfs traitée comme une polarisation*, J. Physiol. Pathol. Gen, 9 (1907), pp. 620–635.

[80] R. B. LEHOUCQ AND D. C. SORENSEN, *Deflation techniques for an implicitly restarted Arnoldi iteration*, SIAM Journal on Matrix Analysis and Applications, 17 (1996), pp. 789–821.

[81] R. B. LEHOUCQ, D. C. SORENSEN, AND C. YANG, *ARPACK users' guide: solution of large-scale eigenvalue problems with implicitly restarted Arnoldi methods*, vol. 6, Siam, 1998.

[82] K. LEVENBERG, *A method for the solution of certain non-linear problems in least squares*, Quarterly of Applied Mathematics, 2 (1944), pp. 164–168.

[83] C. LUKE AND P. COX, *Soil carbon and climate change: from the Jenkinson effect to the compost-bomb instability*, European Journal of Soil Science, 62 (2011), pp. 5–12.

[84] K. MAGINU, *Stability of periodic travelling wave solutions of a nerve conduction equation*, Journal of Mathematical Biology, 6 (1978), pp. 49–57.

[85] K. MAGINU, *Existence and stability of periodic travelling wave solutions to Nagumo's nerve equation*, Journal of Mathematical Biology, 10 (1980), pp. 133–153.

[86] D. W. MARQUARDT, *An algorithm for least-squares estimation of nonlinear parameters*, Journal of the Society for Industrial and Applied Mathematics, 11 (1963), pp. 431–441.

[87] W. D. MCCORMICK, Z. NOSZTICZIUS, AND H. L. SWINNEY, *Interrupted separatrix excitability in a chemical system*, The Journal of Chemical Physics, 94 (1991), pp. 2159–2167.

[88] H. MCKEAN AND V. MOLL, *A threshold for a caricature of the nerve equation*, Bulletin of the American Mathematical Society, 12 (1985), pp. 255–259.

[89] H. P. MCKEAN, *Nagumo's equation*, Advances in Mathematics, 4 (1970), pp. 209–223.

[90] H. P. McKean and V. Moll, *Stabilization to the standing wave in a simple caricature of the nerve equation*, Communications on Pure and Applied Mathematics, 39 (1986), pp. 485–529.

[91] R. Mises and H. Pollaczek-Geiringer, *Praktische verfahren der gleichungsauflösung.*, ZAMM-Journal of Applied Mathematics and Mechanics/Zeitschrift für Angewandte Mathematik und Mechanik, 9 (1929), pp. 152–164.

[92] C. B. Moler, *Numerical computing with MATLAB*, Siam, 2004.

[93] V. Moll and S. Rosencrans, *Calculation of the threshold surface for nerve equations*, SIAM Journal on Applied Mathematics, 50 (1990), pp. 1419–1441.

[94] A. M. Monnier and L. Lapicque, *L'excitation électrique des tissus: essai d'interprétation physique*, Hermann & Cie, (1934).

[95] O. A. Mornev, *On the conditions of excitation of one-dimensional autowave media*, Institute of Applied Physics of the USSR Academy of Sciences, Gorky, 1981, pp. 92–98.

[96] J. D. Murray, *Mathematical biology I: an introduction, vol. 17 of Interdisciplinary Applied Mathematics*, Springer, 2002.

[97] J. D. Murray, *Mathematical biology II: spatial models and biomedical applications, vol. 18 of Interdisciplinary Applied Mathematics*, Springer, 2003.

[98] J. Nagumo, S. Arimoto, and S. Yoshizawa, *An active pulse transmission line simulating nerve axon*, Proceedings of the IRE, 50 (1962), pp. 2061–2070.

[99] J. Nagumo, S. Yoshizawa, and S. Arimoto, *Bistable transmission lines*, IEEE Transactions on Communication Technology, 12 (1965), pp. 400–412.

[100] W. Nernst, *Zur theorie des elektrischen reizes*, Pflügers Archiv European Journal of Physiology, 122 (1908), pp. 275–314.

[101] J. C. Neu, R. S. Preissig, and W. Krassowska, *Initiation of propagation in a one-dimensional excitable medium*, Physica D: Nonlinear Phenomena, 102 (1997), pp. 285–299.

[102] A. C. NEWELL AND J. A. WHITEHEAD, *Finite bandwidth, finite amplitude convection*, Journal of Fluid Mechanics, 38 (1969), pp. 279–303.

[103] D. NOBLE, *The relation of Rushton's 'liminal length' for excitation to the resting and active conductances of excitable cells*, The Journal of Physiology, 226 (1972), pp. 573–591.

[104] D. NOBLE AND R. B. STEIN, *The threshold conditions for initiation of action potentials by excitable cells*, The Journal of Physiology, 187 (1966), pp. 129–162.

[105] J. R. PORTER, J. S. BURG, P. J. ESPENSHADE, AND P. A. IGLESIAS, *Identifying a static nonlinear structure in a biological system using noisy, sparse data*, Journal of Theoretical Biology, 300 (2012), pp. 232–241.

[106] A. PUMIR, A. ARUTUNYAN, V. KRINSKY, AND N. SARVAZYAN, *Genesis of ectopic waves: role of coupling, automaticity, and heterogeneity*, Biophysical Journal, 89 (2005), pp. 2332–2349.

[107] R. J. RADKE, *A MATLAB implementation of the implicitly restarted Arnoldi method for solving large-scale eigenvalue problems*, Master's thesis, Rice University, 1996.

[108] N. RASHEVSKY, *Outline of a physico-mathematical theory of excitation and inhibition*, Protoplasma, 20 (1933), pp. 42–56.

[109] F. RATTAY, L. PAREDES, AND R. LEAO, *Strength–duration relationship for intra- versus extracellular stimulation with microelectrodes*, Neuroscience, 214 (2012), pp. 1–13.

[110] J. N. REDDY, *An introduction to the finite element method*, vol. 2, McGraw-Hill New York, 1993.

[111] J. RINZEL AND J. B. KELLER, *Traveling wave solutions of a nerve conduction equation*, Biophysical Journal, 13 (1973), pp. 1313–1337.

[112] C. ROCCSOREANU, A. GEORGESCU, AND N. GIURGICTEANU, *Dynamic bifurcation for the FitzHugh-Nagumo model*, Springer, 2000, pp. 97–148.

[113] M. ROTH, *The association of clinical and neurological findings and its bearing on the classification and aetiology of Alzheimer's disease*, British Medical Bulletin, 42 (1986), pp. 42–50.

[114] Y. RUCONG, *A two-step shape-preserving advection scheme*, Advances in Atmospheric Sciences, 11 (1994), pp. 479–490.

[115] W. RUSHTON, *Initiation of the propagated disturbance*, Proceedings of the Royal Society of London. Series B, Biological Sciences, 124 (1937), pp. 210–243.

[116] Y. SAAD, *Variations on Arnoldi's method for computing eigenelements of large unsymmetric matrices*, Linear Algebra and its Applications, 34 (1980), pp. 269–295.

[117] J. J. SAKURAI AND J. NAPOLITANO, *Modern quantum mechanics*, Addison-Wesley, 2011.

[118] M. B. SCHIFFER, *Advances in archaeological method and theory*, New York: Academic Press, 1985.

[119] F. SCHLÖGL, *Chemical reaction models for non-equilibrium phase transitions*, Zeitschrift für Physik, 253 (1972), pp. 147–161.

[120] A. SCOTT ET AL., *Encyclopedia of nonlinear science*, Routledge, 2006.

[121] S. K. SCOTT AND K. SHOWALTER, *Simple and complex propagating reaction-diffusion fronts*, The Journal of Physical Chemistry, 96 (1992), pp. 8702–8711.

[122] L. A. SEGEL, *Distant side-walls cause slow amplitude modulation of cellular convection*, Journal of Fluid Mechanics, 38 (1969), pp. 203–224.

[123] G. SEIDEN AND S. CURLAND, *The tongue as an excitable medium*, New Journal of Physics, 17 (2015), p. 033049.

[124] D. SHARMA, R. JIWARI, AND S. KUMAR, *Galerkin-finite element method for the numerical solution of advection-diffusion equation*, International Journal of Pure and Applied Mathematics, 70 (2011), pp. 389–399.

[125] R. SIMITEV AND V. BIKTASHEV, *Asymptotics of conduction velocity restitution in models of electrical excitation in the heart*, Bulletin of Mathematical Biology, 73 (2011), pp. 72–115.

[126] C. F. STARMER, *Initiation of excitation waves*. http://www.scholarpedia.org/article/Initiation_of_excitation_waves.

[127] J. C. STRIKWERDA, *Finite difference schemes and partial differential equations*, Siam, 2004.

[128] V. THOMÉE, *Galerkin finite element methods for parabolic equations*, 25 of Springer Series in Computational Mathematics, (1997).

[129] P. TURCHIN, L. OKSANEN, P. EKERHOLM, T. OKSANEN, AND H. HENTTONEN, *Are lemmings prey or predators?*, Nature, 405 (2000), pp. 562–565.

[130] A. M. TURING, *The chemical basis of morphogenesis*, Philosophical Transactions of the Royal Society of London B: Biological Sciences, 237 (1952), pp. 37–72.

[131] J. J. TYSON AND J. P. KEENER, *Singular perturbation theory of traveling waves in excitable media (a review)*, Physica D: Nonlinear Phenomena, 32 (1988), pp. 327–361.

[132] B. VAN DER POL AND J. VAN DER MARK, *The heartbeat considered as a relaxation oscillation, and an electrical model of the heart*, Philosophical Magazine and Journal of Science, 6 (1928), pp. 763–775.

[133] M. VAN DYKE, *Perturbation methods in fluid mechanics*, Parabolic Press, 1975.

[134] J. WEICKERT, B. T. H. ROMENY, AND M. A. VIERGEVER, *Efficient and reliable schemes for nonlinear diffusion filtering*, IEEE Transactions on Image Processing, 7 (1998), pp. 398–410.

[135] G. WEISS, *Sur la possibilite de rendre comparables entre eux les appareils servant a l'excitation electrique*, Archives Italiennes de Biologie, 35 (1990), pp. 413–445.

[136] U. WINDHORST AND H. JOHANSSON, *Modern techniques in neuroscience research*, Springer, 1999.

[137] S. YOUSEF, *Iterative methods for sparse linear systems*, Siam, 2003.

[138] Y. B. ZEL'DOVICH AND D. FRANK-KAMENETSKY, *Towards the theory of uniformly propagating flames*, in Doklady AN SSSR, vol. 19, 1938, pp. 693–697.

[139] J. ZELDOWITSCH AND D. FRANK-KAMENETZKI, *A theory of thermal propagation of flame*, Acta Physicochimica IJRSS, 9 (1938), pp. 341–350.

[140] D. ZIPES AND J. JALIFE, *Cardiac electrophysiology: from cell to bedside*, WB Saunders CO, 2000.

[141] V. S. ZYKOV, *Excitable media*.
http://www.scholarpedia.org/article/Excitable_media.